Summer 8-15-2015

Topics in Lattice Gauge Theory and Theoretical Physics

Javad Komijani
Washington University in St. Louis

WASHINGTON UNIVERSITY IN ST. LOUIS

Department of Physics

Dissertation Examination Committee:
Claude Bernard, Chair
Carl M. Bender, Co-chair
Mark Alford
John E. McCarthy
Michael C. Ogilvie
Xiang Tang

Topics in Lattice Gauge Theory and Theoretical Physics

by
Javad Komijani

A dissertation presented to the
Graduate School of Art and Sciences
of Washington University in St. Louis in
partial fulfillment of the
requirements for the degree
of Doctor of Philosophy

August 2015
St. Louis, Missouri

Contents

List of Figures

List of Tables

Acknowledgements

During my PhD study, I have had the great opportunity to work with two advisors who helped me to start exploring different areas of the exciting field of theoretical physics. Foremost, I would like to express my sincere gratitude to my advisor Prof. Claude Bernard for the continuous support of my PhD study and research, his enormous patience, encouraging comments, excellent guidance, and immense knowledge. I also would like to thank him, for critically reading this dissertation and for his extremely helpful comments.

Also, my sincere gratitude goes to my other advisor Prof. Carl M. Bender for his inspiration, guidance and continuous support. It was a great pleasure for me to have him as my advisor during my doctoral studies. I have benefited greatly from his knowledge, experience, priceless ideas and inspiring discussions.

I am very grateful to all of the Department faculty members for their help and support. Particularly, I would like to thank Prof. Mark Alford and Prof. Michael C. Ogilvie for their helpful discussions. I also would like to thank Prof. Mehdi Golshani, Prof. Sedigheh Deldar and Prof. Jalil Rashed-Mohassel who encouraged and helped me to join to this great Department.

I take this opportunity to express gratitude to the members of the MILC collaboration. A part of this work would not be possible without their collaboration. I am grateful for their support and friendship. Particularly, I would like to thank Prof. Doug Toussaint and Prof. Carleton DeTar for their hospitality during the MILC workshops, as well as their helpful comments and discussions during this work.

I am indebted to many of my colleagues and friends here, especially Hossein Mahzoon and Saeed Mirshekari for their help and support during the time of writing the thesis. I am also grateful to my family for all the support that they always offer.

to all the people who examine their worlds

ABSTRACT OF THE DISSERTATION

Topics in Lattice Gauge Theory and Theoretical Physics

by

Javad Komijani

Doctor of Philosophy in Physics

Washington University in St. Louis, 2015

Professor Claude Bernard, Chair

Professor Carl M. Bender, Co-chair

This dissertation contains two completely independent parts. In Part I, I investigate effective field theories and their applications in lattice gauge theory. Quantum chromodynamics (QCD) as a part of the standard model (SM) describes the physics of quarks and gluons. There are several numerical and analytical methods to tackle the QCD problems. Lattice QCD is the dominant numerical method. Effective field theories, on the other hand, provide analytic methods to describe the low-energy dynamics of QCD. To use the effective theories in lattice QCD, I develop chiral perturbation theory for heavy-light mesons with staggered quarks—an implementation of fermions on lattice. I use this effective chiral theory to study the pattern of taste splitting in masses of the mesons with staggered quarks. I also calculate the leptonic decay constant of the heavy-light mesons with staggered quarks to one-loop order in the chiral expansion. The resulting chiral formula provides a suitable fit form to combine and analyze a large number of decay constants of heavy-light mesons computed from different lattice ensembles with various choices of input parameters. I perform a comprehensive chiral fit to the lattice data for D mesons computed by the MILC collaboration. Consequently, I determine the physical values of the decay constants of D mesons. These precise results place narrow restrictions on the Cabibbo-Kobayashi-Maskawa (CKM) matrix elements.

In Part II, I introduce the concept of a nonlinear eigenvalue problem by investigating three nonlinear differential equations. First, equation $y'(x) = \cos[\pi x y(x)]$ is investigated. A discrete

set of initial conditions $y(0) = a_n$, leading to unstable separatrix behavior, are identified as the eigenvalues of the problem. I calculate the asymptotic behavior of the initial conditions a_n and their corresponding solutions for large n by reducing the equation to a linear one-dimensional random-walk problem. Second, I investigate equation $y''(x) = 6[y(x)]^2 + x$, whose solutions are called the first Painlevé transcendent. I calculate different types of critical initial conditions that give rise to separatrix solutions for this equation. I work out the asymptotic behaviors of the initial conditions by reducing the problem to a linear Schrödinger equation. Finally, I investigate the second Painlevé transcendent, corresponding to equation $y''(x) = 2[y(x)]^3 + xy(x)$. I find that this equation exhibits patterns similar to the first Painlevé equation.

PART I

Staggered Chiral Perturbation Theory

This part includes three chapters. In Chapter 1 quantum chromodynamics (QCD) is reviewed briefly, and some important numerical and analytical methods to tackle the QCD problems are discussed. Staggered chiral perturbation theory (SχPT) is developed in Chapter 2. Finally, an application of SχPT in calculating the decay constants of D mesons is presented in Chapter 3.

1 Technical Introduction to Part I

1.1 Quantum Chromodynamics

The standard model of strong, weak and electromagnetic interactions is a relativistic quantum field theory that describes all known interactions of quark and leptons. This model is a gauge theory based on the gauge group SU(3)×SU(2)×U(1); the electroweak interactions are described by the SU(2)×U(1) gauge group, and the strong interaction is described by SU(3) gauge group. Quantum chromodynamics (QCD), as a part of the standard model, studies the interactions between quarks and gluons. In the standard model, there are six quark flavors: u (up), d (down), s (strange), c (charm), b (bottom), and t (top), each of which has three colors transforming as a triplet under the fundamental representation of the color SU(3) group.

1.1.1 The QCD action

The QCD action is composed of two parts describing matter (fermionic) and gauge fields

$$S_{\text{QCD}} = \int d^4x[\mathcal{L}_{\text{fermion}} + \mathcal{L}_{\text{gauge}}] \,. \tag{1.1}$$

The fermionic part of the Lagrangian density

$$\mathcal{L}_{\text{fermion}} = \sum_{f=1}^{N_f}\sum_{c=1}^{3} \bar{\psi}_{f,c}(\not{D} - m_f)\psi_{f,c} \,, \qquad \not{D} = i\gamma^\mu(\partial_\mu - ig_S A_\mu) \,, \tag{1.2}$$

describes the quarks, with different flavors and colors, and their interactions with gauge field A_μ. Here, f and c denote the the flavor and the color of fermions, respectively, N_f is the number of flavors, g_S is the strong coupling constant, and the gauge field is a matrix in the color space

$A_\mu = A_\mu^a T^a$, where T^a are the eight generators of the SU(3) gauge group. The gauge part, which describes only the propagation and interactions of eight gluons, is

$$\mathcal{L}_{\text{gauge}} = -\frac{1}{2}\,\text{Tr}\, F^{\mu\nu}F_{\mu\nu}\ , \qquad F_{\mu\nu} = \partial_\mu A_\nu - \partial_\nu A_\mu - ig_S[A_\mu, A_\nu]\ . \tag{1.3}$$

A general feature of gauge theories is that the observable quantities do not change under a gauge transformation. For quark fields, a gauge transformation is a local transformation of fields in the color space given by

$$\psi(x) \ \rightarrow\ V(x)\psi(x)\ , \tag{1.4}$$

where $V(x) \in \text{SU(3)}$. Here a vector notation in the color index is used for ψ. The field strength $F_{\mu\nu}$ consequently transforms as

$$F_{\mu\nu}(x) \ \rightarrow\ V(x)F_{\mu\nu}(x)V(x)^\dagger\ , \tag{1.5}$$

and the QCD Lagrangian is then gauge invariant.

1.1.2 Running coupling constant

Integration of internal loops in Feynman diagrams yields divergent results. To find finite results and make sense of QFT, one needs to regularize the theory. There are several ways to do this, such as momentum cutoff regularization, lattice regularization, and dimensional regularization. These methods, in general, introduce a new energy scale Λ in the theory.[1] Then a change in Λ can be compensated by a change in the parameters of the theory so that all physical quantities become independent of Λ. This leads to the concept of renormalized parameters and renormalization group. The renormalized parameters then depend on the energy scale of the process. This happens even for those parameters of the theory that are (superficially) dimensionless such as g_S.[2] Considering one loop calculation in QCD, the renormalized (effective) strong coupling constant at energy scale μ is

$$\alpha_S(\mu^2) = \frac{g_S^2(\mu^2)}{4\pi} = \frac{12\pi}{(33-2N_f)\ln(\mu^2/\Lambda^2_{\text{QCD}})}\ . \tag{1.6}$$

[1] Even in dimensional regularization, a combination of a fixed dimension and a fixed dummy scale μ can be translated to a cutoff scale Λ. See [1] for more details.

[2] One can interpret the beta function as the anomalous dimension of the coupling constant g_S.

For $N_f < 16$, this relation shows that α_S vanishes as $\mu \to +\infty$, and also suggests that α_S gets large as $\mu \to \Lambda_{\rm QCD}$. These asymptotic behaviors are two important features of QCD, which are referred to as asymptotic freedom and confinement, respectively.

The fundamental scale appearing in Eq. (1.6), $\Lambda_{\rm QCD} \sim 300$MeV, provides a natural scale to separate the quarks based on their masses. A quark Q is called heavy when its mass is much larger than this fundamental scale, $m_Q >> \Lambda_{\rm QCD}$. On the other hand, a quark q is called light when its mass is much lighter than this fundamental scale, $m_Q << \Lambda_{\rm QCD}$. Depending on whether they are light or heavy, quarks show different features in colorless particles such as mesons. For instance, the quarkonium systems ($\bar{Q}Q$) are hydrogen-like, while the corresponding systems with light quarks (pions) are highly relativistic. This stems from the fact that, for a system of heavy quarks, the effective coupling constant $\alpha_S(m_Q^2)$ is small, implying that on length scales comparable to the Compton wavelength $\lambda_Q \sim 1/m_Q$ the strong interactions are perturbative and gluons act like photons in quantum electrodynamics (QCD), while this is not the case for a system of light quarks.

1.1.3 Chiral symmetry

The quarks of the standard model are naturally divided into two classes: u, d and s are light quarks, whereas c, b and t are heavy quarks. The light quarks sector of QCD posses a very important symmetry in the limit of massless u, d, and s quarks.

Using the projection operators $(1 \pm \gamma_5)/2$, one can divide the quark fields into left-handed and right-handed parts as

$$\psi_R = \tfrac{1}{2}(1+\gamma_5)\psi, \qquad \bar{\psi}_R = \bar{\psi}\tfrac{1}{2}(1+\gamma_5), \tag{1.7}$$

$$\psi_L = \tfrac{1}{2}(1-\gamma_5)\psi, \qquad \bar{\psi}_L = \bar{\psi}\tfrac{1}{2}(1-\gamma_5). \tag{1.8}$$

Then, using a matrix notation in flavor space, the light sector of fermionic part of the Lagrangian density in Eq. (1.1) can be written as

$$\mathcal{L}^{\rm light}_{\rm fermion} = \bar{\psi}_L \not{D} \psi_L + \bar{\psi}_R \not{D} \psi_R \; - \bar{\psi}_L M \psi_R - \bar{\psi}_R M \psi_L \; , \tag{1.9}$$

where $M = {\rm diag}(m_u, m_d, m_s)$. In the limit of massless u, d, and s quarks, the Lagrangian density has two parts (the left-handed and right-handed parts) that can be transformed separately in flavor space. Therefore, this Lagrangian density is invariant under a global ${\rm U(3)_L} \times {\rm U(3)_R}$

transformation in the flavor basis

$$\psi_R \to U_R \psi_R, \qquad \bar{\psi}_R \to \bar{\psi}_R U_R^\dagger \,, \tag{1.10}$$

$$\psi_L \to U_L \psi_L, \qquad \bar{\psi}_L \to \bar{\psi}_L U_L^\dagger \,. \tag{1.11}$$

This decomposes to $\mathrm{SU(3)_L} \times \mathrm{SU(3)_R} \times \mathrm{U(1)_V} \times \mathrm{U(1)_A}$, where $\mathrm{U(1)_V}$ is the singlet vector component, *i.e.*, the transformation with $U_L = U_R = exp(i\theta)\, I$, and $\mathrm{U(1)_A}$ is the singlet axial-vector component, *i.e.*, the transformation with $U_L = U_R^\dagger = exp(i\theta)\, I$.[3] Due to the anomaly appearing in the quantum level, $\mathrm{U(1)_A}$ is not a symmetry of QCD even in the limit of massless quarks.

In short, the light sector of the QCD action has $\mathrm{SU(3)_L} \times \mathrm{SU(3)_R} \times \mathrm{U(1)_V}$ symmetry, in the limit of massless quarks. But, this symmetry is assumed to be spontaneously broken, giving rise to eight massless Goldstone bosons. This is addressed in chiral perturbation theory, which is discussed in subsection 1.4.2.

1.2 Overview of approaches to tackle QCD

Straightforward perturbative calculations, in terms of the coupling constant, are not useful when α_S is large. Several numerical and analytical methods have been developed to tackle problems in QCD in this regime. In the numerical approach, lattice QCD is the dominant method to solve QCD problems from first principles. Effective field theories, on the other hand, provide an analytic way to study and organize QCD problems.

1.2.1 Lattice QCD

Lattice QCD is a way to solve the theory from first principles, which is developed based on the Euclidean[4] path integral. In the lattice approach the continuum, infinite volume space-time is replaced with a set of discrete points with finite lattice spacing a and in finite volume. The lattice formulation helps us perform a numerical calculation on quantum field theories. However, in practice, there are some restrictions in lattice calculations. It can be prohibitively expensive to generate sufficiently big and fine lattice configurations. This, in turn, can restrict the values of quark masses to a range which may or may not correspond to their values in the physical world.

[3] Instead of the chiral currents corresponding to the $\mathrm{U(3)_L} \times \mathrm{U(3)_R}$ symmetry, one can use some linear combinations of them, which transform under parity as vector and axial-vector currents. $\mathrm{U(1)_V}$ and $\mathrm{U(1)_A}$ refer to the U(1) component of the vector and the axial-vector currents, respectively.

[4] Euclidean, *i.e.*, imaginary, time is obtained using the Wick rotation: $x^0 \to -ix^4$. In Euclidean space-time, the QCD action is replaced with its Euclidean version; sea Appendix A for details.

Therefore the lattice data needs to be processed in order to extract physical quantities. This process requires setting the lattice scale, taking the finite volume effects into account, tuning quark masses and extrapolating the lattice results to the continuum limit.

Extrapolation and interpolation are essential in extracting desired quantities from lattice data. The process of interpolating and extrapolating, in general, can increase the level of uncertainty. Therefore it is very helpful to take advantage of some analytic methods to restrict the form of the fit functions and decrease the error resulting from extrapolation, and to some degree, interpolation.

1.2.2 Effective field theories

Effective field theory (EFT) is a very powerful tool in quantum field theory. The basic strategy in developing an effective theory is to integrate out unimportant degrees of freedom from the path integral and describe the important physics in hand based on (approximate) symmetries of the remaining degrees of freedom. As an application in QCD, effective theories can describe some aspects of physics of systems involving very heavy and/or very light quarks. Chiral perturbation theory (ChPT) and heavy quark effective theory (HQET) are two well-known effective theories developed to investigate the low-energy dynamics in QCD.

As mentioned, any calculation in lattice QCD requires extrapolations and/or interpolations. The effective field theories can play an important role in decreasing the uncertainty level by providing appropriate fit forms. A simple way to proceed is to use the effective theories developed in the continuum limit. The other option is to develop new effective theories based on the symmetries of a lattice QCD action. This helps us have more control on artifacts of discretization of the lattice action and be able to extrapolate the lattice results to the continuum in a more systematic way.

Lattice actions may have different symmetries depending on the formulations of quantum fields on the lattice. Here our focus is on lattice actions with staggered quarks, for which staggered chiral perturbation theory (SχPT) is developed to study the low energy dynamics of the lattice. The main achievement of the first part of this dissertation is to expand SχPT to heavy-light staggered mesons (mesons with one heavy staggered quark and one light staggered antiquark, or their antiparticles). Then, this theory is applied to extrapolate the lattice results for decay constant of mesons, generated by the MILC collaboration, to the continuum limit while the quark masses are extrapolated/interpolated to their corresponding physical values.

1.3 Lattice QCD

The basic idea in lattice QCD is to replace the continuous Euclidean space-time with a 4 dimensional lattice, with the spacing between the lattice sites denoted by a. The quark fields, $\psi(x)$ and $\bar{\psi}(x)$, (or any other matter field) reside on the lattice sites. Then one needs to formulate a discretized version of the fermionic sector of the QCD action. A simple way to perform this step is to replace the derivatives and the space-time integral with finite differences and a sum over the lattice sites, respectively. However, this introduces a lattice action which is not gauge-invariant for nonzero lattice spacing. Because of the vagaries of renormalization this is likely to mean that the quantized theory still lacks gauge invariance in the limit $a \to 0$ [5]. The alternative is to construct a lattice theory that is gauge invariant even for a nonzero lattice spacing.

1.3.1 The QCD action on lattice

Having placed the quark fields on the lattice sites, one needs to formulate a discretized version of the fermionic sector of the QCD action. This step may violate some of the symmetries that the QCD action posses in the continuum limit, such as Lorentz invariance or the chiral symmetry in the massless quark limit. Consider the continuum action for a free fermion

$$S_{\mathrm{F}}^{0}[\psi,\bar{\psi}] = \int d^4x \psi(x)(\gamma_\mu \partial_\mu + m)\psi(x) \ . \tag{1.12}$$

The partial derivative can be discretized with the symmetric expression

$$\frac{1}{2a}\big(\psi(x+a\hat{\mu}) - \psi(x-a\hat{\mu})\big) \ , \tag{1.13}$$

where x is a lattice site. Then the lattice version of Eq. (1.12) reads

$$S_{\mathrm{F}}^{0}[\psi,\bar{\psi}] = a^4 \sum_x \bar{\psi}(x)\Big(\sum_{\mu=1}^{4}\gamma_\mu \frac{\psi(x+a\hat{\mu}) - \psi(x-a\hat{\mu})}{2a} + m\psi(x)\Big) \ . \tag{1.14}$$

This expression has two problems: it is not gauge-invariant, and it suffers from the existence of *doublers*, unwanted extra states (as explained below).

Under the SU(3) gauge transformation, the quark fields on each site transform as

$$\psi(x) \ \to \ V(x)\psi(x) \tag{1.15}$$

$$\bar{\psi}(x) \ \to \ \bar{\psi}(x)V^{\dagger}(x). \tag{1.16}$$

In order to have a gauge invariant action, the links joining the neighboring sites need to change in a specific way under the gauge transformation. This requires to define a new field, denoted by $U_\mu(x)$ and referred to as *link variable*, which lives on the link connecting the site x to the neighbor site $x + a\hat{\mu}$. The link variables are group members of SU(3) group. Under the gauge transformation they transform as

$$U_\mu(x) \to V(x)U_\mu(x)V^\dagger(x + a\hat{\mu}) \ . \tag{1.17}$$

This property of the link variables is essential to arrive at a gauge-invariant expression for the lattice action

$$S_F^0 = \sum_x \bar{\psi}(x) \left\{ \sum_\mu \gamma_\mu \nabla_\mu \psi(x) + m\, \psi(x) \right\} \ , \tag{1.18}$$

where

$$\nabla_\mu \psi(x) = \frac{1}{2a} \Big(U_\mu(x)\psi(x + a\hat{\mu}) - U_\mu^\dagger(x - a\hat{\mu})\psi(x - a\hat{\mu}) \Big) \ . \tag{1.19}$$

The link variable $U_\mu(x)$ can be associated with the gauge field A_μ via the path ordered integral (defined in the continuum QCD)

$$U_\mu(x) = \mathcal{P} \exp \left\{ ig \int_x^{x+a\hat{\mu}} dy_\nu \, A_\nu(y) \right\} = 1 + iagA_\mu(x + a\hat{\mu}/2) + \dots \ . \tag{1.20}$$

This relation between link variables and gauge field will be used to define gauge actions on the lattice.

To address the second problem, the doubling problem, one can investigate the propagator in momentum space derived from the action Eq. (1.14), with all link fields $U_\mu = 1$,

$$S(ap) = \frac{1}{i \sum_\mu \gamma_\mu \sin(ap_\mu) + am} \ . \tag{1.21}$$

In the massless case, this propagator not only has a pole when $p = 0$, but also when $p_\mu = 0$ or $p_\mu = \pi/a$ for each $\mu = 1, \dots, 4$, *i.e.,* on all 16 corners of the Brillouin zone of the four dimensional lattice. (The problem holds for the massive case as well.) Thus, instead of one fermion, this *naive* action actually has 16 fermions which can appear in the quantum loops and contribute to physical processes. This is the notorious doubling problem of lattice fermions. Several fermion action implementations are proposed to address this issue. We focus on the Kogut-Susskind implementation of fermions [2–4], the so-called staggered fermions.

1.3.2 The gauge-invariant objects and the gauge action

The link variables are introduced in order to build a gauge-invariant expression for the fermionic part of the action. However, one can build gauge invariant objects that do not involve any fermion fields. As a matter of fact these objects can be exploited to construct the gauge action on lattice. This is not surprising because we already know that the link variables are associated with the gauge field.

Consider the products of link variables around an elementary square loop (so-called plaquette)

$$U_{\mu\nu}(x) = U_\mu(x)U_\nu(x + a\hat{\mu})U_\mu^\dagger(x + a\hat{\mu} + a\hat{\nu})U_\nu^\dagger(x + a\hat{\nu}) \; . \tag{1.22}$$

It is easy to verify that $\mathrm{Tr}(U_{\mu\nu})$ is gauge invariant. In general, the trace over products of link variables around any closed loop on the lattice (a so-called Wilson loop) is a gauge invariant quantity. The simplest gauge action, the original form introduce in Ref. [5], is then the sum over all plaquettes

$$S_G = \frac{2}{g^2} \sum_x \sum_{\mu,\nu}^{\mu<\nu} \mathrm{Re}\ \mathrm{Tr}(1 - U_{\mu\nu}(x)) \; , \tag{1.23}$$

where g is the bare coupling constant. This action reduces to $\int d^dx\ \frac{1}{2}\mathrm{Tr}\ F_{\mu\nu}F_{\mu\nu}$ up to terms of $\mathcal{O}(a^2)$. The $\mathcal{O}(a^2)$ corrections can be reduced by using improved actions.

1.3.3 The doubling problem

The basic reason for fermion doubling on the lattice is that the Dirac equation is first order while its lattice Hermitian version is a second order difference equation which doubles the number of generic solutions per dimension. The following toy model shows that the origin of fermion doubling lies in the use of symmetric form for the lattice derivative [6]. Consider the differential equation

$$-i\frac{d}{dt}f(t) - \omega f(t) = 0, \tag{1.24}$$

with the solution $f(t) = f(0)e^{i\omega t}$. There is no unique way to derive the equivalent difference equation in a lattice with finite lattice spacing. For instance, replacing the derivative with the right lattice derivative, one finds

$$-i\ \frac{f\big((n+1)a\big) - f\big(na\big)}{a} - \omega f(na) = 0, \tag{1.25}$$

with can be solved as

$$f(na) = (1 + i\omega a)^n f(0) = e^{n\ln(1+i\omega a)} f(0). \tag{1.26}$$

The continuum limit of this solution, $a \to 0$, recovers the solution of the original differential equation, *i.e.*, $f(t) = f(0)e^{i\omega t}$. However, if one wishes to respect the Hermiticity of the operator $i\frac{d}{dt}$, using the symmetric lattice derivative one obtains

$$-i\,\frac{f\big((n+1)a\big) - f\big((n-1)a\big)}{2a} - \omega f(na) = 0. \tag{1.27}$$

This second order difference equation has two generic solutions:

$$e^{in(\arcsin \omega a)} \text{ and } (-1)^n e^{-in(\arcsin \omega a)}\ , \tag{1.28}$$

where $-\frac{\pi}{2} < \arcsin(\omega a) < \frac{\pi}{2}$. These solutions exhibit different characteristic behaviors in the continuum limit. One solution recovers the solution of the original differential equation, while the other one has an alternating sign factor $(-1)^n$ which does not possess a continuous limit.

Similar to the term with factor $(-1)^n$ in the toy model, the doubler solutions are pure lattice artifacts having no continuum analog. As a matter of fact, these doubler solutions are the fermionic modes appearing at the corners of the Brillouin zone where the function $\sin(p_\mu a)$ vanishes. One possible way to get rid of these unwanted fermionic modes is to decrease the Brillouin zone by doubling the effective lattice spacing for each fermion field. One can think of a 2^4 hypercube of the lattice as a block over which the fermionic degrees of freedom are distributed, in such a way that the effective lattice spacing for each fermion field is twice the original lattice spacing. The Kogut-Susskind fermion formalism, also called the staggered fermions, provides a way to remove some of the unwanted fermionic modes by doubling the effective lattice spacing. In fact this formalism reduces the sixteen-fold degeneracy of the naive discretization to four fermions, which are known as four *tastes*.

1.3.4 Staggered fermions

Consider the naive action for a Dirac field, Eq. (1.18),

$$S_F^0 = \sum_x \bar{\psi}(x) \left\{ \sum_\mu \gamma_\mu \nabla_\mu \psi(x) + m\,\psi(x) \right\}\ .$$

By making a local change of variable

$$\psi(x) = \Gamma_{x/a}\ \chi(x)\ ,\ \ \bar{\psi}(x) = \bar{\chi}(x)\ \Gamma^\dagger_{x/a}\ , \tag{1.29}$$

with

$$\Gamma_{x/a} = \gamma_1^{(x_1/a)}\ \gamma_2^{(x_2/a)}\ \gamma_3^{(x_3/a)}\ \gamma_4^{(x_4/a)}\ , \tag{1.30}$$

the naive fermion action, Eq. (1.18), can be written as

$$S_{KS} = \sum_x \bar{\chi}(x) \left\{ \sum_\mu \eta_\mu(x)\ \nabla_\mu\ \chi(x) + m\chi(x) \right\}\ , \tag{1.31}$$

where

$$\eta_\mu(x) \equiv \Gamma^\dagger_{x/a}\ \gamma_\mu\ \Gamma_{\hat{\mu}+x/a} = (-1)^{(x_1+\cdots+x_{\mu-1})/a}\ . \tag{1.32}$$

In Eq. (1.31), the phase $\eta_\mu(x)$, the only remnant of the original Dirac structure, leaves the action spin-diagonalized. Therefore, the four Dirac components decouple from each other, and the fermion field $\chi(x)$ can be restricted to a single component rather than four components. This, in turn, reduces the doubling by a factor of four, from sixteen to four. The expression in Eq. (1.32), with one-component fermion field $\chi(x)$, is the action of the staggered fermion formulation, and $\chi(x)$ is called the staggered field.

Now, at each block of 2^4 hypercube, labeled by x_{block}, a new field $q_{\alpha i}(x_{\text{block}})$, where both α and i run from 1 to 4, can be constructed from the one-component staggered fermion fields $\chi(x)$ living at the sites within the hypercube. It turns out that α can be interpreted as a Dirac index, while i refers to the taste of the fermion. The taste index is a new quantum number labeling the four remaining fermion species. The field $q_{\alpha i}(x_{\text{block}})$ lives on a *blocked-lattice*, where its effective lattice spacing is twice the original lattice spacing; thereby the effective Brillouin zone is reduced by a factor of two. Thus, as will be discussed later, the new field is free of doublers, and its four tastes have desired continuum forms, unlike the fifteen doubler modes of the naive discretization.

1.3.4.1 Construction of Dirac fields

Dividing the lattice into blocks of 2^4 hypercubes, each block (labeled by y) has 16 sites with coordinate $x = 2y + aA$, where $A_\mu = 0, 1$. It should be emphasized that the blocked-lattice spacing is twice the original lattice spacing; therefore, when the label y refers to the blocks, its units are understood to be twice that of the label x that refers to sites of the original lattice. The one component-staggered fermion fields $\chi(x)$ living at the sites within each block can be

assembled into Dirac fields $q(y)$ as

$$q_{\alpha i}(y) = \frac{1}{8}\sum_A (\Gamma_A)_{\alpha i}\, U_A(y)\, \chi(2y + aA)\ , \tag{1.33}$$

$$\bar{q}_{\alpha i}(y) = \frac{1}{8}\sum_A \bar{\chi}(2y + aA)\, U_A^\dagger(y)\, (\Gamma_A^*)_{\alpha i}\ , \tag{1.34}$$

where α and i label the Dirac and taste indices, respectively, Γ_A is defined in Eq. (1.30), and $U_A(y)$ is a product of the gauge links over some fixed path from $2y$ to $2y + aA$. Both α and i run from 1 to 4 in spin and taste spaces, respectively. Having constructed the Dirac fields in the spin-taste basis, the quark action in Eq. (1.31) can be expressed in terms of $q(y)$. In the free case where $U_\mu(x) = 1$, Eq. (1.31) reads [7]

$$S_{KS} = 16\sum_y \bar{q}(y)\left\{m(I\otimes I) + \sum_\mu \left[(\gamma_\mu \otimes I)\,\nabla_\mu + a\,(\gamma_5 \otimes \xi_\mu\xi_5)\,\Delta_\mu\right]\right\} q(y)\ , \tag{1.35}$$

where I is the identity matrix, and the ξ matrices correspond to the γ matrices in taste space, and ∇_μ and Δ_μ are defined by

$$\nabla_\mu q(y) = \frac{1}{2b}\Big(q(y + b\hat{\mu}) - q(y - b\hat{\mu})\Big)\ , \tag{1.36}$$

$$\Delta_\mu q(y) = \frac{1}{b^2}\Big(q(y + b\hat{\mu}) - 2q(y) + q(y - b\hat{\mu})\Big)\ , \tag{1.37}$$

where $b = 2a$ is the blocked-lattice spacing. The factor of 16 in Eq. (1.35) arises from the fact that there are 1/16 as many y points as x points. In the interacting case, Eq. (1.35) has another dimension-five, $\mathcal{O}(a)$, term, involving the field-strength tensor $\mathcal{F}_{\mu\nu}$, and also higher contributions of $\mathcal{O}(a^2)$ [7]. It is manifest that the theory in the continuum limit has four degenerate tastes, with exact $SU(4)$ symmetry in taste space for each flavor of quark.

In the free case, the propagator in momentum space is (see Appendix B for details)

$$S(p) = \frac{a}{16}\frac{\sum_\mu -i\sin(\frac{1}{2}ap_\mu)\,\Gamma^\mu_{\text{s-t}}(ap) + am}{\sum_\mu \sin^2(\frac{1}{2}ap_\mu) + (am)^2}\ . \tag{1.38}$$

where

$$\Gamma^\mu_{\text{s-t}}(ap) \equiv (\gamma_\mu \otimes I)\exp\left[i\tfrac{1}{2}ap_\mu(\gamma_\mu\gamma_5 \otimes \xi_\mu\xi_5)\right]\ . \tag{1.39}$$

It is noteworthy that $\Gamma^\mu_{\text{s-t}}(p)$ obeys the same anticommutator algebra as $\gamma_\mu \otimes I$. The spin-taste quarks are free of doublers, because the effective Brillouin zone is reduced by a factor of two as is manifest by comparing the denominator of the propagator to Eq. (1.21). However, the taste

degree of freedom itself is an unwanted one and must be removed. The removal, at the quantum loop level, can be accomplished using the so-called fourth-root procedure.

1.3.4.2 Symmetries of the staggered action

The staggered fermion action is invariant under several discrete symmetries such as the shift symmetry of the lattice [8]. Here, our focus is on a very important continuous symmetry of the staggered fermion action for massless quarks. In this limit, the action Eq. (1.31) is invariant under a continuous even/odd $\mathrm{U}(1)_e \times \mathrm{U}(1)_o$ transformation

$$\chi(x) \to \exp\{i\alpha_e\}\chi(x) \ , \ \bar{\chi}(x) \to \bar{\chi}(x)\exp\{-i\alpha_o\} \qquad \text{for } x = \text{even} \ , \tag{1.40}$$

$$\chi(x) \to \exp\{i\alpha_o\}\chi(x) \ , \ \bar{\chi}(x) \to \bar{\chi}(x)\exp\{-i\alpha_e\} \qquad \text{for } x = \text{odd} \ , \tag{1.41}$$

where α_e and α_o are the symmetry parameters, and a site x is called even or odd if $\sum_\mu (x_\mu/a)$ is even or odd, respectively. The physical meaning of this symmetry is that the staggered fermionic degrees of freedom on lattice can be divided into two parts that are decoupled in the massless quark limit. This is a remnant of the usual chiral symmetry for massless fermions in the continuum.

The axial part of the $\mathrm{U}(1)_e \times \mathrm{U}(1)_o$ symmetry, $\alpha_e = -\alpha_o \equiv \alpha_\epsilon$, in the spin-taste basis is

$$q(y) \to \exp\left\{i\alpha_\epsilon\left(\gamma_5 \otimes \xi_5\right)\right\} q(y) \ , \qquad \bar{q}(y) \to \bar{q}(y)\exp\left\{i\alpha_\epsilon\left(\gamma_5 \otimes \xi_5\right)\right\} \ . \tag{1.42}$$

This symmetry, called the $\mathrm{U}(1)_\epsilon$ symmetry, is not a singlet in taste space, thereby it is free from the anomaly at the quantum level. This results in existence of a Goldstone boson on the lattice in the massless quark limit, and guarantees that there is no additive mass renormalization for staggered fermions.

1.3.5 Path integral and numerical calculations

The Euclidean path integral is the basic tool to quantize the field on a lattice; it relates a quantum problem to a statistical-mechanical system. The lattice partition function for a system of fermions and gauge fields is

$$Z = \int \prod_{x,\mu} dU_\mu(x) \prod_x [d\bar{\psi}_x d\psi_x] e^{-S_G(U) - \bar{\psi} M(U) \psi} \ , \tag{1.43}$$

where $S_G(U)$ is the gauge action, while $\bar{\psi}M(U)\psi$ is the fermion action with a matrix notation for the degrees of freedom of the fermion field. Here, $dU_\mu(x)$ is the invariant SU(N) Haar measure and $[d\bar{\psi}_x d\psi_x]$ denotes the integration over the Grassmann fields with all flavors and tastes.

Because of its quadratic form, the integration over the Grassmann fields can be carried out analytically, leading to

$$Z = \int \prod_{x,\mu} dU_\mu(x) \det[M(U)]\ e^{-S_G(U)}\ . \tag{1.44}$$

For staggered fermions, each fermion with a different flavor and taste (in the continuum limit) would get its own determinant factor

$$\det[M(U)] = \prod_{f,t} \det[M(U)_{f,t}]. \tag{1.45}$$

The fourth-root trick is the suggestion to replace $\det[M(U)]$ by its fourth root to get rid of the contributions from taste degree of freedom

$$Z = \int \prod_{x,\mu} dU_\mu(x) \det{}^{\frac{1}{4}}[M(U)]\ e^{-S_G(U)}\ . \tag{1.46}$$

Having defined the partition function, one can calculate the expectation value of some observable $\mathcal{O}$ as

$$\langle \mathcal{O} \rangle = \frac{1}{Z} \int \prod_{x,\mu} dU_\mu(x)\ \mathcal{O}\ \det{}^{\delta}[M(U)]\ e^{-S_G(U)}\ , \tag{1.47}$$

where $\delta = 1/4$ for rooted staggered fermions. Now, some numerical methods like Monte Carlo can be used to compute expectation values of desired observables. The basic idea in the Monte Carlo method is to generate a set of gauge field configurations $\{U_\mu^{(i)}(x)\}$, $i = 1, \ldots, N$, with probability distribution proportional to $\det^{\delta}[M(U)]\ e^{-S_G(U)}$. Expectation values $\langle \mathcal{O} \rangle$ are then computed as an average over the ensemble of gauge field configurations,

$$\langle \mathcal{O} \rangle = \frac{1}{N} \sum_{i=1}^{N} \mathcal{O}(U^{(i)})\ , \tag{1.48}$$

where $\mathcal{O}(U^{(i)})$ is the observable evaluated on the gauge field configuration i.

1.4 Effective Field Theories

As described before, the quarks of the standard model are naturally divided into two classes depending whether they are light or heavy comparing to $\Lambda_{\rm QCD}$. The light class contains u, d and s quarks, whereas the heavy class contains c, b and t quarks. Physical quantities (such as a decay constant) involving light quarks, with mass m_q, can be expressed in powers of $m_q/\Lambda_{\rm QCD}$ (with logarithmic corrections) within the framework of effective field theories. Similarly, physical quantities involving heavy quarks, with mass m_Q, can be expressed in powers of $\Lambda_{\rm QCD}/m_Q$ (with logarithmic corrections). In both limits, where $m_q \to 0$ and/or $m_Q \to \infty$, QCD exhibits new symmetries, which can be used to work out the form of corresponding effective Lagrangians. Chiral perturbation theory (ChPT), is constructed based on the approximate chiral symmetry of the light quarks. It provides a systematic method to study the low energy regime of QCD. On the other hand, to study systems involving heavy quarks, heavy quark effective theory (HQET) is developed based on the approximate spin and flavor symmetries of the heavy quarks of the theory. Both ChPT and HQET can be generalized to include the discretization effects appearing in lattice QCD. This is accomplished through Symanzik's idea to construct a local (continuum-like) effective field theory (EFT) for the lattice theory.

1.4.1 General discussion of EFTs

Effective field theory provides a systematic formalism for the analysis of multi-scale problems [9]. The basic premise of effective theories is that dynamics at low energies (or large distances) does not depend on the details of the dynamics at high energies (or short distances) [10]. The strategy is to integrate out any feature of the physics at distance scales small compared to the scale of interest [11]. This is particularly important in QCD, where quark masses have different energy scales and the $\alpha_S(\mu^2)$ can run dramatically between these energy scales.

Consider a quantum field theory with a large scale M, which could be the mass of a heavy quark or the mass of a meson. Now suppose we are interested in the physics at some lower scale $E << M$. The effect of physics at high energy on the physics at the scale E, can be described by a series of interactions with different dimensions each of which suppressed by an appropriate power of $1/M$ [11]. This can be done in a systematic way in three steps [9]:

1. Choose a cutoff $\Lambda < M$ and divide the fields of the theory into low-frequency and high-frequency modes,

$$\phi = \phi_{\rm L} + \phi_{\rm H}, \tag{1.49}$$

where $\phi_{\rm L}$ contains the Fourier modes with frequency $\omega < \Lambda$, while $\phi_{\rm H}$ contains the remaining modes. ($\phi_{\rm H}$ might be a particle which is too heavy to be excited at energy $E << M$, or just the high-frequency fluctuations of a light particle. The former case can be referred as complete decoupling, and the latter one as partial decoupling [12].) By construction, low-energy physics is described in terms of the $\phi_{\rm L}$ fields.

2. Now integrate out the high-frequency part by doing the path integral over $\phi_{\rm H}$

$$\int \mathcal{D}\phi_{\rm L}\, \mathcal{D}\phi_{\rm H}\, e^{iS(\phi_{\rm L},\phi_{\rm H})} = \int \mathcal{D}\phi_{\rm L}\, e^{iS_\Lambda(\phi_{\rm L})}, \tag{1.50}$$

where

$$e^{iS_\Lambda(\phi_{\rm L})} = \int \mathcal{D}\phi_{\rm H}\, e^{iS(\phi_{\rm L},\phi_{\rm H})} \tag{1.51}$$

is called the Wilsonian effective action. Note that, by construction, this action depends on the choice of the cutoff Λ. S_Λ is non-local on scales $\Delta x \sim 1/\Lambda$, because high-frequency fluctuations have been removed from the theory

3. In the final step, one can expand S_Λ in terms of local operators $\mathcal{O}_i$,

$$S_\Lambda = \int d^D x \sum_i g_i \mathcal{O}_i(x) \equiv \int d^D x\, L_{\rm eff}(x). \tag{1.52}$$

The expansion is called operator product expansion (OPE) which produces the local interactions in the effective theory. The sum runs over all local operators (allowed by the symmetries of the problem) multiplied by coupling constants g_i, which are also referred to as Wilson coefficients. The local operators are, in general, suppressed by powers of $1/M$ depending on their superficial dimension.

The effective Lagrangian is defined as $L_{\rm eff}(x) = \sum_i g_i \mathcal{O}_i(x)$. The local operators $\mathcal{O}_i$ describe the long distance physics (the physics at distance scales bigger than M^{-1}) while the coupling constants g_i incorporate the "unknown physics" in the short distance (the physics at distance scales less than M^{-1}). The process of matching the full theory to the effective theory determines the Wilson coefficients. The effective Lagrangian is written as an infinite sum; however, dimensional analysis shows that only a finite number of these terms are important in the low energy limit. Technically speaking, the low energy physics depends on the short distance theory mainly through the *relevant* and *marginal* couplings, which are not suppressed by powers of M^{-1}, and possibly through some leading *irrelevant* couplings, which are suppressed by powers of M^{-1}, if one measures small enough effects [13].

We construct an effective field theory to study the full theory in the low energy limit, nevertheless it is insightful to consider it the other way around. A crucial insight is that, presumably, no field theory we have ever encountered, and perhaps no field theory of any type, is complete up to arbitrarily high energies [13]. At best it is an EFT valid up to some cutoff "scale of ignorance," which is often a physical scale, such as the mass of a new particle, which has not yet been discovered [9].

One can separate EFTs into two types [14]:

- Those for which the underlying theory is known and the matching can be done perturbatively, such as the Fermi's effective theory (for low energy weak interactions) and the heavy quark effective theory (for mesons with one heavy quark).
- Those for which it is not possible to match, either because the underlying physics is unknown (*e.g.*, the standard model), or because matching is non-perturbative (*e.g.*, chiral perturbation theory, for which the underlying theory is just QCD, but the matching coefficients are not calculable, at least perturbatively).

1.4.2 Chiral perturbation theory

Chiral perturbation theory (ChPT) provides a systematic framework for investigating strong-interaction processes at low energies [15]. This is an effective field theory describing the eight lightest mesons in the nature and their interactions with themselves and with other hadrons. These eight pseudoscalar mesons (π^+, π^-, π^0, K^+, K^-, K^0, $\bar{K}^0$ and η) are distinguished by their relatively small masses compared to the other hadrons. It is well-known that these mesons are the pseudo-Goldstone bosons that arise from the spontaneous breaking of an approximate symmetry in QCD. Hereafter, for simplicity, we use "pions" to refer to these pseudoscalar mesons.

The first step to make an effective field theory for QCD at low-energies is to recognize that, by virtue of the confinement, the hadronic degrees of freedom appear to be the observable degrees of freedom. Then, following the spirit of effective field theories, one can consider a cutoff Λ (say $\Lambda < m_\rho = 770$ MeV) and consequently integrate out all hadronic degrees of freedom that are too heavy to be excited at energy scales $E << \Lambda$. Since we do not have the full theory in terms of the hadronic degrees of freedom to start with, the first step is just a formal step. Having all heavy degrees of freedom integrated out formally, one can construct a suitable phenomenological Lagrangian, by introducing a pion field which obeys the underlying symmetries of the theorem. This phenomenological Lagrangian is constructed based on the chiral

symmetry of QCD in massless quark limit. According to Ref. [16], such a general Lagrangian has no specific dynamical content beyond some general principles such as analyticity, unitarity, and chirality, so that when it is used to calculate pionic S-matrix elements, it yields the most general matrix elements consistent with these general principles, provided that all terms of all orders are included.

1.4.2.1 Chiral symmetry breaking

In the limit of massless quarks, the light sector of the QCD action has $\mathrm{SU(3)_L} \times \mathrm{SU(3)_R} \times \mathrm{U(1)_V}$ symmetry. It is universally believed that in a world with massless quarks the group $\mathrm{SU(3)_L} \times \mathrm{SU(3)_R} \times \mathrm{U(1)_V}$ is spontaneously broken to its subgroup $\mathrm{SU(3)_V} \times \mathrm{U(1)_V}$, for which $U_L = U_R = U_V$ [17]. Therefore, according to the Goldstone theorem, there would have to be eight Goldstone bosons, one for each of the broken operators. These bosons can be parametrized by

$$\Sigma(x) = e^{i2\Phi/f}, \quad \Phi = \phi^a T^a \,, \tag{1.53}$$

where T^a are the eight generators of the SU(3) gauge group. Under a $\mathrm{SU(3))_L} \times \mathrm{SU(3)_R}$ chiral transformation, we can require that Σ and $\Sigma^\dagger$ transform linearly as

$$\Sigma \to U_L \Sigma U_R^\dagger \,, \quad \Sigma^\dagger \to U_R \Sigma^\dagger U_L^\dagger \,. \tag{1.54}$$

But now the Goldstone bosons do not transform linearly, unless $U_L = U_R = U_V$, under which

$$\Sigma \to U_V \Sigma U_V^\dagger = e^{i2U_V \Phi U_V^\dagger / f} \,, \tag{1.55}$$

implying that $\Phi \to U_V \Phi U_V^\dagger$. Now, by choosing different values for U_V, one can identify each element of the Φ matrix with a real particle as

$$\Phi = \begin{pmatrix} \frac{\pi^0}{\sqrt{2}} + \frac{\eta}{\sqrt{6}} & \pi^+ & K^+ \\ \pi^- & -\frac{\pi^0}{\sqrt{2}} + \frac{\eta}{\sqrt{6}} & K^0 \\ K^- & \bar{K^0} & -\frac{2\eta}{\sqrt{6}} \end{pmatrix} . \tag{1.56}$$

We then proceed by building an effective Lagrangian with Σ as the building block in the massless limit.

1.4.2.2 Chiral Lagrangian

Now we can construct the effective Lagrangian to describe only the Goldstone bosons. The Lagrangian must exhibit the same approximate chiral symmetry as QCD, which means that it must be invariant under $\mathrm{SU(3)_L} \times \mathrm{SU(3)_R}$ in the limit of massless quarks. The effect of the mass matrix M, which explicitly breaks the chiral symmetry, can be included systematically, using the so-called *spurion* analysis, by adding new terms suppressed by powers of M. The spurion analysis finds the terms in the chiral Lagrangian that correspond to a given symmetry-breaking term at the QCD level, by temporarily giving a constant parameter (e.g., M) chiral transformation properties to make the term chirally invariant.

The effective Lagrangian can be organized in terms of increasing powers of momentum and mass. With a power counting motivated from physical data, the leading order chiral Lagrangian becomes

$$\begin{aligned} \mathcal{L}_{\mathrm{LO}}^{\mathrm{pion}} &= \frac{f^2}{8}\,\mathrm{Tr}(\partial_\mu \Sigma \partial^\mu \Sigma^\dagger) + \frac{B f^2}{4}\,\mathrm{Tr}(M\Sigma + M^\dagger \Sigma^\dagger) \\ &= \frac{1}{2}\,\mathrm{Tr}(\partial_\mu \Phi \partial^\mu \Phi^\dagger) + \frac{B}{2}\,\mathrm{Tr}(M\Phi^2) + \cdots , \end{aligned} \tag{1.57}$$

where f and B are two low energy constants (LEC) related to the pion decay constant and quark condensation in the chiral limit (*i.e.*, the limit of massless quarks), respectively.

Having the chiral Lagrangian at leading order, the masses of the pseudo-Goldstone bosons can be worked out at leading order

$$\begin{aligned} M_{\pi^\pm}^2 &= B(m_u + m_d), \\ M_{K^\pm}^2 &= B(m_u + m_s), \\ M_{K^0}^2 &= B(m_d + m_s), \\ M_{\pi^0}^2 &\approx B(m_u + m_d), \\ M_\eta^2 &\approx B(m_u + m_d + 4m_s)/3\,. \end{aligned} \tag{1.58}$$

We then recover the Gell-Mann-Okubo relation

$$M_\eta^2 = (2M_{K^+} + 2M_{K^0}^2 - M_\pi^2)/3, \tag{1.59}$$

which relates the mass of η to the masses of the "real" pion and kaons. The result agrees with experimental data within a few percent, which supports the validity of the chiral Lagrangian in describing the light mesons.

The effective Lagrangian can be improved by including next-to-leading order (NLO) terms and so on in a systematic way. Then, by working out the quantum loop effects one can improve the chiral results for quantities such as the masses and the decay constants of pions [15].

1.4.3 Heavy quark effective theory

Consider a $Q\bar{q}$ meson that contains a heavy quark and a light antiquark. Such a system is called a heavy-light meson in which the typical momentum transfer between the heavy and light component arising from nonperturbative QCD dynamics is of the order of $\Lambda_{\rm QCD}$ [111]. An important consequence of this fact is that the heavy quark is nearly on-shell and its momentum may be decomposed as

$$p_Q^\mu = m_Q v^\mu + k^\mu, \tag{1.60}$$

where v is the 4-velocity of the meson containing the heavy quark ($v^2 = 1$), $m_Q v^\mu$ defines the momentum of an on-shell quark, and the residual momentum $k \sim \Lambda_{\rm QCD}$. This is a double-scale problem, with physics at scales $m_Q >> \Lambda_{\rm QCD}$ and $k \sim \Lambda_{\rm QCD}$. By taking the limit of infinite heavy quark mass, in the framework of EFT, the problem reduces to a single-scale one, and also new symmetries appear.

One can divide the Dirac spinor field $Q(x)$ into two components as

$$Q(x) = e^{-im_Q v\cdot x}\left[Q_v(x) + \mathcal{Q}_v(x)\right], \tag{1.61}$$

where

$$Q_v(x) = e^{im_Q v\cdot x}\,\frac{1+\not{v}}{2}\,Q(x),\;\; \mathcal{Q}_v(x) = e^{im_Q v\cdot x}\,\frac{1-\not{v}}{2}\,Q(x)\;. \tag{1.62}$$

It is easy to see that, in the rest frame, $Q_v(x)$ and $\mathcal{Q}_v(x)$ each correspond to two independent components of the four-component $Q(x)$. Now the projection relations

$$\not{v}\,Q_v(x) = Q_v(x)\,, \qquad \not{v}\,\mathcal{Q}_v(x) = -\mathcal{Q}_v(x)\,, \tag{1.63}$$

can be used to show that

$$\begin{aligned}
\mathcal{L}_Q &= \bar{Q}\,(i\not{D} - m_Q)\,Q \\
&= \bar{Q}_v\, i\not{D} Q_v + \bar{\mathcal{Q}}_v\,(i\not{D} - 2m_Q)\,\mathcal{Q}_v + \bar{Q}_v\, i\not{D}\mathcal{Q}_v + \bar{\mathcal{Q}}_v\, i\not{D} Q_v \\
&= \bar{Q}_v\, iv\cdot D\, Q_v + \bar{\mathcal{Q}}_v\,(-iv\cdot D - 2m_Q)\,\mathcal{Q}_v + \bar{Q}_v\, i\not{D}\mathcal{Q}_v + \bar{\mathcal{Q}}_v\, i\not{D} Q_v.
\end{aligned} \tag{1.64}$$

The field Q_v describes a massless fermion, while $\mathcal{Q}_v$ describes a heavy fermion with mass $2m_Q$, and the last two terms couple these two modes. The phase factor in Eq. (1.61) implies the fields $Q_v(x)$ and $\mathcal{Q}_v(x)$ are fluctuations relative to the mass shell of the heavy quark, so they carry the residual momentum k for the system under study. One can conclude that, for a near on-shell quark field $Q(x)$, soft interactions cannot excite $\mathcal{Q}_v(x)$; consequently one can exploit the effective theory technology to integrate it out. This yields

$$\mathcal{L}_{\text{HQET}} = \bar{Q}_v \, iv \cdot D \, Q_v + \mathcal{O}(1/m_Q) \, . \tag{1.65}$$

Note that the covariant derivative contains only the soft gluon field. Hard gluons have been integrated out [9].

Considering the effective Lagrangian for n_Q heavy quarks of the theory, with the same value of the 4-velocity v, one can see that the leading term in the HQET Lagrangian exhibits a new symmetry: U($2n_Q$) spin-flavor symmetry [9]. This symmetry contains the U(n_Q) flavor symmetry and the SU(2) spin symmetry as important subgroup.

1.4.3.1 Heavy-light mesons

The heavy quark symmetry implies a degenerate multiplet of states, such as B and B^*, which have the same quark content (a light u or d quark and a heavy $\bar{b}$ quark) but different spins [111]. It is convenient to have a single object describing the entire multiplet of degenerate states. Therefore one can combine both pseudoscalar field $B(x)$ and the vector field $B^*_\mu(x)$ into a single field with desired transformation properties. The field that destroys a heavy-light meson can be written as

$$H_a = \frac{1+\not{v}}{2} \left[\gamma^\mu B^*_{a\mu} + i\gamma_5 B_a \right] , \tag{1.66}$$

where the index a refers to the light quark flavor of the meson. The field H_a will be used as a building block to construct an effective Lagrangian to describe heavy-light systems.

1.4.3.2 ChPT for heavy-light mesons

In part 1.4.2, we constructed an effective chiral Lagrangian for pseudo-scalar bosons, referred to as pions. Chiral perturbation theory can also be expanded to include the low-energy regime of interaction between pions and heavy-light systems. ChPT for heavy-light systems makes use of spontaneously broken $\text{SU(3)}_\text{L} \times \text{SU(3)}_\text{R}$ chiral symmetry on the light quarks, and spin-flavor symmetry of the heavy quarks [111]. This can be formulated in two steps: replace the full theory

with HQET for an energy cutoff equal to the mass of the heavy quark, then decrease the cutoff and develop a chiral perturbation theory for a cutoff equal to, say, the mass of ρ meson. Recall that the energy of the heavy quark is measured relative to its on-shell mass in HQET, therefore it cannot be integrated out in the second step.

The building blocks to construct and effective Lagrangian are H_a and Σ defined in Eq. (2.21) and Eq. (1.53), respectively. The pions play the role of the gauge field while H_a describes a matter field. A covariant description of the Lagrangian can be achieved by introducing

$$\mathbb{V}_\mu = \frac{i}{2}\left[\sigma^\dagger\partial_\mu\sigma + \sigma\partial_\mu\sigma^\dagger\right] , \tag{1.67}$$

$$\mathbb{A}_\mu = \frac{i}{2}\left[\sigma^\dagger\partial_\mu\sigma - \sigma\partial_\mu\sigma^\dagger\right] , \tag{1.68}$$

where $\sigma = \sqrt{\Sigma}$. The leading order effective Lagrangian is [111]

$$\mathcal{L}_{LO} = -i\,\mathrm{Tr}\big(\overline{H}_a v_\mu(\partial^\mu\delta_{ab} + i\mathbb{V}^\mu_{ba})H_b\big) + g_\pi\,\mathrm{Tr}\big(\overline{H}_a H_b\gamma_\mu\gamma_5\mathbb{A}^\mu_{ba}\big) , \tag{1.69}$$

where Tr means the complete trace over flavor and Dirac indices and g_π is a LEC, which can be fixed by using experimental data. One can proceed to construct a heavy-light current within the framework of HQET. Then, physical quantities such as decay constants and form factors can be worked out.

1.4.4 Symanzik effective theory

The LECs appearing in EFTs can be fixed by the data coming from experiments or numerical calculations. EFTs are particularly useful when there are some lattice data calculated at unphysical points, for instance, the simulations done for unphysical quark masses. These lattice data points can be used to fix the LECs. Then it is straightforward to work out the prediction of the EFTs at the physical points.

In the proceeding section we introduced lattice QCD as a way to solve QCD from first principles. However, there is an outstanding difference between lattice QCD and continuum QCD. Lattice QCD comes with a nonzero lattice spacing a, which in turn introduces an ultraviolet cutoff π/a in momentum space. Any quantity calculated on the lattice needs to be extrapolated to the continuum limit, which increases the uncertainty level. Effective field theories can be used to control the uncertainties associated with lattice calculations.

At scales below the cutoff π/a, one can construct a local (continuum-like) EFT for the lattice theory. This idea is due to Symanzik [19] and referred to as the Symanzik effective theory (SET).

The Symanzik expansion is an expansion in powers of a (or equivalently an expansion in inverse powers of π/a)

$$\mathcal{L}_{\text{SET}} = \mathcal{L}^{(4)} + a\mathcal{L}^{(5)} + a^2\mathcal{L}^{(6)} + \cdots , \tag{1.70}$$

where $\mathcal{L}^{(4)}$ is the continuum QCD Lagrangian and $\mathcal{L}^{(n)}$ contains all acceptable terms with dimension n. The acceptable terms are those which are not banned by the lattice symmetries. SET provides simple semi-quantitative estimates of lattice-spacing effects. More interestingly, it provides strategies for eliminating them, both by parametrically reducing their size, and by giving a framework for combining results from several lattice spacings [20].

1.4.5 Staggered ChPT

Having substituted a lattice action by its SET version, one can proceed to develop new effective theories based on the symmetries present in the SET, which in turn come from the symmetries in the lattice action. Here our focus is on the staggered implementation of quarks on the lattice, where the corresponding Symanzik expansion does not have any dimension five operators that respect all the symmetries of the lattice action [17, 21]. Therefore the nonzero lattice spacing effects appear at $\mathcal{O}(a^2)$. Recall that the staggered action, defined in Eq. (1.35), in the continuum limit has four degenerate tastes, with exact SU(4) symmetry in taste space for each flavor of quark. Therefore, the leading order term in SET, $\mathcal{L}^{(4)}$ in Eq. (1.70), must respect the SU(4) taste symmetry. But, the next-to-leading order terms in SET, which are at $\mathcal{O}(a^2)$, break the taste symmetry of staggered quarks as well as the approximate chiral symmetry of staggered light quarks.

Now we want to argue how one can develop a generalized version of ChPT to describe the staggered meson systems. In principle, this should be done order by order in SET. We do not face any problem at leading order because $\mathcal{L}^{(4)}$ is just the continuum QCD Lagrangian; therefore the corresponding ChPT is the ChPT of the continuum theory, up to an exact SU(4) symmetry in taste space. As it pointed out above, the terms appearing at $\mathcal{O}(a^2)$ explicitly break the taste symmetry of staggered quarks as well as the approximate chiral symmetry of staggered light quarks. It was a remarkable observation that the terms at $\mathcal{O}(a^2)$ can be taken into account using the same technique that we used to import contributions of the nonzero quark masses into ChPT, *i.e.*, the spurion analysis. The resulting theory is, generally, called staggered chiral perturbation theory (SχPT). This theory studies the low-energy dynamics of light staggered mesons with different flavors and tastes. Lee and Sharpe [22], first developed SχPT for the one-flavor case, and then Aubin and Bernard [23, 24] generalized it to the multi-flavor case.

When the fourth-root procedure is taken into account, the corresponding theory is called rooted staggered chiral perturbation theory (rSχPT).

In the SET, the terms appearing at $\mathcal{O}(a^2)$ are dimension six operators, which are described by four-quark operators

$$a^2\mathcal{O}^{ll}_{ss'tt'} = c_1 a^2\ \overline{q}_l(\gamma_s\otimes\xi_t)q_l\ \overline{q}_{l'}(\gamma_{s'}\otimes\xi_{t'})q_{l'}\ , \tag{1.71}$$

$$a^2\mathcal{O}^{lh}_{ss'tt'} = c_2 a^2\ \overline{q}_l(\gamma_s\otimes\xi_t)q_l\ \overline{q}_{h}(\gamma_{s'}\otimes\xi_{t'})q_{h}\ , \tag{1.72}$$

$$a^2\mathcal{O}^{hh}_{ss'tt'} = c_3 a^2\ \overline{q}_h(\gamma_s\otimes\xi_t)q_h\ \overline{q}_{h'}(\gamma_{s'}\otimes\xi_{t'})q_{h'}\ , \tag{1.73}$$

where l and h refer to light and heavy quarks, respectively; s, s' label spins; and t, t' label tastes. The light quark labels l and l' are summed over. In this subsection, our focus is on the light mesons, so we assume that the heavy quarks will be integrated out at some point. The staggered symmetries impose some constraints that restricts the possible operators (see Ref. [8] for a pedagogical review).

As pointed out before, the staggered quarks have an exact SU(4) taste symmetry in the continuum limit. For N_l light flavors of unrooted staggered fermions, in the combined chiral-continuum limit, the theory is invariant under a $\mathrm{SU}(4N_l)_L\times\mathrm{SU}(4N_l)_R\times\mathrm{U}(1)_V$ symmetry. It is assumed that this symmetry is spontaneously broken to the subgroup $\mathrm{SU}(4N_l)_V\times\mathrm{U}(1)_V$, similar to the QCD case. Consequently, there are $(4N_l)^2-1$ massless Goldstone bosons, which can be parametrized by

$$\Sigma(x) = e^{i\Phi/f}, \tag{1.74}$$

where the field Φ is a traceless $4N_l\times 4N_l$ matrix. The field Φ can be parametrized as

$$\Phi = \begin{pmatrix} U & \pi^+ & K^+ & \cdots \\ \pi^- & D & K^0 & \cdots \\ K^- & \bar{K^0} & S & \cdots \\ \vdots & \vdots & \vdots & \ddots \end{pmatrix}, \tag{1.75}$$

where each element of Φ has a 4×4 submatrix structure in taste space as $U=\sum_{\Xi=1}^{16}U_\Xi T_\Xi$, and so forth. Here, T_Ξ are the Hermitian SU(4) taste generators given by

$$T_\Xi = \{\xi_5, i\xi_{\mu 5}, i\xi_{\mu\nu}, \xi_\mu, \xi_I\}\ , \tag{1.76}$$

where the ξ matrices correspond to the γ matrices in taste space.

In addition to the mass term of the fermions, the $\mathcal{O}(a^2)$ terms in SET explicitly break the chiral symmetry. These effects can be incorporated systematically in the theory by using the spurion analysis. With current lattices, the $\mathcal{O}(a^2)$ contributions to the pions masses might be numerically as big as the contributions of the mass matrix of the light quarks. Therefore $\mathcal{O}(a^2)$ corrections to the chiral Lagrangian must be considered as leading order (LO). The complete LO chiral Lagrangian, in Euclidean space-time, is [8, 23]

$$\mathcal{L} = \frac{f^2}{8}\,\mathrm{Tr}(\partial_\mu \Sigma \partial_\mu \Sigma^\dagger) - \frac{1}{4} B f^2\,\mathrm{Tr}(M\Sigma + M\Sigma^\dagger) + \frac{m_0^2}{24}(\mathrm{Tr}(\Phi))^2 + a^2\mathcal{V}\ , \tag{1.77}$$

where the taste-violating potential $\mathcal{V}$ is given by

$$\begin{aligned} -\mathcal{V} \;=\;& C_1\,\mathrm{Tr}(\xi_5^{(N_l)}\Sigma\xi_5^{(N_l)}\Sigma^\dagger) + \frac{C_3}{2}[\mathrm{Tr}(\xi_\nu^{(N_l)}\Sigma\xi_\nu^{(N_l)}\Sigma) + h.c.] \\ &+\frac{C_4}{2}[\mathrm{Tr}(\xi_{\nu 5}^{(N_l)}\Sigma\xi_{5\nu}^{(N_l)}\Sigma) + h.c.] + \frac{C_6}{2}\;\mathrm{Tr}(\xi_{\mu\nu}^{(N_l)}\Sigma\xi_{\nu\mu}^{(N_l)}\Sigma^\dagger) \\ &+\frac{C_{2V}}{4}[\mathrm{Tr}(\xi_\nu^{(N_l)}\Sigma)\,\mathrm{Tr}(\xi_\nu^{(N_l)}\Sigma) + h.c.] + \frac{C_{2A}}{4}[\mathrm{Tr}(\xi_{\nu 5}^{(N_l)}\Sigma)\,\mathrm{Tr}(\xi_{5\nu}^{(N_l)}\Sigma) + h.c.] \\ &+\frac{C_{5V}}{2}[\mathrm{Tr}(\xi_\nu^{(N_l)}\Sigma)\,\mathrm{Tr}(\xi_\nu^{(N_l)}\Sigma^\dagger)] + \frac{C_{5A}}{2}[\mathrm{Tr}(\xi_{\nu 5}^{(N_l)}\Sigma)\,\mathrm{Tr}(\xi_{5\nu}^{(N_l)}\Sigma^\dagger)], \end{aligned} \tag{1.78}$$

with implicit sums over repeated indices. Here, the $4N_l \times 4N_l$ matrices $\xi_\mu^{(N_l)}$ are defined by

$$\left(\xi_\nu^{(N_l)}\right)_{ij} = \xi_\nu \delta_{ij}\ , \tag{1.79}$$

with i and j the $SU(N_l)$ light quark flavor indices, and ξ_ν a 4×4 taste matrix, as in Eq. (1.76). The matrices $\xi_{\mu\nu}^{(n)}$ and $\xi_{\nu 5}^{(n)}$ are defined similarly. In Eq. (1.77), the m_0^2 term suppresses the contribution of $\mathrm{Tr}(\Phi)$ when $m_0 \to \infty$. This is an alternative way to incorporate the chiral anomaly into the theory instead of a traceless parametrization of the Φ field.

Having SχPT one can calculate the $\mathcal{O}(a^2)$ effects on physical quantities such as pion masses and decay constants. This theory provides a framework to combine the lattice results for various lattice spacings and quark masses and fit them together and extract the desired quantities in the continuum limit with tuned quark masses.

1.4.6 Staggered ChPT for heavy-light mesons

Similar to staggered ChPT for light mesons, one can proceed to develop a staggered version of HQET and ChPT for heavy-light systems. Reference [25] works out a staggered version of ChPT for heavy-light mesons with staggered light quark but non-staggered heavy quarks. The main achievement of the first part of this dissertation is to develop SχPT for all-staggered

heavy-light systems. This theory is presented in chapter 2. This effective chiral theory is used to study the pattern of taste splitting in masses of the mesons that are calculated from the lattice configurations generated by the MILC collaboration. The main objective of developing SχPT is to obtain a chiral formula for the decay constants of the heavy-light mesons with staggered quarks. The chiral formula, presented in chapter 2, provides a suitable fit form to combine and analyze a large number of decay constants of heavy-light mesons computed from different lattice ensembles with various choices of input parameters. Chapter 3 presents a comprehensive chiral fit to the lattice data for D mesons computed by the MILC collaboration.

2

Chiral Perturbation Theory for All-Staggered Heavy-Light Mesons

This chapter contains the materials published in a paper with the same title.[1] *This represents work performed by me under the overall supervision of my advisor, C. Bernard.*

2.1 Introduction

Heavy-light meson systems provide some of the best ways to test the standard model and look for signs of new physics. In particular, the constraints on the sides of the unitarity triangle, which come mainly from heavy-light decays and mixings, are limited largely by the size of the theoretical errors in the values of the hadronic matrix elements of weak operators. Lattice QCD provides a means of carrying out non-perturbative calculations of such quantities from first principles and with controlled errors.

In setting up a lattice QCD calculation, a key choice is the form of the lattice action for the quarks. Staggered fermions [2–4] are an efficient approach to simulating light quarks. The "highly improved staggered quark" (HISQ) action [32] makes it possible to treat charm quarks with the same action as the light quarks. Thus "all-staggered" simulations of D and D_s mesons are now possible [33, 34], and even B_s mesons have been treated in this way by pushing up the heavy quark mass on ensembles with the finest available lattice spacings [35].

There are several advantages to this all-staggered approach. Since heavy and light quarks have the same action, there are partially conserved heavy-light axial and vector currents that

[1] C. Bernard and J. Komijani, "Chiral Perturbation Theory for All-Staggered Heavy-Light Mesons," Phys. Rev. D 88, 094017 (2013) [arXiv:1309.4533].

need no renormalization. The tuning of the heavy quark mass is also simplified compared to other approaches (see, for example, Ref. [36]) because difference between "rest" and "kinetic" masses of the heavy quark due to discretization effects may be neglected. Further, the statistical errors of heavy-light pseudoscalars tend to be rather small, as they are for light-light staggered pseudoscalars.

Lattice computations often involve an extrapolation in light quark masses to the physical up and down masses, and always require a continuum extrapolation in lattice spacing. A version of chiral perturbation theory (χPT) that includes the effects of the discretization errors can help to control these extrapolations. Here, we develop chiral perturbation theory for all-staggered heavy-light mesons. We call the theory *heavy-meson, rooted, all-staggered chiral perturbation theory* (HMrASχPT), where "rooted" refers to the fourth root of the staggered determinant, as reviewed below.

Staggered quarks have a four-fold degree of freedom, called taste, which is a remnant of lattice doubling. In the continuum limit, there is an exact $SU(4)$ symmetry acting on tastes; this symmetry is broken at $\mathcal{O}(a^2)$ in the lattice spacing a. The corresponding discretization errors in the light-light sector split the masses of mesons with different tastes, which may be understood using staggered chiral perturbation theory (SχPT) [37, 38]. For typical values of a^2, the taste splittings of light pseudoscalar mesons can be comparable to the masses themselves. In short-hand, we say $a^2 \sim m_\pi^2$, where factors of Λ_{QCD} to balance the dimensions are always assumed in such relations. These taste splittings must therefore be included in the leading order (LO) light-light Lagrangian.

For heavy-light mesons composed of staggered quarks, the situation is different. The LO Lagrangian in the continuum is of $\mathcal{O}(k)$, where k is the residual momentum of the heavy-light meson. We assume $k \sim m_\pi$. Since $a^2 \sim m_\pi^2 \sim k^2$, taste violations are of higher order and will be treated as next-to-leading order (NLO) corrections. The LO heavy-light Lagrangian is then taste invariant. This power counting is consistent with HISQ simulations, where the splittings in *squared* meson masses remain roughly constant as the valence quark mass increases from the light quark regime to the charm regime [39]. Therefore the splittings for the masses themselves are much smaller for heavy-light mesons than for light mesons. For example, the taste splitting at $a \approx 0.12$ fm between the root-mean-squared (RMS) D_s meson and the lightest D_s meson is only about 11 MeV [39], while it is about 110 MeV for the pion.

Reference [25] works out a closely related chiral theory for heavy-light mesons with staggered light quarks but non-staggered heavy quarks (for example, Fermilab [40] or NRQCD [41] quarks). That chiral theory has been called *heavy-meson, rooted staggered chiral perturbation*

theory (HMrSχPT). In HMrSχPT, heavy-light mesons have a single taste degree of freedom associated with the light quark. As in the current case, the LO HMrSχPT Lagrangian in the heavy-light sector is taste invariant.[2] Since the LO Lagrangian determines the propagators and vertices of the one-loop diagrams, those diagrams are very closely related in HMrSχPT and HMrASχPT (the current case). Important differences arise at NLO, however. Such differences affect, for example, the analytic terms that are added on to the one-loop chiral logarithms to give the complete NLO expressions for quantities such as the decay constants. Similarly, mass splittings for heavy-light mesons of different tastes are governed by the analytic NLO terms. Indeed, we prove below that the one-loop diagrams themselves do not give rise to any taste violations in the heavy-light meson masses, despite the fact the light-light masses, which enter those diagrams, do violate taste symmetry. This feature arises from the combination of exact heavy-quark taste symmetry at LO and the all-orders discrete taste symmetry coming from shift invariance.

Thus we need to extend the program developed in Ref. [25] to include staggered heavy quarks with a taste degree of freedom. In this chapter we assume that the staggered action used (*e.g.*, HISQ) is improved sufficiently that we can treat the heavy quark as "continuum-like," with small corrections from cutoff effects. We refer to this assumption in short-hand as taking $am_Q \ll 1$, where m_Q is mass of the heavy quark, although one should keep in mind that corrections in powers of am_Q may in practice be reduced as much or more by the improved action than by the size of am_Q *per se*. Under this assumption, we can use the Symanzik Effective Theory (SET) [44] to describe the discretization effects on the heavy quarks, as well as on the light quarks. The SET is the effective theory for physical momenta p small compared with the cutoff ($ap \ll 1$); it encodes discretization effects in higher-dimensional operators added to continuum QCD.

When the heavy quark is non-staggered, as in HMrSχPT, the heavy-quark doubler states are split from the heavy quark by an amount of order of the cutoff, and are therefore integrated out of the SET. Thus the heavy quark fields have no degree of freedom corresponding to taste, and taste violations at $\mathcal{O}(a^2)$ appear only in four-quark operators composed exclusively of light quarks.

In the all-staggered case, on the other hand, important taste violations at $\mathcal{O}(a^2)$ appear in "mixed" four-quark operators consisting of the product of a heavy quark bilinear and a light quark bilinear, as well as in the product of two light-quark bilinears. These operators break the taste symmetries of both heavy and light quarks. (Products of two heavy-quark bilinears also

[2] There is in fact is no mass splitting of different tastes of heavy-light mesons at any order in HMrSχPT. The absence of splittings is guaranteed by shift symmetry [42, 43], which in the continuum limit is simply a discrete subgroup of continuum $SU(4)$ taste symmetry.

appear in the SET, but their effect on the heavy-light meson Lagrangian is rather trivial since there is at most one heavy quark in all initial and final states considered.)

In the SET, the lattice theory has been replaced by a continuum theory. The lattice spacing a appears only as a parameter multiplying higher-dimensional operators. One can then use the fact that m_Q is large compared to Λ_{QCD}, to organize heavy quark effects with Heavy Quark Effective Theory (HQET). The heavy quark field q_h in both dimension-four and higher-dimension operators is replaced by a HQET field Q, where Q satisfies

$$\frac{1+\not{v}}{2}\, Q = Q \ , \tag{2.1}$$

with v_μ the heavy-quark four-velocity. The dimension-four terms are invariant under heavy-quark spin symmetry, but the higher dimensional terms may violate the symmetry.

Finally, when residual momenta and light quark masses are small compared to the chiral scale $\Lambda_\chi \sim 1$ GeV, the physics of light-light and heavy-light mesons may be described by a chiral effective theory. The dimension-four operators give a standard-looking heavy-meson chiral theory, but with additional taste degrees of freedom for both light and heavy quarks. The higher-dimensional operators may be mapped to the chiral Lagrangian using a spurion analysis. They generate LO terms in the light-light sector that violate light-quark taste symmetry, and NLO terms in the heavy-light sector that violate heavy-quark taste and spin symmetry.

Since the four taste degrees of freedom of a staggered quark are unphysical, the fermion determinant is replaced by its fourth root in simulations. This rooting procedure introduces non-locality: At non-zero lattice spacing, the rooted fermion action is not equivalent to any local action [45], which in turn leads to nonlocal violations of unitarity [45, 46]. In the continuum limit, locality and unitarity are however expected to be restored, an expectation which is supported theoretical arguments [43, 47–49], as well as other analytical and numerical evidence [8, 50–53].

In the chiral theory, rooting is taken into account by multiplying each sea quark loop by a factor of 1/4 [23, 24]. This can be accomplished either by following the quark flow [54] to locate the loops, or — more systematically — by replicating the sea quarks n_r, performing a standard chiral calculation, and taking $n_r = 1/4$ in the result[43, 49]. Here, we follow Ref. [25] and use the quark flow approach.

After the chiral theory is constructed, we first apply it to calculate the taste splittings of heavy-light meson masses at next-to-leading chiral order. Some of the analytic NLO terms break the taste-$SU(4)$ symmetry of the masses down to $SO(4)$ symmetry [37], while others break the

symmetry still further, producing splitting within $SO(4)$ multiplets. Our results can be used to understand the measured lattice splittings [39].

We then calculate the leptonic decay constant of a heavy-light meson at one-loop. The chiral form we obtain is very useful in the analysis of HISQ data for f_{D^+} and f_{D_s} [55]. In general, we work to LO in $1/m_Q$, but some higher order terms (heavy-light hyperfine and flavor splittings) are considered in the decay constant calculation. Following Ref. [56], we argue that the inclusion of those terms (but no other $1/m_Q$ terms) constitutes a systematic approximation in the power counting introduced by Boyd and Grinstein [102].

As is clear from the above, many features of the analysis of Ref. [25] can be used here with only small changes. However, in reexamining the NLO terms in the Lagrangian and current of Ref. [25] for use here, we have discovered some minor mistakes: There are a few terms at NLO that were omitted, and a few of the terms listed in the earlier chapter can be shown either to be absent or to be redundant with terms already present. This occurs only for the complicated terms that violate both (Euclidean) rotation symmetry and taste symmetry. The errors have no consequences for applications of HMrSχPT in the literature.

The remainder of this chapter is organized as follows: In Sec. 2.2, the LO SχPT Lagrangian is constructed for all-staggered heavy-light mesons, and those NLO terms that are the same as in the continuum are briefly discussed. The $\mathcal{O}(a^2)$ terms involving heavy-light mesons are then derived from a spurion analysis in Sec. 2.3, with a needed reduction of a three-index Lorentz tensor into irreducible representations relegated to Appendix C. Section 2.4 focuses on taste splittings of heavy-light mesons. Finally, in Sec. 2.5, the decay constant in heavy-light systems is calculated to NLO. Our conclusions and some discussion of the results follow in Sec. 2.6.

2.2 The staggered chiral Lagrangian with heavy-light mesons

In this section, we first introduce our chiral power counting and give our notation for the various contributions that appear at both LO and NLO. We then consider the LO Lagrangian for both the light mesons and heavy-light mesons. The heavy-light meson field is generalized from that in Ref. [25] so that it carries a heavy-quark taste index, in addition to light-quark taste and flavor — or, equivalently, so that it carries meson taste and light-quark flavor indices. The NLO terms that are invariant under taste symmetry are the same as in the continuum, and are briefly treated in Sec. 2.2.3.

2.2.1 Power counting

We assume the power counting $p_\pi^2 \sim m_\pi^2 \sim m_q \sim a^2$ for the light mesons ("pions") as in Ref. [25]. Here p_π is a typical pion momentum, and factors of Λ_{QCD} are implicit. Two additional scales enter with the inclusion of heavy-light mesons. The first is the residual momentum of the heavy-light meson, k, which we take to be of the same order as p_π. The second scale is the heavy quark mass m_Q. Initially, we keep only the leading order in $1/m_Q$ in the following calculations and derive the decay constant of D at that order. We then follow Ref. [56] to include hyperfine splittings (e.g., $m_D^* - m_D$) and flavor splittings (e.g., $m_{D_s} - m_D$) in the NLO decay constant calculation. These splittings are $\sim$100 MeV, and so not much smaller than m_π, despite the fact that they are formally of order $1/m_Q$. Including the splittings can therefore be important in practical applications of our results, especially since HISQ simulations at physical pion mass are now available [39]. Furthermore it is consistent to include the splittings at NLO in the power counting of Refs. [56, 102],

The LO chiral Lagrangian is therefore $\mathcal{O}(k \sim \sqrt{m_q})$ in the heavy-meson fields and $\mathcal{O}(m_q, a^2)$ in the light-meson fields. (As usual in HQET, terms of $\mathcal{O}(k^0)$ in the heavy-meson fields, *i.e.*, heavy mass terms, are removed by construction.) Since each loop will bring in two powers of p_π or equivalent scales, we consider terms both of order k^2 and of order k^3 in the heavy mesons to be NLO, and similarly next-to-next-to-leading order (NNLO) would include heavy-meson terms of order k^4 and k^5. For our purposes here, we need the complete LO Lagrangian (for both heavy and light mesons), but only the heavy-meson part of the NLO Lagrangian. We therefore write

$$\mathcal{L} = \mathcal{L}_{\rm LO} + \mathcal{L}_{\rm NLO} \,, \tag{2.2}$$

$$\mathcal{L}_{\rm LO} = \mathcal{L}_{\rm LO}^{\rm pion} + \mathcal{L}_1 \,, \tag{2.3}$$

$$\mathcal{L}_{\rm NLO} = \mathcal{L}_2 + \mathcal{L}_3 \tag{2.4}$$

where $\mathcal{L}_{\rm LO}^{\rm pion}$ is the standard LO light meson Lagrangian [38], and $\mathcal{L}_1$, $\mathcal{L}_2$, and $\mathcal{L}_3$ denote the heavy-meson terms of order k^1, k^2 and k^3 (or equivalent scales), respectively.

We will also need $j^{\mu,i\Xi}$, the left-handed heavy-light current for light flavor i and combined taste Ξ. It has the similar expansion

$$j^{\mu,i\Xi} = j_{\rm LO}^{\mu,i\Xi} + j_{\rm NLO}^{\mu,i\Xi} \,, \tag{2.5}$$

$$j_{\rm NLO}^{\mu,i\Xi} = j_1^{\mu,i\Xi} + j_2^{\mu,i\Xi} \,, \tag{2.6}$$

where again the subscripts 1 and 2 denote orders in k.

We can classify contributions to the NLO terms in Eqs. (2.4) and (2.6) by the source of the extra powers of the scale and the nature of any symmetry breaking. The subscript k will denote terms in which the powers come exclusively from additional derivatives as compared to the LO terms, while the subscripts m and a^2 will indicate insertions of mass or taste-violating spurions, respectively (together with possible additional derivatives). The taste-violating terms may be further classified according to whether continuum Euclidean $SO(4)$ rotation symmetry is preserved or broken ("type A" or "type B," respectively), and whether the heavy-quark taste symmetry is preserved or broken ("type 1" or "type 2", respectively). As first pointed out in Ref. [37], type A terms also preserve a $SO(4)$ taste symmetry of the light quarks, and that feature remains true here. Our classification then gives

$$\mathcal{L}_2 = \mathcal{L}_{2,k} + \mathcal{L}_{2,m} + \mathcal{L}^{A1}_{2,a^2} + \mathcal{L}^{B1}_{2,a^2} + \mathcal{L}^{A2}_{2,a^2} + \mathcal{L}^{B2}_{2,a^2} \,, \tag{2.7}$$

$$\mathcal{L}_3 = \mathcal{L}_{3,k} + \mathcal{L}_{3,m} + \mathcal{L}^{A1}_{3,a^2} + \mathcal{L}^{B1}_{3,a^2} + \mathcal{L}^{A2}_{3,a^2} + \mathcal{L}^{B2}_{3,a^2} \,, \tag{2.8}$$

$$j_1^{\mu,i\Xi} = j_{1,k}^{\mu,i\Xi} \,, \tag{2.9}$$

$$j_2^{\mu,i\Xi} = j_{2,k}^{\mu,i\Xi} + j_{2,m}^{\mu,i\Xi} + j_{2,a^2,A1}^{\mu,i\Xi} + j_{2,a^2,B1}^{\mu,i\Xi} + j_{2,a^2,A2}^{\mu,i\Xi} + j_{2,a^2,B2}^{\mu,i\Xi} \,, \tag{2.10}$$

where $j_1^{\mu,i\Xi}$ comes solely from derivative terms, since mass and taste spurions bring in two powers of the small scale.

After introducing our (mainly standard) notation, we give the LO terms $\mathcal{L}_{\rm LO}^{\rm pion}$, $\mathcal{L}_1$, and $j_{\rm LO}^{\mu,i\Xi}$ in the next subsection. NLO terms that are the same as in the continuum, namely $\mathcal{L}_{2,k}$, $\mathcal{L}_{3,k}$, $\mathcal{L}_{2,m}$, $\mathcal{L}_{3,m}$, $j_1^{\mu,i\Xi}$, $j_{2,k}^{\mu,i\Xi}$, and $j_{2,m}^{\mu,i\Xi}$ are then briefly discussed in Sec. 2.2.3. Study of the taste-violating terms, which require a detailed look at the SET, are postponed until Sec. 2.3. Those terms that preserve heavy-quark taste symmetry, namely type A1 and B1 terms, are trivial generalizations of the corresponding terms in [25]. Those that break heavy-quark taste symmetry, namely type A2 and B2, are however completely new.

2.2.2 Leading-order theory

The LO chiral Lagrangian is divided into the light meson part $\mathcal{L}_{\rm LO}^{\rm pion}$ and the heavy meson part $\mathcal{L}_1$, as in Eq. (2.3). The light meson part is standard [38]. However, following Ref. [25], we write the complete Lagrangian in Minkowski space for ease of comparison with the continuum heavy-light literature. If desired, a Wick rotation can be defined everywhere to transform the theory into Euclidean space, corresponding to the Euclidean lattice theory. We have

$$\mathcal{L}_{\rm LO}^{\rm pion} = \frac{f^2}{8}\,\mathrm{Tr}(\partial_\mu\Sigma\partial^\mu\Sigma^\dagger) + \frac{1}{4}\mu f^2\,\mathrm{Tr}(\mathcal{M}\Sigma + \mathcal{M}\Sigma^\dagger) - \frac{2m_0^2}{3}(U_I + D_I + S_I + \ldots)^2 - a^2\mathcal{V}_\Sigma, \tag{2.11}$$

where $\Sigma = \exp[i\Phi/f]$ is a $4n \times 4n$ matrix for n staggered flavors, with Φ given by:

$$\Phi = \begin{pmatrix} U & \pi^+ & K^+ & \cdots \\ \pi^- & D & K^0 & \cdots \\ K^- & \bar{K^0} & S & \cdots \\ \vdots & \vdots & \vdots & \ddots \end{pmatrix} . \tag{2.12}$$

Here $U = \sum_{\Xi=1}^{16} U_\Xi T_\Xi$, *etc.*, with the Hermitian taste generators T_Ξ given by

$$T_\Xi = \{\xi_5, i\xi_{\mu 5}, i\xi_{\mu\nu}, \xi_\mu, \xi_I\} \ . \tag{2.13}$$

As in Ref. [25], we employ Euclidean gamma matrices for ξ_μ, with $\xi_{\mu\nu} \equiv (1/2)[\xi_\mu, \xi_\nu]$ ($\mu < \nu$ in Eq. (2.13)), $\xi_{\mu 5} \equiv \xi_\mu \xi_5$, and $\xi_I \equiv I$, where I is the 4×4 identity matrix. Below, we use a summation convention for indices on the matrices ξ_μ that are repeated twice, but explicit summation for indices that are repeated more than twice. The mass matrix is given by the $4n \times 4n$ matrix

$$\mathcal{M} = \begin{pmatrix} m_u I & 0 & 0 & \cdots \\ 0 & m_d I & 0 & \cdots \\ 0 & 0 & m_s I & \cdots \\ \vdots & \vdots & \vdots & \ddots \end{pmatrix} . \tag{2.14}$$

The potential $\mathcal{V}_\Sigma$, which breaks the taste symmetry of light mesons, is defined in Refs. [25, 38]:

$$\begin{aligned} -\mathcal{V}_\Sigma \ = \ & C_1 \, \mathrm{Tr}(\xi_5^{(n)} \Sigma \xi_5^{(n)} \Sigma^\dagger) + \frac{C_3}{2} [\mathrm{Tr}(\xi_\nu^{(n)} \Sigma \xi_\nu^{(n)} \Sigma) + h.c.] \\ & + \frac{C_4}{2} [\mathrm{Tr}(\xi_{\nu 5}^{(n)} \Sigma \xi_{5\nu}^{(n)} \Sigma) + h.c.] + \frac{C_6}{2} \ \mathrm{Tr}(\xi_{\mu\nu}^{(n)} \Sigma \xi_{\nu\mu}^{(n)} \Sigma^\dagger) \\ & + \frac{C_{2V}}{4} [\mathrm{Tr}(\xi_\nu^{(n)} \Sigma) \, \mathrm{Tr}(\xi_\nu^{(n)} \Sigma) + h.c.] + \frac{C_{2A}}{4} [\mathrm{Tr}(\xi_{\nu 5}^{(n)} \Sigma) \, \mathrm{Tr}(\xi_{5\nu}^{(n)} \Sigma) + h.c.] \\ & + \frac{C_{5V}}{2} [\mathrm{Tr}(\xi_\nu^{(n)} \Sigma) \, \mathrm{Tr}(\xi_\nu^{(n)} \Sigma^\dagger)] + \frac{C_{5A}}{2} [\mathrm{Tr}(\xi_{\nu 5}^{(n)} \Sigma) \, \mathrm{Tr}(\xi_{5\nu}^{(n)} \Sigma^\dagger)] \ . \end{aligned} \tag{2.15}$$

The explicit $4n \times 4n$ matrices $\xi_\mu^{(n)}$ in Eq. (2.15) are defined by

$$\left(\xi_\nu^{(n)}\right)_{ij} = \xi_\nu \delta_{ij} \ , \tag{2.16}$$

with i and j the $SU(n)$ light quark flavor indices, and ξ_ν a 4×4 taste matrix, as in Eq. (2.13). The matrices $\xi_{\mu\nu}^{(n)}$ and $\xi_{\nu 5}^{(n)}$ are defined similarly.

In terms involving heavy-lights, we also need $\sigma \equiv \sqrt{\Sigma} = \exp[i\Phi/2f]$. Both Σ and σ are singlets under the heavy-quark symmetries, while under $SU(4n)_L \times SU(4n)_R$ they transform as

$$\Sigma \to L\Sigma R^\dagger\,, \qquad \Sigma^\dagger \to R\Sigma^\dagger L^\dagger\,, \tag{2.17}$$

$$\sigma \to L\sigma\mathbb{U}^\dagger = \mathbb{U}\sigma R^\dagger\,, \qquad \sigma^\dagger \to R\sigma^\dagger\mathbb{U}^\dagger = \mathbb{U}\sigma^\dagger L^\dagger\,, \tag{2.18}$$

where $L \in SU(4n)_L$, $R \in SU(4n)_R$, and $\mathbb{U}$ is a function of L and R and the pion fields. In the construction of invariant Lagrangian terms it is convenient to define objects involving the σ field that transform only with $\mathbb{U}$ and $\mathbb{U}^\dagger$. The two possibilities with a single derivative are

$$\mathbb{V}_\mu = \frac{i}{2}\left[\sigma^\dagger\partial_\mu\sigma + \sigma\partial_\mu\sigma^\dagger\right]\,, \tag{2.19}$$

$$\mathbb{A}_\mu = \frac{i}{2}\left[\sigma^\dagger\partial_\mu\sigma - \sigma\partial_\mu\sigma^\dagger\right]\,. \tag{2.20}$$

The field that destroys a heavy-light meson can be written as

$$H_{\alpha a} = \frac{1+\not{v}}{2}\left[\gamma^\mu B^*_{\mu\alpha a} + i\gamma_5 B_{\alpha a}\right]\,, \tag{2.21}$$

where v is the meson's velocity, a is the combined flavor-taste index of the light quark, and α is the heavy-quark taste index. To avoid confusion with the covariant derivative $\overrightarrow{D}_\mu$ introduced below, we will use B for now to denote a generic pseudoscalar heavy-light meson and B^* to denote the corresponding vector meson (with $v^\mu B^*_{\mu\alpha a} = 0$), even though the focus of current all-staggered simulations is primarily on the D meson system rather than B meson system. The formalism developed in this chapter applies to both, although $1/m_Q$ corrections are of course larger for D's. The conjugate field that creates a heavy-light meson is

$$\overline{H}_{a\alpha} \equiv \gamma_0 H^\dagger_{a\alpha}\gamma_0 = \left[\gamma^\mu B^{\dagger *}_{\mu a\alpha} + i\gamma_5 B^\dagger_{a\alpha}\right]\frac{1+\not{v}}{2}\,. \tag{2.22}$$

Under the $SU(2)$ heavy-quark spin symmetry, the heavy-light field transforms as

$$\begin{aligned} H &\to SH\,, \\ \overline{H} &\to \overline{H}S^\dagger\,, \end{aligned} \tag{2.23}$$

with $S \in SU(2)$ acting on Dirac index of the heavy-light field. Transformations under the chiral $SU(4n)_L \times SU(4n)_R$ symmetry of the light quarks take the form

$$\begin{aligned} H &\to H\mathbb{U}^\dagger \,, \\ \overline{H} &\to \mathbb{U}\overline{H} \,, \end{aligned} \tag{2.24}$$

with $\mathbb{U} \in SU(4n)$ acting on the combined flavor-taste index a in Eqs. (2.21) and (2.22). Heavy quarks of course do not have a chiral symmetry, but they do have a vector $SU(4)$ taste symmetry (exact in the continuum limit), under which

$$\begin{aligned} H &\to VH \,, \\ \overline{H} &\to \overline{H}V^\dagger \,, \end{aligned} \tag{2.25}$$

with $V \in SU(4)$ acting on the heavy-quark taste index.

We introduce a (chirally) covariant derivative that acts on the heavy-light field or its conjugate as

$$\begin{aligned} (H\overleftarrow{D}_\mu)_{\alpha b} = H_{\alpha c}(\overleftarrow{D}_\mu)_{cb} &\equiv \partial_\mu H_{\alpha b} + iH_{\alpha c}(\mathbb{V}_\mu)_{cb} \,, \\ (\overrightarrow{D}_\mu\overline{H})_{b\alpha} = (\overrightarrow{D}_\mu)_{bc}\overline{H}_{c\alpha} &\equiv \partial_\mu \overline{H}_{b\alpha} - i(\mathbb{V}_\mu)_{bc}\overline{H}_{c\alpha} \,, \end{aligned} \tag{2.26}$$

with implicit sums over repeated indices.

So far H is treated as a $4 \times 4n$ matrix in the taste and the flavor space of quarks. Instead of attaching separate indices for the tastes of the light and heavy quarks of the meson, one can use a single index for the combined meson taste. The field H is then treated as an n-component vector in the flavor space of the light quark, while each element (H_i, $i = 1, \ldots, n$) is a 4×4 matrix in the taste space of the meson, and written as a linear combination of the 16 taste generators T_Ξ, Eq. (2.13). We use Latin indices in the middle of the alphabet ($i, j, ...$) as pure flavor indices, and capital Greek letters such as Ξ to indicate meson tastes. For example, the ith element of the field destroying a heavy-light meson in the light flavor space can be represented by $H_i = \sum_{\Xi=1}^{16} \frac{1}{2} T_\Xi \, H_{i\Xi}$ and its conjugate by $\overline{H}_i = \sum_{\Xi=1}^{16} \frac{1}{2} T_\Xi \, \overline{H}_{i\Xi}$, where the factors of $\frac{1}{2}$ are inserted to ensure that the fields $H_{i\Xi}$ and $\overline{H}_{i\Xi}$ are conventionally normalized.

We can now write down $\mathcal{L}_1$. As discussed in Sec. 2.2.1, lattice corrections are higher order in the heavy-light system, so at LO we just have the continuum-like Lagrangian [25, 111]

$$\mathcal{L}_1 = -i \, \mathrm{Tr}(\overline{H} H v \cdot \overleftarrow{D}) + g_\pi \, \mathrm{Tr}(\overline{H} H \gamma^\mu \gamma_5 \mathbb{A}_\mu) \,, \tag{2.27}$$

Tr means the complete trace over flavor, taste, and Dirac indices. The only difference of $\mathcal{L}_1$ from the continuum LO Lagrangian is addition of the (implicit) taste degrees of freedom of light and heavy quarks. The product $\overline{H}H$ can be treated either as a $4n \times 4n$ matrix in the flavor-taste space of the light quarks: $(\overline{H}H)_{ab} \equiv \overline{H}_{a\alpha}H_{\alpha b}$ (with an implicit sum over α), or equivalently as a $n \times n$ matrix in the flavor space of the light quarks, where each element is itself a 4×4 matrix in the taste space of the meson: $(\overline{H}H)_{ij} \equiv \frac{1}{4}\sum_{\Xi=1}^{16}\sum_{\Xi'=1}^{16}\overline{H}_{i\Xi}H_{j\Xi'}T_\Xi T_{\Xi'}$. Depending on the situation, one of the notations may be more convenient; we must however be careful to be consistent in the treatment of other objects in the same term in the Lagrangian.

For the calculation of the heavy-light decay constants in Sec. 2.5, the chiral representative of the axial heavy-light current is needed. Alternatively, one can work with the left-handed current, whose matrix element between a pseudoscalar meson and the vacuum is proportional to that of the axial current. For the current, it is simplest to treat the heavy-light field as a light-flavor vector whose elements are meson taste matrices. The left-handed current that destroys a heavy-light meson of taste Ξ and light flavor i is $j^{\mu,i\Xi}$, which at LO takes the form

$$j^{\mu,i\Xi}_{\text{LO}} = \frac{\kappa}{2}\,\text{tr}_{D,t}\big(\tfrac{1}{2}T_\Xi\gamma^\mu\,(1-\gamma_5)\,H\sigma^\dagger\lambda^{(i)}\big) \tag{2.28}$$

where κ is a low-energy constant, and $\lambda^{(i)}$ is a constant row vector that fixes the flavor of the light quark: $(\lambda^{(i)})_j = \delta_{ij}$. This expression for the current is a trivial generalization of that in Ref. [111] to include the taste degrees of freedom. It can be checked using the spurion analysis introduced in Sec. 2.3.2 to find the current at next order. The decay constant $f_{B_{i\Xi}}$ is defined by the matrix element

$$\left\langle 0\left|j^{\mu,i'\Xi'}\right|B_{i\Xi}(v)\right\rangle = if_{B_{i\Xi}}m_{B_{i\Xi}}v^\mu\delta_{\Xi\Xi'}\delta_{ii'}\ , \tag{2.29}$$

where relativistic normalization of the state $|B_{i\Xi}(v)\rangle$ is assumed. At LO in the heavy-light chiral theory, $j^{\mu,i'\Xi'}_{\text{LO}} = i\kappa v^\mu B_{i'\Xi'}$, which gives $f^{\text{LO}}_{B_{i\Xi}} = \kappa/\sqrt{m_{B_{i\Xi}}}$. Recall that the factor $\sqrt{m_{B_{i\Xi}}}$ arises from the differences in normalizations between relativistic and non-relativistic states.

2.2.3 Next-to-leading-order terms in the continuum

In the continuum, the NLO terms are of two types: those formed by only adding derivatives to LO terms ($\mathcal{L}_{2,k}$, $\mathcal{L}_{3,k}$, $j^{\mu,i\Xi}_1$, and $j^{\mu,i\Xi}_{2,k}$), and those that involve a mass spurion ($\mathcal{L}_{2,m}$, $\mathcal{L}_{3,m}$, and $j^{\mu,i\Xi}_{2,m}$). The former are not to our knowledge cataloged completely in the literature, and in any case are irrelevant to the heavy meson mass and decay constant to the order we are working: Additional derivatives acting on a heavy-light field vanish on shell ($k = 0$), while those on the light fields contribute only to tree-level diagrams with external pions. We therefore follow

Ref. [25], and simply list some representative terms in $\mathcal{L}_{2,k}$, $\mathcal{L}_{3,k}$, $j_1^{\mu,i\Xi}$, $j_{2,k}^{\mu,i\Xi}$. We have

$$\mathcal{L}_{2,k} = \frac{i\epsilon_1}{\Lambda_\chi}\,\mathrm{Tr}\left((v\cdot\overrightarrow{D}\,\overline{H}H - \overline{H}Hv\cdot\overleftarrow{D})\,\gamma_\mu\gamma_5\mathbb{A}^\mu\right) + \frac{\epsilon_2}{\Lambda_\chi}\,\mathrm{Tr}\left(\overline{H}H(v\cdot\overleftarrow{D})^2\right) + \ldots \quad (2.30)$$

$$\mathcal{L}_{3,k} = \frac{\epsilon_3}{\Lambda_\chi^2}\,\mathrm{Tr}\left(\overline{H}H\gamma_\mu\gamma_5(v\cdot\overrightarrow{D})^2\mathbb{A}^\mu\right) + \frac{\epsilon_4}{\Lambda_\chi^2}\,\mathrm{Tr}\left(\overline{H}H\overrightarrow{\not{D}}\gamma_5\, v\cdot\overrightarrow{D}\,v\cdot\mathbb{A}\right) + \ldots \quad (2.31)$$

$$j_{1,k}^{\mu,i\Xi} = \frac{i\kappa_1}{\Lambda_\chi}\,\mathrm{tr}_{D,t}\big(\tfrac{1}{2}T_\Xi\gamma^\mu\,(1-\gamma_5)\,Hv\cdot\overleftarrow{D}\,\sigma^\dagger\lambda^{(i)}\big) + \frac{\kappa_2}{\Lambda_\chi}\,\mathrm{tr}_{D,t}\big(\tfrac{1}{2}T_\Xi\gamma^\mu\,(1-\gamma_5)\,H\,v\cdot\mathbb{A}\,\sigma^\dagger\lambda^{(i)}\big) + \ldots \quad (2.32)$$

$$j_{2,k}^{\mu,i\Xi} = \frac{\kappa_3}{\Lambda_\chi^2}\,\mathrm{tr}_{D,t}\big(\tfrac{1}{2}T_\Xi\gamma^\mu\,(1-\gamma_5)\,H(v\cdot\overleftarrow{D})^2\sigma^\dagger\lambda^{(i)}\big) + \frac{i\kappa_4}{\Lambda_\chi^2}\,\mathrm{tr}_{D,t}\big(\tfrac{1}{2}T_\Xi\gamma^\mu\,(1-\gamma_5)\,H\,v\cdot\overrightarrow{D}\,v\cdot\mathbb{A}\,\sigma^\dagger\lambda^{(i)}\big) + \ldots \quad (2.33)$$

where the constants ϵ_i, κ_j are taken to be real and dimensionless, Λ_χ is the chiral scale, and

$$\overrightarrow{D}_\nu\mathbb{A}_\mu \equiv \partial_\nu\mathbb{A}_\mu - i[\mathbb{V}_\nu, \mathbb{A}_\mu]\ . \quad (2.34)$$

The only difference from Ref. [25] is a small change of notation because of the taste degree of freedom of the heavy quark: Here the current has meson taste Ξ and light flavor fixed by $\lambda^{(i)}$; whereas in Ref. [25] the current had only light-quark taste and flavor, both of which were fixed by $\lambda^{(i)}$.

The terms induced by single insertions of the light quark mass spurions also follow directly from Ref. [25]. They are:

$$\mathcal{L}_{2,m} = 2\lambda_1\,\mathrm{Tr}\left(\overline{H}H\mathcal{M}^+\right) + 2\lambda_1'\,\mathrm{Tr}\left(\overline{H}H\right)\mathrm{Tr}\left(\mathcal{M}^+\right)\ , \quad (2.35)$$

$$\begin{aligned}\mathcal{L}_{3,m} = {} & ik_1\,\mathrm{Tr}\left(\overline{H}Hv\cdot\overleftarrow{D}\,\mathcal{M}^+ - v\cdot\overrightarrow{D}\,\overline{H}H\,\mathcal{M}^+\right)\\ & + ik_2\,\mathrm{Tr}\left(\overline{H}Hv\cdot\overleftarrow{D} - v\cdot\overrightarrow{D}\,\overline{H}H\right)\mathrm{Tr}(\mathcal{M}^+)\\ & + k_3\,\mathrm{Tr}\left(\overline{H}H\gamma_\mu\gamma_5\{\mathbb{A}^\mu,\mathcal{M}^+\}\right) + k_4\,\mathrm{Tr}\left(\overline{H}H\gamma_\mu\gamma_5\mathbb{A}^\mu\right)\mathrm{Tr}(\mathcal{M}^+)\\ & + k_5\,\mathrm{Tr}\left(\overline{H}H\gamma_\mu\gamma_5\right)\mathrm{Tr}\left(\mathbb{A}^\mu\mathcal{M}^+\right) + k_6\,\mathrm{Tr}\left(\overline{H}H\gamma_\mu[\mathbb{A}^\mu,\mathcal{M}^-]\right)\ , \end{aligned} \quad (2.36)$$

$$\begin{aligned} j_{2,m}^{\mu,i\Xi} = {} & \rho_1\,\mathrm{tr}_{D,t}\left(\tfrac{1}{2}T_\Xi\gamma^\mu(1-\gamma_5)H\mathcal{M}^+\sigma^\dagger\lambda^{(i)}\right) + \rho_2\,\mathrm{tr}_{D,t}\left(\tfrac{1}{2}T_\Xi\gamma^\mu(1-\gamma_5)H\sigma^\dagger\lambda^{(i)}\right)\mathrm{Tr}(\mathcal{M}^+)\\ & + \rho_3\,\mathrm{tr}_{D,t}\left(\tfrac{1}{2}T_\Xi\gamma^\mu(1-\gamma_5)H\mathcal{M}^-\sigma^\dagger\lambda^{(i)}\right) + \rho_4\,\mathrm{tr}_{D,t}\left(\tfrac{1}{2}T_\Xi\gamma^\mu(1-\gamma_5)H\sigma^\dagger\lambda^{(i)}\right)\mathrm{Tr}(\mathcal{M}^-) \end{aligned} \quad (2.37)$$

where $\mathcal{M}^\pm = \frac{1}{2}\left(\sigma\mathcal{M}\sigma \pm \sigma^\dagger\mathcal{M}\sigma^\dagger\right)$ are the light-quark mass spurions.

2.3 Taste Symmetry Breaking

Taste violations first appear at $\mathcal{O}(a^2)$. In the SET, they are described by four-quark (dimension six) operators, which are generated by gluon exchange with total momenta $\sim\pi/a$ between two quark lines. The gluons can change the taste, spin, and color of the quark line, but not its flavor, so the operators take the form of products of two quark bilinears, where each bilinear is made of quark and antiquark fields of a single flavor. In the current case, there are three generic classes of four-quark operators: where both bilinears are of light quarks, where one bilinear is light and the other heavy, and where both bilinears heavy. We write

$$a^2\mathcal{O}^{ll}_{ss'tt'} = c_1 a^2\ \overline{q}_l(\gamma_s\otimes\xi_t)q_l\ \overline{q}_{l'}(\gamma_{s'}\otimes\xi_{t'})q_{l'}\ , \tag{2.38}$$

$$a^2\mathcal{O}^{lh}_{ss'tt'} = c_2 a^2\ \overline{q}_l(\gamma_s\otimes\xi_t)q_l\ \overline{q}_{h}(\gamma_{s'}\otimes\xi_{t'})q_{h}\ , \tag{2.39}$$

$$a^2\mathcal{O}^{hh}_{ss'tt'} = c_3 a^2\ \overline{q}_h(\gamma_s\otimes\xi_t)q_h\ \overline{q}_{h'}(\gamma_{s'}\otimes\xi_{t'})q_{h'}\ . \tag{2.40}$$

where l and h refer to light and heavy quarks, respectively; s, s' label spins; and t, t' label tastes. The light quark labels l and l' are summed over; only a single heavy quark flavor is considered. Color indices, which may be contracted in different ways, are omitted because they have no effect on the chiral operators generated. The operators in Eqs. (2.38) through (2.40) are schematic; they stand for the whole set of possible four-quark operators with the given flavor structure. Similarly, each coefficient c_i represents a set of coefficients of the operators.

The staggered symmetries impose the following constraints on the possible operators[3]

$$U(1)_\epsilon \text{ symmetry} \Rightarrow \{\gamma_5\otimes\xi_5, \gamma_s\otimes\xi_t\} = 0\ , \tag{2.41}$$

$$\text{shift symmetry} \Rightarrow \xi_t = \xi_{t'}\ , \tag{2.42}$$

$$\text{rotational and parity symmetries} \Rightarrow \gamma_t = \gamma_{t'}\ . \tag{2.43}$$

At this point the lattice spacing a has simply become a parameter in the continuum SET theory. We can therefore use the fact that the heavy quark mass m_Q is large compared to Λ_{QCD} to replace the field q_h in Eqs. (2.39) and (2.40) with the HQET field Q, Eq. (2.1). Making in addition the simplifications implied by Eqs. (2.42) and (2.43), we have

$$a^2\mathcal{O}^{ll}_{st} = c_1 a^2\ \overline{q}_l(\gamma_s\otimes\xi_t)q_l\ \overline{q}_{l'}(\gamma_s\otimes\xi_t)q_{l'}\ , \tag{2.44}$$

$$a^2\mathcal{O}^{lh}_{st} = c_2 a^2\ \overline{q}_l(\gamma_s\otimes\xi_t)q_l\ \overline{Q}(\gamma_s\otimes\xi_t)Q\ , \tag{2.45}$$

$$a^2\mathcal{O}^{hh}_{st} = c_3 a^2\ \overline{Q}(\gamma_s\otimes\xi_t)Q\ \overline{Q}(\gamma_s\otimes\xi_t)Q\ . \tag{2.46}$$

[3] See Ref. [8] for a pedagogical review; we follow it closely.

The operators can be further separated into type A and type B operators [37], which are distinguished by whether they break continuum Euclidean rotation symmetry. This breaking occurs when there are indices that are common to both the spin and taste matrices, thereby coupling spin and taste. Type-A operators are invariant under rotation symmetry, while type-B operators break it. Both types of operators break $SU(4)$ taste symmetry. Type-A operators are, however, invariant under an $SO(4)$ taste subgroup, as well as the $SO(4)$ of space-time rotations, whereas type-B operators are invariant only under combined 90° rotations of both spin and taste. There are a total of twelve type-A operators that are named by the spin $\otimes$ taste of their bilinears [37]:

$$\begin{aligned}&[S\times A],\ [S\times V],\ [A\times S],\ [V\times S],\ [P\times A],\ [P\times V],\\&[A\times P],\ [V\times P],\ [T\times V],\ [T\times A],\ [V\times T],\ [A\times T]\ .\end{aligned}\tag{2.47}$$

Each operator will also have the superscript ll, lh, or hh to denote its flavor. Thus, for example

$$[T\times A]^{lh}\equiv a^2\,\overline{q}_l(\gamma_{\mu\nu}\otimes\xi_{\lambda 5})q_l\;\overline{Q}(\gamma^{\nu\mu}\otimes\xi_{5\lambda})Q\ ,\tag{2.48}$$

where $\gamma_{\mu\nu}\equiv(1/2)[\gamma_\mu,\gamma_\nu]$, and we use Minkowski gamma matrices for convenience, corresponding to the fact that we have chosen to write the chiral Lagrangian ultimately in Minkowski space. Taste matrices remain Euclidean, as in Eq. (2.13). Summation over the twice-repeated indices μ,ν,λ is implied.

There are four type-B operators:

$$[T_\mu\times V_\mu],\ [T_\mu\times A_\mu],\ [V_\mu\times T_\mu],\ [A_\mu\times T_\mu],\tag{2.49}$$

where μ is the common index that appears four times. For example, we have

$$[A_\mu\times T_\mu]^{ll}\equiv a^2\sum_\mu\overline{q}_l(i\gamma_\mu\gamma_5\otimes i\xi_{\mu\nu})q_l\;\overline{q}_{l'}(i\gamma^\mu\gamma_5\otimes i\xi_{\mu\nu})q_{l'}\ .\tag{2.50}$$

The index ν, which appears twice, obeys the summation convention, while the sum over an index like μ, which appears four times, is shown explicitly here and below.

We now consider the chiral operators that correspond to the SET/HQET operators, Eqs. (2.44) and (2.46). The light-light operators, Eq. (2.44), are (trivially) invariant under the heavy-quark taste symmetry, while breaking the light-quark taste symmetry, leading to the NLO terms in the Lagrangian and current denoted by $\mathcal{L}^{A1}_{2,a^2}$, $\mathcal{L}^{B1}_{2,a^2}$, $\mathcal{L}^{A1}_{3,a^2}$, $\mathcal{L}^{B1}_{3,a^2}$, $j^{\mu,i\Xi}_{2,a^2,A1}$ and $j^{\mu,i\Xi}_{2,a^2,B1}$ in Eqs. (2.7) through (2.10). They are summarized in the following subsection. The light-heavy operators,

Eq. (2.45), break both the light-quark and heavy-quark taste symmetries. These operators lead to the terms denoted by $\mathcal{L}^{A2}_{2,a^2}$, $\mathcal{L}^{B2}_{2,a^2}$, $\mathcal{L}^{A2}_{3,a^2}$, $\mathcal{L}^{B2}_{3,a^2}$, $j^{\mu,i\Xi}_{2,a^2,A2}$ and $j^{\mu,i\Xi}_{2,a^2,B2}$ in Eqs. (2.7) through (2.10), and are discussed in Sec. 2.3.2. Although the heavy-heavy operators, Eq. (2.46), break the heavy taste symmetry, they do not result in any new chiral operators in the heavy-light chiral Lagrangian or current, for reasons we discuss at the end of Sec. 2.3.2.

2.3.1 Discretization errors at NLO: Light-taste breaking terms

The light-light operators in Eq. (2.44) are trivially invariant under the heavy-quark spin symmetry, in addition to the heavy-quark taste symmetry. Either symmetry alone is enough to guarantee that all corresponding Lagrangian operators are composed of the product $\overline{H}H$. This means that operators determined in Ref. [25] from the light-light four-quark operators can be taken over without change even though the heavy quarks considered there had no taste degree of freedom. Similarly, the spin symmetry alone requires that the left-handed current is constructed from the combination $\gamma^\mu(1-\gamma_5)H$, and the heavy-quark taste symmetry provides no fundamentally new information. Thus the current can also be taken over from Ref. [25], although in this case one needs the same minor notational change to accommodate the heavy-quark taste degree of freedom that we have used above in Eqs. (2.32), (2.33) and (2.37). We have also found it necessary to change a few symbols from those used in Ref. [25] in order to avoid conflict with notation in the present chapter. Moreover, we have discovered a few new terms that were missed in that reference, and have dropped a few terms that are not independent or are absent for other reasons. The changes have no effect on existing calculations in HMrSχPT: the heavy-light leptonic decay constant [25] and the semileptonic form factors for heavy-light meson decays to light [105] or heavy-light [59] mesons.

For type-A operators, the contributions to the chiral Lagrangian are

$$\mathcal{L}^{A1}_{2,a^2} = a^2 \sum_{k=1}^{8} \left\{ K^{A1}_{1,k} \,\mathrm{Tr}\left(\overline{H}H\mathcal{O}^{A1,+}_k\right) + K^{A1}_{2,k} \,\mathrm{Tr}\left(\overline{H}H\right) \mathrm{Tr}(\mathcal{O}^{A1,+}_k) \right\} \tag{2.51}$$

and

$$
\begin{aligned}
\mathcal{L}^{A1}_{3,a^2} &= a^2 \sum_{k=1}^{8} \Bigg\{ i c^{A1}_{1,k} \,\mathrm{Tr}\left(\overline{H} H v\cdot \overleftarrow{D}\, \mathcal{O}^{A1,+}_k - v\cdot \overrightarrow{D}\, \overline{H} H\, \mathcal{O}^{A1,+}_k \right) \\
&\qquad + i c^{A1}_{2,k} \,\mathrm{Tr}\left(\overline{H} H v\cdot \overleftarrow{D} - v\cdot \overrightarrow{D}\, \overline{H} H \right) \mathrm{Tr}(\mathcal{O}^{A1,+}_k) \\
&\qquad + c^{A1}_{3,k} \,\mathrm{Tr}\left(\overline{H} H \gamma_\mu \gamma_5 \{ \mathbb{A}^\mu, \mathcal{O}^{A1,+}_k \} \right) + c^{A1}_{4,k} \,\mathrm{Tr}\left(\overline{H} H \gamma_\mu \gamma_5 \mathbb{A}^\mu \right) \mathrm{Tr}(\mathcal{O}^{A1,+}_k) \\
&\qquad + c^{A1}_{5,k} \,\mathrm{Tr}\left(\overline{H} H \gamma_\mu \gamma_5 \right) \mathrm{Tr}(\mathbb{A}^\mu \mathcal{O}^{A1,+}_k) + c^{A1}_{6,k} \,\mathrm{Tr}\left(\overline{H} H \gamma_\mu [\mathbb{A}^\mu, \mathcal{O}^{A1,-}_k] \right) \\
&\qquad + c^{A1}_{7,k} \Big(\,\mathrm{Tr}\left(\overline{H} H \gamma_\mu \gamma_5 P^{A1}_k \mathbb{A}^\mu \tilde{P}^{A1}_k \right) + \text{p.c.} \Big) \\
&\qquad + c^{A1}_{8,k} \Big(\,\mathrm{Tr}\left(\overline{H} H \gamma_\mu \gamma_5 P^{A1}_k \right) \mathrm{Tr}\left(\mathbb{A}^\mu \tilde{P}^{A1}_k \right) + \text{p.c.} \Big) \Bigg\} \\
&\quad + a^2 \sum_{k=2,5,7,8} c^{A1}_{9,k} \Big(\,\mathrm{Tr}\left(\overline{H} H \gamma_\mu P^{A1}_k \mathbb{A}^\mu \tilde{P}^{A1}_k \right) + \text{p.c.} \Big) \\
&\quad + a^2 \sum_{k=1,2,6,7} c^{A1}_{10,k} \Big(\,\mathrm{Tr}\left(\overline{H} H \gamma_\mu P^{A1}_k \right) \mathrm{Tr}\left(\mathbb{A}^\mu \tilde{P}^{A1}_k \right) + \text{p.c.} \Big) \ . \qquad (2.52)
\end{aligned}
$$

where p.c. denotes the parity conjugate; for example, $\sigma_{\text{p.c.}} = \sigma^\dagger$. Taste violations are encoded in the operators

$$
\begin{aligned}
\mathcal{O}^{A1,\pm}_1 &= (\sigma \xi^{(n)}_5 \Sigma^\dagger \xi^{(n)}_5 \sigma \pm \text{p.c.}) \\
\mathcal{O}^{A1,\pm}_2 &= \left[(\sigma \xi^{(n)}_\nu \sigma) \,\mathrm{Tr}(\xi^{(n)}_\nu \Sigma) \pm \text{p.c.} \right] \\
\mathcal{O}^{A1,\pm}_3 &= (\sigma \xi^{(n)}_\nu \Sigma \xi^{(n)}_\nu \sigma \pm \text{p.c.}) \\
\mathcal{O}^{A1,\pm}_4 &= (\sigma \xi^{(n)}_{\nu 5} \Sigma \xi^{(n)}_{5\nu} \sigma \pm \text{p.c.}) \\
\mathcal{O}^{A1,\pm}_5 &= \left[(\sigma \xi^{(n)}_\nu \sigma) \,\mathrm{Tr}(\xi^{(n)}_\nu \Sigma^\dagger) \pm \text{p.c.} \right] \\
\mathcal{O}^{A1,\pm}_6 &= (\sigma \xi^{(n)}_{\mu\nu} \Sigma^\dagger \xi^{(n)}_{\nu\mu} \sigma \pm \text{p.c.}) \\
\mathcal{O}^{A1,\pm}_7 &= \left[(\sigma \xi^{(n)}_{\nu 5} \sigma) \,\mathrm{Tr}(\xi^{(n)}_{5\nu} \Sigma) \pm \text{p.c.} \right] \\
\mathcal{O}^{A1,\pm}_8 &= \left[(\sigma \xi^{(n)}_{\nu 5} \sigma) \,\mathrm{Tr}(\xi^{(n)}_{5\nu} \Sigma^\dagger) \pm \text{p.c.} \right] \ , \qquad (2.53)
\end{aligned}
$$

and

$$
\begin{aligned}
P_1^{A1} &= \sigma\xi_5^{(n)}\sigma^\dagger\,, & \tilde{P}_1^{A1} &\equiv (P_1^{A1})_{\text{p.c.}} = \sigma^\dagger\xi_5^{(n)}\sigma \\
P_2^{A1} &= \sigma\xi_5^{(n)}\sigma^\dagger\,, & \tilde{P}_2^{A1} &\equiv P_2^{A1} \\
P_3^{A1} &= \sigma\xi_\nu^{(n)}\sigma\,, & \tilde{P}_3^{A1} &\equiv P_3^{A1} \\
P_4^{A1} &= i\sigma\xi_{\nu 5}^{(n)}\sigma\,, & \tilde{P}_4^{A1} &\equiv P_4^{A1} \\
P_5^{A1} &= \sigma\xi_\nu^{(n)}\sigma\,, & \tilde{P}_5^{A1} &\equiv (P_5^{A1})_{\text{p.c.}} = \sigma^\dagger\xi_\nu^{(n)}\sigma^\dagger \\
P_6^{A1} &= i\sigma\xi_{\lambda\nu}^{(n)}\sigma^\dagger\,, & \tilde{P}_6^{A1} &\equiv (P_6^{A1})_{\text{p.c.}} = -i\sigma^\dagger\xi_{\nu\lambda}^{(n)}\sigma \\
P_7^{A1} &= i\sigma\xi_{\lambda\nu}^{(n)}\sigma^\dagger\,, & \tilde{P}_7^{A1} &\equiv P_7^{A1} \\
P_8^{A1} &= i\sigma\xi_{\nu 5}^{(n)}\sigma\,, & \tilde{P}_8^{A1} &\equiv (P_8^{A1})_{\text{p.c.}} = -i\sigma^\dagger\xi_{5\nu}^{(n)}\sigma^\dagger\,.
\end{aligned}
\tag{2.54}
$$

For the current, we have

$$
\begin{aligned}
j_{2,a^2,A1}^{\mu,i\Xi} \;=\; a^2\sum_{k=1}^{8}\Bigg\{ & r_{1,k}^{A1}\,\mathrm{tr}_{D,t}\left(\tfrac{1}{2}T_\Xi\gamma^\mu(1-\gamma_5)H\mathcal{O}_k^{A1,+}\sigma^\dagger\lambda^{(i)}\right) \\
& + r_{2,k}^{A1}\,\mathrm{tr}_{D,t}\left(\tfrac{1}{2}T_\Xi\gamma^\mu(1-\gamma_5)H\sigma^\dagger\lambda^{(i)}\right)\mathrm{Tr}(\mathcal{O}_k^{A1,+}) + r_{3,k}^{A1}\,\mathrm{tr}_{D,t}\left(\tfrac{1}{2}T_\Xi\gamma^\mu(1-\gamma_5)H\mathcal{O}_k^{A1,-}\sigma^\dagger\lambda^{(i)}\right) \\
& + r_{4,k}^{A1}\,\mathrm{tr}_{D,t}\left(\tfrac{1}{2}T_\Xi\gamma^\mu(1-\gamma_5)H\sigma^\dagger\lambda^{(i)}\right)\mathrm{Tr}(\mathcal{O}_k^{A1,-})\Bigg\}\,.
\end{aligned}
\tag{2.55}
$$

Similarly, for type-B operators, we have:

$$
\begin{aligned}
\mathcal{L}_{2,a^2}^{B1} \;=\; a^2\sum_{\mu}\sum_{k=1}^{3}\Bigg\{ & K_{1,k}^{B1}v_\mu v^\mu\,\mathrm{Tr}(\overline{H}H\mathcal{O}_{\mu,k}^{B1,+}) + K_{2,k}^{B1}v_\mu v^\mu\,\mathrm{Tr}(\overline{H}H)\,\mathrm{Tr}(\mathcal{O}_{\mu,k}^{B1,+}) \\
& + K_{3,k}^{B1}v_\mu\,\mathrm{Tr}(\overline{H}H\gamma^\mu\gamma_5\mathcal{O}_{\mu,k}^{B1,-}) + K_{4,k}^{B1}v_\mu\,\mathrm{Tr}(\overline{H}H\gamma^\mu\gamma_5)\,\mathrm{Tr}(\mathcal{O}_{\mu,k}^{B1,-})\Bigg\}\,,
\end{aligned}
\tag{2.56}
$$

where

$$
\begin{aligned}
\mathcal{O}_{\mu,1}^{B1,\pm} &= (\sigma\xi_{\mu\lambda}^{(n)}\Sigma^\dagger\xi_{\lambda\mu}^{(n)}\sigma) \pm \text{p.c.}\,, \\
\mathcal{O}_{\mu,2}^{B1,\pm} &= (\sigma\xi_{\mu}^{(n)}\sigma)\,\mathrm{Tr}(\xi_{\mu}^{(n)}\Sigma^\dagger) \pm \text{p.c.}\,, \\
\mathcal{O}_{\mu,3}^{B1,\pm} &= (\sigma\xi_{\mu 5}^{(n)}\sigma)\,\mathrm{Tr}(\xi_{5\mu}^{(n)}\Sigma^\dagger) \pm \text{p.c.}\,.
\end{aligned}
\tag{2.57}
$$

Note that the above operators explicitly depend on μ, and there is no summation over this index in their definition. (We do sum over λ.) The sum over μ is shown explicitly in Eq. (2.56). The terms proportional to $K_{3,k}^{B1}$ and $K_{4,k}^{B1}$ in Eq. (2.56), which have the form of a product of a

parity-odd combination of the heavy-light mesons times a parity-odd combination of the light mesons, were omitted in Ref. [25]. They are unlikely to be important in practical calculations in either HMrSχPT and HMrASχPT since their first contribution is a NLO correction to the B-B^*-π vertex.

There are many terms in $\mathcal{L}^{B1}_{3,a^2}$, so we separate it for convenience into two parts:

$$\mathcal{L}^{B1}_{3,a^2} = \mathcal{L}^{B1,O}_{3,a^2} + \mathcal{L}^{B1,P}_{3,a^2} \ . \tag{2.58}$$

We then have

$$\begin{aligned}
\mathcal{L}^{B1,O}_{3,a^2} \;=\; & a^2 \sum_{\mu} \sum_{k=1}^{3} \Bigg\{ ic^{B1}_{1,k} \,\mathrm{Tr}\left(\overline{H} H v^\mu \overleftarrow{D}_\mu \, \mathcal{O}^{B1,+}_{\mu,k} - v^\mu \overrightarrow{D}_\mu \, \overline{H} H \, \mathcal{O}^{B1,+}_{\mu,k} \right) \\
& + ic^{B1}_{2,k} \,\mathrm{Tr}\left(\overline{H} H v^\mu \overleftarrow{D}_\mu - v^\mu \overrightarrow{D}_\mu \, \overline{H} H \right) \mathrm{Tr}(\mathcal{O}^{B1,+}_{\mu,k}) \\
& + c^{B1}_{3,k} \,\mathrm{Tr}\left(\overline{H} H \gamma_\mu \gamma_5 \{ \mathbb{A}^\mu, \mathcal{O}^{B1,+}_{\mu,k} \} \right) + c^{B1}_{4,k} \,\mathrm{Tr}\left(\overline{H} H \gamma_\mu \gamma_5 \mathbb{A}^\mu \right) \mathrm{Tr}(\mathcal{O}^{B1,+}_{\mu,k}) \\
& + c^{B1}_{5,k} \,\mathrm{Tr}\left(\overline{H} H \gamma_\mu \gamma_5 \right) \mathrm{Tr}(\mathbb{A}^\mu \mathcal{O}^{B1,+}_{\mu,k}) + c^{B1}_{6,k} \,\mathrm{Tr}\left(\overline{H} H \gamma_\mu [\mathbb{A}^\mu, \mathcal{O}^{B1,-}_{\mu,k}] \right) \\
& + ic^{B1}_{7,k} \, v_\mu v^\mu \,\mathrm{Tr}\left(\overline{H} H v \cdot \overleftarrow{D} \, \mathcal{O}^{B1,+}_{\mu,k} - v \cdot \overrightarrow{D} \, \overline{H} H \, \mathcal{O}^{B1,+}_{\mu,k} \right) \\
& + ic^{B1}_{8,k} \, v_\mu v^\mu \,\mathrm{Tr}\left(\overline{H} H v \cdot \overleftarrow{D} - v \cdot \overrightarrow{D} \, \overline{H} H \right) \mathrm{Tr}(\mathcal{O}^{B1,+}_{\mu,k}) \\
& + c^{B1}_{9,k} \, v_\mu v^\mu \,\mathrm{Tr}\left(\overline{H} H \gamma_\nu \gamma_5 \{ \mathbb{A}^\nu, \mathcal{O}^{B1,+}_{\mu,k} \} \right) + c^{B1}_{10,k} \, v_\mu v^\mu \,\mathrm{Tr}\left(\overline{H} H \gamma_\nu \gamma_5 \mathbb{A}^\nu \right) \mathrm{Tr}(\mathcal{O}^{B1,+}_{\mu,k}) \\
& + c^{B1}_{11,k} \, v_\mu v^\mu \,\mathrm{Tr}\left(\overline{H} H \gamma_\nu \gamma_5 \right) \mathrm{Tr}(\mathbb{A}^\nu \mathcal{O}^{B1,+}_{\mu,k}) + c^{B1}_{12,k} \, v_\mu v^\mu \,\mathrm{Tr}\left(\overline{H} H \gamma_\nu [\mathbb{A}^\nu, \mathcal{O}^{B1,-}_{\mu,k}] \right) \\
& + c^{B1}_{13,k} \, v^\mu \,\mathrm{Tr}\left(\overline{H} H \gamma_\mu \gamma_5 \{ v \cdot \mathbb{A}, \mathcal{O}^{B1,+}_{\mu,k} \} \right) + c^{B1}_{14,k} \, v^\mu \,\mathrm{Tr}\left(\overline{H} H \gamma_\mu \gamma_5 \, v \cdot \mathbb{A} \right) \mathrm{Tr}(\mathcal{O}^{B1,+}_{\mu,k}) \\
& + c^{B1}_{15,k} \, v^\mu \,\mathrm{Tr}\left(\overline{H} H \gamma_\mu \gamma_5 \right) \mathrm{Tr}(v \cdot \mathbb{A} \, \mathcal{O}^{B1,+}_{\mu,k}) + c^{B1}_{19,k} v^\mu \,\mathrm{Tr}\left(\overline{H} H \gamma_{\mu\nu} \{ \mathbb{A}^\nu, \mathcal{O}^{B1,-}_{\mu,k} \} \right) \\
& + c^{B1}_{20,k} v^\mu \,\mathrm{Tr}\left(\overline{H} H \gamma_{\mu\nu} \right) \mathrm{Tr}\left(\mathbb{A}^\nu \mathcal{O}^{B1,-}_{\mu,k} \right) \Bigg\},
\end{aligned} \tag{2.59}$$

and

$$
\begin{aligned}
\mathcal{L}^{B1,P}_{3,a^2} \;=\; a^2 \sum_\mu \Bigg\{ \sum_{k=1}^{4} \Bigg[& c^{B1}_{21,k} \Big(\mathrm{Tr}\left(\overline{H} H \gamma_\mu \gamma_5 P^{B1}_{\mu,k} \mathbb{A}^\mu \tilde{P}^{B1}_{\mu,k}\right) + \mathrm{p.c.} \Big) \\
& + c^{B1}_{22,k} \Big(\mathrm{Tr}\left(\overline{H} H \gamma_\mu \gamma_5 P^{B1}_{\mu,k}\right) \mathrm{Tr}\left(\mathbb{A}^\mu \tilde{P}^{B1}_{\mu,k}\right) + \mathrm{p.c.} \Big) \\
& + c^{B1}_{23,k} v_\mu v^\mu \Big(\mathrm{Tr}\left(\overline{H} H \gamma_\nu \gamma_5 P^{B1}_{\mu,k} \mathbb{A}^\nu \tilde{P}^{B1}_{\mu,k}\right) + \mathrm{p.c.} \Big) \\
& + c^{B1}_{24,k} v_\mu v^\mu \Big(\mathrm{Tr}\left(\overline{H} H \gamma_\nu \gamma_5 P^{B1}_{\mu,k}\right) \mathrm{Tr}\left(\mathbb{A}^\nu \tilde{P}^{B1}_{\mu,k}\right) + \mathrm{p.c.} \Big) \\
& + c^{B1}_{25,k} v^\mu \Big(\mathrm{Tr}\left(\overline{H} H \gamma_\mu \gamma_5 P^{B1}_{\mu,k} v\cdot\mathbb{A}\, \tilde{P}^{B1}_{\mu,k}\right) + \mathrm{p.c.} \Big) \\
& + c^{B1}_{26,k} v^\mu \Big(\mathrm{Tr}\left(\overline{H} H \gamma_\mu \gamma_5 P^{B1}_{\mu,k}\right) \mathrm{Tr}\left(v\cdot\mathbb{A}\, \tilde{P}^{B1}_{\mu,k}\right) + \mathrm{p.c.} \Big) \Bigg] \\
& + \sum_{k=2,3,4} \Bigg[c^{B1}_{29,k} \Big(\mathrm{Tr}\left(\overline{H} H \gamma_\mu P^{B1}_{\mu,k} \mathbb{A}^\mu \tilde{P}^{B1}_{\mu,k}\right) + \mathrm{p.c.} \Big) \\
& \qquad + c^{B1}_{30,k} v_\mu v^\mu \Big(\mathrm{Tr}\left(\overline{H} H \gamma_\nu P^{B1}_{\mu,k} \mathbb{A}^\nu \tilde{P}^{B1}_{\mu,k}\right) + \mathrm{p.c.} \Big) \Bigg] \\
& + \sum_{k=1,4} \Bigg[c^{B1}_{31,k} \Big(\mathrm{Tr}\left(\overline{H} H \gamma_\mu P^{B1}_{\mu,k}\right) \mathrm{Tr}\left(\mathbb{A}^\mu \tilde{P}^{B1}_{\mu,k}\right) + \mathrm{p.c.} \Big) \\
& \qquad + c^{B1}_{32,k} v_\mu v^\mu \Big(\mathrm{Tr}\left(\overline{H} H \gamma_\nu P^{B1}_{\mu,k}\right) \mathrm{Tr}\left(\mathbb{A}^\nu \tilde{P}^{B1}_{\mu,k}\right) + \mathrm{p.c.} \Big) \Bigg] \\
& + c^{B1}_{33,1} v^\mu \Big(\mathrm{Tr}\left(\overline{H} H \gamma_{\mu\nu} P^{B1}_{\mu,1} \mathbb{A}^\nu \tilde{P}^{B1}_{\mu,1}\right) + \mathrm{p.c.} \Big) \\
& + \sum_{k=2,3} \Bigg[c^{B1}_{34,k} v^\mu \Big(\mathrm{Tr}\left(\overline{H} H \gamma_{\mu\nu} P^{B1}_{\mu,k}\right) \mathrm{Tr}\left(\mathbb{A}^\nu \tilde{P}^{B1}_{\mu,k}\right) + \mathrm{p.c.} \Big) \Bigg] \Bigg\} \,, \qquad (2.60)
\end{aligned}
$$

where

$$
\begin{aligned}
P^{B1}_{\mu,1} &= i\sigma \xi^{(n)}_{\mu\lambda} \sigma^\dagger \,, & \tilde{P}^{B1}_{\mu,1} &\equiv (P^{B1}_{\mu,1})_{\mathrm{p.c.}} = -i\sigma^\dagger \xi^{(n)}_{\lambda\mu} \sigma \\
P^{B1}_{\mu,2} &= \sigma \xi^{(n)}_{\mu} \sigma \,, & \tilde{P}^{B1}_{\mu,2} &\equiv (P^{B1}_{\mu,2})_{\mathrm{p.c.}} = \sigma^\dagger \xi^{(n)}_{\mu} \sigma^\dagger \\
P^{B1}_{\mu,3} &= i\sigma \xi^{(n)}_{\mu 5} \sigma \,, & \tilde{P}^{B1}_{\mu,3} &\equiv (P^{B1}_{\mu,3})_{\mathrm{p.c.}} = -i\sigma^\dagger \xi^{(n)}_{5\mu} \sigma^\dagger \\
P^{B1}_{\mu,4} &= i\sigma \xi^{(n)}_{\mu\lambda} \sigma^\dagger \,, & \tilde{P}^{B1}_{\mu,4} &\equiv P^{B1}_{\mu,4} \,. \qquad (2.61)
\end{aligned}
$$

A comparison of Eq. (2.59) with Eq. (59) in Ref. [25] shows that we have dropped the terms with coefficients $c^B_{16,k}$, $c^B_{17,k}$, and $c^B_{18,k}$ because one can write them as linear combinations of other terms in the Lagrangian using Eqs. (2.78) and (2.82) below and the cyclic property of the trace. For example, the term with coefficient $c^B_{16,k}$ is linearly dependent on the terms with coefficients $c^B_{9,k}$ and $c^B_{13,k}$. Terms with coefficients $c^B_{27,k}$ and $c^B_{28,k}$ in Eq. (60) of Ref. [25] have been dropped in Eq. (2.60) for the same reason.

For the type-B contributions to the current, we have:

$$
\begin{aligned}
j^{\mu,i\Xi}_{2,a^2,B1} \;=\; a^2 \sum_{k=1}^{3} \sum_{\nu} \Bigg\{ & r^{B1}_{5,k}\, \mathrm{tr}_{D,t}\left(\tfrac{1}{2} T_\Xi \gamma^\mu (1-\gamma_5) H v_\nu v^\nu \mathcal{O}^{B1,+}_{\nu,k} \sigma^\dagger \lambda^{(i)}\right) \\
& + r^{B1}_{6,k}\, \mathrm{tr}_{D,t}\left(\tfrac{1}{2} T_\Xi \gamma^\mu (1-\gamma_5) H \sigma^\dagger \lambda^{(i)}\right) v_\nu v^\nu\, \mathrm{Tr}(\mathcal{O}^{B1,+}_{\nu,k}) \\
& + r^{B1}_{7,k}\, \mathrm{tr}_{D,t}\left(\tfrac{1}{2} T_\Xi \gamma^\mu (1-\gamma_5) H v_\nu v^\nu \mathcal{O}^{B1,-}_{\nu,k} \sigma^\dagger \lambda^{(i)}\right) \\
& + r^{B1}_{8,k}\, \mathrm{tr}_{D,t}\left(\tfrac{1}{2} T_\Xi \gamma^\mu (1-\gamma_5) H \sigma^\dagger \lambda^{(i)}\right) v_\nu v^\nu\, \mathrm{Tr}(\mathcal{O}^{B1,-}_{\nu,k}) \\
& + r^{B1}_{9,k}\, \mathrm{tr}_{D,t}\left(\tfrac{1}{2} T_\Xi \gamma^\mu (1-\gamma_5) H \gamma^\nu v_\nu \mathcal{O}^{B1,+}_{\nu,k} \sigma^\dagger \lambda^{(i)}\right) \\
& + r^{B1}_{10,k}\, \mathrm{tr}_{D,t}\left(\tfrac{1}{2} T_\Xi \gamma^\mu (1-\gamma_5) H \gamma^\nu \sigma^\dagger \lambda^{(i)}\right) v_\nu\, \mathrm{Tr}(\mathcal{O}^{B1,+}_{\nu,k}) \\
& + r^{B1}_{11,k}\, \mathrm{tr}_{D,t}\left(\tfrac{1}{2} T_\Xi \gamma^\mu (1-\gamma_5) H \gamma^\nu v_\nu \mathcal{O}^{B1,-}_{\nu,k} \sigma^\dagger \lambda^{(i)}\right) \\
& + r^{B1}_{12,k}\, \mathrm{tr}_{D,t}\left(\tfrac{1}{2} T_\Xi \gamma^\mu (1-\gamma_5) H \gamma^\nu \sigma^\dagger \lambda^{(i)}\right) v_\nu\, \mathrm{Tr}(\mathcal{O}^{B1,-}_{\nu,k}) \Bigg\} \,. \qquad (2.62)
\end{aligned}
$$

Here we have omitted terms in Ref. [25] with coefficients $r_{1,k}$ through $r_{4,k}$. These terms have the (Lorentz and taste) index ν set to μ and not summed over. We believe such terms are inconsistent with heavy-quark spin symmetry, which is not broken by light-light four-quark operators in the SET. In the next subsection, we give a more detailed discussion about type-B contributions to the current, which will further elucidate the reason for dropping these terms.

2.3.2 Discretization errors at NLO: Heavy-taste breaking terms

We now proceed to determine the chiral representatives of the light-heavy terms in the SET, Eq. (2.45). The spin and taste matrices between $\overline{Q}$ and Q in this case mean that heavy-quark spin and taste symmetries are broken. The corresponding chiral operators are completely new, unrelated to those in Ref. [25], and we must determine them from scratch. That requires defining spurions to make the operators "invariant," and then constructing the possible chiral operators in terms of those spurions. Initially, we do not allow additional derivatives (*i.e.*, either the covariant derivative, $\overrightarrow{D}_\mu$ or the axial current $\mathbb{A}$), and find the chiral operators summarized by the terms $\mathcal{L}^{A2}_{2,a^2}$, $\mathcal{L}^{B2}_{2,a^2}$, $j^{\mu,i\Xi}_{2,a^2,A2}$ and $j^{\mu,i\Xi}_{2,a^2,B2}$ in Eqs. (2.7) and (2.10). We then consider terms with a single additional derivative, which are summarized in $\mathcal{L}^{A2}_{3,a^2}$ and $\mathcal{L}^{B2}_{3,a^2}$, Eq. (2.8).

We take the type-A operator $\big[V \times P\big]^{lh}$ as an example:

$$\begin{aligned} a^2\mathcal{O}_{[V\times P]^{lh}} &\equiv a^2\ \overline{q}(\gamma^\mu \otimes \xi_5) q\ \overline{Q}(\gamma_\mu \otimes \xi_5) Q, \\ &= a^2[\overline{q}^L(\gamma^\mu \otimes \xi_5) q^L + \overline{q}^R(\gamma^\mu \otimes \xi_5) q^R]\ [\overline{Q}(\gamma_\mu \otimes \xi_5) Q], \\ &= a^2[\overline{q}^L(\gamma^\mu \otimes A_1) q^L + \overline{q}^R(\gamma^\mu \otimes A_2) q^R]\ [\overline{Q}\left(B(\mu) \otimes C\right) Q]\ , \end{aligned} \tag{2.63}$$

with $q^L = [(1-\gamma_5)/2]\, q$ and $q^R = [(1+\gamma_5)/2]\, q$. Note that Eq. (2.63) is written in Minkowski space for consistency with the conventions of this chapter. We have introduced four spurions, A_1, A_2, $B(\mu)$, and C, which transform as:

$$A_1 \rightarrow L A_1 L^\dagger\ , \tag{2.64}$$

$$A_2 \rightarrow R A_2 R^\dagger\ , \tag{2.65}$$

$$B(\mu) \rightarrow S\, B(\mu)\, S^\dagger\ , \tag{2.66}$$

$$C \rightarrow V C V^\dagger\ . \tag{2.67}$$

Here A_1 and A_2 are light-quark spurions that transform according to the chiral flavor-taste symmetry, while $B(\mu)$ and C transform to maintain the spin and taste symmetry, respectively, of the heavy quark. We will use them as building blocks for the chiral theory, and eventually let them take the values

$$A_1 = a\xi_5^{(n)} \equiv a\xi_5 \otimes I_{\text{flavor}}\ , \tag{2.68}$$

$$A_2 = a\xi_5^{(n)} \equiv a\xi_5 \otimes I_{\text{flavor}}\ , \tag{2.69}$$

$$B(\mu) = \gamma_\mu\ , \tag{2.70}$$

$$C = a\xi_5\ , \tag{2.71}$$

where I_{flavor} is the identity in flavor space. We employ two separate heavy quark spurions so that we can let $B(\mu)$ take its final value before A_1, A_2, and C do. This two-stage procedure is useful in elucidating the implications of Lorentz (or, equivalently, Euclidean rotation) invariance. Since Lorentz transformations include heavy-quark spin transformations, once $B(\mu)$ is introduced in the last line of Eq. (2.63), the 4-quark operator no longer transforms as a Lorentz scalar field. The chiral operators we construct from A_1, A_2, and $B(\mu)\otimes C$ will thus be invariants under heavy quark spin, heavy quark taste, and light quark chiral transformations, but not under Lorentz transformations. However, once we replace $B(\mu)$ by γ_μ (and sum over μ), the 4-quark operator is once again a Lorentz scalar, and so must be the resulting chiral operators.

In constructing chiral operators from these spurions, we first note that A_1 and A_2 may be

combined with σ and $\sigma^\dagger$ in order to form objects that transform with $\mathbb{U}$ under the light-quark symmetries. This is convenient because H and $\overline{H}$ transform in that way, Eq. (2.24). We note

$$\sigma^\dagger A_1 \sigma \;\to\; \mathbb{U}\,(\sigma^\dagger A_1 \sigma)\,\mathbb{U}^\dagger\,, \tag{2.72}$$

$$\sigma A_2 \sigma^\dagger \;\to\; \mathbb{U}\,(\sigma A_2 \sigma^\dagger)\,\mathbb{U}^\dagger\,. \tag{2.73}$$

We can now easily make chiral operators that are invariant under heavy and light taste symmetry and spin symmetry, and are bilinear in $B(\mu)\otimes C$ and A_1 or A_2. (Terms with more spurions are higher order.) We find the following operators:

$$\mathrm{Tr}\left[\overline{H}\,(B(\mu)\otimes C)\,H\,\Gamma_1\sigma^\dagger A_1\sigma\right], \qquad \mathrm{Tr}\left[\overline{H}\,(B(\mu)\otimes C)\,H\,\Gamma_2\sigma A_2\sigma^\dagger\right],$$
$$\mathrm{Tr}\left[\overline{H}\,(B(\mu)\otimes C)\,H\,\Gamma_3\right]\mathrm{Tr}\left[\sigma^\dagger A_1\sigma\right], \qquad \mathrm{Tr}\left[\overline{H}\,(B(\mu)\otimes C)\,H\,\Gamma_4\right]\mathrm{Tr}\left[\sigma A_2\sigma^\dagger\right],$$

where $\Gamma_1,\cdots,\Gamma_4$ are (for the moment, arbitrary) combinations of γ matrices and components of the heavy quark velocity v, which are the only additional factors allowed at this order. Replacing $B(\mu)$ by γ_μ, we may then demand Lorentz (and parity) invariance. The resulting operators are

$$v^\mu\,\mathrm{Tr}\left(\overline{H}\gamma_\mu C H\sigma^\dagger A_1\sigma\right) + v^\mu\,\mathrm{Tr}\left(\overline{H}\gamma_\mu C H\sigma A_2\sigma^\dagger\right)\,, \tag{2.74}$$

$$\mathrm{Tr}\left(\overline{H}\gamma_\mu C H\gamma^\mu\sigma^\dagger A_1\sigma\right) + \mathrm{Tr}\left(\overline{H}\gamma_\mu C H\gamma^\mu\sigma A_2\sigma^\dagger\right)\,, \tag{2.75}$$

$$v^\mu\,\mathrm{Tr}\left(\overline{H}\gamma_\mu C H\right)\mathrm{Tr}\left(\sigma^\dagger A_1\sigma\right) + v^\mu Tr\left(\overline{H}\gamma_\mu C H\right)\mathrm{Tr}\left(\sigma A_2\sigma^\dagger\right)\,, \tag{2.76}$$

$$\mathrm{Tr}\left(\overline{H}\gamma_\mu C H\gamma^\mu\right)\mathrm{Tr}\left(\sigma^\dagger A_1\sigma\right) + \mathrm{Tr}\left(\overline{H}\gamma_\mu C H\gamma^\mu\right)\mathrm{Tr}\left(\sigma A_2\sigma^\dagger\right)\,, \tag{2.77}$$

Here, parity invariance requires that A_1 and A_2 enter symmetrically; there are no parity-odd bilinears in H and $\overline{H}$ that could be multiplied by an antisymmetric combination of A_1 and A_2. We have also omitted the direct product symbol $\otimes$ where the meaning is clear from context. Since $\mathrm{Tr}\left(\sigma^\dagger A_1\sigma\right) = 0 = \mathrm{Tr}\left(\sigma^\dagger A_2\sigma\right)$ once A_1 and A_2 take their final values, Eq. (2.76) and Eq. (2.77) may be dropped. On the other hand, various simplifications of terms involving H and $\overline{H}$ are possible here and below, due to the overall factors of $(1+\not{v})$ in their definitions [Eqs. (2.21) and (2.22)], the fact that $v^2 = 1$, and the relation $v^\mu B^*_{\mu\alpha a} = 0$ for the vector meson field B^*. We

list some relations that are useful for simplifying terms:

$$\not{v}\not{B}^* = -\not{B}^*\not{v} \quad \Rightarrow \quad \not{v}H = -H\not{v}, \tag{2.78}$$

$$(1+\not{v})\not{v} = (1+\not{v}), \tag{2.79}$$

$$(1+\not{v})\gamma_5(1+\not{v}) = 0, \tag{2.80}$$

$$(1+\not{v})\gamma_\mu(1+\not{v}) = (1+\not{v})v_\mu(1+\not{v}), \tag{2.81}$$

$$(1-\not{v})\gamma_{\mu\nu}(1+\not{v}) = (1-\not{v})\left(\gamma_\mu v_\nu - \gamma_\nu v_\mu\right)(1+\not{v}), \tag{2.82}$$

$$\mathrm{tr}_D(\overline{H}H\gamma_\mu) = -v_\mu \mathrm{tr}_D(\overline{H}H), \tag{2.83}$$

where tr_D is a trace over Dirac indices only, and Eq. (2.83) is actually a simple consequence of Eqs. (2.78) and (2.81) and the cyclic property of the trace. With these relations, it is straightforward show that Eq. (2.74) and Eq. (2.75) are both proportional to

$$a^2\,\mathrm{Tr}\left(\overline{H}\xi_5 H\sigma^\dagger\xi_5^{(n)}\sigma\right) + a^2\,\mathrm{Tr}\left(\overline{H}\xi_5 H\sigma\xi_5^{(n)}\sigma^\dagger\right)\,, \tag{2.84}$$

where we wave inserted final values of the spurions from Eqs. (2.68), (2.69) and (2.71). We then follow the same procedure for other type-A operators. For clarity, we write the terms with a single trace and terms with two traces separately. First, we list the single-trace terms:

$$[S\times A] \;\to\; a^2\,\mathrm{Tr}\left(\overline{H}\xi_{5\mu} H\sigma^\dagger\xi_{\mu 5}^{(n)}\sigma^\dagger\right) + a^2\,\mathrm{Tr}\left(\overline{H}\xi_{5\mu} H\sigma\xi_{\mu 5}^{(n)}\sigma\right)\,, \tag{2.85}$$

$$[S\times V] \;\to\; a^2\,\mathrm{Tr}\left(\overline{H}\xi_{\mu} H\sigma^\dagger\xi_{\mu}^{(n)}\sigma^\dagger\right) + a^2\,\mathrm{Tr}\left(\overline{H}\xi_{\mu} H\sigma\xi_{\mu}^{(n)}\sigma\right)\,, \tag{2.86}$$

$$[P\times A] \;\to\; 0\,, \tag{2.87}$$

$$[P\times V] \;\to\; 0\,, \tag{2.88}$$

$$[T\times A] \;\to\; a^2\,\mathrm{Tr}\left(\overline{H}\gamma_{\lambda\nu}\xi_{5\mu} H\gamma^{\nu\lambda}\sigma^\dagger\xi_{\mu 5}^{(n)}\sigma^\dagger\right) + a^2\,\mathrm{Tr}\left(\overline{H}\gamma_{\lambda\nu}\xi_{5\mu} H\gamma^{\nu\lambda}\sigma\xi_{\mu 5}^{(n)}\sigma\right)\,, \tag{2.89}$$

$$[T\times V] \;\to\; a^2\,\mathrm{Tr}\left(\overline{H}\gamma_{\lambda\nu}\xi_{\mu} H\gamma^{\nu\lambda}\sigma^\dagger\xi_{\mu}^{(n)}\sigma^\dagger\right) + a^2\,\mathrm{Tr}\left(\overline{H}\gamma_{\lambda\nu}\xi_{\mu} H\gamma^{\nu\lambda}\sigma\xi_{\mu}^{(n)}\sigma\right)\,, \tag{2.90}$$

$$[V\times S] \;\to\; a^2\,\mathrm{Tr}\left(\overline{H}H\right)\,, \tag{2.91}$$

$$[V\times P] \;\to\; a^2\,\mathrm{Tr}\left(\overline{H}\xi_5 H\sigma^\dagger\xi_5^{(n)}\sigma\right) + a^2\,\mathrm{Tr}\left(\overline{H}\xi_5 H\sigma\xi_5^{(n)}\sigma^\dagger\right)\,, \tag{2.92}$$

$$[V\times T] \;\to\; a^2\,\mathrm{Tr}\left(\overline{H}\xi_{\nu\lambda} H\sigma^\dagger\xi_{\lambda\nu}^{(n)}\sigma\right) + a^2\,\mathrm{Tr}\left(\overline{H}\xi_{\nu\lambda} H\sigma\xi_{\lambda\nu}^{(n)}\sigma^\dagger\right)\,, \tag{2.93}$$

$$[A\times S] \;\to\; a^2\,\mathrm{Tr}\left(\overline{H}\gamma_{5\mu} H\gamma^{\mu 5}\right)\,, \tag{2.94}$$

$$[A\times P] \;\to\; a^2\,\mathrm{Tr}\left(\overline{H}\gamma_{5\mu}\xi_5 H\gamma^{\mu 5}\sigma^\dagger\xi_5^{(n)}\sigma\right) + a^2\,\mathrm{Tr}\left(\overline{H}\gamma_{5\mu}\xi_5 H\gamma^{\mu 5}\sigma\xi_5^{(n)}\sigma^\dagger\right)\,, \tag{2.95}$$

$$[A\times T] \;\to\; a^2\,\mathrm{Tr}\left(\overline{H}\gamma_{5\mu}\xi_{\nu\lambda} H\gamma^{\mu 5}\sigma^\dagger\xi_{\lambda\nu}^{(n)}\sigma\right) + a^2\,\mathrm{Tr}\left(\overline{H}\gamma_{5\mu}\xi_{\nu\lambda} H\gamma^{\mu 5}\sigma\xi_{\lambda\nu}^{(n)}\sigma^\dagger\right)\,. \tag{2.96}$$

As before, all twice-repeated indices are summed. The double-trace terms are:

$$\begin{aligned}
\big[S\times A\big] &\to a^2\,\mathrm{Tr}\left(\overline{H}\xi_{5\mu}H\right)\mathrm{Tr}\left(\sigma^\dagger\xi^{(n)}_{\mu5}\sigma^\dagger\right)+a^2\,\mathrm{Tr}\left(\overline{H}\xi_{5\mu}H\right)\mathrm{Tr}\left(\sigma\xi^{(n)}_{\mu5}\sigma\right)\,, && (2.97)\\
\big[S\times V\big] &\to a^2\,\mathrm{Tr}\left(\overline{H}\xi_{\mu}H\right)\mathrm{Tr}\left(\sigma^\dagger\xi^{(n)}_{\mu}\sigma^\dagger\right)+a^2\,\mathrm{Tr}\left(\overline{H}\xi_{\mu}H\right)\mathrm{Tr}\left(\sigma\xi^{(n)}_{\mu}\sigma\right)\,, && (2.98)\\
\big[P\times A\big] &\to 0\,, && (2.99)\\
\big[P\times V\big] &\to 0\,, && (2.100)\\
\big[T\times A\big] &\to a^2\,\mathrm{Tr}\left(\overline{H}\gamma_{\lambda\nu}\xi_{5\mu}H\gamma^{\lambda\nu}\right)\mathrm{Tr}\left(\sigma^\dagger\xi^{(n)}_{\mu5}\sigma^\dagger\right)+a^2\,\mathrm{Tr}\left(\overline{H}\gamma_{\lambda\nu}\xi_{5\mu}H\gamma^{\lambda\nu}\right)\mathrm{Tr}\left(\sigma\xi^{(n)}_{\mu5}\sigma\right), && (2.101)\\
\big[T\times V\big] &\to a^2\,\mathrm{Tr}\left(\overline{H}\gamma_{\lambda\nu}\xi_{\mu}H\gamma^{\lambda\nu}\right)\mathrm{Tr}\left(\sigma^\dagger\xi^{(n)}_{\mu}\sigma^\dagger\right)+a^2\,\mathrm{Tr}\left(\overline{H}\gamma_{\lambda\nu}\xi_{\mu}H\gamma^{\lambda\nu}\right)\mathrm{Tr}\left(\sigma\xi^{(n)}_{\mu}\sigma\right), && (2.102)\\
\big[V\times S\big] &\to 0\,, && (2.103)\\
\big[V\times P\big] &\to 0\,, && (2.104)\\
\big[V\times T\big] &\to 0 && (2.105)\\
\big[A\times S\big] &\to 0\,, && (2.106)\\
\big[A\times P\big] &\to 0\,, && (2.107)\\
\big[A\times T\big] &\to 0\,. && (2.108)
\end{aligned}$$

In Eqs. (2.85) through (2.108), we have again used the fact that Lorentz-invariant, parity-odd bilinears in H and $\overline{H}$ [such as $\mathrm{tr}_D(\overline{H}H\gamma_5)$, $\mathrm{tr}_D(\overline{H}\gamma^\mu H\gamma_{\mu5})$, or $\mathrm{tr}_D(\overline{H}\gamma^{\mu\nu}H\gamma_{\nu\mu}\gamma_5)$] vanish. The reason for this is that, once the Dirac traces are performed, the only objects from which to form invariants in the heavy-meson sector are B, $B^\dagger$, B^*_μ, $B^{\dagger*}_\nu$, and v_λ, and it is not possible to make a Lorentz-invariant bilinear in the meson fields that is parity odd out of these ingredients. This eliminates the possibility of antisymmetric combinations of the light quark spurions, multiplied by parity-odd combinations of the heavy-meson fields.

We now consider the type-B operators. The procedure here is a bit more complicated because these operators violate Lorentz invariance in a particular way, and we must ensure that the chiral operators do the same. Our approach is based on that introduced by Sharpe and Van de Water [60] to find light-meson chiral representatives of type-B operators. We take $\big[T_\mu\times A_\mu\big]$ as an example:

$$a^2\mathcal{O}_{[T_\mu\times A_\mu]}\equiv a^2\sum_\mu\left\{\overline{q}_l(\gamma^{\mu\nu}\otimes\xi_{\mu5})q_l\overline{q}_h(\gamma_{\nu\mu}\otimes\xi_{5\mu})q_h-\overline{q}_l(\gamma^{\mu\nu5}\otimes\xi_{\mu5})q_l\overline{q}_h(\gamma_{5\nu\mu}\otimes\xi_{5\mu})q_h\right\}\,. \quad (2.109)$$

The second term in this expression removes the Lorentz-singlet component. However, it is unnecessary to keep both terms here because the second term can be written as a linear combination of the first term and $\big[T\times A\big]$, which has already have been taken into account. Further, it is useful for the moment to remove the sums (explicit or implicit) over the indices μ,ν. Thus we

are led to consider the operator

$$\begin{aligned} a^2\mathcal{O}(\mu,\nu) &\equiv a^2\overline{q}(\gamma^{\mu\nu}\otimes\xi_{\mu 5})q\;\overline{Q}(\gamma_{\nu\mu}\otimes\xi_{5\mu})Q, \\ &= a^2\Big[\overline{q}^L(\gamma^{\mu\nu}\otimes\xi_{\mu 5})q^R+\overline{q}^R(\gamma^{\mu\nu}\otimes\xi_{\mu 5})q^L\Big]\Big[\overline{Q}(\gamma_{\nu\mu}\otimes\xi_{5\mu})Q\Big], \\ &= \Big[\overline{q}^L\big(\gamma^{\mu\nu}\otimes A_1(\mu)\big)q^R+\overline{q}^R\big(\gamma^{\mu\nu}\otimes A_2(\mu)\big)q^L\Big]\Big[\overline{Q}\big(B(\nu,\mu)\otimes C(\mu)\big)Q\Big] \end{aligned} \tag{2.110}$$

where μ and ν are fixed. With the spurions $A_1(\mu)$, $A_2(\mu)$, and $B(\nu,\mu)\otimes C(\mu)$, we can construct two single-trace $\mathcal{O}(a^2)$ terms that are invariant under heavy and light taste symmetry and heavy-quark spin symmetry:

$$\begin{aligned} &\mathrm{Tr}\left[\overline{H}\big(B(\nu,\mu)\otimes C(\mu)\big)H\Gamma_1\,\sigma^\dagger A_1(\mu)\sigma^\dagger\right], \\ &\mathrm{Tr}\left[\overline{H}\big(B(\nu,\mu)\otimes C(\mu)\big)H\Gamma_2\,\sigma A_2(\mu)\sigma\right], \end{aligned} \tag{2.111}$$

where Γ_1 and Γ_2 are as-yet undetermined combinations of γ matrices and components of v. There are also two-trace versions of these operators, in which the heavy- and light-quark factors are separately traced, but for simplicity we focus on the single-trace case here.

We now replace the spurion $B(\nu,\mu)$ with its value $\gamma_{\nu\mu}$. We also restore the sum over ν (but not μ), considering chiral representatives of the operator $a^2\mathcal{O}(\mu)=a^2\sum_\nu\mathcal{O}(\mu,\nu)$:

$$a^2\mathcal{O}(\mu) = \Big[\overline{q}^L\gamma^{\mu\nu}A_1(\mu)q^R+\overline{q}^R\gamma^{\mu\nu}A_2(\mu)q^L\Big]\Big[\overline{Q}\gamma_{\nu\mu}C(\mu)Q\Big] \quad (\mu\text{ fixed}), \tag{2.112}$$

with the $\otimes$ symbols and the sum on ν implicit. The operator $\mathcal{O}(\mu)$ is the ${}^{\mu}{}_{\mu}$ component of a two-index Lorentz tensor, and is therefore a linear combination of an element of a symmetric traceless tensor and a Lorentz singlet (the trace). The singlet piece, in which the sum over the Lorentz index μ is decoupled from the taste label μ of the spurions, is simply a repeat of the corresponding type-A operator; only the symmetric tensor is new. Thus the desired chiral operators are ${}^{\mu}{}_{\mu}$ components of two-index Lorentz tensors, where it is not necessary to insist on tracelessness because the trace term again will repeat one of the type-A chiral operators. From the possibilities in Eq. (2.111), two independent operators may now be constructed:

$$\begin{aligned} &\mathrm{Tr}\left[\overline{H}\gamma_{\nu\mu}C(\mu)H\gamma^{\mu\nu}\left(\sigma^\dagger A_1(\mu)\sigma^\dagger+\sigma A_2(\mu)\sigma\right)\right], \\ &\mathrm{Tr}\left[\overline{H}\gamma_{\nu\mu}C(\mu)H\gamma^{\mu\nu}\gamma_5\left(\sigma^\dagger A_1(\mu)\sigma^\dagger-\sigma A_2(\mu)\sigma\right)\right], \end{aligned} \tag{2.113}$$

with μ still fixed. Using Eqs. (2.78) through (2.82), it is not hard to show that choices other than $\gamma^{\mu\nu}$ for the Γ_i factors following the H field either vanish identically (*e.g.*, for the choice $\gamma^\mu v^\nu$) or are proportional to one of the terms listed (*e.g.*, for the choice $v^\mu\gamma^\nu$). The symmetric

combination of A_1 and A_2 in the first term, as well as the antisymmetric combination in the second, are required by parity.

Finally, we put in the fixed values of the spurions $A_1(\mu)$, $A_2(\mu)$, and $C(\mu)$, and restore the sum on μ, giving the two operators

$$a^2 \sum_\mu \left\{ \mathrm{Tr}\left[\overline{H} \gamma_{\nu\mu} \xi_{5\mu} H \gamma^{\mu\nu} \left(\sigma^\dagger \xi^{(n)}_{\mu 5} \sigma^\dagger + \sigma \xi^{(n)}_{\mu 5} \sigma \right) \right] \right\} , \tag{2.114}$$

$$a^2 \sum_\mu \left\{ \mathrm{Tr}\left[\overline{H} \gamma_{\nu\mu} \xi_{5\mu} H \gamma^{\mu\nu} \gamma_5 \left(\sigma^\dagger \xi^{(n)}_{\mu 5} \sigma^\dagger - \sigma \xi^{(n)}_{\mu 5} \sigma \right) \right] \right\} . \tag{2.115}$$

As mentioned earlier, terms like Eq. (2.115) (odd in the light spurions) are ruled out in the type-A case by parity and Lorentz invariance. Here, however, Lorentz invariance is broken, and $\mathrm{tr}_D \left(\overline{H} \gamma_{\nu\mu} H \gamma^{\mu\nu} \gamma_5 \right)$ does not vanish since the sum on μ is not free, but coupled to the taste sum. Further, one can check that the term in Eq. (2.115) is Hermitian and time-reversal invariant; for details of how time-reversal symmetry acts on relevant quantities, see Ref. [25], Sec. III D.

We derive the other type-B terms similarly. For clarity, we write the single-trace terms and the double-trace terms separately. The single-trace terms are:

$$\begin{aligned}
\left[T_\mu \times A_\mu \right] \quad \to \quad & a^2 \sum_\mu \left\{ \mathrm{Tr}\left[\overline{H} \gamma_{\nu\mu} \xi_{5\mu} H \gamma^{\mu\nu} \left(\sigma^\dagger \xi^{(n)}_{\mu 5} \sigma^\dagger + \sigma \xi^{(n)}_{\mu 5} \sigma \right) \right] \right\} , \\
& a^2 \sum_\mu \left\{ \mathrm{Tr}\left[\overline{H} \gamma_{\nu\mu} \xi_{5\mu} H \gamma^{\mu\nu} \gamma_5 \left(\sigma^\dagger \xi^{(n)}_{\mu 5} \sigma^\dagger - \sigma \xi^{(n)}_{\mu 5} \sigma \right) \right] \right\} ; \qquad (2.116) \\
\left[T_\mu \times V_\mu \right] \quad \to \quad & a^2 \sum_\mu \left\{ \mathrm{Tr}\left[\overline{H} \gamma_{\nu\mu} \xi_{\mu} H \gamma^{\mu\nu} \left(\sigma^\dagger \xi^{(n)}_{\mu} \sigma^\dagger + \sigma \xi^{(n)}_{\mu} \sigma \right) \right] \right\} , \\
& a^2 \sum_\mu \left\{ \mathrm{Tr}\left[\overline{H} \gamma_{\nu\mu} \xi_{\mu} H \gamma^{\mu\nu} \gamma_5 \left(\sigma^\dagger \xi^{(n)}_{\mu} \sigma^\dagger - \sigma \xi^{(n)}_{\mu} \sigma \right) \right] \right\} ; \qquad (2.117) \\
\left[A_\mu \times T_\mu \right] \quad \to \quad & a^2 \sum_\mu \left\{ \mathrm{Tr}\left[\overline{H} \gamma_{5\mu} \xi_{\nu\mu} H \gamma^{\mu 5} \left(\sigma^\dagger \xi^{(n)}_{\mu\nu} \sigma + \sigma \xi^{(n)}_{\mu\nu} \sigma^\dagger \right) \right] \right\} , \\
& a^2 \sum_\mu \left\{ \mathrm{Tr}\left[\overline{H} \gamma_{5\mu} \xi_{\nu\mu} H \gamma^{\mu} \left(\sigma^\dagger \xi^{(n)}_{\mu\nu} \sigma - \sigma \xi^{(n)}_{\mu\nu} \sigma^\dagger \right) \right] \right\} ; \qquad (2.118) \\
\left[V_\mu \times T_\mu \right] \quad \to \quad & a^2 \sum_\mu \left\{ v^\mu v_\mu \, \mathrm{Tr}\left[\overline{H} \xi_{\nu\mu} H \left(\sigma^\dagger \xi^{(n)}_{\mu\nu} \sigma + \sigma \xi^{(n)}_{\mu\nu} \sigma^\dagger \right) \right] \right\} , \\
& a^2 \sum_\mu \left\{ v^\mu \, \mathrm{Tr}\left[\overline{H} \xi_{\nu\mu} H \gamma_{\mu 5} \left(\sigma^\dagger \xi^{(n)}_{\mu\nu} \sigma - \sigma \xi^{(n)}_{\mu\nu} \sigma^\dagger \right) \right] \right\} . \qquad (2.119)
\end{aligned}$$

The double-trace terms are:

$$\begin{aligned}
[T_\mu \times A_\mu] \;&\to\; a^2 \sum_\mu \mathrm{Tr}\left(\overline{H}\gamma_{\nu\mu}\xi_{5\mu}H\gamma^{\mu\nu}\right)\left\{\mathrm{Tr}\left(\sigma^\dagger\xi^{(n)}_{\mu 5}\sigma^\dagger\right)+\mathrm{Tr}\left(\sigma\xi^{(n)}_{\mu 5}\sigma\right)\right\}\,, \\
&\quad\; a^2 \sum_\mu \mathrm{Tr}\left(\overline{H}\gamma_{\nu\mu}\xi_{5\mu}H\gamma^{\mu\nu}\gamma_5\right)\left\{\mathrm{Tr}\left(\sigma^\dagger\xi^{(n)}_{\mu 5}\sigma^\dagger\right)-\mathrm{Tr}\left(\sigma\xi^{(n)}_{\mu 5}\sigma\right)\right\}\,; \quad (2.120) \\
[T_\mu \times V_\mu] \;&\to\; a^2 \sum_\mu \mathrm{Tr}\left(\overline{H}\gamma_{\nu\mu}\xi_{\mu}H\gamma^{\mu\nu}\right)\left\{\mathrm{Tr}\left(\sigma^\dagger\xi^{(n)}_{\mu}\sigma^\dagger\right)+\mathrm{Tr}\left(\sigma\xi^{(n)}_{\mu}\sigma\right)\right\}\,, \\
&\quad\; a^2 \sum_\mu \mathrm{Tr}\left(\overline{H}\gamma_{\nu\mu}\xi_{\mu}H\gamma^{\mu\nu}\gamma_5\right)\left\{\mathrm{Tr}\left(\sigma^\dagger\xi^{(n)}_{\mu}\sigma^\dagger\right)-\mathrm{Tr}\left(\sigma\xi^{(n)}_{\mu}\sigma\right)\right\}\,; \quad (2.121) \\
[A_\mu \times T_\mu] \;&\to\; 0\,, \quad (2.122) \\
[V_\mu \times T_\mu] \;&\to\; 0\,. \quad (2.123)
\end{aligned}$$

The Lagrangian terms $\mathcal{L}^{A2}_{2,a^2}$ and $\mathcal{L}^{B2}_{2,a^2}$, Eq. (2.7), collect the (heavy-quark taste violating) chiral operators that we have derived so far. To make the notation a bit more compact, we first define the operators:

$$\begin{aligned}
P^\pm_5 &= \frac{1}{2}(\sigma\xi^{(n)}_5\sigma^\dagger \pm \text{p.c.}), \\
P^\pm_{\mu\nu} &= \frac{1}{2}(\sigma\xi^{(n)}_{\mu\nu}\sigma^\dagger \pm \text{p.c.}), \\
P^\pm_{\mu} &= \frac{1}{2}(\sigma\xi^{(n)}_{\mu}\sigma \pm \text{p.c.}), \\
P^\pm_{\mu 5} &= \frac{1}{2}(\sigma\xi^{(n)}_{\mu 5}\sigma \pm \text{p.c.})\,. \quad (2.124)
\end{aligned}$$

We then have

$$\begin{aligned}
\mathcal{L}^{A2}_{2,a^2} \;=\; a^2\Big\{ & K^{A2}_{1,0}\,\mathrm{Tr}\left(\overline{H}H\right) + K^{A2}_{1,1}\,\mathrm{Tr}\left(\overline{H}\xi_5 H P^+_5\right) + K^{A2}_{1,2}\,\mathrm{Tr}\left(\overline{H}\xi_\mu H P^+_\mu\right) \\
& + K^{A2}_{1,3}\,\mathrm{Tr}\left(\overline{H}\xi_{5\mu}H P^+_{\mu 5}\right) + K^{A2}_{1,4}\,\mathrm{Tr}\left(\overline{H}\xi_{\mu\nu}H P^+_{\nu\mu}\right) + K^{A2}_{1,5}\,\mathrm{Tr}\left(\overline{H}\gamma_{5\mu}H\gamma^{\mu 5}\right) \\
& + K^{A2}_{1,6}\,\mathrm{Tr}\left(\overline{H}\gamma_{5\mu}\xi_5 H\gamma^{\mu 5}P^+_5\right) + K^{A2}_{1,7}\,\mathrm{Tr}\left(\overline{H}\gamma_{\mu\nu}\xi_\lambda H\gamma^{\nu\mu}P^+_\lambda\right) \\
& + K^{A2}_{1,8}\,\mathrm{Tr}\left(\overline{H}\gamma_{\mu\nu}\xi_{5\lambda}H\gamma^{\nu\mu}P^+_{\lambda 5}\right) + K^{A2}_{1,9}\,\mathrm{Tr}\left(\overline{H}\gamma_{5\mu}\xi_{\nu\lambda}H\gamma^{\mu 5}P^+_{\lambda\nu}\right) \quad (2.125) \\
& + K^{A2}_{2,1}\,\mathrm{Tr}\left(\overline{H}\xi_\mu H\right)\mathrm{Tr}\left(P^+_\mu\right) + K^{A2}_{2,2}\,\mathrm{Tr}\left(\overline{H}\xi_{5\mu}H\right)\mathrm{Tr}\left(P^+_{\mu 5}\right) \\
& + K^{A2}_{2,3}\,\mathrm{Tr}\left(\overline{H}\gamma_{\mu\nu}\xi_\lambda H\gamma^{\nu\mu}\right)\mathrm{Tr}\left(P^+_\lambda\right) + K^{A2}_{2,4}\,\mathrm{Tr}\left(\overline{H}\gamma_{\mu\nu}\xi_{5\lambda}H\gamma^{\nu\mu}\right)\mathrm{Tr}\left(P^+_{\lambda 5}\right)\Big\}\,,
\end{aligned}$$

where ten terms are single-trace and four are double-trace. For completeness we have kept the trivial term $a^2K^{A2}_{1,0}\,\mathrm{Tr}\left(\overline{H}H\right)$ even though it does not break any symmetries and just gives equal mass shifts to all tastes of pseudoscalar and vector heavy-light mesons. In fact, this term also

would appear in $\mathcal{L}^{A1}_{2,a^2}$ but was dropped from Ref. [25] due to its triviality. It is worth mentioning that the terms breaking the spin symmetry by $\gamma_{\mu\nu}$ in Eq. (2.125) can be replaced with simpler terms using the following identity:

$$\overline{H}\gamma_{\mu\nu}T_\Xi H\gamma^{\nu\mu} = \overline{H}\gamma_5\gamma_{\mu\nu}T_\Xi H\gamma_5\gamma^{\nu\mu} = -2\overline{H}\gamma_{5\rho}T_\Xi H\gamma^{\rho 5}, \tag{2.126}$$

where the first equality follows from the fact that the γ_5 factors just interchange the components of $\gamma_{\mu\nu}$, and the second can be proved using Eqs. (2.79), (2.80) and (2.82).

For $\mathcal{L}^{B2}_{2,a^2}$ we have

$$\begin{aligned}
\mathcal{L}^{B2}_{2,a^2} \;=\; & a^2\sum_\mu\Big\{ K^{B2}_{1,1}\,\mathrm{Tr}\left(\overline{H}\gamma_{\nu\mu}\xi_\mu H\gamma^{\mu\nu}P^+_\mu\right) + K^{B2}_{1,2}\,\mathrm{Tr}\left(\overline{H}\gamma_{\nu\mu}\xi_{5\mu}H\gamma^{\mu\nu}P^+_{\mu 5}\right) \\
& + K^{B2}_{1,3}v^\mu v_\mu\,\mathrm{Tr}\left(\overline{H}\xi_{\nu\mu}HP^+_{\mu\nu}\right) + K^{B2}_{1,4}\,\mathrm{Tr}\left(\overline{H}\gamma_{5\mu}\xi_{\nu\mu}H\gamma^{\mu 5}P^+_{\mu\nu}\right) \\
& + K^{B2}_{1,5}\,\mathrm{Tr}\left(\overline{H}\gamma_{\nu\mu}\xi_\mu H\gamma^{\mu\nu}\gamma_5P^-_\mu\right) + K^{B2}_{1,6}\,\mathrm{Tr}\left(\overline{H}\gamma_{\nu\mu}\xi_{5\mu}H\gamma^{\mu\nu}\gamma_5P^-_{\mu 5}\right) \\
& + K^{B2}_{1,7}v^\mu\,\mathrm{Tr}\left(\overline{H}\xi_{\nu\mu}H\gamma_{\mu 5}P^-_{\mu\nu}\right) + K^{B2}_{1,8}v^\mu\,\mathrm{Tr}\left(\overline{H}\gamma_{5\mu}\xi_{\nu\mu}HP^-_{\mu\nu}\right) \\
& + K^{B2}_{2,1}\,\mathrm{Tr}\left(\overline{H}\gamma_{\nu\mu}\xi_\mu H\gamma^{\mu\nu}\right)\mathrm{Tr}\left(P^+_\mu\right) + K^{B2}_{2,2}\,\mathrm{Tr}\left(\overline{H}\gamma_{\nu\mu}\xi_{5\mu}H\gamma^{\mu\nu}\right)\mathrm{Tr}\left(P^+_{\mu 5}\right) \\
& + K^{B2}_{2,3}\,\mathrm{Tr}\left(\overline{H}\gamma_{\nu\mu}\xi_\mu H\gamma^{\mu\nu}\gamma_5\right)\mathrm{Tr}\left(P^-_\mu\right) + K^{B2}_{2,4}\,\mathrm{Tr}\left(\overline{H}\gamma_{\nu\mu}\xi_{5\mu}H\gamma^{\mu\nu}\gamma_5\right)\mathrm{Tr}\left(P^-_{\mu 5}\right)\Big\}\,.
\end{aligned} \tag{2.127}$$

where eight terms are single-trace and four are double-trace.

There are a large number of terms contributing to the remaining NLO parts of the Lagrangian, $\mathcal{L}^{A2}_{3,a^2}$ and $\mathcal{L}^{B2}_{3,a^2}$. An extra derivative, either in the form of the covariant derivative D_ν or the axial current $\mathbb{A}_\nu$, can be added to the terms in $\mathcal{L}^{A2}_{2,a^2}$ and $\mathcal{L}^{B2}_{2,a^2}$ in many ways when one takes into account the ordering of terms and the various possibilities for contracting indices. Faced with this explosion of terms, we content ourselves with listing some representative contributions. For all practical applications at NLO that we can envision, this will be sufficient, since in a lattice computation of some physical quantity one is only interested in knowing what analytic terms are possible, and whether the coefficients of these terms are linearly dependent or independent, and not in knowing how to write those coefficients as combinations of the low energy constants in the chiral Lagrangian. This is the case for the heavy-light decay constant, discussed in Sec. 2.5. For the NLO taste splittings of the masses of heavy-light mesons, treated Sec. 2.4, the quantities $\mathcal{L}^{A2}_{3,a^2}$ and $\mathcal{L}^{B2}_{3,a^2}$ are in fact irrelevant, because they either have an extra factor of the residual momentum k, which vanishes on shell at this order, or because they have an extra pion field at tree level.

Some representative contributions to $\mathcal{L}^{A2}_{3,a^2}$ are:

$$\begin{aligned}
\mathcal{L}^{A2}_{3,a^2} \;=\; & a^2\Bigg\{\Bigg[ic^{A2}_{1,0}\,\mathrm{Tr}\left(\overline{H}Hv\cdot\overleftarrow{D}-v\cdot\overrightarrow{D}\,\overline{H}H\right)+\cdots \\
& +ic^{A2}_{1,9}\,\mathrm{Tr}\left(\overline{H}\gamma_{5\mu}\xi_{\nu\lambda}H\gamma^{\mu 5}v\cdot\overleftarrow{D}\,P^+_{\lambda\nu}-v\cdot\overrightarrow{D}\,\overline{H}\gamma_{5\mu}\xi_{\nu\lambda}H\gamma^{\mu 5}P^+_{\lambda\nu}\right)\Bigg] \\
& +\Bigg[ic^{A2}_{2,1}\,\mathrm{Tr}\left(\overline{H}\xi_\mu Hv\cdot\overleftarrow{D}\,-v\cdot\overrightarrow{D}\,\overline{H}\xi_\mu H\right)\mathrm{Tr}\left(P^+_\mu\right)+\cdots \\
& +ic^{A2}_{2,4}\,\mathrm{Tr}\left(\overline{H}\gamma_{\mu\nu}\xi_{5\lambda}H\gamma^{\nu\mu}v\cdot\overleftarrow{D}\,-v\cdot\overrightarrow{D}\,\overline{H}\gamma_{\mu\nu}\xi_{5\lambda}H\gamma^{\nu\mu}\right)\mathrm{Tr}\left(P^+_{\lambda 5}\right)\Bigg] \\
& +\Bigg[c^{A2}_{3,0}\,\mathrm{Tr}\left(\overline{H}H\gamma_\sigma\gamma_5\mathbb{A}^\sigma\right)+\cdots+c^{A2}_{3,9}\,\mathrm{Tr}\left(\overline{H}\gamma_{5\mu}\xi_{\nu\lambda}H\gamma^{\mu 5}\gamma_\sigma\gamma_5\{\mathbb{A}^\sigma,P^+_{\lambda\nu}\}\right)\Bigg] \\
& +\Bigg[c^{A2}_{4,1}\,\mathrm{Tr}\left(\overline{H}\xi_\mu H\gamma_\sigma\gamma_5\mathbb{A}^\sigma\right)\mathrm{Tr}\left(P^+_\mu\right)+\cdots+c^{A2}_{4,4}\,\mathrm{Tr}\left(\overline{H}\gamma_{\mu\nu}\xi_{5\lambda}H\gamma^{\nu\mu}\gamma_\sigma\gamma_5\mathbb{A}^\sigma\right)\mathrm{Tr}\left(P^+_{\lambda 5}\right)\Bigg] \\
& +\Bigg[c^{A2}_{5,1}\,\mathrm{Tr}\left(\overline{H}\xi_5 H\gamma_\sigma\gamma_5\right)\mathrm{Tr}\left(\mathbb{A}^\sigma P^+_5\right)+\cdots+c^{A2}_{5,9}\,\mathrm{Tr}\left(\overline{H}\gamma_{5\mu}\xi_{\nu\lambda}H\gamma^{\mu 5}\gamma_\sigma\gamma_5\right)\mathrm{Tr}\left(\mathbb{A}^\sigma P^+_{\lambda\nu}\right)\Bigg] \\
& +\Bigg[c^{A2}_{6,1}\,\mathrm{Tr}\left(\overline{H}\xi_5 H\gamma_\sigma\gamma_5[\mathbb{A}^\sigma,P^-_5]\right)+\cdots+c^{A2}_{6,9}\,\mathrm{Tr}\left(\overline{H}\gamma_{5\mu}\xi_{\nu\lambda}H\gamma^{\mu 5}\gamma_\sigma\gamma_5[\mathbb{A}^\sigma,P^-_{\lambda\nu}]\right)\Bigg] \\
& +\cdots\Bigg\}\,. \qquad (2.128)
\end{aligned}$$

The expressions inside of each square bracket are constructed by adding a derivative-containing factor in the same way to each of the single-trace or the double-trace terms of Eq. (2.125), so the ellipses in the square brackets may easily be filled in if desired. On the other hand, the final ellipsis in Eq. (2.128) represents entirely new terms in which the operators breaking the heavy-quark spin symmetry are contracted with $\mathbb{A}^\mu$ or D^μ. An example is

$$\mathrm{Tr}\left(\overline{H}\gamma_{5\mu}\xi_{\nu\lambda}H\{\mathbb{A}^\mu,P^+_{\lambda\nu}\}\right)\;. \qquad (2.129)$$

Similarly, for $\mathcal{L}^{B2}_{3,a^2}$ we have:

$$\begin{aligned}
\mathcal{L}^{B2}_{3,a^2} \;=\; a^2 \sum_\mu \Bigg\{ & \left[ic^{B2}_{1,1} \,\mathrm{Tr}\left(\overline{H}\gamma_{\nu\mu}\xi_\mu H v\cdot\overleftarrow{D}\,\gamma^{\mu\nu} P^+_\mu - v\cdot\overrightarrow{D}\,\overline{H}\gamma_{\nu\mu}\xi_\mu H\gamma^{\mu\nu}P^+_\mu \right) + \cdots \right] \\
& + \left[ic^{B2}_{2,1} \,\mathrm{Tr}\left(\overline{H}\gamma_{\nu\mu}\xi_\mu H v\cdot\overleftarrow{D}\,\gamma^{\mu\nu} - v\cdot\overrightarrow{D}\,\overline{H}\gamma_{\nu\mu}\xi_\mu H\gamma^{\mu\nu} \right) \mathrm{Tr}\left(P^+_\mu \right) + \cdots \right] \\
& + \left[c^{B2}_{3,1} \,\mathrm{Tr}\left(\overline{H}\gamma_{\nu\mu}\xi_\mu H\gamma^{\mu\nu}\gamma_\sigma\gamma_5 \{\mathbb{A}^\sigma, P^+_\mu\} \right) + \cdots \right] \\
& + \left[c^{B2}_{4,1} \,\mathrm{Tr}\left(\overline{H}\gamma_{\nu\mu}\xi_\mu H\gamma^{\mu\nu}\gamma_\sigma\gamma_5 \mathbb{A}^\sigma \right) \mathrm{Tr}\left(P^+_\mu \right) + \cdots \right] \\
& + \left[c^{B2}_{5,1} \,\mathrm{Tr}\left(\overline{H}\gamma_{\nu\mu}\xi_\mu H\gamma^{\mu\nu}\gamma_\sigma\gamma_5 \right) \mathrm{Tr}\left(\mathbb{A}^\sigma P^+_5 \right) + \cdots \right] \\
& + \left[c^{A2}_{6,1} \,\mathrm{Tr}\left(\overline{H}\gamma_{\nu\mu}\xi_\mu H\gamma^{\mu\nu}\gamma_\sigma\gamma_5 [\mathbb{A}^\sigma, P^-_5] \right) + \cdots \right] \\
& + \cdots \Bigg\} \,. \qquad (2.130)
\end{aligned}$$

The case of the type-A contributions to the current, $j^{\mu,i\Xi}_{2,a^2,A2}$, is more straightforward, since we need only insert the heavy-quark and light-quark spurions, without any additional derivatives, and Lorentz invariance is not broken. Still, there are many terms, since parity places no restrictions on the low energy constants in the left-handed current, but merely relates them to those of the right-handed current. Further, many of the simplifying relations, Eqs. (2.78) through (2.83), have no counterpart in the current, where there is only a single heavy-meson

field. We therefore again only give some representative terms:

$$
\begin{aligned}
j^{\mu,i\Xi}_{2,a^2,A2} \;=\; a^2\Bigg\{ & r^{A2}_{0,0}\,\mathrm{tr}_{D,t}\left(\tfrac{1}{2}T_\Xi\gamma^\mu(1-\gamma_5)H\sigma^\dagger\lambda^{(i)}\right) + r^{A2}_{0,1}\,\mathrm{tr}_{D,t}\left(\tfrac{1}{2}T_\Xi\gamma^\mu(1-\gamma_5)\gamma_\nu H\gamma^\nu\sigma^\dagger\lambda^{(i)}\right) \\
& + r^{A2}_{1,1}\,\mathrm{tr}_{D,t}\left(\tfrac{1}{2}T_\Xi\gamma^\mu(1-\gamma_5)\xi_5 HP^+_5\sigma^\dagger\lambda^{(i)}\right) + r^{A2}_{1,2}\,\mathrm{tr}_{D,t}\left(\tfrac{1}{2}T_\Xi\gamma^\mu(1-\gamma_5)\xi_\rho HP^+_\rho\sigma^\dagger\lambda^{(i)}\right) \\
& + r^{A2}_{1,3}\,\mathrm{tr}_{D,t}\left(\tfrac{1}{2}T_\Xi\gamma^\mu(1-\gamma_5)\xi_{5\rho} HP^+_{\rho 5}\sigma^\dagger\lambda^{(i)}\right) + r^{A2}_{1,4}\,\mathrm{tr}_{D,t}\left(\tfrac{1}{2}T_\Xi\gamma^\mu(1-\gamma_5)\xi_{\beta\rho} HP^+_{\rho\beta}\sigma^\dagger\lambda^{(i)}\right) \\
& + r^{A2}_{1,5}\,\mathrm{tr}_{D,t}\left(\tfrac{1}{2}T_\Xi\gamma^\mu(1-\gamma_5)\gamma_\nu\xi_5 H\gamma^\nu P^+_5\sigma^\dagger\lambda^{(i)}\right) \\
& + r^{A2}_{1,6}\,\mathrm{tr}_{D,t}\left(\tfrac{1}{2}T_\Xi\gamma^\mu(1-\gamma_5)\gamma_{\nu\beta}\xi_\rho H\gamma^\beta v^\nu P^+_\rho\sigma^\dagger\lambda^{(i)}\right) \\
& + r^{A2}_{1,7}\,\mathrm{tr}_{D,t}\left(\tfrac{1}{2}T_\Xi\gamma^\mu(1-\gamma_5)\gamma_{\nu\beta}\xi_{5\rho} H\gamma^\beta v^\nu P^+_{\rho 5}\sigma^\dagger\lambda^{(i)}\right) \\
& + r^{A2}_{1,8}\,\mathrm{tr}_{D,t}\left(\tfrac{1}{2}T_\Xi\gamma^\mu(1-\gamma_5)\gamma_\nu\xi_{\beta\rho} H\gamma^\nu P^+_{\rho\beta}\sigma^\dagger\lambda^{(i)}\right) \\
& + r^{A2}_{2,1}\,\mathrm{tr}_{D,t}\left(\tfrac{1}{2}T_\Xi\gamma^\mu(1-\gamma_5)\xi_\rho H\sigma^\dagger\lambda^{(i)}\right)\mathrm{Tr}\left(P^+_\rho\right) + \cdots \\
& + r^{A2}_{3,1}\,\mathrm{tr}_{D,t}\left(\tfrac{1}{2}T_\Xi\gamma^\mu(1-\gamma_5)\xi_5 HP^-_5\sigma^\dagger\lambda^{(i)}\right) + \cdots \\
& + r^{A2}_{4,1}\,\mathrm{tr}_{D,t}\left(\tfrac{1}{2}T_\Xi\gamma^\mu(1-\gamma_5)\xi_\rho H\sigma^\dagger\lambda^{(i)}\right)\mathrm{Tr}\left(P^-_\rho\right) + \cdots\Bigg\}\,. \qquad (2.131)
\end{aligned}
$$

Here we have divided the terms into five sub-classes: terms with no $P^\pm$ factors, single traces with P^+, double traces with P^+, single traces with P^-, and double traces with P^-. The terms with no factors of $P^\pm$ (coefficients $r^{A2}_{0,0}$ and $r^{A2}_{0,1}$) are rather trivial and break no taste symmetries, although the second does break heavy-quark spin symmetry. The ellipses in Eq. (2.131) may easily be filled based on the terms of the sub-class of single traces with P^+. In deriving Eq. (2.131) we have used the fact that a factor of γ_5 before or after the H field has no (nontrivial) effect, due to the presence of the left projector, $(1-\gamma_5)$. Thus, for example, terms generated by $[A\times S]$, $[A\times P]$, and $[A\times T]$ are identical to those from $[V\times S]$, $[V\times P]$, $[V\times T]$, respectively.

As we will see more explicitly in the discussion of $j^{\mu,i\Xi}_{2,a^2,B2}$ that follows, the Lorentz structures that follow H in Eq. (2.131) are not fixed by the spurions, but can be any combination of the available four-vectors γ^α and v^λ consistent with Lorentz invariance. For example, the factor $\gamma^\beta v^\nu$ following H in the $r^{A2}_{1,6}$ term, could also in principle be replaced by $\gamma^{\beta\nu}$. However, such a term would vanish due to the identity $\gamma^{\beta\nu}\gamma^\mu\gamma_{\nu\beta}=0$.

Finally we turn to the type-B contributions to the current, $j^{\mu,i\Xi}_{2,a^2,B2}$. The reasoning is very similar in principle to that for the type-B Lagrangian, but the presence of an additional Lorentz index in the current increases the complexity, so we describe some of the details. Up to this point, we have not explicitly employed a formal spurion analysis for the current, but it now

becomes necessary. At the SET/HQET level, the left-handed current is

$$j^{\mu,i\Xi} = \bar{q}\big(\lambda^{(i)}\ \tfrac{1}{2}T^{\Xi}\gamma^{\mu}(1-\gamma_5)\big)Q = \bar{q}\big(F(\mu)\otimes E\big)Q\ , \tag{2.132}$$

where we have introduced a taste spurion E and a spin spurion $F(\mu)$. They transform as

$$E \ \to\ LEV^{\dagger}, \qquad [\Rightarrow\ \sigma^{\dagger}E \to \mathbb{U}\sigma^{\dagger}EV^{\dagger}]\ , \tag{2.133}$$

$$F(\mu) \ \to\ F(\mu)S^{\dagger}\ , \tag{2.134}$$

and ultimately take the values

$$E \ =\ \lambda^{(i)}\ \tfrac{1}{2}T^{\Xi}\ , \tag{2.135}$$

$$F(\mu) \ =\ \gamma^{\mu}(1-\gamma_5)\ . \tag{2.136}$$

For an example, we again take the $[T_\mu \times A_\mu]$ type-B operator, and introduce spurions for it as in Eq. (2.112), except we replace the index μ there with ν (and ν with β) so as not to conflict with the index of the current. The terms we seek are trilinear in the spurions $F(\mu)\otimes E$, $B(\beta,\nu)\otimes C(\nu)$, and either $A_1(\nu)$ or $A_2(\nu)$. Since parity does not constrain the terms in the current, we use just $A_1(\nu)$ in this example. Demanding heavy and light taste symmetry and heavy-quark spin symmetry, a possible chiral operator has the form

$$\mathrm{tr}_{D,t}\Big\{\big(F(\mu)\otimes\sigma^{\dagger}E\big)\big(B(\beta,\nu)\otimes C(\nu)\big)H\Gamma\sigma^{\dagger}A_1(\nu)\sigma^{\dagger}\Big\}\ , \tag{2.137}$$

where μ, ν, and β are fixed, and Γ is some combination of components of γ matrices and of v, to be determined.

After replacing the spin spurions $F(\mu)$ and $B(\beta,\nu)$ with their values, and reintroducing the sum over β, the current becomes the $^{\mu}$ component of a Lorentz vector, and the 4-quark operator becomes the $_{\nu}{}^{\nu}$ component of a symmetric two-index tensor. As before, we may take the latter to be traceless. At the SET level, call the three-index tensor coming from the product of the two representations X. As worked out in Appendix C, the element $X^{\mu}{}_{\nu}{}^{\nu}$ is a linear combination of elements of three irreducible representations: a completely symmetric traceless three-index tensor (S), a three-index tensor with mixed symmetry (A), and a vector (W). From Lorentz symmetry alone, the chiral operators for each of these three representations could have independent LECs. Fixing the spin spurions in Eq. (2.137), however, tells us that

the corresponding chiral operator is required by spin symmetry to have the form

$$\tilde{X}^{\mu}{}_{\nu}{}^{\nu} = \mathrm{tr}_{D,t}\left\{\sigma^{\dagger}E\gamma^{\mu}(1-\gamma_5)\gamma_{\beta\nu}C(\nu)H\,\Gamma^{\nu\beta}\sigma^{\dagger}A_1(\nu)\sigma^{\dagger}\right\}\ , \tag{2.138}$$

with an implicit sum over β, but not over ν. Given a choice for $\Gamma^{\nu\beta}$ (for example, $v^{\nu}v^{\beta}$), the corresponding elements of the individual representations at the chiral level, $\tilde{S}^{\mu}{}_{\nu}{}^{\nu}$, $\tilde{A}^{\mu}{}_{\nu}{}^{\nu}$, and $\tilde{W}^{\mu}$, which are formed by permuting indices and taking traces of $\tilde{X}$, will not in general have the form of Eq. (2.138) unless the properties of H and the Dirac trace conspire to allow them to be rewritten in that form. We have checked that, for the four possible choices for $\Gamma^{\nu\beta}$ ($\gamma^{\nu}\gamma^{\beta}$, $\gamma^{\nu}v^{\beta}$, $v^{\nu}\gamma^{\beta}$, and $v^{\nu}v^{\beta}$), the generic situation obtains.[4] Thus the relative normalization of the LECs of the individual representations are fixed to be the same as in Eq. (C.7), and $\tilde{X}^{\mu}{}_{\nu}{}^{\nu}$ is the only possible chiral operator. Setting the remaining spurions to their fixed values, and restoring the sum over ν, then gives the final chiral operators. For the choice $\Gamma^{\nu\beta} = \gamma^{\nu}\gamma^{\beta}$, we find the operators

$$\mathrm{tr}_{D,t}\left\{\tfrac{1}{2}T_{\Xi}\gamma^{\mu}(1-\gamma_5)\gamma_{\nu\beta}\xi_{5\nu}H\gamma^{\beta\nu}P^{\pm}_{\nu 5}\sigma^{\dagger}\lambda^{(i)}\right\}\ , \tag{2.139}$$

where $P^{\pm}_{\nu 5}$ arises from the sum and difference of Eq. (2.138) with the corresponding operator after the replacement $A_1(\nu) \to A_2(\nu)$.

Following this procedure for other heavy-light terms in the SET, we then have

$$\begin{aligned}
j^{\mu,i\Xi}_{2,a^2,B2} \;=\; a^2\sum_{\nu}\Bigg\{ & r^{B2}_{1,1}\,\mathrm{tr}_{D,t}\left(\tfrac{1}{2}T_{\Xi}\gamma^{\mu}(1-\gamma_5)\gamma_{\nu\beta}\xi_{\nu}H\gamma^{\beta\nu}P^{+}_{\nu}\sigma^{\dagger}\lambda^{(i)}\right)\\
& + r^{B2}_{1,2}\,\mathrm{tr}_{D,t}\left(\tfrac{1}{2}T_{\Xi}\gamma^{\mu}(1-\gamma_5)\gamma_{\nu\beta}\xi_{5\nu}H\gamma^{\beta\nu}P^{+}_{\nu 5}\sigma^{\dagger}\lambda^{(i)}\right)\\
& + r^{A2}_{1,3}\,\mathrm{tr}_{D,t}\left(\tfrac{1}{2}T_{\Xi}\gamma^{\mu}(1-\gamma_5)\gamma_{\nu}\xi_{\nu\rho}H\gamma^{\nu}P^{+}_{\rho\nu}\sigma^{\dagger}\lambda^{(i)}\right)\\
& + r^{A2}_{1,4}\,\mathrm{tr}_{D,t}\left(\tfrac{1}{2}T_{\Xi}\gamma^{\mu}(1-\gamma_5)\gamma_{\nu}\xi_{\nu\rho}Hv^{\nu}P^{+}_{\rho\nu}\sigma^{\dagger}\lambda^{(i)}\right)+\cdots\\
& + r^{B2}_{2,1}\,\mathrm{tr}_{D,t}\left(\tfrac{1}{2}T_{\Xi}\gamma^{\mu}(1-\gamma_5)\gamma_{\nu\beta}\xi_{\nu}H\gamma^{\beta\nu}\sigma^{\dagger}\lambda^{(i)}\right)\mathrm{Tr}\left(P^{+}_{\nu}\right)+\cdots\\
& + r^{B2}_{3,1}\,\mathrm{tr}_{D,t}\left(\tfrac{1}{2}T_{\Xi}\gamma^{\mu}(1-\gamma_5)\gamma_{\nu\beta}\xi_{\nu}H\gamma^{\beta\nu}P^{-}_{\nu}\sigma^{\dagger}\lambda^{(i)}\right)+\cdots\\
& + r^{B2}_{4,1}\,\mathrm{tr}_{D,t}\left(\tfrac{1}{2}T_{\Xi}\gamma^{\mu}(1-\gamma_5)\gamma_{\nu\beta}\xi_{\nu}H\gamma^{\beta\nu}\sigma^{\dagger}\lambda^{(i)}\right)\mathrm{Tr}\left(P^{-}_{\nu}\right)+\cdots\Bigg\}\ ,
\end{aligned} \tag{2.140}$$

where again we have not written the complete set of contributions, but only some representative terms.

[4] Note that the trivial choice $\Gamma^{\nu\beta} = \delta^{\nu\beta}$ vanishes after the trace on $\nu = \beta$ is subtracted, so only a type-A chiral operator can be formed in that way.

One can use a similar spurion analysis to check the type-B contributions to the current coming from the light-light four-quark operators, Eq. (2.62). In that case, the only Dirac matrix coming before the H field is the $\gamma^\mu(1-\gamma_5)$ spin spurion from the current, and the matrix corresponding to $\Gamma^{\nu\beta}$ after H is simply the ${}_\nu{}^\nu$ component of a two-index symmetric, traceless tensor. The choices $v_\nu v^\nu$ and $v_\nu\gamma^\nu$ for this matrix ($\gamma_\nu\gamma^\nu$ is clearly trivial) give the terms in Eq. (2.62). The incorrect additional terms listed in Ref. [25] came from ignoring the consequences of heavy-quark spin symmetry, and using Lorentz-symmetry considerations only.

This completes the discussion of the effects of light-heavy terms in the SET, Eq. (2.45). There are still the heavy-heavy terms, Eq. (2.46) to consider. However, it is now easy to see that the heavy-heavy terms do not produce any new nontrivial chiral operators in the Lagrangian or current. These 4-quark operators contain two heavy-quark spurions, and no light-quark spurions. Since the heavy-quark spurions transform on both sides with heavy-quark spin matrices and heavy-quark taste matrices, they both must be placed between the $\overline{H}$ and H fields in the Lagrangian. One then just gets the product of the two spurions, which is proportional to the identity. So the heavy-heavy 4-quark operators in the SET lead simply to trivial chiral Lagrangian operators, which are already present as the first operators in Eqs. (2.125) and (2.128). For the same reason, they lead to a trivial current operator, $a^2\mathrm{tr}_{D,t}\left(\frac{1}{2}T_\Xi\gamma^\mu(1-\gamma_5)H\sigma^\dagger\lambda^{(i)}\right)$, which does not break any symmetries and just adds a constant term proportional to a^2 to any LO matrix element.

2.4 Taste splittings of heavy-light meson masses

In this section, we calculate the mass splitting between heavy-light mesons of different tastes in terms of the low energy constants in the chiral Lagrangian. With reasonable assumptions about which operators give dominant effects, we are able to explain the observed pattern of taste splittings.

We first show that the one-loop diagrams give taste-invariant masses to the heavy-light mesons, even though the diagrams contain pion propagators, which break taste symmetry. Taste-independence of one-loop chiral logs follows from the exact $SU(4)$ taste symmetry of the heavy quark at LO in the chiral theory, as well as the shift symmetry of the staggered action [42]. The latter can be represented at the SET and chiral levels as an exact, discrete taste symmetry that

acts jointly on both heavy and light quarks [43]. This symmetry is

$$q_i \to (I \otimes \xi_\nu) q_i \,, \qquad \bar{q}_i \to \bar{q}_i (I \otimes \xi_\nu) \,, \tag{2.141}$$

$$Q \to (I \otimes \xi_\nu) Q \,, \qquad \bar{Q} \to \bar{Q} (I \otimes \xi_\nu) \,, \tag{2.142}$$

at the level of the Symanzik action, and

$$\begin{aligned} \Sigma &\to \xi_\nu^{(n)} \Sigma \xi_\nu^{(n)} \,, \\ \sigma &\to \xi_\nu^{(n)} \sigma \xi_\nu^{(n)} \,, \\ H &\to \xi_\nu H \xi_\nu^{(n)} \,, \\ \overline{H} &\to \xi_\nu^{(n)} \overline{H} \xi_\nu \,, \end{aligned} \tag{2.143}$$

at the chiral level. Note that the symmetry is diagonal in flavor; the transformation acts only on the taste indices and affects all light quark flavors, as well as the heavy quark, identically.

Using the $SU(4)$ heavy-quark taste symmetry of the LO Lagrangian, one can undo the action of the discrete taste symmetry on the heavy quark. Taking $V = \xi_\nu$ in Eq. (2.25), we have the following symmetry of the LO Lagrangian:

$$\begin{aligned} \Sigma &\to \xi_\nu^{(n)} \Sigma \xi_\nu^{(n)} \,, \\ \sigma &\to \xi_\nu^{(n)} \sigma \xi_\nu^{(n)} \,, \\ H &\to H \xi_\nu^{(n)} \,, \\ \overline{H} &\to \xi_\nu^{(n)} \overline{H} \,, \end{aligned} \tag{2.144}$$

We call this symmetry *light-quark discrete taste symmetry*. In applying it, it is convenient to think of H in the way described above Eq. (2.27), as a light flavor vector (index i) with components that are 4×4 taste matrices

$$H_i^{\alpha\beta} = \sum_{\Xi=1}^{16} \tfrac{1}{2} T_\Xi^{\alpha\beta} \, H_{i\Xi} \quad . \tag{2.145}$$

Here α and β are the heavy and light quark tastes, respectively.

We can now show that the heavy-light meson propagator is taste invariant if the $SU(4)$ heavy-quark taste symmetry is exact. This implies that the one-loop diagrams for the propagator are taste invariant, since they use LO propagators and vertices. Consider the propagator

$$\langle 0 | H_i^{\alpha\beta}(x) \overline{H}_j^{\beta'\alpha'}(y) | 0 \rangle \equiv \delta_{ij} K^{\alpha\alpha'}(\beta, \beta', x, y, i) \,, \tag{2.146}$$

where we have used flavor conservation. Then the heavy taste symmetry implies

$$K^{\alpha\alpha'} = (VKV^\dagger)^{\alpha\alpha'} \tag{2.147}$$

for any $SU(4)$ taste transformation V. Thus K is proportional to the identity, which gives

$$\langle 0|H_i^{\alpha\beta}(x)\overline{H}_j^{\beta'\alpha'}(y)|0\rangle \equiv \delta_{ij}\delta^{\alpha\alpha'}G^{\beta'\beta}(x,y,i) = \delta_{ij}\delta^{\alpha\alpha'}\sum_{\Xi=1}^{16}\tfrac{1}{2}T_\Xi^{\beta'\beta}\,g_\Xi(x,y,i)\ , \tag{2.148}$$

where we have defined (equivalent) new functions $G^{\beta'\beta}$ and g_Ξ. Light-quark discrete taste symmetry, Eq. (2.144), implies

$$\sum_{\Xi=1}^{16} T_\Xi\, g_\Xi(x,y,i) = \sum_{\Xi=1}^{16}\xi_\nu T_\Xi \xi_\nu\, g_\Xi(x,y,i)\ . \tag{2.149}$$

Each T_Ξ has a unique signature of four signs determined by whether $\xi_\nu T_\Xi \xi_\nu$ is $+T_\Xi$ or $-T_\Xi$, for $\nu = 1,\cdots,4$. Clearly only $T_\Xi = I$ has signature $(+,+,+,+)$. One may then conclude from Eq. (2.149) that $g_\Xi = 0$ for $\Xi \neq I$ and

$$\langle 0|H_i^{\alpha\beta}(x)\overline{H}_j^{\beta'\alpha'}(y)|0\rangle = \tfrac{1}{2}\delta_{ij}\delta^{\alpha\alpha'}\,\delta^{\beta\beta'}g_I(x,y,i)\ . \tag{2.150}$$

Multiplying with $\frac{1}{2}T_\Xi^{\beta\alpha}$ and $\frac{1}{2}T_{\Xi'}^{\alpha'\beta'}$ and summing repeated indices gives the final form

$$\langle 0|H_{i\Xi}(x)\overline{H}_{j\Xi'}(y)|0\rangle = \tfrac{1}{2}\delta_{ij}\delta_{\Xi\Xi'}\,g_I(x,y,i)\ . \tag{2.151}$$

Thus the one-loop heavy-light meson propagator is taste invariant, so the masses (as well as the wave function renormalization) at one-loop are invariant. This means that all taste-violations in the heavy-light masses at NLO come from the NLO terms in the HMrASχPT Lagrangian, treated at tree level, and may be analyzed straightforwardly.

From now on we refer to the heavy-light pseudoscalar meson as a D (not B) meson, because the lattice data from MILC that we show later is for D mesons. To determine the taste splittings in the meson masses, we need only consider the taste-violating NLO Lagrangian terms $\mathcal{L}^{A1}_{2,a^2}$, $\mathcal{L}^{B1}_{2,a^2}$, $\mathcal{L}^{A2}_{2,a^2}$ and $\mathcal{L}^{B2}_{2,a^2}$. Taste-violating terms in $\mathcal{L}_3$ lead only to wave-function renormalization, since the LO pole in the propagator is at residual momentum $k = 0$, and these terms either have an addition factor of k or at least one pion field. Further, one easily sees that $\mathcal{L}^{A1}_{2,a^2}$ and $\mathcal{L}^{B1}_{2,a^2}$, Eqs. (2.51) and (2.56), produce no taste splittings of D mesons because their taste-noninvariant factors, $\mathcal{O}_k^{A1,+}$ and $\mathcal{O}_{\mu,k}^{B1,+}$ [Eqs. (2.53) and (2.57)], either vanish or go to the identity matrix when there are no pion fields at tree level. Thus taste splittings of D meson masses at NLO

(*i.e.*, $\mathcal{O}(a^2)$) come only from the terms that break heavy-quark taste and spin symmetry, namely $\mathcal{L}^{A2}_{2,a^2}$ and $\mathcal{L}^{B2}_{2,a^2}$. From Eqs. (2.125) and (2.127), we can then easily find all the terms that contribute to taste splittings of the D masses at $\mathcal{O}(a^2)$:

$$\begin{aligned}
\delta\mathcal{L}_{m_Q} \;=\; & a^2\Big\{ K^{A2}_{1,1}\,\mathrm{Tr}\left(\overline{H}\xi_5 H\xi_5\right) + K^{A2}_{1,2}\,\mathrm{Tr}\left(\overline{H}\xi_\mu H\xi_\mu\right) \\
& + K^{A2}_{1,3}\,\mathrm{Tr}\left(\overline{H}\xi_{5\mu} H\xi_{\mu 5}\right) + K^{A2}_{1,4}\,\mathrm{Tr}\left(\overline{H}\xi_{\mu\nu} H\xi_{\nu\mu}\right) \\
& + K^{A2}_{1,6}\,\mathrm{Tr}\left(\overline{H}\gamma_{5\mu}\xi_5 H\gamma^{\mu 5}\xi_5\right) + K^{A2}_{1,7}\,\mathrm{Tr}\left(\overline{H}\gamma_{\mu\nu}\xi_\lambda H\gamma^{\nu\mu}\xi_\lambda\right) \\
& + K^{A2}_{1,8}\,\mathrm{Tr}\left(\overline{H}\gamma_{\mu\nu}\xi_{5\lambda} H\gamma^{\nu\mu}\xi_{\lambda 5}\right) + K^{A2}_{1,9}\,\mathrm{Tr}\left(\overline{H}\gamma_{5\mu}\xi_{\nu\lambda} H\gamma^{\mu 5}\xi_{\lambda\nu}\right)\Big\} \\
& + a^2\sum_\mu\Big\{ K^{B2}_{1,1}\,\mathrm{Tr}\left(\overline{H}\gamma_{\nu\mu}\xi_\mu H\gamma^{\mu\nu}\xi_\mu\right) + K^{B2}_{1,2}\,\mathrm{Tr}\left(\overline{H}\gamma_{\nu\mu}\xi_{5\mu} H\gamma^{\mu\nu}\xi_{\mu 5}\right) \\
& + K^{B2}_{1,3} v^\mu v_\mu\,\mathrm{Tr}\left(\overline{H}\xi_{\nu\mu} H\xi_{\mu\nu}\right) + K^{B2}_{1,4}\,\mathrm{Tr}\left(\overline{H}\gamma_{5\mu}\xi_{\nu\mu} H\gamma^{\mu 5}\xi_{\mu\nu}\right)\Big\}\,, \qquad (2.152)
\end{aligned}$$

where we have set the pion fields σ and $\sigma^\dagger$ to the identity. The sum of the mass contributions from these terms has the form

$$\delta\mathcal{L}_{m_Q} = -\sum_\Xi D^\dagger_\Xi D_\Xi \triangle_{m_Q}(T_\Xi) + \cdots\,, \qquad (2.153)$$

where $\triangle_{m_Q}(T_\Xi)$ is the mass shift of the D meson with taste Ξ, and $\cdots$ represents D^* mass terms, which we are not interested in here.

TABLE 2.1: Taste splittings due to type-A operators

$\triangle_{m_Q}(.)$	ξ_5	$\xi_{\mu 5}$	$\xi_{\mu\nu}$	ξ_μ	I
$2a^2(K^{A2}_{1,1} - 3K^{A2}_{1,6})$	+1	-1	+1	-1	+1
$2a^2(K^{A2}_{1,2} + 6K^{A2}_{1,7})$	-4	+2	0	-2	+4
$2a^2(K^{A2}_{1,3} + 6K^{A2}_{1,8})$	-4	-2	0	+2	+4
$2a^2(K^{A2}_{1,4} - 3K^{A2}_{1,9})$	+12	0	-4	0	+12

For a static D meson, where $v_i = 0$, the corrections on the D masses from $\delta\mathcal{L}_{m_Q}$ are:

$$\begin{aligned}
\triangle_{m_Q}(\xi_5) &= 2a^2\Big\{(K^{A2}_{1,1} - 3K^{A2}_{1,6}) - 4(K^{A2}_{1,2} + 6K^{A2}_{1,7}) - 4(K^{A2}_{1,3} + 6K^{A2}_{1,8}) \\
&\quad + 12(K^{A2}_{1,4} - 3K^{A2}_{1,9}) - 6K^{B2}_{1,1} - 6K^{B2}_{1,2} + 3K^{B2}_{1,3} - 9K^{B2}_{1,4}\Big\} \qquad (2.154) \\
\triangle_{m_Q}(\xi_{05}) &= 2a^2\Big\{-(K^{A2}_{1,1} - 3K^{A2}_{1,6}) + 2(K^{A2}_{1,2} + 6K^{A2}_{1,7}) - 2(K^{A2}_{1,3} + 6K^{A2}_{1,8}) \\
&\quad + 6K^{B2}_{1,1} - 6K^{B2}_{1,2} - 3K^{B2}_{1,3} - 3K^{B2}_{1,4}\Big\} \qquad (2.155) \\
\triangle_{m_Q}(\xi_{i5}) &= 2a^2\Big\{-(K^{A2}_{1,1} - 3K^{A2}_{1,6}) + 2(K^{A2}_{1,2} + 6K^{A2}_{1,7}) - 2(K^{A2}_{1,3} + 6K^{A2}_{1,8}) \\
&\quad + 2K^{B2}_{1,1} - 2K^{B2}_{1,2} + K^{B2}_{1,3} + K^{B2}_{1,4}\Big\} \qquad (2.156) \\
\triangle_{m_Q}(\xi_{ij}) &= 2a^2\Big\{(K^{A2}_{1,1} - 3K^{A2}_{1,6}) - 4(K^{A2}_{1,4} - 3K^{A2}_{1,9}) - 2K^{B2}_{1,1} - 2K^{B2}_{1,2} \\
&\quad - K^{B2}_{1,3} + 3K^{B2}_{1,4}\Big\} \qquad (2.157) \\
\triangle_{m_Q}(\xi_{i0}) &= 2a^2\Big\{(K^{A2}_{1,1} - 3K^{A2}_{1,6}) - 4(K^{A2}_{1,4} - 3K^{A2}_{1,9}) + 2K^{B2}_{1,1} + 2K^{B2}_{1,2} \\
&\quad - K^{B2}_{1,3} + 3K^{B2}_{1,4}\Big\} \qquad (2.158) \\
\triangle_{m_Q}(\xi_i) &= 2a^2\Big\{-(K^{A2}_{1,1} - 3K^{A2}_{1,6}) - 2(K^{A2}_{1,2} + 6K^{A2}_{1,7}) + 2(K^{A2}_{1,3} + 6K^{A2}_{1,8}) \\
&\quad - 2K^{B2}_{1,1} + 2K^{B2}_{1,2} + K^{B2}_{1,3} + K^{B2}_{1,4}\Big\} \qquad (2.159) \\
\triangle_{m_Q}(\xi_0) &= 2a^2\Big\{-(K^{A2}_{1,1} - 3K^{A2}_{1,6}) - 2(K^{A2}_{1,2} + 6K^{A2}_{1,7}) + 2(K^{A2}_{1,3} + 6K^{A2}_{1,8}) \\
&\quad - 6K^{B2}_{1,1} + 6K^{B2}_{1,2} - 3K^{B2}_{1,3} - 3K^{B2}_{1,4}\Big\} \qquad (2.160) \\
\triangle_{m_Q}(I) &= 2a^2\Big\{(K^{A2}_{1,1} - 3K^{A2}_{1,6}) + 4(K^{A2}_{1,2} + 6K^{A2}_{1,7}) + 4(K^{A2}_{1,3} + 6K^{A2}_{1,8}) \\
&\quad + 12(K^{A2}_{1,4} - 3K^{A2}_{1,9}) + 6K^{B2}_{1,1} + 6K^{B2}_{1,2} + 3K^{B2}_{1,3} - 9K^{B2}_{1,4}\Big\} \qquad (2.161)
\end{aligned}$$

The results are summarized in Tables 2.1 and 2.2, which help us see the patterns of taste splittings.

The type-A terms split the heavy-light masses into the five $SO(4)$ taste multiplets: P, A,

TABLE 2.2: Taste splittings due to type-B operators

$\triangle_{m_Q}(.)$	ξ_5	ξ_{05}	ξ_{i5}	ξ_{ij}	ξ_{i0}	ξ_i	ξ_0	I
$2a^2K_{1,1}^{B2}$	-6	+6	+2	-2	+2	-2	-6	+6
$2a^2K_{1,2}^{B2}$	-6	-6	-2	-2	+2	+2	+6	+6
$2a^2K_{1,3}^{B2}$	+3	-3	+1	-1	-1	+1	-3	+3
$2a^2K_{1,4}^{B2}$	-9	-3	+1	+3	+3	+1	-3	-9

T, V and S (pseudoscalar, axial-vector, tensor, vector and singlet tastes). The type-B terms split these multiplets and give different masses to the time and spatial components, such as ξ_0 and ξ_i for the vector taste multiplet. The staggered lattice symmetries guarantee that the eight multiplets shown in Table 2.2 cannot be be broken further; for example, the three tastes ξ_i must remain degenerate. On the other hand, it is straightforward to check that any pattern of splitting of the eight multiplets is possible, given arbitrary values of the parameters $K_{1,n}^{A2}$ and $K_{1,m}^{B2}$.

Further progress in understanding the actual pattern of splittings determined in simulations is therefore only possible with some assumptions about which of the corresponding chiral operators are likely to give dominant contributions to the masses. Experience with the pion (light-light pseudoscalar) splittings is helpful in guiding these assumptions, so we first review what happens in that case. The staggered pion masses at LO are

$$m_{ab,\Xi}^2 = \mu(m_a + m_b) + a^2\Delta_\Xi \ , \tag{2.162}$$

where m_a and m_b are light quark masses, μ is the low-energy constant from Eq. (2.11), and $a^2\Delta_\Xi$ is the splitting of taste Ξ. The pions have $SO(4)$ taste symmetry; their masses form five multiplets with tastes P, A, T, V and S. Simulations with the asqtad and HISQ actions give approximately equal splittings of squared masses between the P, A, T, V and S tastes (and with that ordering, from lowest to highest) [8, 39, 61]. These equal splittings imply that the dominant chiral operator contributing to taste splittings of pion masses is the operator multiplied by C_4 in $-a^2V_\Sigma$, Eq. (2.15), namely

$$a^2\left[\mathrm{Tr}(\xi_{\nu5}^{(n)}\Sigma\xi_{5\nu}^{(n)}\Sigma) + h.c.\right] \ . \tag{2.163}$$

This operator is generated by the four-quark operators $[S\times A]^{ll}$, $[P\times A]^{ll}$ and $[T\times A]^{ll}$ in the SET, Eq. (2.44). Note that, for the pions, only type-A operators are relevant at LO, because type-B operators have no chiral representatives to this order. The non-trivial space-time structure in

the type-B case requires more at least two derivatives in the light-light chiral operators, making their representatives NLO in the chiral expansion [37].

We now carry over this experience to the heavy-light case. We have assumed above that the lattice is sufficiently fine, or the charmed quark is sufficiently improved, that it may treated as a "continuum-like," and corrections of order $(am_Q)^2$ may be neglected. This means that the contributions of the heavy quark to the SET are identical to those of a light quark. In particular, the same four-quark operators that dominated for light quarks, namely $[S \times A]$, $[P \times A]$ and $[T \times A]$, are expected to be the dominant type-A operators in the heavy-light case. Taste splittings of heavy-light meson masses can come only from the "heavy-light" versions of these operators. From Eqs. (2.85), (2.87) and (2.89), these operators give rise to chiral representatives with coefficients $K_{1,3}^{A2}$ and $K_{1,8}^{A2}$ in Eq. (2.152). From Table 2.1, we then deduce the same equal-spacing pattern for heavy-light $SO(4)$ representations that is familiar from the pions. For type-B operators, one may guess that the $[T_\mu \times A_\mu]$ SET operator would be dominant, since it is the only type-B operator that has the same spin and taste as one of the dominant type-A operators. From Eq. (2.116), this four-quark operator gives rise to the chiral representative with coefficient $K_{1,2}^{B2}$ in Eq. (2.152). Referring to the second line of Table 2.2, we see that this operator produces equal splitting within the A, T, and V $SO(4)$ multiplets. Further, the multiplicity-weighted average splitting between $SO(4)$ multiplets for this type-B operator is the same as for the dominant type-A operators (equal splitting with the order P, A, T, V, S), so this operator does not spoil that overall $SO(4)$ pattern, but only produces splittings within multiplets.

The patterns of splitting expected from the discussion in the previous paragraph are qualitatively present in the MILC data, shown in Fig. 2.1. Note in particular the "sc" case, which gives heavy-light meson splittings with small enough errors that the pattern of $SO(4)$ breaking is clear. It is non-trivial that the time component of taste is higher than the space components in two cases (ξ_0 *vs.* ξ_i and ξ_{i0} *vs.* ξ_{ij}) but not in the third case (ξ_{05} *vs.* ξ_{i5}), just as in the second line of Table 2.2. Further, the figure shows roughly equal splittings within $SO(4)$ multiplets, as well as between (the center of gravity of) $SO(4)$ multiplets. Although the chiral theory is not applicable to the "cc" case, it is interesting to see that the structure that would correspond to the dominant type-B operator gets particularly strong there, with near degeneracies of between members of different $SO(4)$ multiplets, in particular ξ_0 and I, or ξ_{i0} and ξ_i.

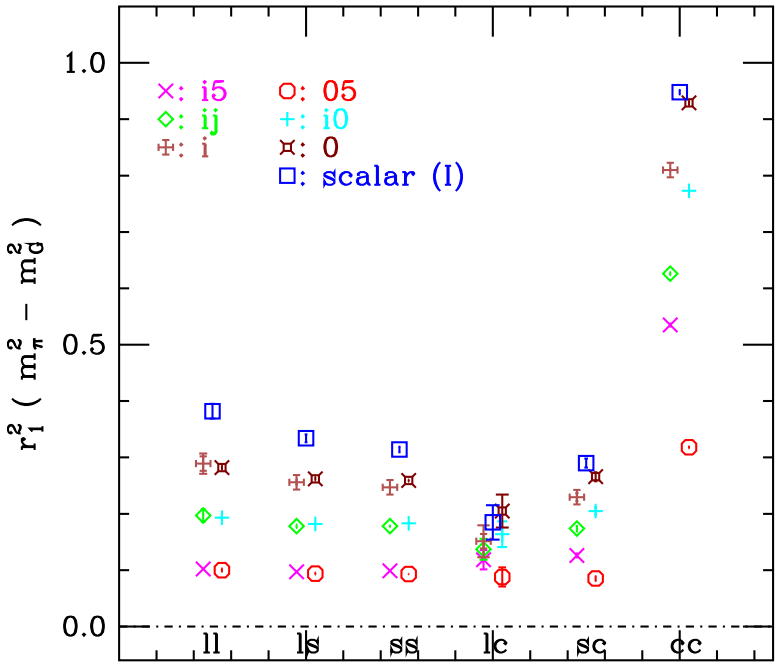

FIGURE 2.1: Meson mass splitting for the MILC HISQ ensemble at $a \approx 0.15$ fm and $m_l = 0.2m_s$ [39]. Squared mass splitting between pions of different tastes and the Goldstone pion in units of r_1 are shown. The types of quarks in the mesons are shown on the abscissa: l, s, and c stand for light (u,d), strange, and charm quarks, respectively.

2.5 Decay constants of the D meson at NLO

In this section, we calculate the decay constant of the D meson at one loop in HMrASχPT. We can express the decay constant at this order as

$$f_{D_{x\Xi}}\sqrt{M_{D_{x\Xi}}} = \kappa\left(1 + \frac{1}{16\pi^2 f^2}\,\delta f_{D_x} + \text{analytic terms}\right)\,, \tag{2.164}$$

where x labels the light valence flavor in the meson, Ξ labels the meson taste, κ is the LO low-energy constant in the current, Eq. (2.28), and δf_{D_x} denotes the sum of the chiral logarithm terms, coming from the one-loop diagrams. We will allow for the possibility of partial quenching, so the valence quark mass m_x may be different from any of the sea-quark masses. The analytic terms arise from tree-level contributions from the NLO Lagrangian and current and will include taste symmetry violations, due to the taste-violating terms $\mathcal{L}^{A2}_{3,a^2}$, $\mathcal{L}^{B2}_{3,a^2}$, $j^{\mu,i\Xi}_{2,a^2,A2}$ and $j^{\mu,i\Xi}_{2,a^2,B2}$.

By following the same approach as we used to show the one-loop contribution to the heavy-light meson propagator is taste independent, it is straightforward to show that the one-loop term δf_{D_x} is independent of taste of the meson. We simply replace the field $H_i^{\alpha\beta}$ in Eq. (2.146) with

the leading order current

$$j_{\rm LO}^{\mu,i,\alpha\beta} = \sum_{\Xi} \tfrac{1}{2} T_{\Xi}^{\alpha\beta} j_{\rm LO}^{\mu,i\Xi} = \frac{\kappa}{2} \sum_{\Xi} \tfrac{1}{2} T_{\Xi}^{\alpha\beta} \ {\rm tr}_{D,t}\big(\tfrac{1}{2} T_{\Xi} \gamma^{\mu} \left(1-\gamma_5\right) H \sigma^{\dagger} \lambda^{(i)}\big) \ , \tag{2.165}$$

where we have used Eq. (2.28) for $j_{\rm LO}^{\mu,i\Xi}$. Note that $j_{\rm LO}^{\mu,i,\alpha\beta}$ transforms under heavy-quark taste symmetry and light-quark discrete taste symmetry exactly as $H_i^{\alpha\beta}$ does. Identical manipulations to those in Sec. 2.4 thus show that the two-point function of the current and the field is taste-independent:

$$\langle 0 | j_{\rm LO}^{\mu,i\Xi}(x) \overline{H}_{j\Xi'}(y) | 0 \rangle = \tfrac{1}{2} \delta_{ij} \delta_{\Xi\Xi'} \, h_I(x,y,i) \ , \tag{2.166}$$

where we have introduced a new function h_I. Up to an additional term coming from the one-loop wave function renormalization, δf_{D_x} is proportional to the one-loop contribution to the two-point function in Eq. (2.166). Since we know from Sec. 2.4 that the wave function contribution is taste-independent, we have proven the taste-independence of δf_{D_x}. Furthermore, it is now easy to see that δf_{D_x} in our theory, HMrASχPT, is identical to the corresponding contribution in HMrSχPT calculated in Ref. [25]. The only difference between the LO Lagrangians in the two theories is the extra taste degree of freedom of the heavy quark in HMrASχPT. Since we have seen that heavy-quark taste is conserved in the one-loop diagrams, the heavy taste degree of freedom just flows through the diagram and has no effect on the result. Note that virtual heavy quark loops are forbidden in our theory since the residual energy is low; if they were allowed the heavy-quark taste would lead to an extra counting factor in loops.

We thus take over the result from Ref. [25] for δf_{D_x} without change, except for trivial changes in notation. The analytic terms, which come from the NLO Lagrangian, will be different in the two theories, however. The terms $\mathcal{L}_{3,a^2}^{A2}$, $\mathcal{L}_{3,a^2}^{B2}$, $j_{2,a^2,A2}^{\mu,i\Xi}$ and $j_{2,a^2,B2}^{\mu,i\Xi}$ give contributions that depend on the taste of meson.

Following Ref. [25] for the one loop terms, we then get, for the 1+1+1 partially quenched case with all masses unequal:

$$\begin{aligned}
\frac{f_{D_{x\Xi}} \sqrt{M_{D_{x\Xi}}}}{\kappa} \ = \ & 1 + \frac{1}{16\pi^2 f^2} \frac{1+3g_\pi^2}{2} \Bigg\{ -\frac{1}{16} \sum_{\mathcal{S},\Xi'} \ell(m^2_{x\mathcal{S},\Xi'}) \\
& - \frac{1}{3} \sum_{j \in \mathcal{M}_I^{(3,x)}} \frac{\partial}{\partial m^2_{X,I}} \Big[R_j^{[3,3]}(\mathcal{M}_I^{(3,x)}; \mu_I^{(3)}) \ell(m_j^2) \Big] \\
& - \Bigg(a^2 \delta'_V \sum_{j \in \mathcal{M}_V^{(4,x)}} \frac{\partial}{\partial m^2_{X,V}} \Big[R_j^{[4,3]}(\mathcal{M}_V^{(4,x)}; \mu_V^{(3)}) \ell(m_j^2) \Big] + [V \to A] \Bigg) \Bigg\} \\
& + c_s(m_u + m_d + m_s) + c_v m_x + c_{a,\Xi} a^2 \ ,
\end{aligned} \tag{2.167}$$

where x is the valence flavor, Ξ is the valence taste, $\mathcal{S}$ runs over the three sea quarks u, d, and s, and Ξ' runs over the 16 meson tastes. The chiral logarithm function ℓ and the residue functions R are defined by

$$\ell(m^2) \equiv m^2 \ln \frac{m^2}{\Lambda_\chi^2}, \tag{2.168}$$

$$R_j^{[n,k]}(\{m\};\{\mu\}) \equiv \frac{\prod_{i=1}^{k}(\mu_i^2 - m_j^2)}{\prod_{r\neq j}(m_r^2 - m_j^2)}\ , \tag{2.169}$$

with the sets of masses in the residues given by

$$\mu^{(3)} = \{m_U^2, m_D^2, m_S^2\}\ , \tag{2.170}$$

$$\mathcal{M}^{(3,x)} = \{m_X^2, m_{\pi^0}^2, m_\eta^2\}\ , \tag{2.171}$$

$$\mathcal{M}^{(4,x)} = \{m_X^2, m_{\pi^0}^2, m_\eta^2, m_{\eta'}^2\}\ . \tag{2.172}$$

Here taste labels (*e.g.*, I or V for the masses) are implicit. In Eq. (2.167), $c_{a,\Xi}$ is the only coefficient that depends on the taste of the heavy meson. It can be written as a linear function of constants appearing in $\mathcal{L}^{A2}_{3,a^2}$, $\mathcal{L}^{B2}_{3,a^2}$, $j^{\mu,i\Xi}_{2,a^2,A2}$ and $j^{\mu,i\Xi}_{2,a^2,B2}$. It is straightforward to check that these terms are sufficient to break the taste symmetry down to the lattice symmetry. Thus the coefficients $c_{a,\Xi}$ are independent for the eight multiplets listed in Table 2.2.

Now we include the effects of hyperfine and flavor splittings of the heavy-light mesons in one-loop diagrams. We follow the argument of Ref. [56] and briefly describe how one can adjust Eq. (2.167) to include these splittings. In Eq. (2.167), the contributions proportional to g_π^2 come from diagrams with internal D^* propagators, and the contributions with no factor of g_π^2 come from diagrams with light-meson ("pion") tadpoles. Thus we must only adjust the former contributions. The splittings in diagrams with internal D^* propagators depend on whether the pion line is connected, which results in the term with the sum over $\mathcal{S}$ in Eq. (2.167), or disconnected, which results in the terms with the factors of the residue function R in Eq. (2.167). (See Fig. 5 in Ref. [25] for the structure of the quark flow in these diagrams.) In the disconnected case, the valence x quark in the external $D_{x\Xi}$ flows into the pion propagator and then returns the way it came (a "hairpin" diagram) and enters the D^* propagator. Thus the internal D^* always has the same flavor as the external $D_{x\Xi}$, so there is no flavor splitting between the two, only a hyperfine splitting. In the connected case, the D^* in the loop has the flavor of the virtual sea quark loop (which we labeled by $\mathcal{S}$ in Eq. (2.167)), so there is flavor splitting with the external $D_{x\Xi}$, in addition to the hyperfine splitting.

We let Δ^* be the lowest-order hyperfine splitting, and $\delta_{\mathcal{S}x}$ be the flavor splitting between

a heavy-light meson with light quark of flavor $\mathcal{S}$ and one of flavor x. At lowest order, $\delta_{\mathcal{S}x}$ is proportional to the quark-mass difference, which can be written in terms of the parameter λ_1 in Eq. (2.35):

$$\delta_{\mathcal{S}x} \cong 2\lambda_1(m_{\mathcal{S}} - m_x) \cong \frac{\lambda_1}{\mu}(m^2_{\mathcal{S}\mathcal{S},\xi_5} - m^2_{xx,\xi_5}), \tag{2.173}$$

where the final expression expresses the result in terms of pion masses.

Since the mass of the external D is removed in HQET, the mass shell is at $k = 0$. When there is no splitting, the internal D^* has its pole at the same place, which makes the integrals simple and gives rise to the chiral log function $\ell(m^2)$. In the presence of a splitting Δ between the internal D^* and the external D, the integrals involve the more complicated function

$$J(m, \Delta) = (m^2 - 2\Delta^2)\log(m^2/\Lambda^2) + 2\Delta^2 - 4\Delta^2 F(m/\Delta). \tag{2.174}$$

Here the function F is [62, 63]

$$F(1/x) = \begin{cases} -\frac{\sqrt{1-x^2}}{x}\left[\frac{\pi}{2} - \tan^{-1}\frac{x}{\sqrt{1-x^2}}\right], & \text{if } |x| \le 1, \\ \frac{\sqrt{x^2-1}}{x}\ln(x + \sqrt{x^2-1}), & \text{if } |x| \ge 1 \quad . \end{cases} \tag{2.175}$$

We may now generalize Eq. (2.167) to include splittings. We simply replace

$$\ell(m^2) \to J(m, \Delta) \tag{2.176}$$

in the terms proportional to g_π^2, taking care to include the flavor splittings ($\Delta = \Delta^* + \delta_{\mathcal{S}x}$) for terms from connected-pion diagrams, and to omit the flavor splittings ($\Delta = \Delta^*$) for terms from

disconnected-pion diagrams. The result for the leptonic decay constant is then

$$\begin{aligned}
\frac{f_{D_{x\Xi}}\sqrt{M_{D_{x\Xi}}}}{\kappa} &= 1 + \frac{1}{16\pi^2 f^2}\frac{1}{2}\Bigg\{ -\frac{1}{16}\sum_{\mathcal{S},\Xi'} \ell(m^2_{\mathcal{S}x,\Xi'}) \\
&\quad - \frac{1}{3}\sum_{j\in\mathcal{M}_I^{(3,x)}} \frac{\partial}{\partial m^2_{X,I}}\left[R_j^{[3,3]}(\mathcal{M}_I^{(3,x)};\mu_I^{(3)})\ell(m_j^2)\right] \\
&\quad - \left(a^2\delta'_V \sum_{j\in\mathcal{M}_V^{(4,x)}} \frac{\partial}{\partial m^2_{X,V}}\left[R_j^{[4,3]}(\mathcal{M}_V^{(4,x)};\mu_V^{(3)})\ell(m_j^2)\right] + [V\to A]\right) \\
&\quad - 3g_\pi^2\frac{1}{16}\sum_{\mathcal{S},\Xi'} J(m_{\mathcal{S}x,\Xi'},\Delta^* + \delta_{\mathcal{S}x}) \\
&\quad - g_\pi^2 \sum_{j\in\mathcal{M}_I^{(3,x)}} \frac{\partial}{\partial m^2_{X,I}}\left[R_j^{[3,3]}(\mathcal{M}_I^{(3,x)};\mu_I^{(3)})J(m_j,\Delta^*)\right] \\
&\quad - 3g_\pi^2\left(a^2\delta'_V \sum_{j\in\mathcal{M}_V^{(4,x)}} \frac{\partial}{\partial m^2_{X,V}}\left[R_j^{[4,3]}(\mathcal{M}_V^{(4,x)};\mu_V^{(3)})J(m_j,\Delta^*)\right] + [V\to A]\right)\Bigg\} \\
&\quad + c_s(m_u+m_d+m_s) + c_v m_x + c_{a,\Xi}a^2 \ . \qquad (2.177)
\end{aligned}$$

We can also include the finite-volume effects for a spatial volume L^3 into Eq. (2.177). Following Ref. [56], we replace

$$\ell(m^2) \ \to \ \ell(m^2) + m^2\delta_1(mL), \qquad (2.178)$$

$$J(m,\Delta) \ \to \ J(m,\Delta) + \delta J(m,\Delta,L), \qquad (2.179)$$

where

$$\delta J(m,\Delta,L) = \frac{m^2}{3}\delta_1(mL) - 16\pi^2\left[\frac{2\Delta}{3}J_{FV}(m,\Delta,L) + \frac{\Delta^2-m^2}{3}K_{FV}(m,\Delta,L)\right] \ , \qquad (2.180)$$

with

$$K_{FV}(m,\Delta,L) \equiv \frac{\partial}{\partial\Delta}J_{FV}(m,\Delta,L), \qquad (2.181)$$

and with $\delta_1(mL)$ and $J_{FV}(m,\Delta,L)$ defined in Refs. [105, 106].

Reference [56] also discusses the extent to which including the splittings as in Eq. (2.177), and not other possible $1/m_Q$ effects, is a systematic improvement on Eq. (2.167). In that discussion the power counting introduced by Boyd and Grinstein [102] is applied, which assumes

$$\frac{\Delta^2,\ \Delta m,\ m^2}{m_Q} \ll \Delta \sim m \ , \qquad (2.182)$$

where Δ is a generic splitting (Δ^* or δ_{Sx} or a linear combination of the two), m is a generic light pseudoscalar *meson* mass, and m_Q is the heavy quark mass. In the lattice simulations of Ref. [56], the lowest pion masses were about half the physical kaon mass, and the power counting of Ref. [102] was only marginally applicable to the data. However, for simulations on the HISQ ensembles generated by the MILC Collaboration [39, 61], the lowest pion masses are physical, and the assumptions of the Boyd-Grinstein power counting are well satisfied. Furthermore, including the splittings with such data is not optional: for D mesons the hyperfine splitting $\Delta^* = 142.1$ MeV, and the flavor splitting $\delta_{sd} = 98.9$ MeV, clearly non-negligible compared to the physical pion mass.

Since we have included hyperfine and flavor splittings, which are empirically large even though they are formally of order $1/m_Q$, it is important to consider whether splittings coming from taste violations should also be included in the heavy-light propagators at one loop. As discussed in the introduction, taste splittings in squared meson masses are roughly constant as the masses increase from pions to D mesons, which means that taste splittings in the heavy-light masses themselves are quite small, ~ 11 MeV at $a \approx 0.12$ fm for the HISQ action. The taste splittings are indeed higher order compared to the physical hyperfine and flavor splittings. We note that the taste-violating Lagrangian terms in Eqs. (2.125) and (2.127) also lead to $\mathcal{O}(a^2)$ contributions to hyperfine splittings. Those effects have not been measured in lattice simulations, but we think it is reasonable to assume they are comparable in size to the taste splittings since in most cases the same operators produce both effects.

There is also the question of whether other $1/m_Q$ continuum effects should be included along with the hyperfine and flavor splittings. As discussed in Ref. [56], such terms only change the overall normalization of the result for the quantity δf_{D_x} in Eq. (2.164) by relatively small amount, of order Λ_{QCD}/m_Q. Since in any case the value of f in Eq. (2.164) may be considered uncertain by as much as 20% (the difference between f_π and f_K), these additional $1/m_Q$ terms have no practical implications for our results.

2.6 Conclusions

We have generalized the chiral Lagrangian for heavy-light mesons to the case where both heavy and light quarks have the staggered action. A fundamental assumption of our work is that lattice spacings is sufficiently small, or the heavy-quark action is sufficiently improved, that we may treat am_Q as a small parameter, where m_Q is the heavy quark mass. This is the same assumption required in order to describe heavy quarks with the HISQ staggered action in simulations.

The heavy-light part of the LO staggered chiral Lagrangian we obtain is identical to that in the continuum, except for extra taste degrees of freedom of the light and heavy quarks. In contrast with the light-light part of the chiral Lagrangian, which includes taste splittings at LO, the heavy-light part of the LO chiral Lagrangian is taste-invariant, with three key symmetries: heavy quark spin symmetry, chiral symmetry of the light quarks (including taste and flavor symmetries), and $SU(4)$ taste symmetry of the heavy quarks. Complications arise at NLO, where these symmetries of the heavy-light Lagrangian may be broken by lattice artifacts, as well as by light-quark mass terms. Those NLO contributions that arise from terms in the Symanzik effective theory composed exclusively of light quarks may be taken over directly from Ref. [25]. In doing so, we have corrected some minor errors in that reference, which do not affect any existing calculations within that framework. Terms in the Symanzik effective theory with heavy staggered quarks are new. We have derived their consequences for the NLO heavy-light Lagrangian, as well as the left-handed current, in some detail. In some cases, though, we have not attempted to find the complete set of possible terms, and have contented ourselves with simply listing sufficient numbers of terms relevant to foreseeable practical applications.

We have then applied our Lagrangian to calculate, through NLO, the taste splitting of heavy-light mesons and the heavy-light leptonic decay constant. In both these cases, we are able to prove that the one-loop diagrams are taste invariant, despite the fact that they contain pion propagators that break taste symmetry. This means that taste violations in these quantities at NLO come exclusively from analytic terms, which arise from the NLO Lagrangian and current. Using our results for the mass splittings, and making assumptions about the dominant operators based on experience with light-light quantities, we find that we can qualitatively understand the pattern of splittings seen in heavy-light HISQ data.

For the decay constant, the NLO taste violations produce a single analytic term that depends on taste of the meson, the term $c_{a,\Xi}a^2$ in Eqs. (2.167) and (2.177). The one-loop diagrams give rise to the same chiral logarithms derived in Ref. [25], because in both cases they are taste invariant. Following Ref. [56], we include the modifications of these chiral logarithms due to heavy-light hyperfine and flavor splittings, which are comparable in size to the physical pion mass, and therefore important for describing modern simulations in which the light quark masses are physical or close to physical. The resulting chiral form is being used to fit HISQ data for decay constants of the D system [55]. Although such fits may be bypassed for data at physical quark masses [34], the chiral fits allow one to include data at unphysical quark masses, and thereby one can hope to obtain smaller statistical errors and better control over continuum extrapolation errors. The work in progress indicates that these hopes are realized in practice.

3

Charmed Pseudoscalar Meson Decay Constants

The MILC Collaboration has been generating a large library of gauge configuration ensembles with four dynamical quark flavors—up, down, strange, and charm—using highly improved staggered quark (HISQ) action. These ensembles have both physical and unphysical values of the light sea-quark masses with four values of the lattice spacing ranging from 0.06 to 0.15 fm. The decay constants of D and D_s mesons are among many other quantities computed from these ensembles. Using the chiral formula derived in the previous chapter, Eq. (2.177), we combine the data computed from different ensembles. By fitting the chiral result to the lattice data, the unknown LECs appearing in the decay constant formula are determined. Then, a combined chiral extrapolation/interpolation and continuum extrapolations is performed, and consequently the physical values of the D^+ and D_s meson decay constants are obtained. This work is an important part of the paper[1] published by the MILC and Fermilab lattice collaborations on the decay constants of pseudoscalar mesons. This chapter contains the complete paper, but my main contributions are subsection 3.4.2, which discusses chiral perturbation theory analysis of f_D and f_{D_s}, and section 3.5, which discusses the final results.

3.1 Introduction and motivation

The leptonic decays of pseudoscalar mesons enable precise determinations of Cabibbo-Kobayashi-Maskawa (CKM) quark-mixing matrix elements within the Standard Model. In particular, experimental rates for the decays $D^+ \to \mu^+\nu$, $D_s \to \mu^+\nu$ and $D_s \to \tau^+\nu$, when combined

[1] A. Bazavov, C. Bernard, C.M. Bouchard, C. DeTar, D. Du, A.X. El-Khadra, J. Foley, E.D. Freeland, E. Gámiz, Steven Gottlieb, U.M. Heller, J. Kim, J. Komijani, A.S. Kronfeld, J. Laiho, L. Levkova, P.B. Mackenzie, E.T. Neil, J.N. Simone, R.L. Sugar, D. Toussaint, R.S. Van de Water, R. Zhou, "Charmed and light pseudoscalar meson decay constants from four-flavor lattice QCD with physical light quarks," Phys. Rev. D 90, 074509 (2014) [arXiv:1407.3772].

with lattice calculations of the charm-meson decay constants f_{D^+} and f_{D_s}, allow one to obtain $|V_{cd}|$ and $|V_{cs}|$. Indeed, this approach results in the most precise current determination of $|V_{cd}|$. Similarly, the light-meson decay-constant ratio f_{K^+}/f_{π^+} can be used to extract $|V_{us}|/|V_{ud}|$ from the experimental ratio of kaon and pion leptonic decay widths [65, 66]. Here we calculate the charm decay constants for the first time using physical values for the light sea-quark mass. We obtain f_{D^+} and f_{D_s} to about 0.5% precision and their ratio f_{D_s}/f_{D^+} to about 0.3% precision; we also update our earlier calculation of f_{K^+}/f_{π^+} [67] to almost 0.2% precision. This is the most precise lattice calculation of the charm decay constants to date, and improves upon previous results by a factor of two to four. We also compute the quark-mass ratios m_c/m_s and m_s/m_l, which are fundamental parameters of the Standard Model.

We use the lattice ensembles generated by the MILC Collaboration with four flavors ($n_f = 2+1+1$) of dynamical quarks using the highly improved staggered quark (HISQ) action, and a one-loop tadpole improved Symanzik improved gauge action [68–71]. The generation algorithm uses the fourth-root procedure to remove the unwanted taste degrees of freedom [72–84]. Our data set includes ensembles with four values of the lattice spacing ranging from approximately 0.15 fm to 0.06 fm, enabling good control over the continuum extrapolation. The data set includes both ensembles with the light (up-down), strange, and charm sea-masses close to their physical values ("physical-mass ensembles") and ensembles where either the light sea-mass is heavier than in nature, or the strange sea-mass is lighter than in nature, or both.

The physical-mass ensembles enable us to perform first a straightforward analysis that does not require chiral fits. This analysis, which we refer to as the "physical-mass analysis" below, gives our results for f_{K^+}/f_{π^+}, as well as ratios of physical quark masses. The quark-mass ratios are then used as input to a more sophisticated analysis of the charm decay constants that includes the ensembles with unphysical sea-quark masses. In this second analysis, referred to as the "chiral analysis," we analyze our complete data set within the framework of staggered chiral perturbation theory (SχPT) for all-staggered heavy-light mesons [23, 24, 85, 86]. The inclusion of the unphysical-mass ensembles gives us tighter control on discretization effects because SχPT connects the quark-mass and lattice-spacing dependence of the data, reducing the statistical errors on the decay constants significantly, and allowing us to make more refined adjustments for mistuning of masses. We therefore take our final central values for f_{D^+}, f_{D_s}, and f_{D_s}/f_{D^+} from the chiral analysis. The physical-mass analysis provides a cross check of the chiral analysis and is used in our final estimate of systematic uncertainties.

An earlier result for f_{K^+}/f_{π^+} was presented in Ref. [67]. Here we update this analysis with slightly more statistics and improved estimates for the systematic errors. Preliminary results for the charm decay constants and quark masses were presented in Ref. [87].

This chapter is organized as follows. Section 3.2 gives details about the lattice ensembles used in our calculation and the method for extracting the decay constants from two-point correlation functions. As discussed in Sec. 3.3, the first stage in our analysis is to fit the two-point correlators to determine the meson masses and decay amplitudes for each pair of valence-quark masses. Section 3.4 presents the main body of our analysis, which proceeds in two stages. In the first stage, described in Sec. 3.4.1, we use the physical-mass ensembles to compute quark-mass ratios and f_{K^+}/f_{π^+}, as well as some additional intermediate quantities required for the later chiral analysis of the D-meson decay constants. In the first part of the physical-mass analysis, Sec. 3.4.1.1, we fit the valence-quark mass dependence of the masses and amplitudes, and evaluate the decay amplitudes at the resulting tuned valence masses. Next, in Sec. 3.4.1.2, we adjust the quark-mass ratios and decay amplitudes to account for the slight sea-quark mass mistuning and extrapolate these results to the continuum. In the last part of the physical-mass analysis, Sec. 3.4.1.3, we consider systematic errors from finite-volume and electromagnetic effects. In the second analysis stage described in Sec. 3.4.2, we use heavy-light staggered chiral perturbation theory to combine the unphysical light- and strange-quark mass ensembles with the nearly-physical quark mass ensembles to obtain the charm-meson decay constants. We first present the chiral perturbation theory for all-staggered heavy-light mesons in Sec. 3.4.2.1. We then discuss the required mass-independent scale setting in Sec. 3.4.2.2, where we take care to correct for effects on the scale and quark-mass estimates of mistunings of the sea-quark masses. We present the chiral-continuum fits in Sec. 3.4.2.3, and discuss the systematic errors from the continuum extrapolation, as well as from other sources, in Sec. 3.4.2.4. We present our final results for the decay constants and quark-mass ratios with error budgets in Sec. 2.6, in which we also compare our results to other unquenched lattice calculations. Finally, we discuss the impact of our results on CKM phenomenology in Sec. 3.6. Appendix **??** gives details about the inclusion of nonleading heavy-quark effects in our chiral formulas.

3.2 Lattice simulation parameters and methods

Table 3.1 summarizes the lattice ensembles used in this calculation. Discussion of the parameters relevant to the lattice generation, such as integration step sizes and acceptance rates, choice of the RHMC or RHMD algorithm, and autocorrelations of various quantities can be found in Ref. [71]. In particular, we find that the effects of using the RHMD algorithm rather than the RHMC algorithm in some of our ensembles are negligible. The dependence of error estimates for the decay constants in this work on the jackknife block size is consistent with the more general results on autocorrelations in Ref. [71]. Reference [71] also shows the molecular dynamics time

TABLE 3.1: Ensembles used in this calculation. The first column is the gauge coupling $\beta = 10/g^2$, and the next three columns are the sea-quark masses in lattice units. The primes on the masses indicate that they are the values used in the runs, and in general differ from the physical values either by choice, or because of tuning errors. The lattice spacings in this table are obtained separately on each ensemble using f_{π^+} as the length standard, following the procedure described in Sec. 3.4.1.1. (In Sec. 3.4.2 we use a mass-independent lattice spacing, described there.) The lattice spacings here differ slightly from those in Ref. [71] since we use f_{π^+} as the length scale, while those in Ref. [71] were determined using F_{p4s} (discussed at the beginning of Sec. 3.4.1). Values of the strange quark mass chosen to be unphysical are marked with a dagger (†); while the asterisk (*) marks an ensemble that we expect to extend in the future.

β	am'_l	am'_s	am'_c	$(L/a)^3 \times (T/a)$	N_{lats}	a (fm)	L (fm)	$M_\pi L$	M_π (MeV)
5.80	0.013	0.065	0.838	$16^3 \times 48$	1020	0.14985(38)	2.38	3.8	314
5.80	0.0064	0.064	0.828	$24^3 \times 48$	1000	0.15303(19)	3.67	4.0	214
5.80	0.00235	0.0647	0.831	$32^3 \times 48$	1000	0.15089(17)	4.83	3.2	130
6.00	0.0102	0.0509	0.635	$24^3 \times 64$	1040	0.12520(22)	3.00	4.5	299
6.00	0.0102	0.03054†	0.635	$24^3 \times 64$	1020	0.12104(26)	2.90	4.5	307
6.00	0.00507	0.0507	0.628	$24^3 \times 64$	1020	0.12085(28)	2.89	3.2	221
6.00	0.00507	0.0507	0.628	$32^3 \times 64$	1000	0.12307(16)	3.93	4.3	216
6.00	0.00507	0.0507	0.628	$40^3 \times 64$	1028	0.12388(10)	4.95	5.4	214
6.00	0.01275	0.01275†	0.640	$24^3 \times 64$	1020	0.11848(26)	2.84	5.0	349
6.00	0.00507	0.0304†	0.628	$32^3 \times 64$	1020	0.12014(16)	3.84	4.3	219
6.00	0.00507	0.022815†	0.628	$32^3 \times 64$	1020	0.11853(16)	3.79	4.2	221
6.00	0.00507	0.012675†	0.628	$32^3 \times 64$	1020	0.11562(14)	3.70	4.2	226
6.00	0.00507	0.00507†	0.628	$32^3 \times 64$	1020	0.11311(19)	3.62	4.2	230
6.00	0.0088725	0.022815†	0.628	$32^3 \times 64$	1020	0.12083(17)	3.87	5.6	286
6.00	0.00184	0.0507	0.628	$48^3 \times 64$	999	0.12121(10)	5.82	3.9	133
6.30	0.0074	0.037	0.440	$32^3 \times 96$	1011	0.09242(21)	2.95	4.5	301
6.30	0.00363	0.0363	0.430	$48^3 \times 96$	1000	0.09030(13)	4.33	4.7	215
6.30	0.0012	0.0363	0.432	$64^3 \times 96$	1031	0.08779(08)	5.62	3.7	130
6.72	0.0048	0.024	0.286	$48^3 \times 144$	1016	0.06132(22)	2.94	4.5	304
6.72	0.0024	0.024	0.286	$64^3 \times 144$	1166	0.05937(10)	3.79	4.3	224
6.72	0.0008	0.022	0.260	$96^3 \times 192$	583*	0.05676(06)	5.44	3.7	135

evolution of the topological charge for many of these ensembles and histograms of the topological charge. We have since also verified that on the $a \approx 0.06$ fm physical quark mass ensemble the autocorrelation time for the topological charge is much shorter than the topological charge autocorrelation time on the $a \approx 0.06$ fm $m'_l = m'_s/5$ ensemble shown in Fig. 2 of Ref. [71]. The dependence on the light-quark mass can be understood by thinking of the decorrelation process as a random walk in the topological charge.

Our extraction of the pseudoscalar decay constants with staggered quarks follows that used for asqtad quarks [66, 88] and for f_{K^+} with the HISQ action [67, 89]. The decay constant f_{PS} is given by the matrix element of $\bar{\psi}\gamma_5\psi$ between the vacuum and the pseudoscalar meson. For staggered fermions, using the pion taste corresponding to the axial symmetry broken only by

quark masses, this becomes the operator

$$\mathcal{O}_P(\mathbf{x},t) = \bar{\chi}^a(\mathbf{x},t)(-1)^{x+y+z+t}\chi^a(\mathbf{x},t) \quad , \tag{3.1}$$

where a is a color index. The desired matrix element can be obtained from the amplitude of a correlator using this operator at the source and sink,

$$P_{PP}(t) = \frac{1}{V_s}\sum_{\mathbf{y}}\langle\mathcal{O}_P(\mathbf{y},0)\mathcal{O}_P(\mathbf{0},t)\rangle = C_{PP}e^{-Mt} + \text{excited state contributions} \quad , \tag{3.2}$$

where V_s is the spatial volume, M is the pseudoscalar meson mass and the sum over $\mathbf{y}$ isolates the zero spatial momentum states. Then the decay constant is given by [90, 91]

$$f_{PS} = (m_A + m_B)\sqrt{\frac{V_s}{4}}\sqrt{\frac{C_{PP}}{M^3}} \quad , \tag{3.3}$$

where m_A and m_B are valence quark masses and M is the pseudoscalar meson mass.

In our computations, we use a "random-wall" source for the quark propagators, where a randomly oriented unit vector in color space is placed on each spatial site at the source time. Then quark and antiquark propagators originating on different lattice sites are zero when averaged over the sources. We use three such source vectors for each source time slice.

We also compute pion correlators using a "Coulomb-wall" source, where the gauge field is fixed to the lattice Coulomb gauge, and then a uniform color vector source is used at each spatial site. In practice these vectors are the "red", "green," and "blue" color axes. The Coulomb-wall source correlators are somewhat less contaminated by excited states than the random wall source correlators, so by simultaneously fitting the correlators with common masses we are able to determine the masses better, and hence get a better determined amplitude for the random-wall source correlator.

Four source time slices are used on each lattice, with the exception of the 0.06 fm physical quark-mass ensemble where, because these lattices are longer in the Euclidean time direction, six source time slices are used. The location of the source time slices on successive lattices is advanced by an amount close to one half of the spacing between sources, but incommensurate with the lattice time size, so that the source location cycles among all possible values.

In each lattice ensemble, two-point correlators are computed for a range of valence-quark masses. The complete set of valence-quark masses is given in Table 3.2. The lightest valence mass used is one-tenth the strange quark mass for the coarser ensembles with heavier sea-quark masses, 1/20 the strange quark mass for the $a \approx 0.06$ fm ensembles with heavier than physical sea-quark

TABLE 3.2: Valence-quark masses used in this project. Correlators with random wall and Coulomb-wall sources are computed for each possible pair of valence-quark masses. Light valence masses m_v are given in units of the (ensemble value of the) sea strange quark mass m'_s. Note that for the four ensembles with near-physical sea-quark mass, the lightest valence mass is the same as the light sea mass. The two heavy valence masses are in units of the charm sea-quark mass m'_c. For the ensembles with unphysical strange quark mass (included in "All" at $\beta = 6.0$), the valence masses are given in units of the approximate physical strange quark mass, 0.0507.

β	sea quark masses			light valence masses	charm valence masses
	am'_l	am'_s	am'_c	m_v/m'_s	m_v/m'_c
5.80	0.013	0.065	0.838	0.1,0.15,0.2,0.3,0.4,0.6,0.8,1.0	0.9,1.0
5.80	0.0064	0.064	0.828	0.1,0.15,0.2,0.3,0.4,0.6,0.8,1.0	0.9,1.0
5.80	0.00235	0.0647	0.831	0.036,0.07,0.1,0.15,0.2,0.3,0.4,0.6,0.8,1.0	0.9,1.0
6.00	0.0102	All	0.635	0.1,0.15,0.2,0.3,0.4,0.6,0.8,1.0	0.9,1.0
6.00	0.00507	All	0.628	0.1,0.15,0.2,0.3,0.4,0.6,0.8,1.0	0.9,1.0
6.00	0.00184	0.0507	0.628	0.036,0.073,0.1,0.15,0.2,0.3,0.4,0.6,0.8,1.0	0.9,1.0
6.30	0.0074	0.037	0.440	0.1,0.15,0.2,0.3,0.4,0.6,0.8,1.0	0.9,1.0
6.30	0.00363	0.0363	0.430	0.1,0.15,0.2,0.3,0.4,0.6,0.8,1.0	0.9,1.0
6.30	0.0012	0.0363	0.432	0.033,0.066,0.1,0.15,0.2,0.3,0.4,0.6,0.8,1.0	0.9,1.0
6.72	0.0048	0.024	0.286	0.05,0.1,0.15,0.2,0.3,0.4,0.6,0.8,1.0	0.9,1.0
6.72	0.0024	0.024	0.286	0.05,0.1,0.15,0.2,0.3,0.4,0.6,0.8,1.0	0.9,1.0
6.72	0.0008	0.022	0.260	0.036,0.068,0.1,0.15,0.2,0.3,0.4,0.6,0.8,1.0	0.9,1.0

mass, and the physical light-quark mass for the ensembles with physical sea-quark mass. The valence masses chosen then cover the range from this lightest mass up to the estimated strange-quark mass. We then choose additional masses at the estimated charm-quark mass (the same as the charm-quark mass in the sea), as well as nine-tenths of that value, so that we can make adjustments for mistuning of the charm-quark mass. For these last two quarks, the coefficient of the three-link term in the fermion action (the "Naik term") is adjusted to improve the quark's dispersion relation [92]. Specifically, the expansion resulting from combining Eqs. (24) and (26) of Ref. [92] is used; the improvement has been checked in HISQ simulations [70, 92].

3.3 Two-point correlator fits

To find the pseudoscalar masses and decay amplitudes, the random-wall and Coulomb-wall correlators are fitted to common masses but independent amplitudes. With staggered quarks the Goldstone-taste pseudoscalar correlators with unequal quark masses contain contributions from opposite-parity states, which show up as exponentials multiplied by an alternating sign, $(-1)^t$. For valence-quark masses up to and including the strange quark mass these contributions are small, and good fits can be obtained while neglecting them. In fact, in our previous analyses with the asqtad quark action, these states were not included in the two-point fits. However,

with these data sets, slightly better fits are obtained when an opposite-parity state is included in the light-light fits, and so we include such a state in the unequal quark mass correlators.

The light-charm correlators (where "light" here includes masses up to the physical strange quark mass m_s) are more difficult to fit than the light-light correlators for several reasons. First, because the difference in the valence-quark mass is large, the amplitude of the opposite-parity states is not small. Second, the mass splitting between the ground state and the lowest excited single particle state is smaller. For the light-light correlators, the approximate chiral symmetry makes the ground state mass smaller than typical hadronic scales, which has the side effect of making the mass gap to the excited single particle states large, and these excited states can be suppressed by simply taking a large enough minimum distance. For the charm-light correlators we include an excited state in the fit function. (In principle, multiparticle states also appear in these correlators. For example, the lowest excited state in the pion correlator would be a three-pion state. Empirically these states do not enter with large amplitudes, and the important excited states correspond more closely to single particle states.)

To make the fits converge reliably, it is necessary to loosely constrain the masses of the opposite-parity and excited states by Gaussian priors. The central value of the gap between the ground state and opposite parity states is taken to be 400 MeV, motivated by the 450 MeV gap between the D mass and the 0^+ light-charm mass, and the 350 MeV gap between the D_s mass and a poorly established 0^+ strange-charm meson [93]. The central value for the gap between the ground state and excited state masses is taken to be 700 MeV, motivated by the 660 MeV gap between the η_c and the corresponding 2S state. In most cases the widths of the priors for the opposite-parity and excited state gaps are taken to be 200 MeV and 140 MeV respectively, although in some cases these need to be adjusted to get all of the jackknife fits to converge.

Another factor that makes the light-charm correlators more difficult to fit is the faster growth of the statistical error. The time dependence of the variance of a correlator is expected to depend on time as $e^{-E_2 t}$, where E_2 is the energy of the lowest lying state created by $\mathcal{O}\mathcal{O}^\dagger$, where $\mathcal{O}$ is the source operator for the correlator itself, with the proviso that quark and antiquark lines all go from source to sink, rather than coming back to the source [94]. For the pion correlator, the state created by $\mathcal{O}\mathcal{O}^\dagger$ is just the two pion state, leading to the expectation that the fractional statistical error on the pion correlator is roughly independent of distance. However, for the light-charm correlator, the quarks and antiquarks created by $\mathcal{O}\mathcal{O}^\dagger$ can pair up to form an η_c and a pion. Then, the reduction of the pion's mass from chiral symmetry makes this state much lighter than $2M_D$, so the fractional error of the propagator grows rapidly with distance. This makes it essential to use smaller minimum distances in the fit range for the light-charm correlators, which

of course makes the problem of excited states discussed in the previous paragraph even more serious.

Table 3.3 shows our expectations for the states controlling the growth of statistical errors for the various pseudoscalar correlators. Figure 3.1 shows the fractional errors for the random-wall correlators for the 0.09 fm physical quark-mass ensemble, with comparison to the slopes expected from Table 3.3. With the exception of the charm-charm correlator, the behavior of the statistical error agrees with our theoretical expectations.

Figures 3.2 and 3.3 show the masses in the 2+1 state fits for the light-charm correlators in the $a \approx 0.09$ fm physical quark-mass ensemble as a function of the minimum distance included in the fit, where the light-quark mass is the physical $(m_u + m_d)/2$ (Fig. 3.2) and m_s (Fig. 3.3). Fit ranges are chosen from graphs like this for all the ensembles, and analogous graphs for the light-light and charm-charm correlators. We show this ensemble because it, together with the $a \approx 0.06$ fm physical mass ensemble, is the most important to the final results. In these graphs the error bars on the right show the central values and widths of the priors used for the opposite-parity and excited masses. At short distances, these masses are more accurately determined by the data, while at larger D_{min} the input prior controls the mass. The linear sizes of the symbols in these figures are proportional to the p value of the fit, with the size of the symbols in the legend corresponding to 50%. In the two-point correlator fits used to choose the fit types and ranges, as in Figs. 3.2 and 3.3, autocorrelations among the lattices are minimized by first blocking the data in blocks of four lattices, or 10 to 24 molecular dynamics time units. However, statistical errors on results in later sections are obtained from the jackknife procedures described in Secs. 3.4.1 and 3.4.2. In these analyses the two-point fits are repeated in each jackknife resampling. From these and similar graphs for other ensembles and different numbers of excited states, keeping the minimum distance in physical units reasonably constant, the minimum distances and fit forms in Table 3.4 are chosen. The need for using a smaller minimum distance and including an excited state in the heavy-light fits is consistent with our expectations from Table 3.3 and Fig. 3.1. Because the statistical errors increase with distance from the source, the fits are much less sensitive to the choice of maximum distance. In most cases the maximum distance is taken to be one less than the midpoint of the lattice. However, in the $a \approx 0.09$ and 0.06 fm ensembles, the light-charm and charm-charm fits used a smaller maximum distance because having fewer points in the fit gave a better conditioned covariance matrix. These maximum distances are also included in Table 3.4.

TABLE 3.3: States expected to control the statistical errors on the correlators, for the pseudoscalars with physical valence-quark masses. The second column shows the state expected to control the growth of the statistical error on the correlator, the third column the mass gap between half the mass of the error state and the particle mass, and the fourth column the length scale for the growth of the fractional statistical error. Here $\bar{s}s$ is the unphysical flavor nonsinglet state, with mass 680 MeV.

State	Error	Energy gap (MeV)	Growth length (fm)
π	2π	0	∞
K	$\pi + \bar{s}s$	90	2.26
η_c	$2\eta_c$	0	∞
D_s	$\eta_c + \bar{s}s$	140	1.42
D	$\eta_c + \pi$	310	0.64

TABLE 3.4: Fit forms and minimum distance included for the two-point correlator fits. Here the fit form is the number of negative parity (*i.e.*, pseudoscalar) states "plus" the number of positive parity states. When the valence quarks have equal masses, the opposite-parity states are not included. In this work the charm-charm fits are needed only for computing the mass of the η_c meson, used as a check on the quality of our charm physics.

	light-light			light-charm			charm-charm		
	form	D_{min}	D_{max}	form	D_{min}	D_{max}	form	D_{min}	D_{max}
$a \approx 0.15$ fm	1+1	16	23	2+1	8	23	2+0	9	23
$a \approx 0.12$ fm	1+1	20	31	2+1	10	31	2+0	12	23
$a \approx 0.09$ fm	1+1	30	47	2+1	15	37	2+0	18	35
$a \approx 0.06$ fm	1+1	40	71	2+1	20	51	2+0	21	50

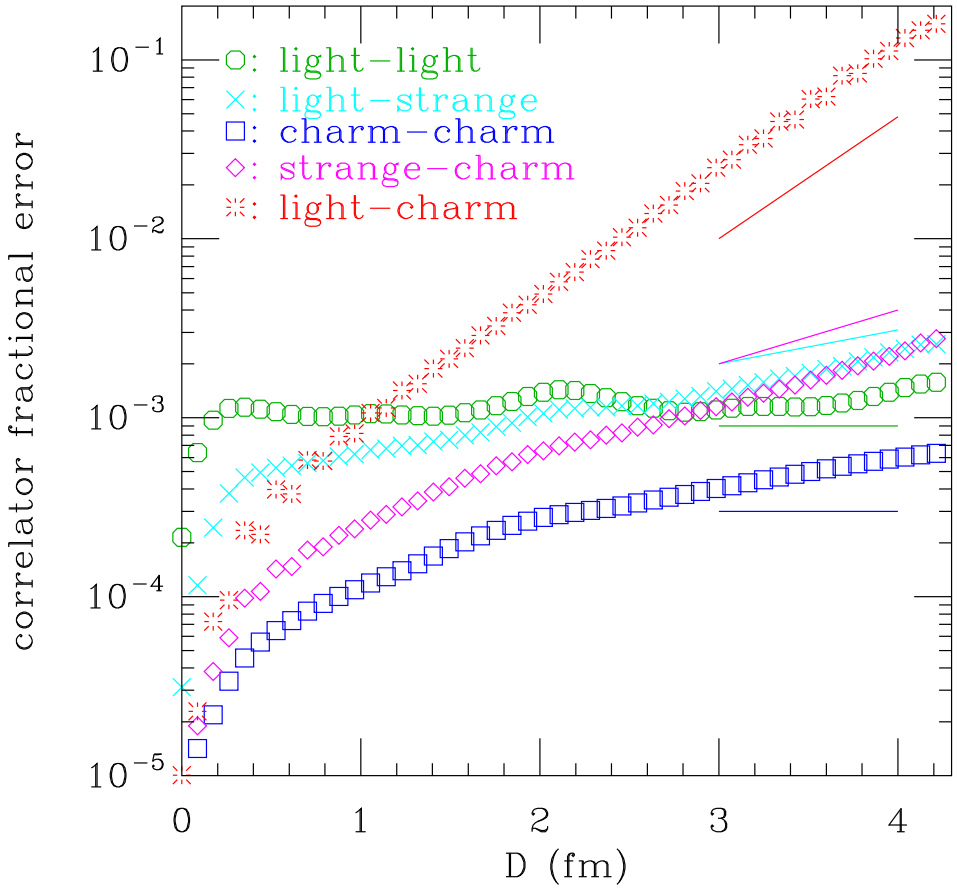

FIGURE 3.1: Fractional errors for pseudoscalar correlators as a function of distance from the 0.09 fm physical quark-mass ensemble. The line segments show the slope expected from the states in Table 3.3, which give a good approximation to the observed growth of the errors with the exception of the charm-charm correlator.

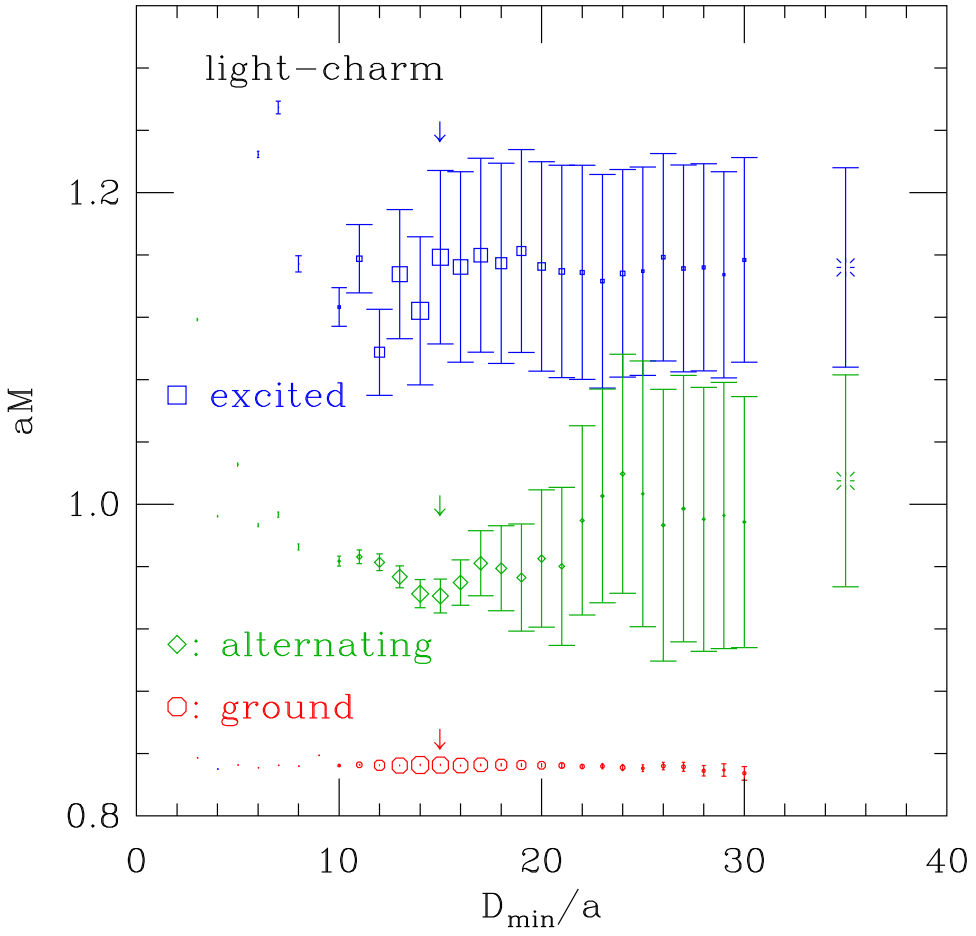

FIGURE 3.2: Fits for the light-charm pseudoscalar correlator (mass M) in the ensemble with $a \approx 0.09$ fm and physical sea-quark masses. We plot the ground state, alternating state (opposite parity) and excited state masses as a function of minimum distance included in the fit. The size of the symbols is proportional to the p value of the fit, with the size of the symbols in the legend corresponding to 0.5. The two bursts on the right show the priors and their errors for the alternating and excited masses. The vertical arrows at $D_{min} = 15$ indicate the fit that is chosen. Further discussion is in the text. Here the masses and distance are in units of the lattice spacing.

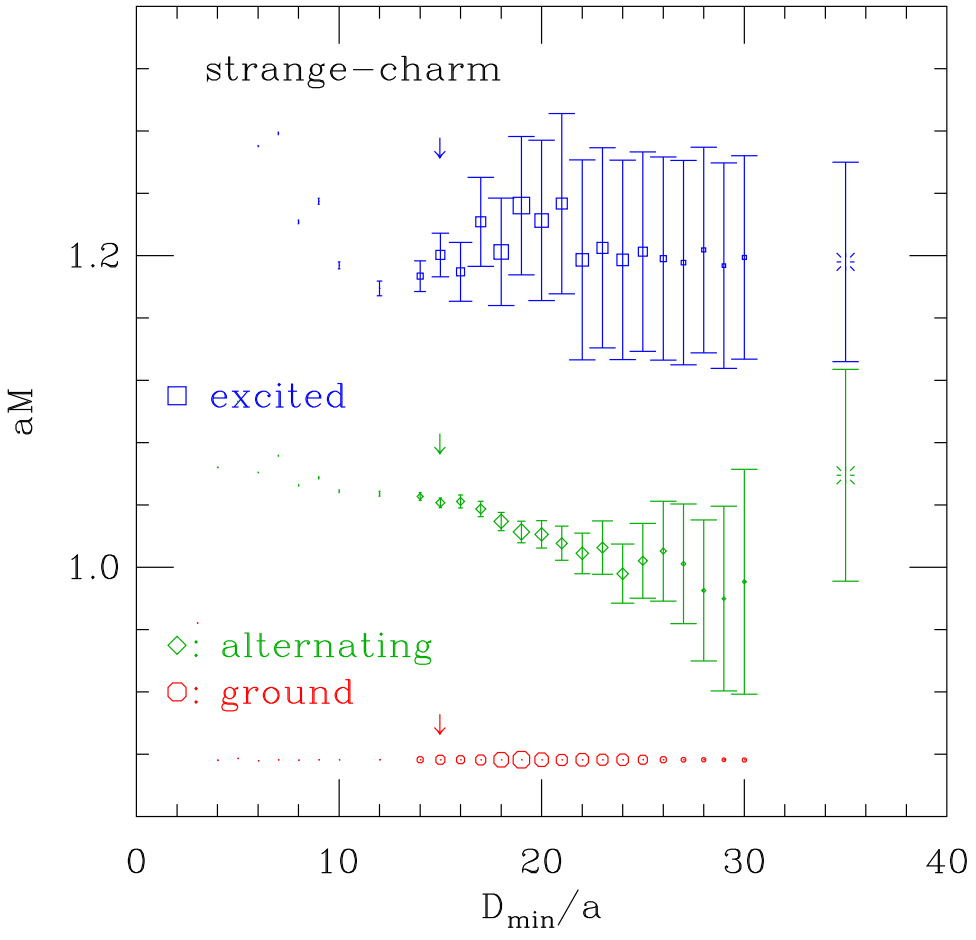

FIGURE 3.3: Fits for the strange-charm correlator in the ensemble with $a \approx 0.09$ fm and physical sea-quark masses. The format and symbols are the same as in Fig. 3.2.

3.4 Determination of decay constants and quark-mass ratios

This section describes the details of the analyses that produce our results for light-light and heavy-light decay constants and the ratios of quark masses. We perform two versions of the analysis. The first, the "physical-mass analysis" described in Sec. 3.4.1, is a straightforward procedure that essentially uses only the physical-quark mass ensembles. On these ensembles, a chiral extrapolation is not needed: only interpolations are required in order to find the physical quark-mass point. The physical-mass analysis produces our results for quark-mass ratios and f_{K^+}/f_{π^+}, as well as some additional intermediate quantities required for the chiral analysis of the D meson decay constants, which follows. The second analysis of charm decay constants, described in Sec. 3.4.2, uses chiral perturbation theory to perform a combined fit to all of our physical-mass and unphysical-mass data, and to thereby significantly reduce the statistical uncertainties of the results. We take the more precise values of f_{D^+}, f_{D_s}, and their ratio from the chiral analysis as our final results, and use those from the simpler physical-mass analysis only as a consistency check, and to aid in the estimation of systematic errors.

In the physical-mass analysis of Sec. 3.4.1, we first determine the lattice spacing and quark masses separately for each ensemble, using, in essence, the five experimental values of f_{π^+}, M_{π^0}, M_{K^0}, M_{K^+} and M_{D_s}, as explained in Sec. 3.4.1.1. In order to adjust for mistuning of the sea-quark masses, we perform a parallel scale-setting and quark-mass determination on the unphysical-mass ensembles; there, however, an extrapolation in the valence-quark mass is generally required. We extrapolate the quark-mass ratios to the continuum, after small sea-quark mistuning adjustments, in Sec. 3.4.1.2. We follow the same procedure on the physical-mass ensembles to also obtain values for decay constants. In particular, we update our result for f_{K^+}/f_{π^+} from Ref. [67]. Although the results for charm decay constants from the physical-mass analysis are not taken as our final values, they are used as additional inputs in the estimation of systematic errors from the continuum extrapolation. Finally, the physical-mass analysis allows us to make straightforward estimates of systematic errors coming from finite-volume and electromagnetic (EM) effects on the decay constants and quark-mass ratios, as described in Sec. 3.4.1.3.

The values of the physical quark-mass ratios m_c/m_s, m_s/m_l, and (to a lesser extent, in order to take into account isospin-violating effects) m_u/m_d obtained in Sec. 3.4.1 are used in the subsequent chiral analysis in Sec. 3.4.2. Further, in the physical-mass analysis, we determine the useful quantity F_{p4s} [71], which is the light-light pseudoscalar decay constant F evaluated at a fiducial point with both valence masses equal to $m_{p4s} \equiv 0.4 m_s$ and physical sea-quark masses. The meson mass at the same fiducial point, M_{p4s}, as well as the ratio $R_{p4s} \equiv F_{p4s}/M_{p4s}$, are

similarly determined. The unphysical decay constant F_{p4s} provides an extremely precise and convenient quantity to set the relative scale in the chiral analysis (see Sec. 3.4.2.2), while we use R_{p4s} to tune the strange sea-quark mass.

The chiral analysis of the decay constants of charm mesons is described in detail in Sec. 3.4.2. With chiral perturbation theory, one can take advantage of all our data by including both the physical-mass and unphysical-mass ensembles in a unified procedure. In particular, the statistical error in Φ_{D^+} is slightly more than a factor of two smaller with the chiral analysis than in the physical-mass analysis of Sec. 3.4.1. In addition, the use of the relevant form of staggered chiral perturbation theory for this case, heavy-meson, rooted, all-staggered chiral perturbation theory (HMrASχPT) [86], allows us to relate the quark-mass and lattice-spacing dependence of the data, and thereby use the unphysical-mass ensembles to tighten the control of the continuum extrapolation. Our final central values for the charm decay constants given in the conclusions are taken from the chiral analysis. We increase some of the systematic uncertainties, however, to take into account differences with the results of the physical-mass analysis.

3.4.1 Simple analysis from physical quark-mass ensembles

Here we determine the quark-mass ratios and decay constants employing primarily the physical quark-mass ensembles. First, in Sec. 3.4.1.1, we determine the lattice spacing, quark masses, and decay constants separately for each ensemble. Next, in Sec. 3.4.1.2, we adjust the quark masses and decay constants for slight sea-quark mass mistuning, and extrapolate to the continuum. Finally, we estimate the systematic uncertainties in the quark-mass ratios and decay constants in Sec. 3.4.1.3. We present results and error budgets for these quantities obtained from the physical mass analysis in Table 3.6.

3.4.1.1 Valence-quark mass interpolation

In this stage of the analysis we determine tuned quark masses and the lattice spacing (using f_{π^+} to fix the scale) for each ensemble, and then find the decay constants by interpolation or extrapolation in valence-quark mass to these corrected quark masses. There are a number of possible choices for the procedure used, and we include the differences among a few sets of choices in our systematic error estimate. It is important to remember that there is inherent ambiguity in defining a lattice spacing for ensembles with unphysical sea-quark masses, but all sensible choices should have the same limit at zero lattice spacing and physical sea-quark masses. For example, in the ensemble-by-ensemble fitting procedure described in this section, we take

the value of f_{π^+} on each ensemble to be 130.41 MeV, independent of sea-quark masses, while for the chiral perturbation theory analysis we take the lattice spacing to be independent of the sea-quark masses.

Figure 3.4 illustrates some of the features of our procedure, and referring to it may help clarify the following description. Since the decay amplitude F depends on valence-quark mass, and we wish to use $f_{\pi^+} = 130.41$ MeV to set the lattice scale, we must determine the lattice spacing and tuned light-quark mass simultaneously. To do so, we find the light valence-quark mass where the mass and amplitude of the pseudoscalar meson with degenerate valence quarks have the physical ratio of $M_\pi^2/f_{\pi^+}^2$. (Actually we adjust this ratio for finite size effects, using the pion mass and decay constant in a 5.5 fm box. This correction is discussed in Sec. 3.4.1.3.) This light-quark mass is the average of the up and down quark masses, $m_l = (m_u + m_d)/2$. Here we use the mass of the π^0, since it is less affected by electromagnetic corrections than the π^+. Since the π^+ contains one up and one down quark, the error in f_{π^+} from using degenerate light valence quarks is negligible. This tuning is illustrated in the upper left panel of Fig. 3.4, which shows this ratio as a function of light valence mass for the 0.09 fm physical quark-mass ensemble, one of the two ensembles that are most important in our analysis. The octagons in this panel are the ratio at the valence-quark masses where we calculated correlators, with error bars that are too small to be visible. The horizontal red line is the desired value of this ratio, and the green vertical line shows the light-quark mass where the ratio has its desired value. With the tuned light-quark mass determined, we use the decay amplitude at this mass, f_{π^+}, to fix the lattice spacing. In performing the interpolation or extrapolation of M_π^2/f_π^2 we use points with degenerate light valence-quark mass $m_{\rm v}$ and employ a continuum, partially quenched, SU(2) χPT form [23, 95],

$$\begin{aligned}
\frac{M_\pi^2}{f_\pi^2} &= \frac{B2m_{\rm v}}{f^2}\left\{1 + \frac{1}{16\pi^2 f^2}\left[B(4m_{\rm v} - 2m_l')\log(2Bm_{\rm v}/\Lambda_\chi^2)\right.\right. \\
&\qquad \left.\left. +4B(m_{\rm v} + m_l')\log(B(m_{\rm v} + m_l')/\Lambda_\chi^2)\right] + Cm_{\rm v}\right\} \\
f_\pi &= f\left\{1 - \frac{2B(m_{\rm v} + m_l')}{16\pi^2 f^2}\log(B(m_{\rm v} + m_l')/\Lambda_\chi^2) + Cm_{\rm v} + Dm_{\rm v}^2\right\}\ , \qquad (3.4)
\end{aligned}$$

where m_l' is the light sea-quark mass and Λ_χ is the chiral scale. In applying Eq. (3.4), we fix the low energy constants B and f in the coefficients of the logarithms to values determined from lowest order χPT using the smallest valence-quark mass. We then fix the coefficients of $m_{\rm v}$ and $m_{\rm v}^2$ in M_π^2/f_π^2 using the smallest two valence-quark masses available, and we fix the

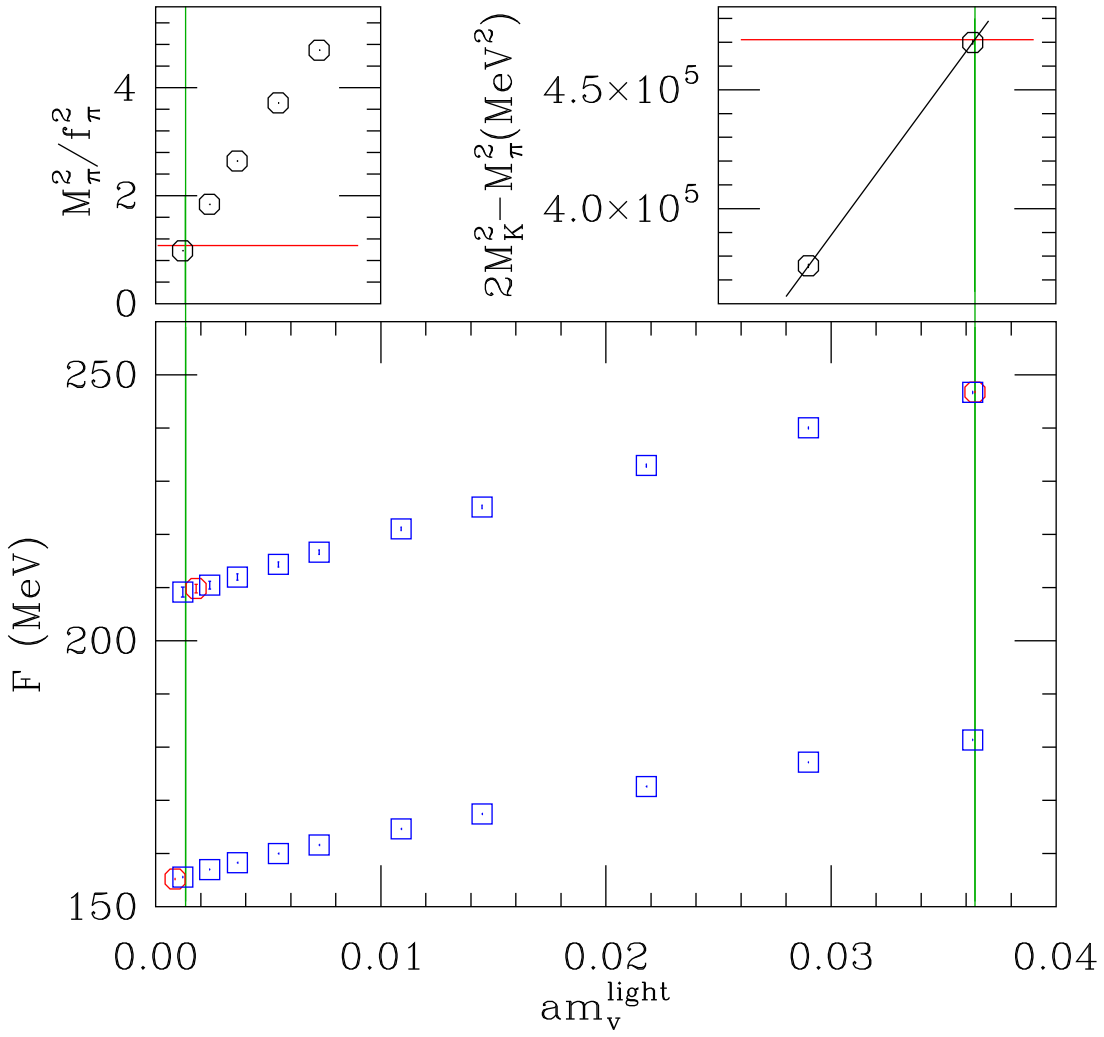

FIGURE 3.4: Illustration of the "f_π" tuning for the $a \approx 0.09$ fm physical quark mass ensemble. F is the decay constant of a generic pseudoscalar meson. The procedure illustrated is described in the text.

analytic coefficients in f_π using the three smallest valence-quark masses. In the physical quark-mass ensembles, such as the one shown in Fig. 3.4, this is only a small correction to the quark mass. On the other hand, in most of the ensembles with $m'_l/m'_s = 0.1$ or 0.2, the lightest valence-quark mass is $0.05m'_s$ or $0.1m'_s$, and a significant extrapolation is made. However, these unphysical-mass ensembles are used only in the analysis of this section to correct the results of the physical-mass ensembles for small mistunings of the sea masses in the physical-mass ensembles.

We then fix the tuned strange quark mass to the mass that gives the correct $2M_K^2 - M_\pi^2$. This is illustrated in the upper right panel of Fig. 3.4. In all of our ensembles, we use valence "strange" quark masses at the expected strange quark mass and at 0.8 times this mass. The two data points shown in the figure have these strange masses and the lightest available light-quark valence mass. A linear interpolation or extrapolation is performed through these two points. Again, the horizontal red line shows the desired value of this mass difference, and the vertical green line the resulting value of m_s. In this stage of the tuning the kaon mass is corrected for finite volume effects, electromagnetic effects and isospin breaking effects, where again we defer the details to the discussion of systematic errors in Sec. 3.4.1.3.

Next we determine the up-down quark mass difference, and hence the up and down quark masses. We use the difference in K^0 and K^+ masses,

$$m_d - m_u = \frac{M^2_{K^0_{\rm adj}} - M^2_{K^+_{\rm adj}}}{\frac{\partial M_K^2}{\partial m_l}} \quad . \tag{3.5}$$

Here the kaon masses are adjusted for finite volume and electromagnetic effects, and again we defer the details to Sec. 3.4.1.3. We note that the electromagnetic corrections are a small effect on the strange quark mass tuning, but are absolutely crucial in the determination of $m_d - m_u$. To estimate the derivative $\partial M_K^2/\partial m_l$, we use the masses of kaons containing a valence quark near the strange quark mass and a second valence quark that is one of the two lightest valence quarks we have.

Then the tuned charm quark mass is determined from the experimental value of M_{D_s}. We use M_{D_s} rather than M_D because it has much smaller statistical errors. In all of our ensembles we have correlators with valence-quark masses at the expected charm quark mass and at 0.9 times this mass. Using linear interpolations in m_s of the D_s meson mass at these two "charm" masses to the strange quark mass found earlier, and a linear interpolation in m_c between these, we find a tuned charm quark mass.

Now that we have found the lattice spacing and tuned quark masses, we can find decay constants and masses of other mesons by interpolating or extrapolating to these quark masses.

TABLE 3.5: Tuned lattice spacings (using f_{π^+} to set the scale) and quark masses for the physical quark-mass ensembles. The quark mass entries show the light, strange and charm quark masses in units of the lattice spacing. The column labeled am' gives the run values of the sea quark masses.

a_{approx}(fm)	a_{tuned}(fm)	am'	am_{tuned}
0.15	0.15089(17)	0.00235/0.0647/0.831	0.002426(8)/0.06730(16)/0.8447(15)
0.12	0.12121(10)	0.00184/0.0507/0.628	0.001907(5)/0.05252(10)/0.6382(8)
0.09	0.08779(8)	0.0012/0.0363/0.432	0.001326(4)/0.03636(9)/0.4313(6)
0.06	0.05676(6)	0.0008/0.0220/0.260	0.000799(3)/0.02186(6)/0.2579(4)

The bottom panel of Fig. 3.4 illustrates this process. The lower set of points in this graph are the decay constants at each light valence mass, interpolated using the two "strange" valence masses to the tuned strange quark mass. Then f_{K^+} is found by extrapolating these points to the tuned m_u, illustrated by the red octagon at the lower left. Similarly, the upper set of data points is the decay constant at each light-quark mass, linearly interpolated or extrapolated using the two "charm" valence masses to the tuned m_c. This graph is then interpolated or extrapolated to the tuned m_d to find f_{D^+}, shown in the red octagon at the upper left, or to the tuned m_s to find f_{D_s}, shown by the red octagon at the upper right.

As checks on our procedure, we also similarly interpolate or extrapolate in the meson masses to find M_{D^0}, M_{D^+} and M_{η_c}.

3.4.1.2 Sea-quark mass adjustment and continuum extrapolation

In this stage we combine the results from the individual ensembles and fit to a function of the lattice spacing to find the continuum limit. We use the ensembles with unphysical sea-quark masses to make small adjustments for the fact that the sea-quark masses in the physical quark-mass ensembles were fixed after short tuning runs, and inevitably turned out to be slightly mistuned when the full runs are done. The amount of mistuning is shown in Table 3.5, which gives the sea-quark masses and the tuned quark masses for the physical quark-mass ensembles.

Fitting to the lattice spacing dependence is straightforward, because the results from each ensemble are statistically independent. We have performed continuum extrapolations for the ratios of quark masses, m_u/m_d, m_s/m_l, and m_c/m_s, which come automatically from the fitting for each ensemble described in Sec. 3.4.1.1. Figures 3.5, 3.6, and 3.7 show the results for each ensemble, together with fits to the lattice spacing dependence. In these plots the abscissa is $a^2\alpha_S$, where α_S is an effective coupling constant determined from taste violations in the pion masses. The relative value of α_S at a given coupling β, compared to its value at a fixed, fiducial

coupling β_0, is given by

$$\frac{\alpha_S(\beta)}{\alpha_S(\beta_0)} = \sqrt{\frac{(a^2\bar{\Delta})_\beta \; a^2(\beta_0)}{(a^2\bar{\Delta})_{\beta_0} \; a^2(\beta)}} \,, \tag{3.6}$$

where $(a^2\bar{\Delta})_\beta$ is the mean squared taste splitting at coupling β, and $a(\beta)$ is the lattice spacing given below in Table 3.8. Equation (3.6) assumes that $a^2\bar{\Delta}$ is proportional to $\alpha_S^2 a^2$, its leading behavior. We use $\beta_0 = 5.8$ in these plots, and scale α_S to agree with the coupling α_V at $\beta_0 = 5.8$, which in turn may be determined from the plaquette [96] as explained after Eq. (9) of Ref. [71].

In these figures the fit used to determine the central value is shown in black. This is a quadratic polynomial fit through the four physical quark-mass points. In this fit, small adjustments have been made to compensate for sea-quark mass mistuning. To make these adjustments, the derivative of each quantity with respect to sea-quark mass is found from a fit including both the physical quark-mass ensembles and the $0.1m'_s$ ensembles, and this derivative is used to adjust each point in the fit. The resulting adjustments are too small to be visible in Figs. 3.5, 3.6, and 3.7. Other fits shown in these figures are used in estimating the systematic error resulting from our choice of fitting forms. The blue lines in each figure show the fit including the $0.1m'_s$ points, where the fit is quadratic in a^2 and linear in m'_l/m'_s. Here the solid line is the fit evaluated at the physical sea-quark mass, and the dashed line is the fit evaluated at $m'_l = 0.1m'_s$. The red lines are extrapolations using only the finer lattice spacings: the curved solid line is a quadratic through the 0.06, 0.09 and 0.12 fm ensembles, and the dashed straight line is a line through the finest two points. The diamonds at $\alpha_S a^2 = 0$ indicate the continuum extrapolations of the various fits. It is clear from the curvature in Figs. 3.5, 3.6, and 3.7 that a quadratic term is needed. However, it makes only a negligible difference whether this quadratic term is taken to be $(\alpha_S a^2)^2$, as is done here for convenience, or simply $(a^2)^2$. Other continuum extrapolations not shown here use $\alpha_V a^2$, where α_V is the strong coupling constant computed from the plaquette, or simply a^2 as the abscissa.

The four extrapolations in Figs. 3.5, 3.6, and 3.7, together with quadratic fits to the physical mass points using $\alpha_V a^2$ or a^2 as the abscissa, make a set of six continuum extrapolations for these and other quantities. The six versions are used to estimate the systematic errors of the quark mass ratios and light-meson decay constants, and to inform the systematic error analysis of Sec. 3.4.2.4.

In Fig. 3.5 and, to a lesser extent in Figs. 3.6 and 3.7, the points at small lattice spacing with unphysical light sea quark masses deviate strongly from the physical sea quark mass points. This is mostly a partial quenching effect that shows up for valence quark masses small compared to the light sea quark mass. In particular, the squared pseudoscalar meson mass is increased by a partially quenched chiral log, which means that a smaller tuned light valence quark mass is

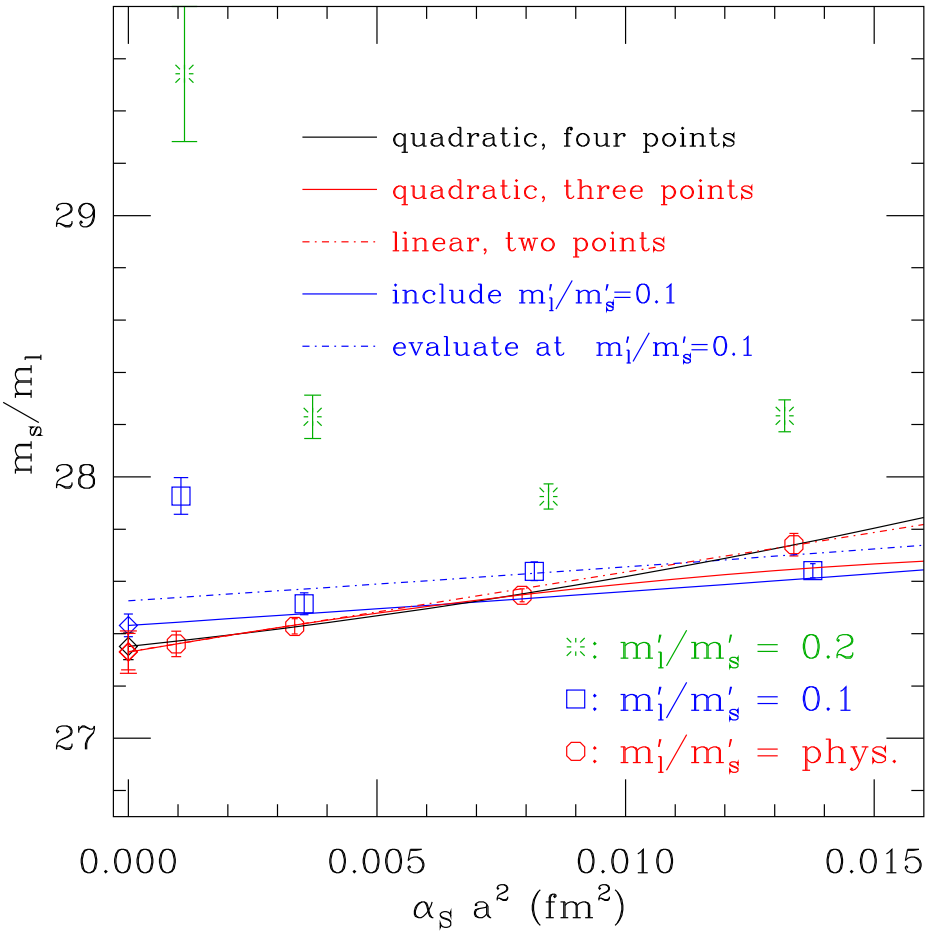

FIGURE 3.5: The tuned ratio of strange quark mass to light-quark mass, m_s/m_l, on each ensemble, for the physical quark-mass ensembles (red octagons), for $m'_l/m'_s = 0.1$ (blue squares) and for $m'_l/m'_s = 0.2$ (green bursts). The fits shown in this and subsequent figures are described in the text. The diamonds at the left indicate the continuum extrapolations of the various fits.

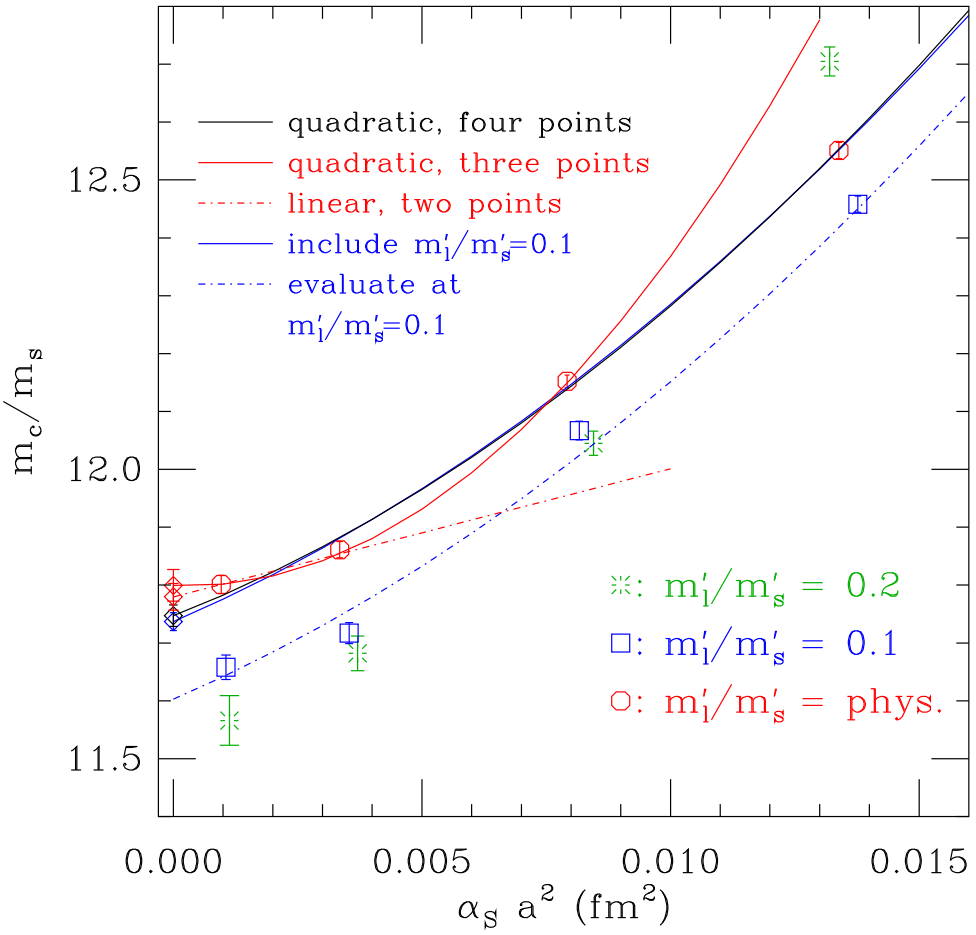

FIGURE 3.6: The tuned ratio of charm quark mass to strange quark mass, m_c/m_s, on each ensemble. The notation and choice of fits is the same as in Fig. 3.5.

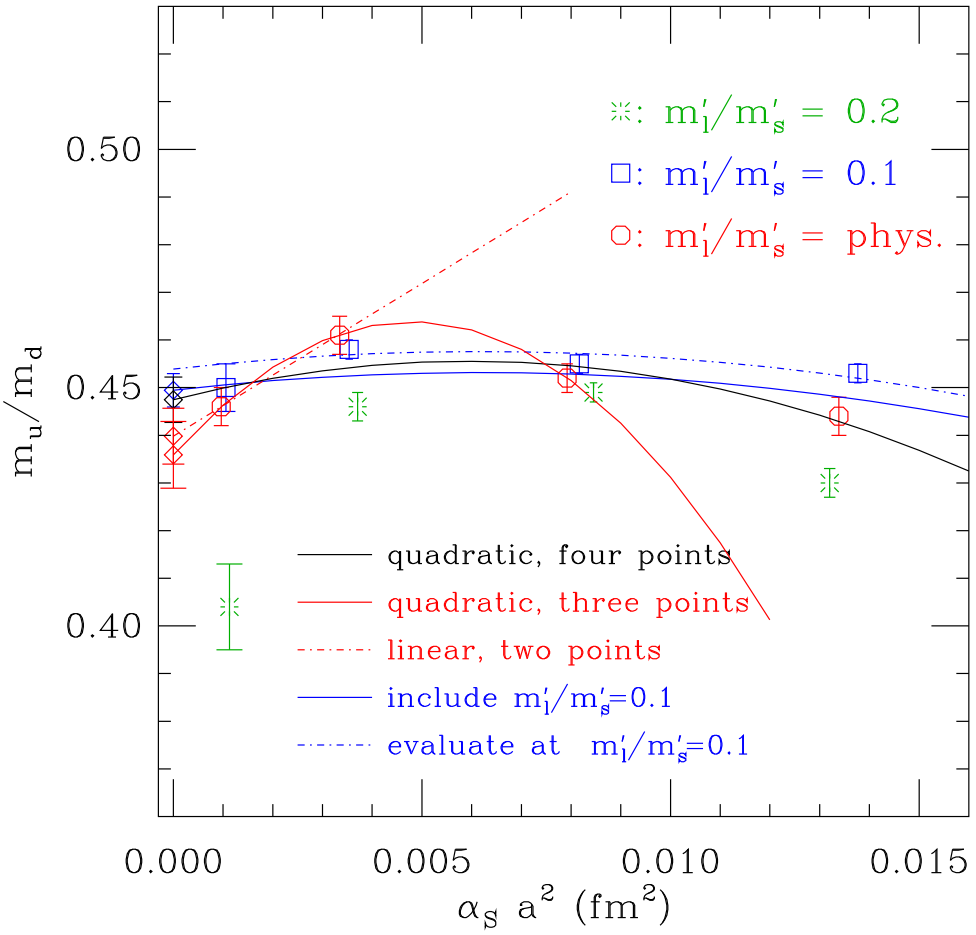

FIGURE 3.7: The ratio of up quark mass to down quark mass, m_u/m_d, on each ensemble. The notation and choice of fits is the same as in Fig. 3.5.

needed to give the desired M^2/F^2. This has the direct effect of increasing m_s/m_l, with smaller effects on all other quantities. This is mostly seen at the smallest lattice spacing because at larger lattice spacings taste violations smear out the chiral logs. Note that this partial quenching effect has negligible effect on our results for m_s/m_l and m_c/m_s, which depend almost exclusively on the data from the physical-mass ensembles.

We perform similar continuum extrapolations for the ratios of decay constants F_{p4s}/f_{π^+}, f_{K^+}/f_{π^+}, f_{D^+}/f_{π^+}, f_{D_s}/f_{π^+}, and f_{D_s}/f_{D^+}, and for M_{p4s} and $R_{p4s} = F_{p4s}/M_{p4s}$. Figure 3.8 shows the individual ensemble values and the same set of continuum extrapolations for the ratio f_{K^+}/f_{π^+}. As an example of a quantity involving a charm quark, Fig. 3.9 shows values and continuum extrapolations for the ratio f_{D_s}/f_{π^+}. The extrapolated value for f_{K^+}/f_{π^+} is our result for this quantity. Figure 3.10 shows the continuum extrapolations for F_{p4s} and $R_{p4s} \equiv F_{p4s}/M_{p4s}$. The resulting continuum values for F_{p4s} and R_{p4s} are used in the later analysis in Sec. 3.4.2. The values for the charm-meson decay constants provide consistency checks on the analysis in Sec. 3.4.2, and the spread in continuum values among the different extrapolations is included in our estimates of the systematic uncertainty from the continuum extrapolation. Finally, as a check, we extrapolate the mass of the η_c meson. These continuum extrapolations and their statistical errors are shown in Table 3.6.

Statistical errors on these quark mass ratios and decay constants are estimated with a jackknife method, where for each ensemble we perform the entire fitting procedure eliminating one configuration at a time. Autocorrelations are handled by estimating the final error from the variance of the jackknife resamples, after first blocking the jackknife results in blocks of 20 (eliminated) lattices, which corresponds to 50 molecular dynamics time units for the $a \approx 0.15$ fm physical quark mass ensemble, 100 molecular dynamics time units for the other $a \approx 0.15$ fm and the 0.12 fm ensembles and 120 time units for the $a \approx 0.09$ and 0.06 fm ensembles.

3.4.1.3 Finite volume and electromagnetic uncertainties

Our treatment of finite volume effects on the pion and kaon masses and decay constants is the same as described in Ref. [67], and we refer the reader to the discussion there. To summarize very briefly, we adjust these masses and decay constants to their values in a 5.5 fm box, the size of our physical quark mass lattices, and use these adjusted values in the tuning procedure described above. After the tuning and continuum extrapolation, at which point we have determined f_{K^+} in a 5.5 fm box, the adjustment is removed to get our result for f_{K^+} in infinite volume. As an estimate of the remaining finite size uncertainty we use the difference between results using staggered chiral perturbation theory and continuum chiral perturbation theory (NNLO for M_π

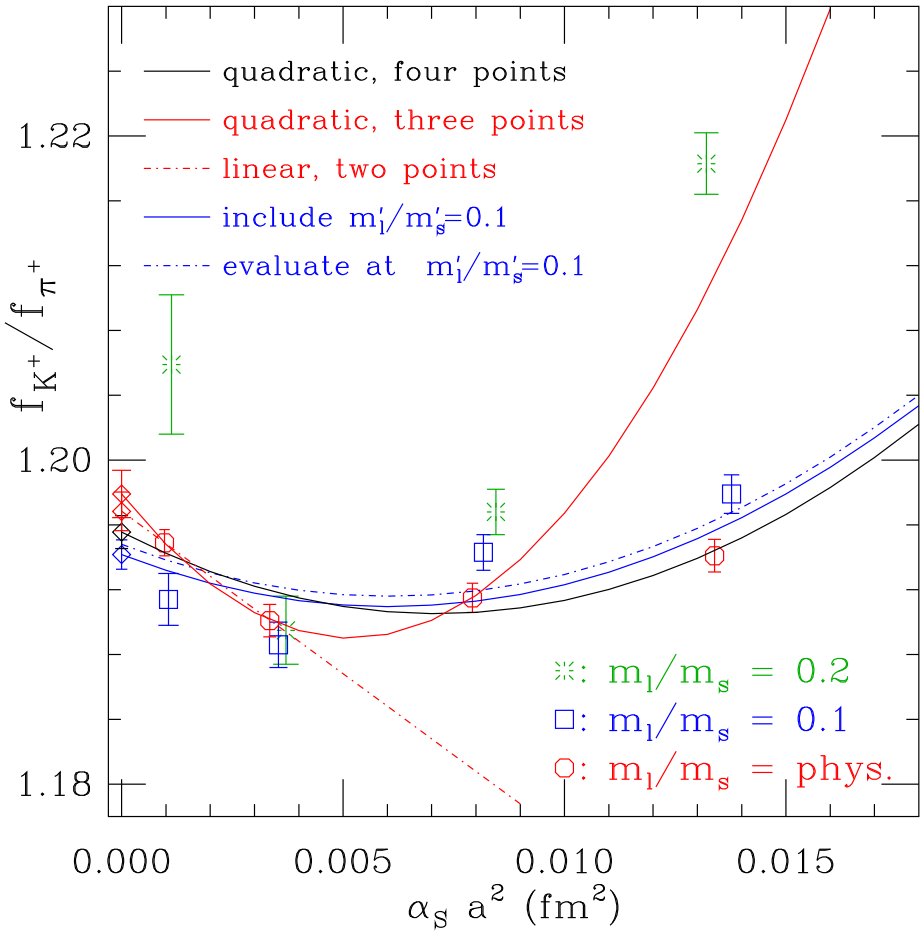

FIGURE 3.8: The ratio f_{K^+}/f_{π^+} on each ensemble, The notation and choice of fits is the same as in Fig. 3.5.

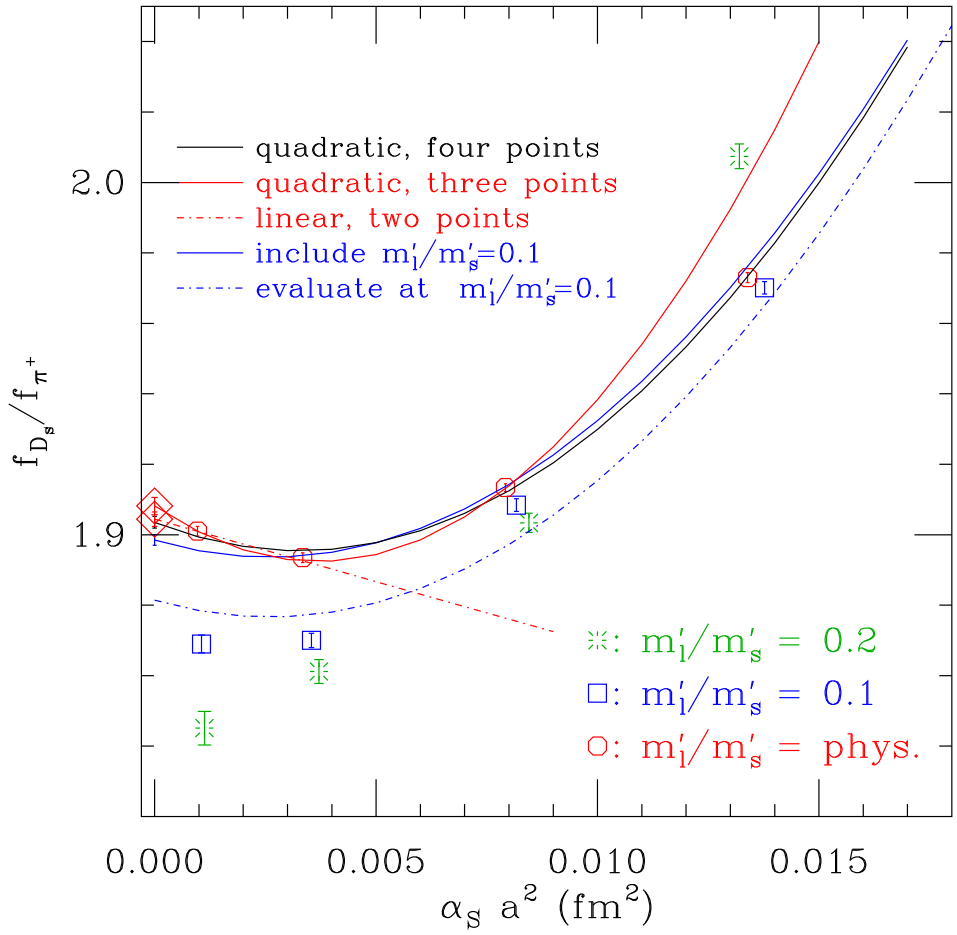

FIGURE 3.9: The ratio f_{D_s}/f_{π^+} on each ensemble. The notation and choice of fits is the same as in Fig. 3.5.

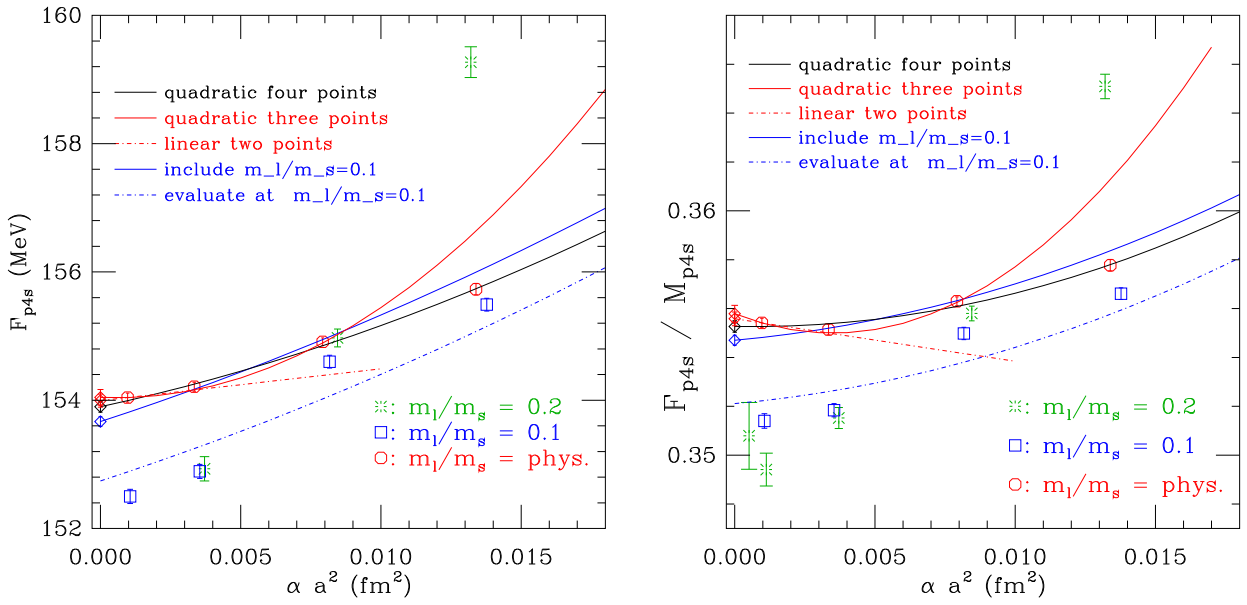

FIGURE 3.10: F_{p4s} and the ratio F_{p4s}/M_{p4s} on each ensemble. Here $f_\pi = 130.41$ MeV was used to set the scale to express F_{p4s} in MeV. The notation and choice of fits is the same as in Fig. 3.5.

and f_{π^+}, NLO for M_K and f_{K^+}) [67]. This difference, along with other systematic effects, is tabulated in Table 3.6. Finite size effects on the charm-meson masses and decay constants are, as expected, quite small. Figure 3.11 shows the charm-meson masses and decay constants on the three ensembles differing only in spatial size, showing no detectable finite size effects.

Our treatment of EM effects also follows Ref. [67], which in turn follows Ref. [66]. The current analysis uses updated inputs for the electromagnetic effects, so we repeat some of the discussion. Because our sea quarks are isospin symmetric, we adjust the experimental inputs to what they would be in a world without electromagnetism or sea-quark isospin violation before matching the simulation data to experiment to find the strange quark mass m_s and the average light-quark mass $\hat{m} = (m_u + m_d)/2$. Specifically, we do not adjust the neutral pion mass because the leading-order isospin correction to $M_{\pi^0}^2$ is $\propto (m_u - m_d)^2/\Lambda_\chi^2$ in χPT and therefore small,

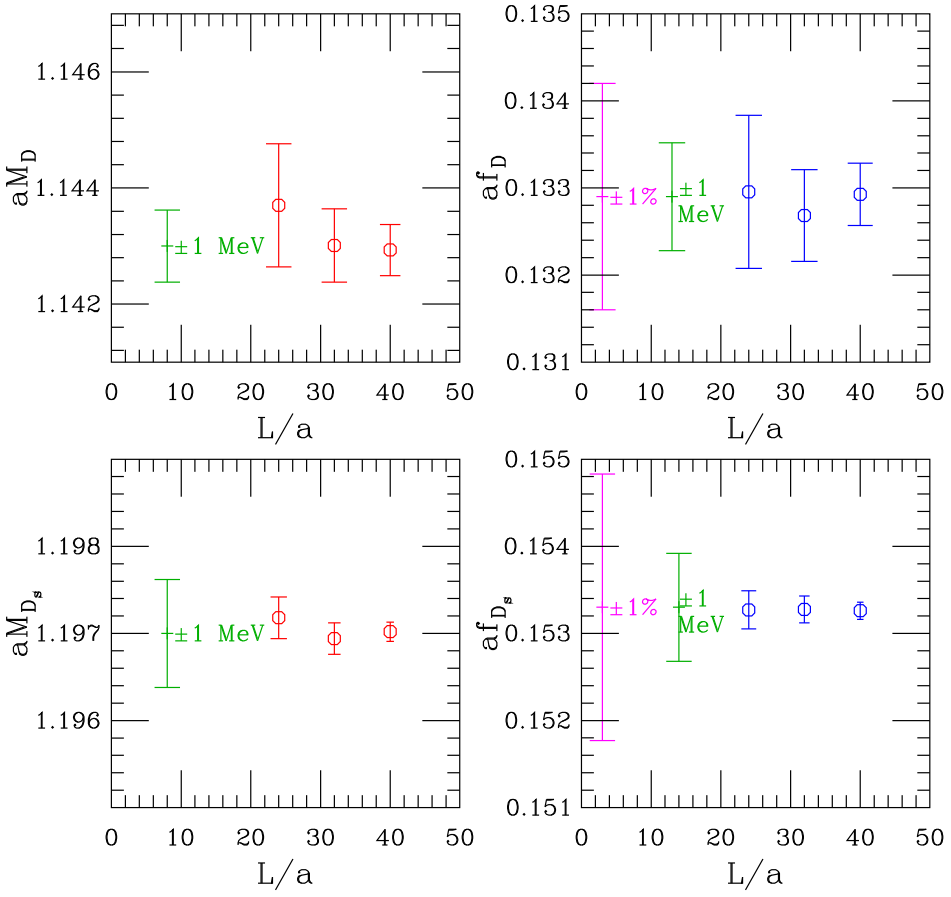

FIGURE 3.11: Spatial size effects on M_D, M_{D_s}, f_D and f_{D_s}, as determined by comparison of ensembles with $L/a = 24$, 32, and 40 at $\beta = 6.0$ ($a \approx 0.12$ fm). To show the magnitude of the effects, green error bars show an arbitrary value ± 1 MeV, and magenta error bars $\pm 1\%$.

TABLE 3.6: Values for various physical quantities evaluated at zero lattice spacing, as well as statistical and systematic errors, obtained from the simple physical-mass ensemble analysis. Here $\Phi_{D^+} \equiv f_{D^+}\sqrt{M_{D^+}}$ etc. We also include the p value of the central fit of this analysis. For the systematic errors, we tabulate the amount by which the central values change. Finite size errors are the difference between results using staggered chiral perturbation theory and continuum chiral perturbation theory (NNLO for M_π and f_{π^+}, NLO for M_K and f_{K^+}) [67]. "EM1" is the effect of varying ϵ by 0.021, or one standard deviation. "EM2" is the effect of subtracting 450 MeV^2 from M_K^2. "EM3" is the effect of lowering the D_s meson mass by 1 MeV. "Cont. extrap." is the full amount of variation among the alternative continuum extrapolation fits. "Priors" is the effect of using narrower priors for the mass gaps in the 0.09 and 0.06 fm physical quark mass correlator fits. More details on these systematic effects are in the text.

Quantity	Central value	Stat.	p val.	Finite size	EM1	EM2	EM3	Cont. extrap.	Priors
M_{η_c} (MeV)	2982.33	0.35	0.18	0.29	0.11	0.35	−1.81	$^{+1.41}_{-0.88}$	0.01
f_{K^+}/f_{π^+}	1.1956	0.0010	0.025	−0.0010	−0.0003	−0.0004	0.0000	$^{+0.0023}_{-0.0014}$	0.0002
F_{p4s} (MeV)	153.90	0.09	0.10	−0.15	−0.02	−0.05	0.00	$^{+0.14}_{-0.23}$	0.00
M_{p4s} (MeV)	433.24	0.17	0.11	−0.02	−0.12	−0.41	0.00	$^{+0.01}_{-0.33}$	−0.01
R_{p4s}	0.35527	0.00024	0.035	−0.00030	0.00007	0.00023	0.00000	$^{+0.00052}_{-0.00015}$	0.00001
m_u/m_d	0.4482	0.0048	0.025	0.0001	−0.0156	0.0000	0.0000	$^{+0.0021}_{-0.0115}$	0.0000
m_s/m_l	27.352	0.051	0.72	−0.039	−0.015	−0.053	0.000	$^{+0.080}_{-0.020}$	−0.001
m_c/m_s	11.747	0.019	0.010	−0.006	0.009	0.025	−0.010	$^{+0.052}_{-0.032}$	0.001
f_{D_s}/f_{D^+}	1.1736	0.0036	0.97	0.0003	−0.0003	−0.0003	0.0000	$^{+0.0004}_{-0.0015}$	−0.0002
f_{D^+}/f_{π^+}	1.6232	0.0057	0.59	−0.0016	0.0003	0.0000	−0.0001	$^{+0.0097}_{-0.0034}$	0.0006
f_{D_s}/f_{π^+}	1.9035	0.0017	0.010	−0.0015	−0.0001	−0.0004	−0.0001	$^{+0.0089}_{-0.0050}$	−0.0001
Φ_{D^+} (MeV$^{3/2}$)	9161.5	33.7	0.61	−9.3	1.6	0.6	−3.1	$^{+16.1}_{-44.9}$	3.0
Φ_{D_s} (MeV$^{3/2}$)	11012.9	9.7	0.007	−8.9	−0.7	−2.6	−3.4	$^{+51.6}_{-28.8}$	−0.1

and the electromagnetic corrections vanish in the chiral limit for neutral mesons and are thus also small. For the kaon, we consider the isospin-averaged mass $M_{\widehat{K}}^2 = (M_{K^+}^2 + M_{K^0}^2)_{\rm QCD}/2$, where the subscript "QCD" indicates that the leading EM effects in the masses are removed from the experimental masses [93]. To remove these effects we use results from our ongoing lattice QED+QCD simulations with asqtad sea quarks [97, 98] for the parameter ϵ that characterizes violations of Dashen's theorem:

$$(M_{K^\pm}^2 - M_{K^0}^2)^\gamma = (1+\epsilon)(M_{\pi^\pm}^2 - M_{\pi^0}^2)^\gamma \ , \tag{3.7}$$

where the superscript γ denotes the EM contribution to the splittings. In Refs. [97, 98], we found $\epsilon = 0.65(7)(14)(10)$, but this result did not yet adjust for finite volume effects on the photon field. A recent preliminary result [99] including finite volume effects is $\epsilon = 0.84(21)$, and we use that here.

We estimate the uncertainty due to EM effects by varying the values of the EM-subtracted meson masses used in the quark-mass tuning; this affects m_u the most. We vary the parameter

ϵ by its error. We also consider possible EM effects on the neutral kaon mass itself, which are less well understood than the EM effects on the K^+–K^0 splitting that are described by ϵ. In Ref. [98], the EM contribution to the squared K^0 mass was estimated to be about 900 MeV^2. However, this estimate did not take into account the effects of EM quark mass renormalization, which should be subtracted from the result. A rough calculation of the renormalization effect (using one-loop perturbation theory) suggests it is of order of half the size of the contribution. We thus include as a systematic error the effect of shifting the squared K^0 mass by 450 MeV^2. We do not consider direct EM effects on the weak matrix elements f_{π^+}, f_{K^+}, f_{D^+} and f_{D_s}, which are by definition pure QCD quantities [93]. Such direct EM effects, however, are relevant in the extraction of CKM elements by comparison with experimental rates, as described in Sec. 3.6.

The shifts in various quantities resulting from these electromagnetic uncertainties are also tabulated in Table 3.6. The two effects labeled "EM1" and "EM2" are combined in quadrature to give our quoted EM systematic errors for m_s/m_l and f_{K^+}/f_{π^+}. The "EM3" column in Table 3.6 shows the effect of lowering the input D_s meson mass by 1 MeV, an order-of-magnitude estimate for the electromagnetic effect on this mass, which affects the tuning of the charm-quark mass. This effect has not been directly determined in QCD+QED simulations. Assuming that the EM effect on M_{D^+} is approximately the same as on M_{D_s}, since the two mesons have the same charge, the EM3 error on the decay constants of these mesons is negligible: To very good approximation, the changes in Φ_{D^+} and Φ_{D_s} due to the change in the estimate of the charm-quark mass, are canceled by the changes in the factors of $M_{D^+}^{1/2}$ or $M_{D_s}^{1/2}$ in these quantities. The fact that the decay constants themselves are only mildly dependent on the heavy-quark mass (for example, the difference between f_{D_s} and f_{B_s} is only about 10% [100]) indicates that such cancellations must take place. The EM3 error does lead to a significant uncertainty on m_c/m_s, and we include it in our systematic error estimate for that quantity.

3.4.2 Chiral perturbation theory analysis of f_D and f_{D_s} including unphysical quark-mass ensembles

In this section, we present the combined chiral extrapolation/interpolation and continuum extrapolations used to obtain the physical values of the D^+ and D_s meson decay constants. We first discuss chiral perturbation theory for all-staggered heavy-light mesons in Sec. 3.4.2.1, giving the formulas used for the chiral fits and describing our method for incorporating discretization effects into the extrapolation. An explanation of our method for setting the lattice scale follows in Sec. 3.4.2.2. Chiral perturbation theory assumes a mass-independent scale-setting procedure. In practice, we use F_{p4s} to set the scale and F_{p4s}/M_{p4s} to tune the strange sea-quark mass.

We take these values from the physical quark-mass analysis in Sec. 3.4.1. This means that the absolute scale comes ultimately from f_{π^+}, which is used to set the scale in Sec. 3.4.1.

The chiral fits themselves are presented in Sec. 3.4.2.3, while systematic errors in the chiral analysis are described in Sec. 3.4.2.4. Chiral/continuum extrapolation errors are found by considering a large number (18) of alternative chiral fits, as well as six versions of the continuum extrapolation of the inputs, resulting in 108 possibilities. We also estimate finite volume and EM errors within the chiral analysis by propagating the errors in the corresponding inputs through the chiral fits. Equations (3.28)–(3.30) show our results for the charm decay constants from the self-contained chiral analysis with complete systematic error budgets.

3.4.2.1 Chiral perturbation theory for f_{D^+} and f_{D_s}

The quark-mass and lattice-spacing dependence of the decay constant has been derived at one loop in heavy-meson, rooted, all-staggered chiral perturbation theory (HMrASχPT) in Ref. [86]. At fixed heavy-quark mass m_Q, one may argue following Ref. [101] that inclusion of hyperfine splittings (*e.g.*, $M_D^* - M_D$) and flavor splittings (*e.g.*, $M_{D_s} - M_D$), but no other $1/m_Q$ effects, constitutes a systematic approximation at NLO in HMrASχPT. The argument is based on the power counting introduced by Boyd and Grinstein [102]. With v denoting the light valence quark, Y the v$\bar{\text{v}}$ valence meson, and $\Phi_{D_\text{v}} \equiv f_{D_\text{v}}\sqrt{M_{D_\text{v}}}$, Ref. [86] obtains for the pseudoscalar-taste heavy-light meson:

$$
\begin{aligned}
\Phi_{D_\text{v}} \;=\; \Phi_0\Bigg\{ & 1 + \frac{1}{16\pi^2 f^2}\frac{1}{2}\Bigg(-\frac{1}{16}\sum_{\mathcal{S},\Xi}\ell(M^2_{\mathcal{S}\text{v},\Xi}) - \frac{1}{3}\sum_{j\in\mathcal{M}_I^{(3,\text{v})}}\frac{\partial}{\partial M^2_{Y,I}}\left[R_j^{[3,3]}(\mathcal{M}_I^{(3,\text{v})};\mu_I^{(3)})\ell(M_j^2)\right] \\
& - \Big(a^2\delta'_V \sum_{j\in\mathcal{M}_V^{(4,\text{v})}}\frac{\partial}{\partial M^2_{Y,V}}\left[R_j^{[4,3]}(\mathcal{M}_V^{(4,\text{v})};\mu_V^{(3)})\ell(M_j^2)\right] + [V\to A]\Big) \\
& - 3g_\pi^2\frac{1}{16}\sum_{\mathcal{S},\Xi}J(M_{\mathcal{S}\text{v},\Xi},\Delta^* + \delta_{\mathcal{S}\text{v}}) - g_\pi^2\sum_{j\in\mathcal{M}_I^{(3,\text{v})}}\frac{\partial}{\partial M^2_{Y,I}}\left[R_j^{[3,3]}(\mathcal{M}_I^{(3,\text{v})};\mu_I^{(3)})J(M_j,\Delta^*)\right] \\
& - 3g_\pi^2\Big(a^2\delta'_V\sum_{j\in\mathcal{M}_V^{(4,\text{v})}}\frac{\partial}{\partial M^2_{Y,V}}\left[R_j^{[4,3]}(\mathcal{M}_V^{(4,\text{v})};\mu_V^{(3)})J(M_j,\Delta^*)\right] + [V\to A]\Big)\Bigg) \\
& + L_\text{s}(x_u + x_d + x_s) + L_\text{v}x_\text{v} + L_a\frac{x_{\bar{\Delta}}}{2}\Bigg\}\,,
\end{aligned}
\tag{3.8}
$$

where Φ_0, L_s, L_v, and L_a are low-energy constants (LECs); the indices $\mathcal{S}$ and Ξ run over sea-quark flavors and meson tastes, respectively; Δ^* is the lowest-order hyperfine splitting; $\delta_{\mathcal{S}\text{v}}$ is the flavor splitting between a heavy-light meson with light quark of flavor $\mathcal{S}$ and one of flavor v;

and g_π is the D-D^*-π coupling. In infinite volume, the chiral logarithm functions ℓ and J are defined by [23, 101]

$$\ell(m^2) = m^2 \ln \frac{m^2}{\Lambda_\chi^2} \qquad \text{[infinite volume]}, \tag{3.9}$$

$$J(M,\Delta) = (M^2 - 2\Delta^2)\log(M^2/\Lambda^2) + 2\Delta^2 - 4\Delta^2 F(M/\Delta) \qquad \text{[infinite volume]}, \tag{3.10}$$

with [103]

$$F(1/x) \equiv \begin{cases} -\frac{\sqrt{1-x^2}}{x}\left[\frac{\pi}{2} - \tan^{-1}\frac{x}{\sqrt{1-x^2}}\right], & \text{if } |x| \le 1, \\ \frac{\sqrt{x^2-1}}{x}\ln(x+\sqrt{x^2-1}), & \text{if } |x| \ge 1. \end{cases} \tag{3.11}$$

The residue functions $R_j^{[n,k]}$ are given by

$$R_j^{[n,k]}(\{m\};\{\mu\}) \equiv \frac{\prod_{i=1}^{k}(\mu_i^2 - m_j^2)}{\prod_{r\neq j}^{n}(m_r^2 - m_j^2)} \,. \tag{3.12}$$

The sets of masses in the residues are

$$\mu^{(3)} = \{m_U^2, m_D^2, m_S^2\} \,, \tag{3.13}$$

$$\mathcal{M}^{(3,\mathrm{v})} = \{m_Y^2, m_{\pi^0}^2, m_\eta^2\} \,, \tag{3.14}$$

$$\mathcal{M}^{(4,\mathrm{v})} = \{m_Y^2, m_{\pi^0}^2, m_\eta^2, m_{\eta'}^2\} \,. \tag{3.15}$$

Here taste labels (*e.g.*, I or V for the masses) are implicit. We define dimensionless quark masses and a measure of the taste splitting by

$$x_{u,d,s,\mathrm{v}} \equiv \frac{4B}{16\pi^2 f_\pi^2} m_{u,d,s,\mathrm{v}} \,, \text{ and} \qquad x_{\bar{\Delta}} \equiv \frac{2}{16\pi^2 f_\pi^2} a^2\bar{\Delta} \,, \tag{3.16}$$

where B is the LEC that gives the Goldstone pion mass $M_\pi^2 = B(m_u + m_d)$, and $a^2\bar{\Delta}$ is the mean-squared pion taste splitting. The x_i are natural variables of HMrASχPT; the LECs L_s, L_v, and L_a are therefore expected to be $\mathcal{O}(1)$. All ensembles in the current analysis have degenerate light sea quarks: $x_u = x_d \equiv x_l$. The taste splittings have been determined to $\sim$1–10% precision [71] and are used as input to Eq. (3.8), as are the taste-breaking hairpin parameters δ'_A and δ'_V, whose ranges are taken from chiral fits to light pseudoscalar mesons [104].

To include the finite-volume effects for a spatial volume L^3 in Eq. (3.8), we replace [101]

$$\ell(m^2) \to \ell(m^2) + m^2\delta_1(mL) \qquad \text{[finite volume]}, \tag{3.17}$$

$$J(m,\Delta) \to J(m,\Delta) + \delta J(m,\Delta,L) \qquad \text{[finite volume]}, \tag{3.18}$$

where

$$\delta J(m,\Delta,L) = \frac{m^2}{3}\delta_1(mL) - 16\pi^2\left[\frac{2\Delta}{3}J_{FV}(m,\Delta,L) + \frac{\Delta^2-m^2}{3}K_{FV}(m,\Delta,L)\right], \quad (3.19)$$

with

$$K_{FV}(m,\Delta,L) \equiv \frac{\partial}{\partial\Delta}J_{FV}(m,\Delta,L), \quad (3.20)$$

and with $\delta_1(mL)$ and $J_{FV}(m,\Delta,L)$ defined in Refs. [105, 106].

Because we have data with $\sim 1\%$ to less than 0.1% statistical errors and 314 to 366 data points (depending on whether $a \approx 0.15$ fm is included), NLO HMrASχPT is not adequate to describe fully the quark-mass dependence, in particular for masses near m_s. We therefore include all NNLO and NNNLO mass-dependent analytic terms. There are four independent functions of $x_{\rm v}$, x_l and x_s at NNLO and seven at NNNLO, for a total of eleven additional fit parameters. It is not necessary to keep all the seven terms appearing at NNNLO to get a good fit, nevertheless we include all of them to make it a systematic approximation at the level of analytic terms.

While Eq. (3.8) is a systematic NLO approximation for the decay constant at fixed m_Q, we have data on each ensemble with two different values of the valence charm mass: m_c' and $0.9m_c'$, where m_c' is the value of the charm sea mass of the ensembles, and is itself not precisely equal to the physical charm mass m_c because of tuning errors, which are in some cases as large as this difference (*i.e.*, 10% of m_c'). Since such changes in the value of the charm mass lead to corrections to decay constants that are comparable in size to those from the pion masses at NLO, Eq. (3.8) needs to be modified in order to fit the data. We therefore allow the LEC Φ_0 to depend on m_Q as suggested by HQET. For acceptable fits to the highly correlated data at valence charm masses m_c' and $0.9m_c'$, we need to introduce both $1/m_Q$ and $1/m_Q^2$ terms. (For more details see Appendix D.) Furthermore, Φ_0 has generic lattice-spacing dependence that must be included to obtain good fits. With HISQ quarks, the leading generic discretization errors are $\mathcal{O}(\alpha_S a^2)$. But because the high degree of improvement in the HISQ action drastically reduces the coefficient of these leading errors, formally higher $\mathcal{O}(a^4)$ errors are also apparent, as can be seen from the curvature in Figs. 3.5 – 3.10. In Eq. (3.8), we thus replace

$$\Phi_0 \to \Phi_0\left(1 + k_1\frac{\Lambda_{\rm HQET}}{m_Q} + k_2\frac{\Lambda_{\rm HQET}^2}{m_Q^2}\right)\left(1 + c_1\alpha_S(a\Lambda)^2 + c_2(a\Lambda)^4\right), \quad (3.21)$$

where the k_i are new physical LECs, c_i are additional fit parameters, $\Lambda_{\rm HQET}$ is a physical scale for HQET effects, and Λ is the scale of discretization effects.

In cases where the valence and sea values of the charm quark mass differ, m_Q in Eq. (3.21) is taken equal to the valence mass. This is based on the expectation from decoupling [107] that effects due to variations in the charm sea mass on low-energy physical quantities are small. Note that HQET tells us that heavy-light decay constants come from the physics of the light-quark at scale $\Lambda_{\rm QCD}$, despite the presence of the heavy valence quark. Thus we do not introduce extra terms corresponding to the charm sea mass here. As discussed in Sec. 3.4.2.4, however, such terms are included in alternative fits used to estimate systematic errors.

Generic dependence on a is also allowed for the physical LECs $L_{\rm s}$, $L_{\rm v}$, k_1 and k_2. However, because these parameters first appear at NLO in the chiral or HQET expansions, it is sufficient to include at most the leading a-dependence, for example:

$$L_{\rm v} \to L_{\rm v} + L_{\rm v\delta}\ \alpha_S(a\Lambda)^2 \tag{3.22}$$

Thus we add 4 fit parameters related to generic discretization effects: $L_{\rm v\delta}$, $L_{\rm s\delta}$, $k_{1\delta}$, and $k_{2\delta}$. There are also 3 parameters related to taste-violation effects: L_a, δ'_A and δ'_V. These parameters are taken proportional to the measured average taste splitting $a^2\bar{\Delta}$, which depends on a approximately as $\alpha_S^2 a^2$ [71]. In addition, we find that m_Q-dependent discretization errors must be considered if data at the coarsest lattice spacing ($a \approx 0.15$ fm) is included in the fits. This is not surprising because $am_c^{\rm phys} \approx 0.84$ at this lattice spacing, which by the power counting estimates of Ref. [68] suggests $\sim$5% discretization errors (although this may be reduced by dimensionless factors). We therefore add $c_3\alpha_S(am_Q)^2 + c_4(am_Q)^4$ to the analytic terms in Eq. (3.8), where m_Q is taken to denote the valence charm mass. If the $a \approx 0.15$ fm data are omitted, good fits may be obtained with c_3 and c_4 set to zero. As discussed below, one can also add similar terms for the charm sea mass.

For the LEC g_π, a reasonable range is $g_\pi = 0.53(8)$, which comes from recent lattice calculations [108, 109]. When this central value and range are included as Bayesian priors, fits to our full data set tend to pull g_π low, several sigma below 0.53. Hence, we simply fix $g_\pi = 0.45$, 1-sigma below its nominal value, in our central fit. This problem is ameliorated for alternative fits, used to estimate the systematic errors, that drop the data at $a \approx 0.15$ fm or that use the experimental value of f_{K^+}, rather than that of f_{π^+}, for f in Eq. (3.8). Other alternatives considered in the systematic error estimates are to allow g_π to be a free parameter, or to keep it fixed at its nominal value. We give more details about fits with varying treatments of g_π in Sec. 3.4.2.4.

3.4.2.2 Setting the relative lattice scale

Relative scale setting in the combined chiral analysis is done using F_{p4s}. The value of F_{p4s} in physical units, which is only needed at the end of this analysis, has been obtained by comparison with f_{π^+} in Sec. 3.4.1, as are the other needed inputs: $R_{p4s} \equiv F_{p4s}/M_{p4s}$ and the quark-mass ratios m_c/m_s, m_s/m_l and m_u/m_d. All those quantities are listed in Table 3.6, and Fig. 3.10 shows the data and continuum extrapolations used to determine F_{p4s} and R_{p4s}.

We use F_{p4s} in the chiral analysis, rather than f_{π^+} itself, for several reasons. First of all, F_{p4s} gives highly-precise relative lattice spacings between ensembles. Precision scale setting is required in order to get good chiral fits to our large partially-quenched data set (366 points) with large correlations of the points within each ensemble. Second, F_{p4s} can be accurately adjusted for mistunings in the sea-quark masses using unphysical-mass ensembles for which the physical valence-quark mass values needed to find f_{π^+} can only be reached by extrapolation. Finally, and perhaps most importantly, there are no logarithms of light pseudoscalar masses ($\sim m_\pi$) in the SχPT expression for the decay constant [23] evaluated at the relevant quark masses for F_{p4s}. The lightest meson that enters is a valence-sea meson for quark masses $0.4m_s$ and m_l, which has mass $\sim$325 MeV (for the Goldstone taste). This means that F_{p4s} should be well approximated by its Taylor series in a^2, and we do not need to modify Eq. (3.8) to take into account chiral logarithms that enter through the scale-setting procedure. We have checked this assumption by performing a more complicated three-step analysis: (1) The degenerate light-light decay-constant data for all ensembles are fit to the NLO SχPT form of Ref. [23]. (2) From the fit, we determine F_{p4s} as a function of a^2. (3) The data for $\Phi_{D_v}/F_{p4s}^{3/2}$ are fit to Eq. (3.8) divided by the 3/2 power of $F_{p4s}(a^2)$. The results of this procedure differ from the results reported in Table 3.9 below by less than half of the statistical errors, and the systematic errors are essentially the same in both approaches.

We use a mass-independent scale-setting scheme. We first determine aF_{p4s} and am_{p4s} on the physical-mass ensembles; then, by definition, all ensembles at the same β as a given physical-mass ensemble have a lattice spacing a and value of am_{p4s} equal to those of the physical-mass ensemble. Since we do not know the correct strange-quark mass until after the lattice spacing is fixed, aF_{p4s} and am_{p4s} must be determined self-consistently. We find am_{p4s} and aF_{p4s} on a given physical-mass ensemble by adjusting am_v until $aF/(aM)$ has the expected physical ratio R_{p4s}.

To determine aF_{p4s} and am_{p4s} accurately, data must be adjusted for mistunings in the sea-quark masses. The sea-quark masses of the physical-mass ensembles are tuned relatively well

(especially at 0.09 and 0.06 fm), and adjustments are small. Nevertheless, the adjustments may change the final results of f_{D^+} and f_{D_s} by more than the size of the statistical errors.

To make these adjustments, we first find an approximate value of am_{p4s} on each physical-mass ensemble by passing a parabola through $(M/F)^2$ as a function of $m_{\rm v}$, for the three values of $m_{\rm v}$ closest to m_{p4s}. The sea-quark masses are kept fixed (initially, to their values in the run) in this process. We use $(M/F)^2$ here rather than F/M, since we expect M^2 to be approximately linear in $\rm m_v$, and F^2 to be approximately constant. The value of $am_{\rm v}$ where the ratio takes its expected value $1/R^2_{p4s}$ is the tentative value of am_{p4s}, and the corresponding value of aF is the tentative value of aF_{p4s}. The procedure also gives tentative values of the physical sea-quark masses in lattice units: $am_s \cong 2.5\, am_{p4s}$, $am_l \cong 2.5\, am_{p4s}/(m_s/m_l)$, and $am_c \cong 2.5\, am_{p4s}(m_c/m_s)$. We then adjust the data for aF and aM to the values they would have at the tentative new sea-quark masses, and iterate the whole process until it converges.

The adjustment of the data requires a determination of the following derivatives

$$\frac{\partial F^2}{\partial m'_l}, \frac{\partial F^2}{\partial m'_s}, \frac{\partial F^2}{\partial m'_c}, \frac{\partial M^2}{\partial m'_l}, \frac{\partial M^2}{\partial m'_s}, \frac{\partial M^2}{\partial m'_c}, \frac{\partial^2 M^2}{\partial m'_l \partial m_{\rm v}}, \frac{\partial^2 M^2}{\partial m'_s \partial m_{\rm v}}, \frac{\partial^2 M^2}{\partial m'_c \partial m_{\rm v}}, \tag{3.23}$$

where the derivatives should be evaluated at $m_{\rm v} = m_{p4s}$, and with m'_l, m'_s and m'_c at their physical values. All quantities here are in "$p4s$ units", which are (semi-) physical units in which aF and aM have been divided by (the tentative value of) aF_{p4s}, and quark masses in lattice units have been divided by (the tentative value of) am_{p4s} (and therefore do not require renormalization). The mixed partial derivatives with $m_{\rm v}$ are needed because we must adjust the data at different values of $m_{\rm v}$ in order to iterate the process. Because M^2 is approximately linear in $m_{\rm v}$, the effect of the mixed partials in Eq. (3.23) is non-negligible, while mixed partials of F^2 may be neglected. Since the effects of mistunings are already not much larger than our statistical errors, we expect that we may neglect discretization errors and any mistuning effects in the derivatives themselves. This means that we may use, at all lattice spacings, the values determined for the derivatives in Eq. (3.23) at any one lattice spacing. This expectation is confirmed by alternative determinations of the derivatives, which give results in agreement with the method we now describe.

Many of the derivatives may be calculated using the twelve ensembles that we have at $a \approx 0.12$ fm. Figure 3.12 shows the light and strange sea masses of these ensembles. Most of the ensembles have the same charm sea masses, which allows us to determine the derivatives with respect to m'_l and m'_s accurately. We first convert the lattice data to $p4s$ units using (tentative values of) am_{p4s} and aF_{p4s}. Ensembles in which the light sea mass is tuned close to $0.1m'_s$, shown inside the dashed blue ellipse in Fig. 3.12, are then used to determine $\partial F^2/\partial m'_s$, $\partial M^2/\partial m'_s$ and

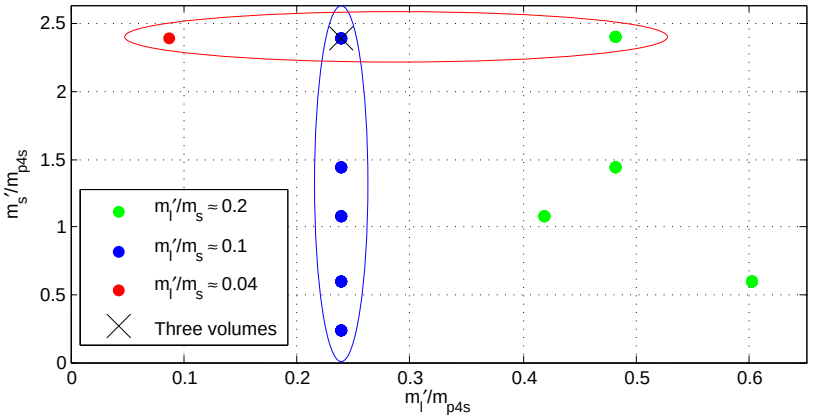

FIGURE 3.12: Values of m'_s and m'_l of the ensembles at $\beta = 6.0$. At one value of m'_s and m'_l, indicated by the black cross, we have three ensembles with different volumes; the intermediate volume ensemble, which is equal in volume to all the other ensembles shown here, is used in our calculation of the derivatives. Five ensembles inside the blue ellipse are used to calculate $\partial F^2/\partial m'_s$, $\partial M^2/\partial m'_s$, and $\partial^2 M^2/\partial m'_s \partial m_v$. These five ensembles have the same charm sea masses. Three ensembles inside the red ellipse are used to calculate $\partial F^2/\partial m'_l$, $\partial M^2/\partial m'_l$, and $\partial^2 M^2/\partial m'_l \partial m_v$. One of these ensembles has a slightly different charm sea mass, which is adjusted before calculating the derivatives.

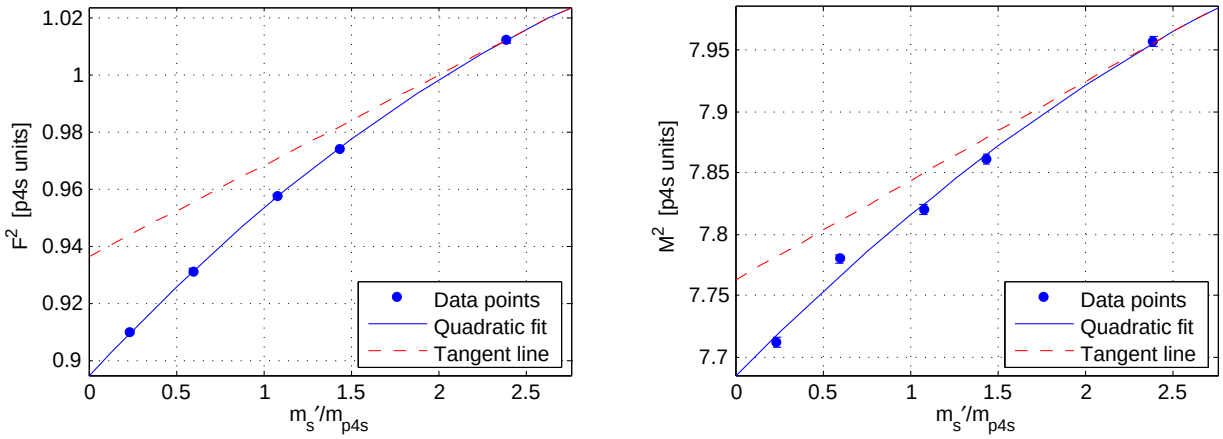

FIGURE 3.13: Data from the $a \approx 0.12$ fm, $m'_l/m_s \approx 0.1$ ensembles, which are shown inside the blue ellipse in Fig. 3.12. F_{p4s} and M_{p4s} are the light-light pseudoscalar decay constant and mass for $m_v = m_{p4s}$; quantities are expressed in $p4s$ units, as described in the text. The needed derivatives are given by the slope of the tangent line at m'_s/m_{p4s}=2.5

$\partial^2 M^2/\partial m'_s \partial m_v$. The three derivatives with respect to m'_s are found by fitting a quadratic function to the corresponding quantities of these ensembles, as shown in Fig. 3.13.

To calculate $\partial F^2/\partial m'_l$, $\partial M^2/\partial m'_l$ and $\partial^2 M^2/\partial m'_l \partial m_v$, we use the three ensembles with strange sea mass close to its physical value, the ensembles inside the red ellipse in Fig. 3.12. We fit straight lines to the corresponding data, as shown in Fig. 3.14. Note that there are small differences in the charm and strange sea masses of these ensembles, but they are taken into account by a small adjustment using the derivatives with respect to m'_s and m'_c.

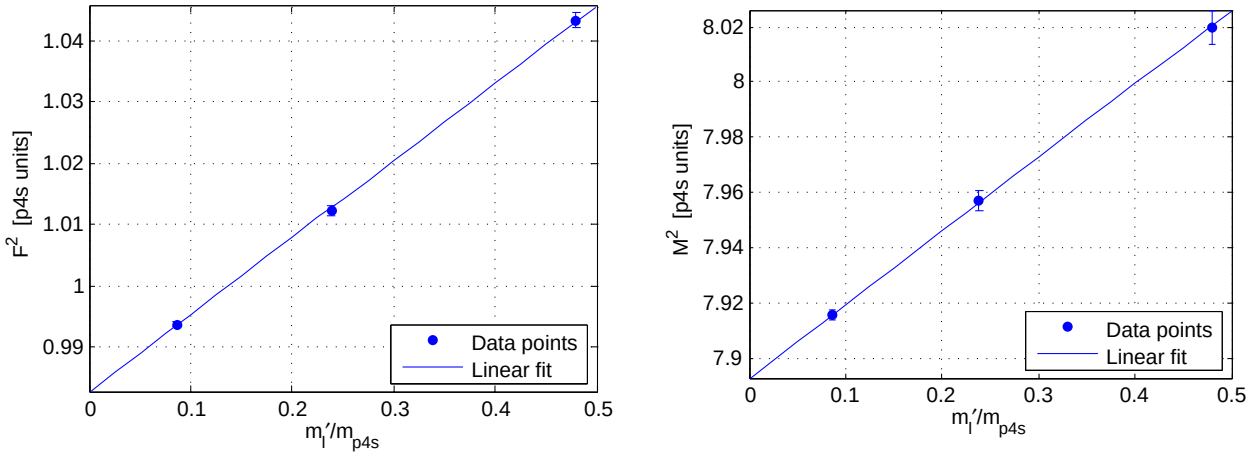

FIGURE 3.14: Data from three ensembles with strange sea masses tuned close to m_s, the ensembles inside the red ellipse in Fig. 3.12.

TABLE 3.7: The values of derivatives needed for adjusting the data for mistunings. All the derivatives are in $p4s$ units, and are evaluated at the valence mass $m_{\rm v} = m_{p4s}$ and at physical values of sea masses m_l, m_s, and m_c. Derivatives are found using 0.12 fm and 0.06 fm ensembles, as described in the text.

$\frac{\partial F^2}{\partial m_l'}$	0.1255(32)	$\frac{\partial M^2}{\partial m_l'}$	0.266(15)	$\frac{\partial^2 M^2}{\partial m_l' \partial m_{\rm v}}$	0.182(55)
$\frac{\partial F^2}{\partial m_s'}$	0.0318(17)	$\frac{\partial M^2}{\partial m_s'}$	0.0810(85)	$\frac{\partial^2 M^2}{\partial m_s' \partial m_{\rm v}}$	0.060(30)
$\frac{\partial F^2}{\partial m_c'}$	0.00554(85)	$\frac{\partial M^2}{\partial m_c'}$	0.0209(41)	$\frac{\partial^2 M^2}{\partial m_c' \partial m_{\rm v}}$	0.023(13)

The derivatives with respect to m_c' cannot be calculated directly, because we do not have a group of ensembles with different charm sea masses but equal light and strange sea masses. So we have to determine the charm-mass derivatives indirectly, by investigating ensembles with different charm sea masses after adjusting for their differences in strange and light sea masses. This procedure can be carried out using the three ensembles available at ≈ 0.06 fm. Since m_s' and m_c' vary by about 10% on these three ensembles, the lever arm is large enough to calculate the derivatives with respect to m_c'. We first use the derivatives with respect to m_s' obtained at ≈ 0.12 fm to adjust the data at ≈ 0.06 fm for mistuning of the strange sea masses, so only m_l' and m_c' dependence remains. Then we calculate the m_c' derivatives by passing a function linear in both m_l' and m_c' through the three data points for each quantity. The m_c' derivatives thus found feed back into the small adjustments needed at $a \approx 0.12$ fm in order to calculate m_l' derivatives, as discussed in the preceding paragraph. Our estimates of all the needed derivatives are tabulated in Table 3.7.

It is noteworthy that we can analytically determine the first order derivatives with respect to m_c' by integrating out the charm quark for processes that occur at energies well below its mass.

By decoupling [107], the effect of a heavy (enough) sea quark on low-energy quantities occurs only through the change it produces in the effective value of $\Lambda_{\rm QCD}$ in the low-energy (three-flavor) theory [110]. (For a pedagogical discussion see Sec. 1.5 of Ref. [111].) Thus, assuming m'_c is heavy enough, we may calculate the m'_c derivatives of any quantity that is proportional to $\Lambda_{\rm QCD}$, where the proportionality constant is some pure number, independent of the light quark masses. Examples of such quantities are the LEC B in Eq. (3.16) and the light-light decay constant in the chiral limit, f. At leading order in weak-coupling perturbation theory, one then obtains (see Eq.(1.114) in Ref. [111]),

$$\frac{\partial B}{\partial m'_c} = \frac{2}{27}\frac{B}{m'_c} \ , \qquad \frac{\partial f}{\partial m'_c} = \frac{2}{27}\frac{f}{m'_c} \ . \tag{3.24}$$

At the nonzero values of $m_{\rm v}$, m'_l, and m'_s at which we need to evaluate the derivatives in Eq. (3.23), there are corrections to these expressions. However, chiral perturbation theory suggests that such corrections are relatively small. At the relevant light masses, we therefore expect

$$\frac{\partial F^2}{\partial m'_c} = 2F\frac{\partial F}{\partial m'_c} \approx \frac{4}{27}\frac{F^2}{m'_c} = 0.00504 \quad [p4s \text{ units}], \tag{3.25}$$

$$\frac{\partial M^2}{\partial m'_c} \approx 2m_{p4s}\frac{\partial B}{\partial m'_c} \approx \frac{2}{27}\frac{M^2}{m'_c} = 0.01998 \quad [p4s \text{ units}], \tag{3.26}$$

which agree with our numerical results within 10%; see Table 3.7. Indeed, the fact that the agreement is this close is probably due to chance, especially for the derivative of the decay constant: Our argument has neglected the difference between f and F_{p4s}, but that difference is $\sim$40%.

Having the required derivatives, we now iteratively adjust for mistunings. We first compute am_{p4s} and aF_{p4s}, then adjust the data, and repeat the entire process two more times. The values of am_{p4s} and aF_{p4s} have then converged to well within their statistical errors. The results for the lattice spacing a and am_s are listed in Table 3.8. The error estimates of these quantities will be discussed below. Our investigation shows that the errors in the derivatives change a and am_s by less than their statistical errors, so those errors are not included in the analysis.

Comparing Table 3.8 with Table 3.5, which uses f_{π^+} to set the scale, we see significant differences at the coarser lattice spacings, but not at the finest spacing. This is as expected for two different schemes, which should only agree exactly in the continuum limit.

TABLE 3.8: Lattice spacing a and am_s, as a function β, in the $p4s$ mass-independent scale-setting scheme.

$\beta = 5.8$	$a = 0.15305(17)_{\text{stat}}(^{+46}_{-23})_{a^2\,\text{extrap}}(29)_{\text{FV}}(4)_{\text{EM}}$ fm $am_s = 0.06863(16)_{\text{stat}}(^{+43}_{-24})_{a^2\,\text{extrap}}(26)_{\text{FV}}(7)_{\text{EM}}$ [lattice units]
$\beta = 6.0$	$a = 0.12232(14)_{\text{stat}}(^{+36}_{-19})_{a^2\,\text{extrap}}(23)_{\text{FV}}(3)_{\text{EM}}$ fm $am_s = 0.05304(13)_{\text{stat}}(^{+33}_{-18})_{a^2\,\text{extrap}}(20)_{\text{FV}}(6)_{\text{EM}}$ [lattice units]
$\beta = 6.3$	$a = 0.08791(10)_{\text{stat}}(^{+26}_{-13})_{a^2\,\text{extrap}}(17)_{\text{FV}}(2)_{\text{EM}}$ fm $am_s = 0.03631(9)_{\text{stat}}(^{+23}_{-13})_{a^2\,\text{extrap}}(14)_{\text{FV}}(4)_{\text{EM}}$ [lattice units]
$\beta = 6.72$	$a = 0.05672(7)_{\text{stat}}(^{+17}_{-9})_{a^2\,\text{extrap}}(11)_{\text{FV}}(1)_{\text{EM}}$ fm $am_s = 0.02182(5)_{\text{stat}}(^{+14}_{-8})_{a^2\,\text{extrap}}(8)_{\text{FV}}(2)_{\text{EM}}$ [lattice units]

3.4.2.3 Chiral-continuum fits to D system

So far, we have introduced eight fit parameters related to discretization effects (c_1, c_2, c_3, c_4, $L_{\text{v}\delta}$, $L_{\text{s}\delta}$, $k_{1\delta}$, and $k_{2\delta}$) and three parameters related to taste-violation effects (L_a, δ'_{A}, and δ'_{V}). The latter parameters appear at NLO in SχPT and must be kept since our expansion is supposed to be completely systematic through NLO. This is not the case for the former parameters; several of them (c_2, c_3, c_4, $L_{\text{v}\delta}$, $L_{\text{s}\delta}$, and $k_{2\delta}$) are formally NNLO and may be dropped. We indeed get acceptable fits when some of these parameters are dropped, especially if the $a \approx 0.15$ fm data are omitted. In order to see the effects of these parameters, we present the results of two fits, with different sets of parameters, to data at the three finer lattice spacings, and we study the extrapolation of the chiral fit back to the coarsest lattice spacing ($a \approx 0.15$ fm, $\beta = 5.8$).

Figure 3.15 shows a fit to partially quenched data at the three finer lattice spacings. (The $a \approx 0.15$ fm data are omitted.) Among the introduced fit parameters related to discretization effects, only c_1 in Eq. (3.21) and $k_{1\delta}$ in Eq. (3.22) are taken as free parameters in this fit, and the others are set to zero. This fit gives $p = 0.033$, and as illustrated in Fig. 3.15, the extrapolation of the fit to the coarsest lattice spacing does not follow the corresponding data points. We note that this fit and all other chiral fits in this chapter include additional data (not shown) from ensembles at $a \approx 0.12$ fm ($\beta = 6.0$) either with m'_s lighter than physical, or with volumes $24^3 \times 64$ and $40^3 \times 64$, which were generated to check finite volume effects. (See Table 3.1.) Moreover, it is important to realize that the biggest source of variation in the data in the four plots shown in Fig. 3.15 is not discretization errors, but mistunings of the strange and, most importantly, charm-quark masses.

Adding $c_3\alpha_S(am_Q)^2 + c_4(am_Q)^4$ to the analytic terms in Eq. (3.8), as well as including c_2 in Eq. (3.21), we get a new fit to the partially quenched data at the three finer lattice spacings. By including these three extra parameters, an excellent fit is achieved, as shown in Fig. 3.16, and

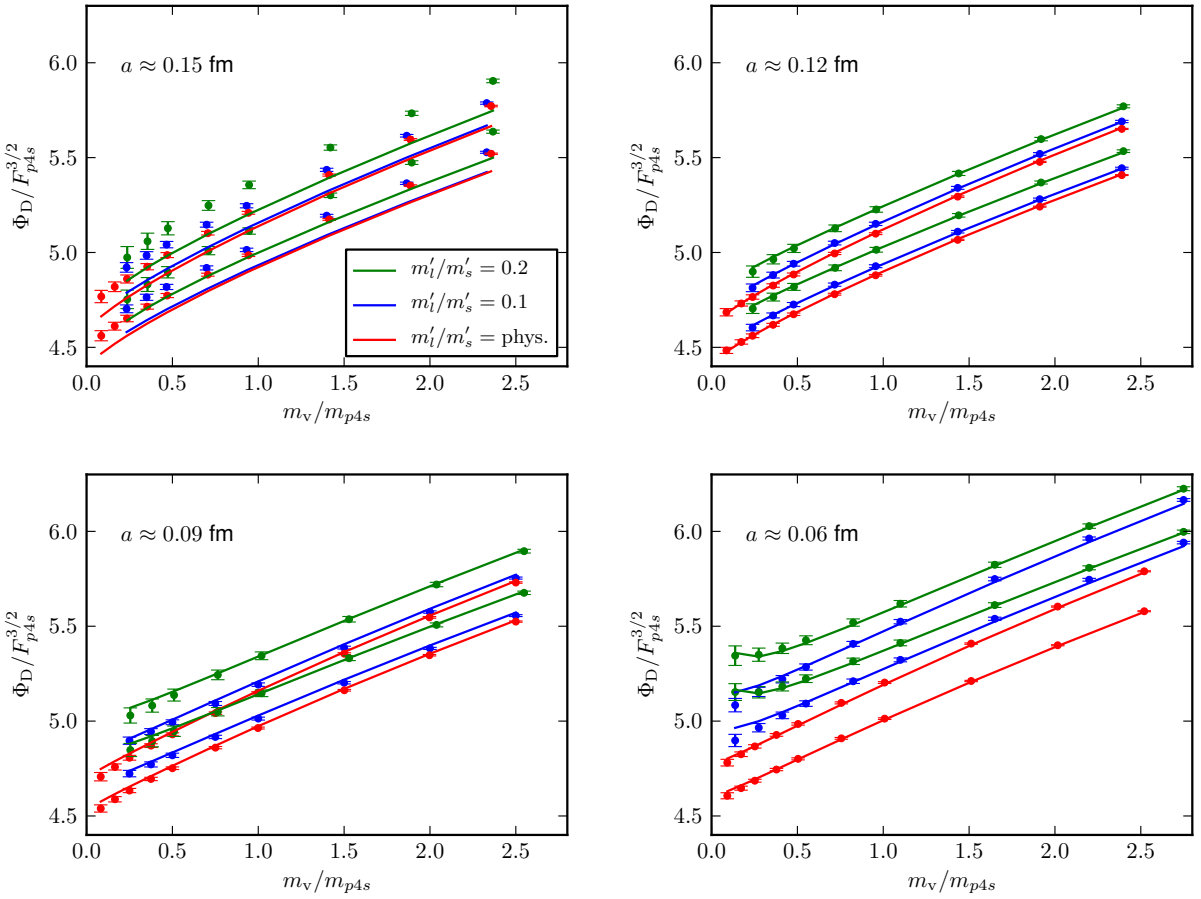

FIGURE 3.15: Simultaneous chiral fit to Φ_D as a function of m_v, the valence-quark mass (in units of m_{p4s}), at the three finer lattice spacings. The $a \approx 0.15$ fm ($\beta = 5.8$) data is not included in the fit, although the data and the extrapolation of the chiral fit to it are shown at the left in the top row. At the right of the top row we show the $a \approx 0.12$ fm ($\beta = 6.0$) data, and in the bottom row are $a \approx 0.09$ fm ($\beta = 6.3$, left) and $a \approx 0.06$ fm ($\beta = 6.72$, right). The colors denote different light sea-quark masses, as indicated. For each color there are two lines, one for heavy valence-quark mass $\approx m'_c$ (higher line), and one for $\approx 0.9m'_c$. In this fit, g_π is fixed to 0.53. The fit has $\chi^2/\text{dof} = 339/293$, giving $p = 0.033$.

extrapolation of the fit to the coarsest lattice spacing gives lines that pass relatively well through the corresponding data points. This comparison makes clear that higher-order discretization errors are important for the HISQ data, in which the leading-order discretization effects are suppressed.

We have a total of 18 acceptable ($p > 0.1$) versions of the continuum/chiral fits. Five of the fits drop the $a \approx 0.15$ fm ensembles; the rest keep those ensembles. The chiral coupling f is generally set to f_{π^+}, except for two fits with the coupling constant set to f_{K^+}. The LEC g_π is usually fixed to either its nominal value or to 1σ below its nominal value, however it is allowed to be a free parameter in four of the fits. The LEC B in Eq. (3.16) is generally determined for

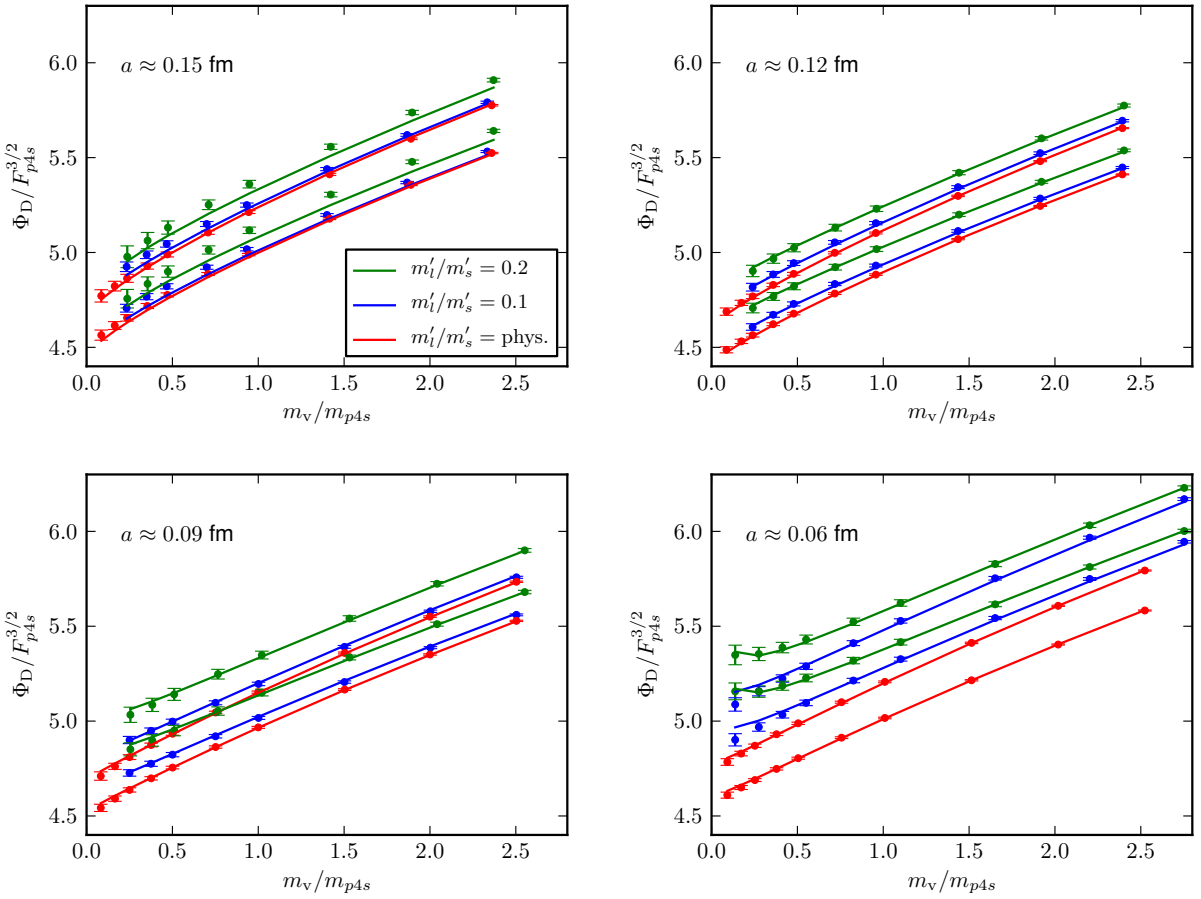

FIGURE 3.16: Simultaneous chiral fit to Φ_D as a function of m_v at the three finer lattice spacings. Similar to the fit in Fig. 3.15, but with three extra fit parameters: c_2, c_3, and c_4. This fit has $\chi^2/\text{dof} = 239/290$, giving $p = 0.986$.

each lattice spacing separately by fitting all data for the squared meson mass M^2 vs. the sum of the valence masses to a straight line. (At $a \approx 0.12$ fm only the ensembles with strange sea masses close to its physical mass are included in the fit.) However, in two versions of the chiral fits, B is determined from just the data on the physical-mass ensembles at each lattice spacing.

Another difference among the fits is how we determine the strong coupling α_S in discretization terms such as those with coefficients c_1 and c_3. Since the coefficients are free parameters, all that we actually need in the fits is the relative value of α_S at a given coupling β compared to its value at a fixed, fiducial coupling β_0. In most of the fits, we have used measured light-light pseudoscalar taste splittings to fix this relative value, as in Eq. (3.6). An alternative, which is used in two of our fits, is to use for α_S the coupling α_V, determined from the plaquette [96]. The scale for α_V is taken to be $q^* = 2.0/a$. Note that the NLO perturbative corrections to α_V have not been calculated for the HISQ action, so we use the result for the asqtad action.

Since the n_f dependence of the NLO result is small, we expect the difference to have negligible effects on the results of the fit. This expectation can be tested by, for example, flipping the sign of the n_f term in the asqtad result, which is likely a much bigger change than would actually come from changing from asqtad to HISQ. When we do this, we find that the results change by amounts comparable to or smaller than the statistical errors, and significantly smaller than the total systematic errors. Similar, but usually smaller, changes result from replacing $q^* = 2.0/a$ with $q^* = 1.5/a$, which is another reasonable choice, as discussed in Ref. [71].

We have introduced eight fit parameters related to discretization effects (c_1, c_2, c_3, c_4, $L_{\mathrm{v}\delta}$, $L_{\mathrm{s}\delta}$, $k_{1\delta}$, and $k_{2\delta}$), but it is not necessary to keep all of them to get an acceptable fit. Dropping some of these parameters, we have different continuum/chiral fits with the number of parameters ranging from 23 to 28. We may also choose to constrain, with priors, the LECs in higher-order (NNLO and NNNLO) analytic terms to be $\mathcal{O}(1)$ in natural units (as explained following Eq. (3.16)). (Through NLO, where we have the complete chiral expression, including logarithms, we always leave the LECs Φ_0, L_{s}, L_{v}, and L_a completely unconstrained, while g_π, δ'_A, and δ'_V are constrained by independent analyses as discussed above.) We may similarly constrain the coefficients of discretization terms to be $\mathcal{O}(1)$ when the terms are written in terms of a reasonable QCD scale (which we take, conservatively, to be 600 MeV). Among the 18 fits we consider, some have higher-order chiral terms and discretization terms completely unconstrained, and others constrain either the chiral terms, or the discretization terms, or both.

In Eq. (3.21), m_Q denotes the valence charm mass. To take into account the physical effects of the charm sea masses we can introduce a parameter k'_1 to Eq. (3.21):

$$\Phi_0 \to \Phi_0 \left(1 + k_1 \frac{\Lambda_{\mathrm{HQET}}}{m_Q} + k_2 \frac{\Lambda^2_{\mathrm{HQET}}}{m_Q^2} + k'_1 \frac{\Lambda_{\mathrm{HQET}}}{m'_c}\right) \left(1 + c_1 \alpha_S (a\Lambda)^2 + c_2 (a\Lambda)^4\right) , \qquad (3.27)$$

where m'_c is the mass of the charm mass in the sea. One of our 18 fits adds the parameter k'_1. Further, discretization errors coming from the charm sea masses can be included by adding $c'_3 \alpha_S (am'_c)^2 + c'_4 (am'_c)^4$ to the analytic terms in Eq. (3.8), and one of the fits makes that addition. It is interesting to note that it is possible to obtain another acceptable fit in which c_2 in Eq. (3.21) is restricted by priors to be much smaller than its value in the central fit, but the c'_3 and c'_4 terms are added. This shows that our lattice data cannot distinguish in detail between various sources of higher-order discretization effects. However, the results in the continuum limit are rather insensitive to these differences.

Since all 18 fits considered have acceptable p values and give correction terms reasonably consistent with expectations from chiral perturbation theory and power counting, whether or

not such terms are constrained, we have no strong reason to choose one fit or groups of fits as preferred in comparison to the rest. We therefore choose our "central fit" simply by requiring that it be a fit to all ensembles and that it give results for Φ_{D+} and Φ_{D_s} that are as close as possible to the center of the histograms for these quantities from all the fits and from all systematic variations in the inputs (*i.e.*, from the "continuum extrapolation" column in Table 3.6). This central fit has 27 free parameters, with g_π fixed to 1-sigma below its nominal value, and with the k_1', c_3', and c_4' terms discussed in the previous paragraph dropped, but all discretization terms aside from c_3' and c_4' kept. In the central fit, c_2 in Eq. (3.21) is equal to 1.3 with $\Lambda = 600$ MeV; while the HQET parameters are $k_1 = -1.0$ and $k_2 = 0.5$, with $\Lambda_{\rm HQET} = 600$ MeV.

Figure 3.17 shows our central fit to partially quenched data at all four lattice spacings. Extrapolating the parameters to the continuum, adjusting the strange sea-quark mass and charm valence- and sea-quark masses to their physical values, and setting the light sea-quark mass equal to the light valence mass (up to the small difference between m_d and $m_l = (m_u + m_d)/2$) gives the orange band. Putting in the physical light-quark mass then gives the black burst, which is the result for Φ_{D^+}. Note that the effect of isospin violation in the valence quarks is included in our result. The effect of isospin violation in the sea has not been included, but we may easily estimate its size by putting in our values for m_u and m_d (instead of the average sea mass m_l) in Eq. (3.8) and in the NNLO and NNNLO analytic terms. This results in a change of only 0.01% in f_{D^+}, and a still smaller change in f_{D_s}.

The width of the band shows the statistical error coming from the fit, which is only part of the total statistical error, since it does not include the statistical errors in the inputs of the quark masses and the lattice scale. To determine the total statistical error of each output quantity, we divide the full data set into 100 jackknife resamples. The complete calculation, including the determination of the inputs, is performed on each resample, and the error is computed as usual from the variations over the resamples. (For convenience, we kept the covariance matrix fixed to that from the full data set, rather than recomputing it for each resample.) Each jackknife resample drops approximately ten consecutive stored configurations (50 to 60 trajectories) from each ensemble with ≈ 1000 configurations. This procedure controls for autocorrelations, since all our measures of the autocorrelations of these quantities indicate that they are negligible after four or eight consecutive configurations. For the physical-mass 0.06 fm ensemble with 583 configurations, we are forced to drop only about six consecutive stored configurations at a time. Our expectation is that the effect of any remaining autocorrelations, while perhaps not completely negligible, is small compared to other sources of error. The total statistical errors computed from the jackknife procedure are only about 10% larger than the statistical error from the chiral/continuum fit, indicating that the inputs are statistically quite well determined.

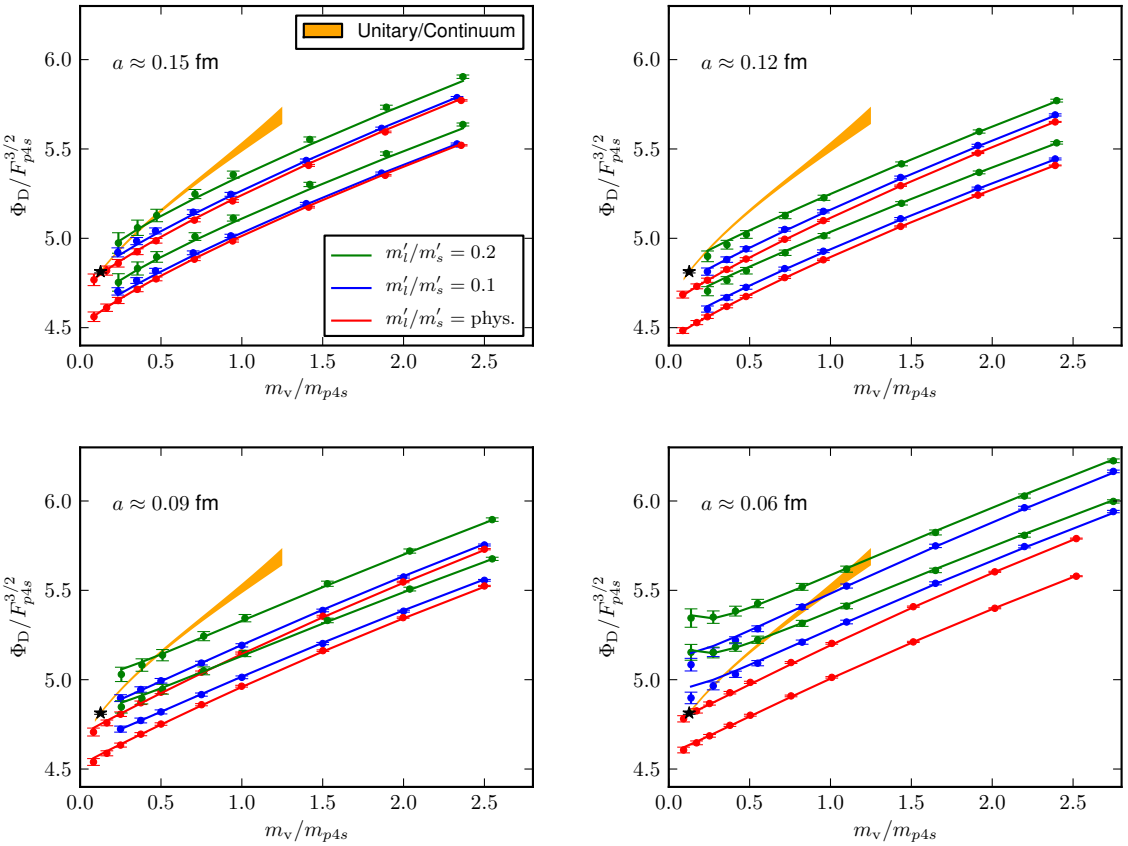

FIGURE 3.17: Simultaneous chiral fit to Φ_D as a function of m_v, the valence-quark mass (in units of m_{p4s}), at all four lattice spacings: $a \approx 0.15$ fm and 0.12 fm (top row), and 0.09 fm and 0.06 fm (bottom row). This fit has $\chi^2/\text{dof} = 347/339$, giving $p = 0.36$. In the fit lines for each ensemble, the light valence-quark mass varies, with all sea-quark masses held fixed. The orange band, labeled as "unitary/continuum," is identical in each panel. It gives the result after extrapolating to the continuum, setting the light valence-quark and sea-quark masses equal (up to the small difference between m_d and $m_l = (m_u + m_d)/2$), and adjusting the strange and charm masses to their physical values. The width of the band shows the statistical error coming from the fit. The black bursts indicate the value of Φ_{D^+} at the physical light-quark mass point.

The same procedure is performed to find the total statistical error of a and am_s at each lattice spacing.

Figure 3.18 illustrates how data for Φ_{D^+} and Φ_{D_s} depend on lattice spacing after adjustment to physical values of the quark masses (blue circles). There is a 2–3% variation between these points and the continuum value (green square at $a^2 = 0$). Note that there is clear curvature in the plot, evidence of significant a^4 terms in addition to the formally leading $\alpha_S a^2$ terms. Both the small absolute size of the errors, and the competition between formally leading and subleading terms, are typical of highly improved actions such as the HISQ action. The red stars show the contribution from the chiral logarithms (with known taste splittings) to the a^2

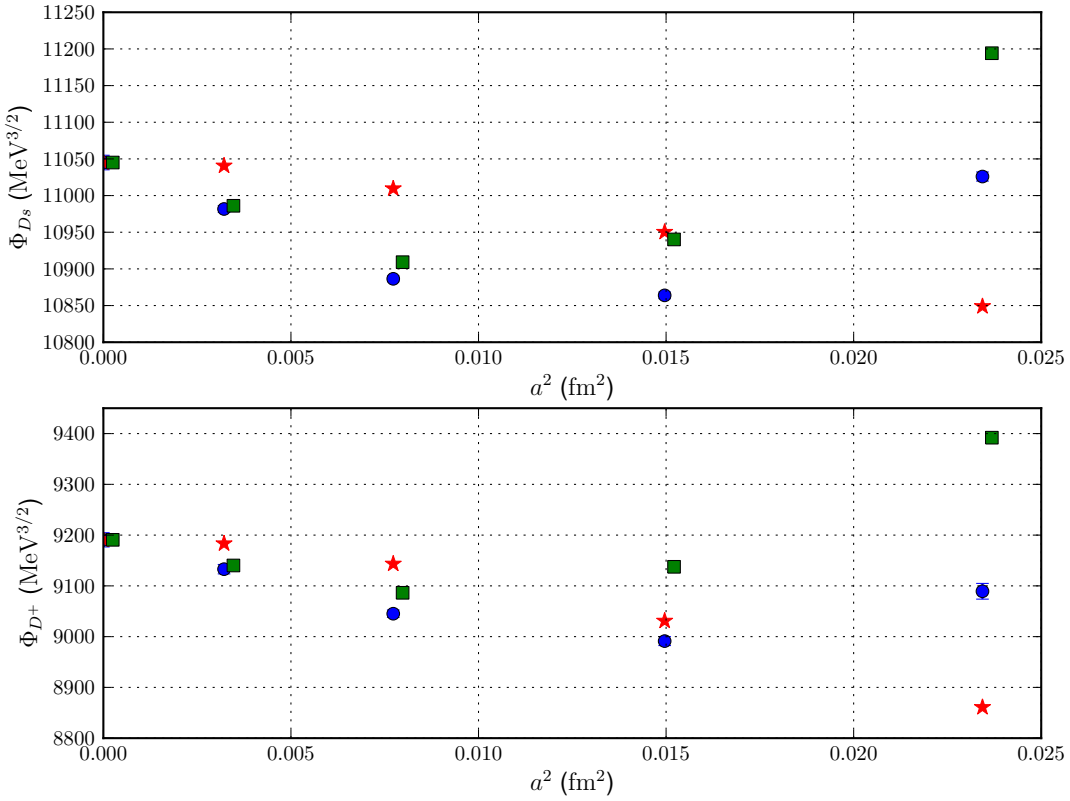

FIGURE 3.18: Lattice spacing dependence of Φ_{D^+} and Φ_{D_s}. The blue circles show the lattice data, after adjustment for mistunings of valence- and sea-quark masses. The red stars show the modification of each continuum value by the a^2 dependence of the chiral logarithms, while the green squares show the corresponding modification by the a^2 dependence induced by the fit parameters. Red stars and green squares overlap at $a^2 = 0$ (only the green square is visible). Neglecting small cross terms, the deviation of the blue circles from the continuum value are given by the algebraic sum of the deviations of the red stars and the green squares.

dependence of the chiral fit function. The green squares show the corresponding contribution from the analytic fit parameters. The two effects are of comparable magnitudes but the relative sign changes with lattice spacing; both are needed to describe the a^2 dependence of the data.

3.4.2.4 Continuum extrapolation and systematic uncertainties

To determine the systematic error associated with the continuum extrapolation (and chiral interpolation) of the charm decay constants in the chiral perturbation theory analysis, we rerun the analysis with alternative continuum/chiral fits, and with alternative inputs that come from different continuum extrapolations of the physical-mass analysis, listed in the "continuum extrapolation" column in Table 3.6.

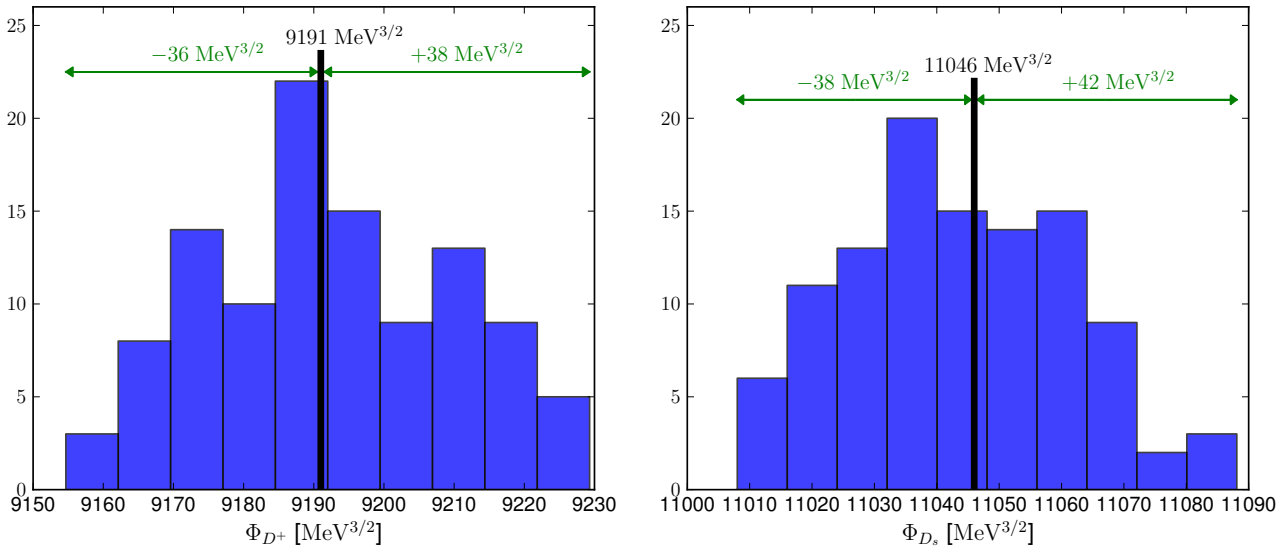

FIGURE 3.19: Histograms of Φ_{D^+} and Φ_{D_s} values obtained from various versions of the continuum/chiral extrapolation and various inputs of quark masses and scale values from the physical-mass analysis. Our central fit gives $\Phi_{D^+} = 9191$ MeV$^{3/2}$ and $\Phi_{D_s} = 11046$ MeV$^{3/2}$; those values are marked with vertical black lines. At the top of each histogram, we show the range taken as the systematic error of the self-contained chiral analysis of the current section.

As mentioned above, we have a total of 18 acceptable versions of the continuum/chiral fits. We also have the six versions of the continuum extrapolations used in the physical-mass analysis that leads to the inputs of quark masses and the lattice scale. This gives a total of 108 versions of the analysis. Histograms of the 108 results for Φ_{D^+} and Φ_{D_s} are shown in Fig. 3.19. Conservatively, we take the maximum difference seen in these results with our central values as the "self-contained" estimate of the continuum extrapolation errors within this chiral analysis. The central fit is chosen to give results that are close to the centers of the histograms, which results in more symmetrical error bars than in the preliminary analysis reported in Ref. [87]. Note that the "acceptable" fits entering the histograms all have $p > 0.1$. If the cutoff is instead taken to be $p > 0.05$, the additional fits allowed would not change the error estimates. However a cutoff of 0.01 or lower would give some additional outliers that would increase the width of the histograms.

As mentioned in Sec. 3.4.2.1, the chiral fits tend to pull g_π to low values. We can now look at this effect quantitatively. The central fit, which has g_π fixed to 0.45, 1σ below its nominal value of 0.53, has $p = 0.36$ and gives $\Phi_{D^+} = 9191(14)$ MeV$^{3/2}$, where the statistical error comes only from the fit and not from the errors in the inputs. Allowing g_π to be a free parameter, with prior range 0.53(8), we find $g_\pi = 0.26(5)$, about 3σ below its nominal value, and $p = 0.71$. However, Φ_{D^+} then is 9184(15) MeV$^{3/2}$, a change of only half the statistical error, and much less than the systematic error from the range over the results of all chiral/continuum fits. Alternatively, fixing

g_π to its nominal value gives $\Phi_{D^+} = 9195(13)\,\mathrm{MeV}^{3/2}$, $p = 0.16$. We can also consider the effect in fits that drop the data with $a \approx 0.15$ fm and consequently use fewer lattice-spacing-dependent parameters. When g_π is a free parameter with prior range 0.53(8), we find $g_\pi = 0.37(6)$, 2σ below the nominal value, and $\Phi_{D^+} = 9189(12)\,\mathrm{MeV}^{3/2}$, $p = 0.37$. The corresponding fits with g_π fixed to its nominal value or one sigma below that value give $\Phi_{D^+} = 9196(13)\,\mathrm{MeV}^{3/2}$, $p = 0.18$ and $\Phi_{D^+} = 9192(12)\,\mathrm{MeV}^{3/2}$, $p = 0.30$, respectively. Thus, the systematic error on Φ_{D^+} associated with the value of g_π is small compared to our other errors. The systematic error from g_π on Φ_{D_s} is a factor of two smaller still.

The fact that a wide range of g_π values give good fits indicates that our data has little to say about the physical value of that parameter. Indeed, even fits with g_π set equal to zero have very good p values, and do not change Φ_{D^+} by more than one statistical σ. Such a fit that includes all data gives $\Phi_{D^+} = 9180(13)\,\mathrm{MeV}^{3/2}$, $p = 0.83$, and one that drops the data with $a \approx 0.15$ fm gives $\Phi_{D^+} = 9181(13)\,\mathrm{MeV}^{3/2}$, $p = 0.52$.

In practice, the NLO finite volume corrections are included in our fit function, Eq. (3.8), when it is applied to the data, and the volume is sent to infinity when the continuum results are extracted. We may conservatively estimate the residual finite volume error in the heavy-light data either by turning off all finite volume corrections and repeating the fit, or by using the current fit to find the size of the NLO finite volume correction on our most-important, 0.06 fm physical-mass ensemble. Yet another way to make the estimate is by direct comparison of our results on the $32^3 \times 64$, $\beta = 6.0$, $m'_l/m'_s = 0.1$ ensemble (which is similar in physical size to our other $m'_l/m'_s = 0.1$ ensembles) and the $40^3 \times 64$, $\beta = 6.0$, $m'_l/m'_s = 0.1$ ensemble. All three methods indicate that there are negligible direct finite volume effects in the heavy-light lattice data. Nevertheless, there are non-negligible finite volume effects in our final answers, which appear due to the scale setting in the light-quark sector through, ultimately, f_{π^+}. (The value of F_{p4s} in physical units that we use comes by comparison with f_{π^+}.) We then propagate the errors in the inputs through our analysis. Electromagnetic errors in the light quark masses are similarly propagated through our analysis.

Results for Φ_{D^+}, Φ_{D_s} and their ratio at various values of the mass ratio of light to strange sea quarks are shown in Table 3.9; only the top subsection of the table gives physical results. Note that the valence masses do not vary in the three different subsections of the table, so changes in results show only the effects of the light sea mass. The EM error associated with the masses of the heavy-light mesons, which we call "EM3," is *not* included in any of the quoted EM errors in the table. As explained in Sec. 3.4.1.3, that is because the error cancels to good approximation when one extracts the decay constants f_{D^+}, f_{D_s} from Φ_{D^+}, Φ_{D_s}. One should use

TABLE 3.9: Results for Φ from the chiral analysis, for three choices of the light sea mass m'_l. Φ_D is the value of Φ when the light valence mass $m_v = m_l \equiv (m_u + m_d)/2$. Valence masses here are always taken to be the physical values m_d, m_s or m_l, independent of the value of m'_l, and the strange sea mass is always physical ($m'_s = m_s$). In the EM errors on these quantities, we have not included the "EM3" error coming from the EM effects on the masses of the corresponding heavy-light mesons. Such errors largely cancel when we compute f_{D^+} and f_{D_s} from Φ_{D^+} and Φ_{D_s} using the experimental meson masses. For Φ_D and f_D, the situation is more complicated — see text. The negative central value of $\Phi_{D^+} - \Phi_D$ for $m'_l/m_s = 0.2$ is an effect of partial quenching, but note that the systematic errors are large in this case.

$m'_l = m_l$	$\Phi_{D^+} = 9191 \pm 16_{\text{stat}} \,^{+38}_{-36}\vert_{a^2\,\text{extrap}} \pm 13_{\text{FV}} \pm 1_{\text{EM}}$ MeV$^{3/2}$ $\Phi_{D_s} = 11046 \pm 12_{\text{stat}} \,^{+42}_{-38}\vert_{a^2\,\text{extrap}} \pm 12_{\text{FV}} \pm 4_{\text{EM}}$ MeV$^{3/2}$ $\Phi_{D_s}/\Phi_{D^+} = 1.2018 \pm 0.0010_{\text{stat}} \,^{+0.0024}_{-0.0032}\vert_{a^2\,\text{extrap}} \pm 0.0004_{\text{FV}} \pm 0.0005_{\text{EM}}$ $\Phi_D = 9168 \pm 16_{\text{stat}} \,^{+39}_{-40}\vert_{a^2\,\text{extrap}} \pm 13_{\text{FV}} \pm 1_{\text{EM}}$ MeV$^{3/2}$ $\Phi_{D^+} - \Phi_D = 23.6 \pm 0.3_{\text{stat}} \,^{+4.7}_{-1.6}\vert_{a^2\,\text{extrap}} \pm 0.1_{\text{FV}} \pm 1.0_{\text{EM}}$ MeV$^{3/2}$
$m'_l/m_s = 0.1$	$\Phi_{D^+} = 9412 \pm 16_{\text{stat}} \,^{+46}_{-86}\vert_{a^2\,\text{extrap}} \pm 13_{\text{FV}} \pm 1_{\text{EM}}$ MeV$^{3/2}$ $\Phi_{D_s} = 11128 \pm 13_{\text{stat}} \,^{+36}_{-42}\vert_{a^2\,\text{extrap}} \pm 12_{\text{FV}} \pm 4_{\text{EM}}$ MeV$^{3/2}$ $\Phi_{D_s}/\Phi_{D^+} = 1.1824 \pm 0.0010_{\text{stat}} \,^{+0.0078}_{-0.0036}\vert_{a^2\,\text{extrap}} \pm 0.0004_{\text{FV}} \pm 0.0003_{\text{EM}}$ $\Phi_D = 9402 \pm 16_{\text{stat}} \,^{+48}_{-95}\vert_{a^2\,\text{extrap}} \pm 13_{\text{FV}} \pm 1_{\text{EM}}$ MeV$^{3/2}$ $\Phi_{D^+} - \Phi_D = 10.4 \pm 0.3_{\text{stat}} \,^{+9.4}_{-2.4}\vert_{a^2\,\text{extrap}} \pm 0.1_{\text{FV}} \pm 0.5_{\text{EM}}$ MeV$^{3/2}$
$m'_l/m_s = 0.2$	$\Phi_{D^+} = 9709 \pm 19_{\text{stat}} \,^{+53}_{-140}\vert_{a^2\,\text{extrap}} \pm 13_{\text{FV}} \pm 2_{\text{EM}}$ MeV$^{3/2}$ $\Phi_{D_s} = 11250 \pm 15_{\text{stat}} \,^{+44}_{-47}\vert_{a^2\,\text{extrap}} \pm 12_{\text{FV}} \pm 4_{\text{EM}}$ MeV$^{3/2}$ $\Phi_{D_s}/\Phi_{D^+} = 1.1588 \pm 0.0011_{\text{stat}} \,^{+0.0140}_{-0.0038}\vert_{a^2\,\text{extrap}} \pm 0.0003_{\text{FV}} \pm 0.0002_{\text{EM}}$ $\Phi_D = 9714 \pm 19_{\text{stat}} \,^{+56}_{-154}\vert_{a^2\,\text{extrap}} \pm 13_{\text{FV}} \pm 2_{\text{EM}}$ MeV$^{3/2}$ $\Phi_{D^+} - \Phi_D = -5.3 \pm 0.3_{\text{stat}} \,^{+15.0}_{-3.3}\vert_{a^2\,\text{extrap}} \pm 0.1_{\text{FV}} \pm 0.0_{\text{EM}}$ MeV$^{3/2}$

the experimental masses $M_{D^+} = 1869.62$ MeV, $M_{D_s} = 1968.50$ MeV [93] in this extraction; the experimental errors in these masses are negligible at the current level of precision.

To quantify the effect of isospin violations, we also report Φ_D and $\Phi_{D^+} - \Phi_D$, where Φ_D is the value of Φ in the isospin limit, when the light valence mass is equal to $m_l = (m_u + m_d)/2$ instead of m_d. In this case, the EM errors in the heavy-light meson masses do affect the errors in the corresponding decay constant difference because of the difference between the EM effect in the charged M_{D^+} and in the neutral M_{D^0}, which are averaged to obtain M_D. We estimate this error when we quote $f_{D^+} - f_D$ below.

In Table 3.10, we report additional results for the case when the light valence mass is kept equal to the light sea mass and $m'_l/m_s = 0.1$ or 0.2. These unphysical results may be useful for normalizing other calculations, such as those of B-system decay constants, as described in Sec. 2.6.

At each β value, we have reported, in Table 3.8, the values for the lattice spacing a and the strange mass in lattice units am_s, which come from our scale-setting procedure using M_{p4s}/F_{p4s} and aF_{p4s}. For the estimates of the extrapolation errors in these quantities, we have used the

TABLE 3.10: Results for Φ for two choices of light sea masses. Here the valence mass for Φ_D is taken equal to the light sea mass: $m_v = m'_l$. The quantities denoted by "phys" are those tabulated in Table 3.9 for the case $m'_l = m_l$.

$m'_l/m_s = 0.1$	$\Phi_D = 9477 \pm 15_{\rm stat}\ ^{+39}_{-66}|_{a^2\,\rm extrap} \pm 13_{\rm FV} \pm 2_{\rm EM}$ MeV$^{3/2}$
	$\Phi_{D_s} = 11128 \pm 13_{\rm stat}\ ^{+36}_{-42}|_{a^2\,\rm extrap} \pm 12_{\rm FV} \pm 4_{\rm EM}$ MeV$^{3/2}$
	$\Phi_D/\Phi_D^{\text{"phys"}} = 1.0338 \pm 0.0005_{\rm stat}\ ^{+0.0009}_{-0.0031}|_{a^2\,\rm extrap} \pm 0.0000_{\rm FV} \pm 0.0001_{\rm EM}$
	$\Phi_D/\Phi_{D^+}^{\text{"phys"}} = 1.0311 \pm 0.0004_{\rm stat}\ ^{+0.0010}_{-0.0036}|_{a^2\,\rm extrap} \pm 0.0000_{\rm FV} \pm 0.0002_{\rm EM}$
	$\Phi_{D_s}/\Phi_{D_s}^{\text{"phys"}} = 1.0075 \pm 0.0003_{\rm stat}\ ^{+0.0005}_{-0.0006}|_{a^2\,\rm extrap} \pm 0.0000_{\rm FV} \pm 0.0000_{\rm EM}$
$m'_l/m_s = 0.2$	$\Phi_D = 9870 \pm 17_{\rm stat}\ ^{+39}_{-71}|_{a^2\,\rm extrap} \pm 13_{\rm FV} \pm 2_{\rm EM}$ MeV$^{3/2}$
	$\Phi_{D_s} = 11250 \pm 15_{\rm stat}\ ^{+44}_{-47}|_{a^2\,\rm extrap} \pm 12_{\rm FV} \pm 4_{\rm EM}$ MeV$^{3/2}$
	$\Phi_D/\Phi_D^{\text{"phys"}} = 1.0766 \pm 0.0011_{\rm stat}\ ^{+0.0017}_{-0.0038}|_{a^2\,\rm extrap} \pm 0.0001_{\rm FV} \pm 0.0002_{\rm EM}$
	$\Phi_D/\Phi_{D^+}^{\text{"phys"}} = 1.0738 \pm 0.0011_{\rm stat}\ ^{+0.0017}_{-0.0043}|_{a^2\,\rm extrap} \pm 0.0001_{\rm FV} \pm 0.0002_{\rm EM}$
	$\Phi_{D_s}/\Phi_{D_s}^{\text{"phys"}} = 1.0185 \pm 0.0007_{\rm stat}\ ^{+0.0014}_{-0.0010}|_{a^2\,\rm extrap} \pm 0.0000_{\rm FV} \pm 0.0000_{\rm EM}$

six versions of the continuum extrapolation for the inputs, which are the quark-mass ratios, M_{p4s}/F_{p4s}, and F_{p4s} in physical units. Finite volume and electromagnetic errors come simply from propagating the errors in f_{π^+} and the light quark masses through the analysis.

The self-contained chiral analysis of the current section gives:

$$f_{D^+} = 212.6 \pm 0.4_{\rm stat}\ ^{+0.9}_{-0.8}|_{a^2\,\rm extrap} \pm 0.3_{\rm FV} \pm 0.0_{\rm EM} \pm 0.3_{f_\pi\,\rm PDG}\ \text{MeV}\,, \quad (3.28)$$

$$f_{D_s} = 249.0 \pm 0.3_{\rm stat}\ ^{+1.0}_{-0.9}|_{a^2\,\rm extrap} \pm 0.2_{\rm FV} \pm 0.1_{\rm EM} \pm 0.4_{f_\pi\,\rm PDG}\ \text{MeV}\,, \quad (3.29)$$

$$f_{D_s}/f_{D^+} = 1.1712(10)_{\rm stat}(^{+24}_{-31})_{a^2\,\rm extrap}(3)_{\rm FV}(5)_{\rm EM}\,, \quad (3.30)$$

$$f_{D^+} - f_D = 0.47(1)_{\rm stat}(^{+11}_{-\ 4})_{a^2\,\rm extrap}(0)_{\rm FV}(4)_{\rm EM}\ \text{MeV}\,, \quad (3.31)$$

where f_D is the decay constant in the isospin limit, $m_u = m_d = m_l$. In finding $f_{D^+} - f_D$ from $\Phi_{D^+} - \Phi_D$ in Table 3.9, we use the experimental value for M_{D^+} and our result, $M_{D^+} - M_{D^0} = 2.6$ MeV, obtained from the pure-QCD analysis in Sec. 3.4.1. Comparison with the experimental mass difference $M_{D^+} - M_{D^0} = 4.8$ MeV indicates that the EM effect on this difference is $\sim$2.2 MeV. We take half of this difference, namely 1.1 MeV, as our estimate of the "EM3" effect on the heavy-light masses, and propagate this error to $f_{D^+} - f_D$, adding it in quadrature with other EM errors to get the error quoted in Eq. (3.31).

3.5 Results and conclusions

Our main results are for the charm decay constants and their ratio. We take the more precise determinations from the self-contained chiral perturbation theory analysis using the full set of sea-quark ensembles, Eqs. (3.28)–(3.30), for our best estimate of the central values and statistical

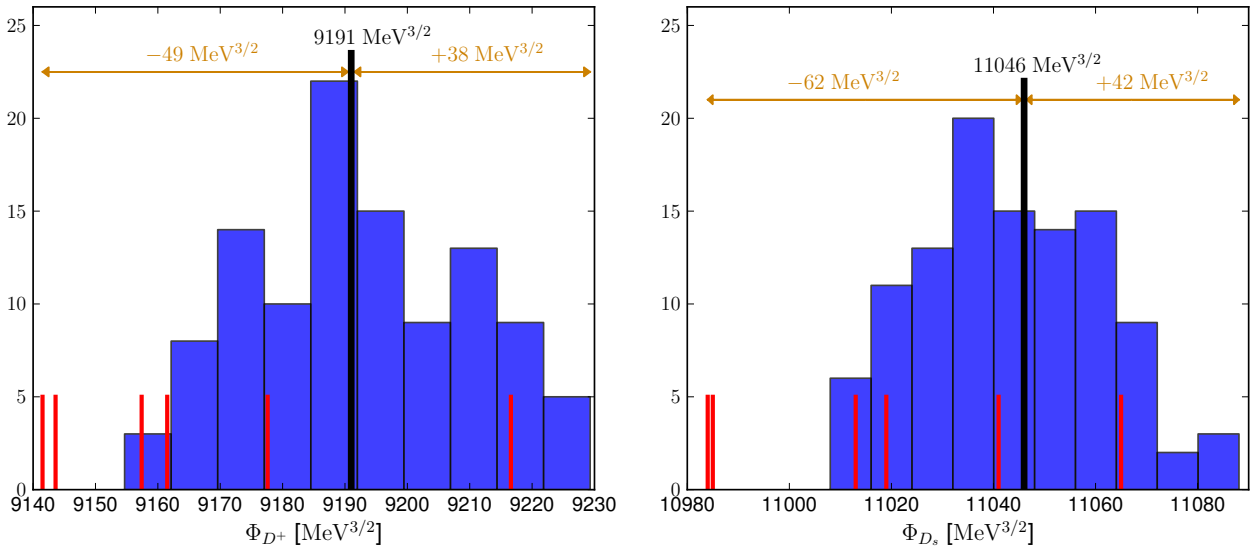

FIGURE 3.20: The same as Fig. 3.19, but the histograms of Φ_{D^+} and Φ_{D_s} from the chiral analysis have been overlaid with results from various continuum extrapolations in the physical-mass analysis, shown as vertical red lines. We take the full ranges shown at the top of each plot as the final estimates of the systematic errors coming from the continuum extrapolation.

errors. We then use the results of the simpler physical-mass analysis to help estimate the systematic uncertainties. For the continuum extrapolation error, we consider the differences in the central values of f_{D^+}, f_{D_s}, and f_{D_s}/f_{D^+}, obtained with various continuum-extrapolation Ansätze in the physical-mass analysis, and take those differences as the uncertainty whenever they are larger than the error from the chiral analysis. Figure 3.20 shows the histograms from Fig. 3.19 overlaid with the results from the various continuum extrapolations considered in Sec. 3.4.1 (vertical red lines), as well as our final estimates for the systematic errors of the continuum extrapolation. The analysis on the physical-mass ensembles also gives alternative, and comparably-sized, estimates for the finite-volume and EM errors to those in Eqs. (3.28)–(3.30) (see Table 3.6), and we take the larger value as the uncertainty in each case. This procedure yields our final results for f_{D^+}, f_{D_s} and f_{D_s}/f_{D^+}:

$$f_{D^+} = 212.6 \pm 0.4_{\text{stat}} \, {}^{+0.9}_{-1.1}|_{a^2\,\text{extrap}} \pm 0.3_{\text{FV}} \pm 0.1_{\text{EM}} \pm 0.3_{f_\pi\,\text{PDG}} \text{ MeV}\,, \tag{3.32}$$

$$f_{D_s} = 249.0 \pm 0.3_{\text{stat}} \, {}^{+1.0}_{-1.4}|_{a^2\,\text{extrap}} \pm 0.2_{\text{FV}} \pm 0.1_{\text{EM}} \pm 0.4_{f_\pi\,\text{PDG}} \text{ MeV}\,, \tag{3.33}$$

$$f_{D_s}/f_{D^+} = 1.1712(10)_{\text{stat}}(^{+28}_{-31})_{a^2\,\text{extrap}}(3)_{\text{FV}}(6)_{\text{EM}}\,. \tag{3.34}$$

For the effects of isospin violation we find

$$f_{D^+} - f_D = 0.47(1)_{\text{stat}}(^{+25}_{-\ 4})_{a^2\,\text{extrap}}(0)_{\text{FV}}(4)_{\text{EM}} \text{ MeV}, \tag{3.35}$$

where the continuum-extrapolation error has been increased relative to that in Eq. (3.31) to take into account the difference from the result of the physical-mass analysis.

We also update our determination of the decay-constant ratio f_{K^+}/f_{π^+} in Ref. [67] from the physical-mass analysis using additional configurations on the 0.06 fm physical quark mass ensemble, and include results for quark-mass ratios coming from the tuning procedure and continuum extrapolation described in Sec. 3.4.1:

$$f_{K^+}/f_{\pi^+} = 1.1956(10)_{\rm stat}\,{}^{+23}_{-14}|_{a^2\,\rm extrap}(10)_{\rm FV}(5)_{\rm EM}\,, \tag{3.36}$$

$$m_s/m_l = 27.352(51)_{\rm stat}\,{}^{+80}_{-20}|_{a^2\,\rm extrap}(39)_{\rm FV}(55)_{\rm EM}\,, \tag{3.37}$$

$$m_c/m_s = 11.747(19)_{\rm stat}\,{}^{+52}_{-32}|_{a^2\,\rm extrap}(6)_{\rm FV}(28)_{\rm EM}\,. \tag{3.38}$$

Although our analysis also determines m_u/m_d, we do not quote a final result, because the errors in this ratio are dominated by electromagnetic effects. If we take the results from our preliminary study of EM effects on pion and kaon masses reported in Ref. [99] at face value, we obtain a central value for $m_u/m_d = 0.4482(48)_{\rm stat}\,{}^{+21}_{-115}|_{a^2\,\rm extrap}(1)_{\rm FV}$, where we include the uncertainties from all sources other than EM. Once the full analysis of m_u/m_d from our QCD+QED simulations is complete, we expect the EM error to lie between 0.0150 and 0.0230. Even the more conservative estimate for the EM error on m_u/m_d, however, would not impact the uncertainties on our final results in Eqs. (3.32) through (3.38) significantly; the electromagnetic error is subdominant for most of these quantities, and one of several comparably sized errors in the case of m_s/m_l. With the charm-quark mass tuned to match the D_s mass, our analysis gives a mass for the η_c of $2982.33(0.35)(^{+2.34}_{-2.07})$ MeV. While this mass is in good agreement with the experimental value, it should be remembered that our calculation does not include the effects of disconnected contractions or decay channels to the η_c mass. Finally, we note that we are computing the values of the decay constants as they are conventionally defined, in a pure-QCD world. Comparison to experiment thus requires a matching of the decay rates between QCD and QCD+QED. The errors in such a matching are not included in our error budgets for the decay constants, but are accounted for in our determinations of CKM matrix elements in Sec. 3.6.

Figures 3.21, 3.22, 3.23 and 3.24 compare our results for m_s/m_l, m_c/m_s, f_{K^+}/f_{π^+} and the charm decay constants with other unquenched calculations. Our results agree with most determinations at the 1–2σ level. In particular, our value for f_{D_s} agrees with the second-most-precise determination from HPQCD obtained using HISQ valence quarks on the (2+1)-flavor MILC Asqtad ensembles [112]. We disagree slightly with HPQCD's determination of the ratio f_{D_s}/f_{D^+} [113], but only by 1.2σ. Our result for f_{D_s} is more precise than previous determinations primarily for two reasons. First, the statistical errors in our data points for the decay amplitudes

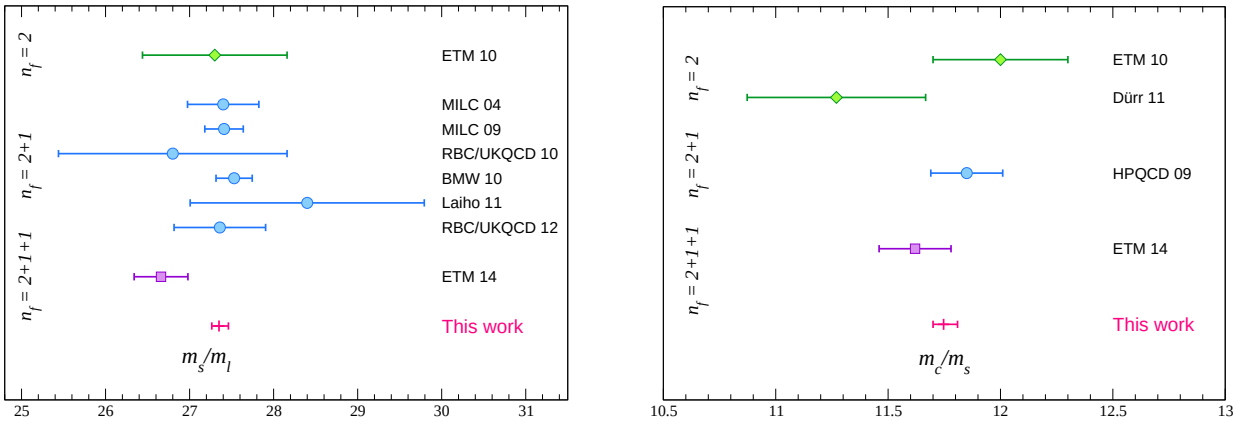

FIGURE 3.21: Unquenched lattice results for m_s/m_l [88, 114–119] and m_c/m_s [114, 120–122]. Results are grouped by the number of flavors from top to bottom: $n_f = 2$ (green diamonds), $n_f = 2+1$ (blue circles), and $n_f = 2+1+1$ (purple squares). Within each grouping, the results are in chronological order. Our new results are denoted by magenta crosses and displayed at the bottom of each plot.

are two or more times smaller than those obtained by, for example, HPQCD [112]. Second, our use of ensembles with the physical light-quark mass eliminates the significant (although not dominant) uncertainty from the chiral extrapolation. For f_{D^+} and f_{D_s}/f_{D^+}, we also have significantly smaller continuum-extrapolation errors due to the use of the HISQ sea-quark action and lattice spacings down to $a \approx 0.06$ fm.

The dominant source of uncertainty in our results is from the continuum extrapolation, and will be reduced once we include a still finer ensemble in our analysis with $a \approx 0.045$ fm and $m_l/m_s = 0.2$, generation of which is in progress. In fact, we already have some preliminary data on this ensemble, albeit with small statistics, and have tried including these data in the current chiral fits. The fits have acceptable p values and give results that are less than one statistical sigma away from those in Eqs. (3.32) through (3.36). Once we have ensembles with lattice spacings as fine as $a \approx 0.03$ fm, we expect to be able to use the same methods employed here to compute bottom decay constants. In the meantime, however, our results for D-meson decay constants using HISQ charm quarks can be combined with calculations of the ratios Φ_{B_s}/Φ_{D_s} using Fermilab heavy quarks to improve the determinations of decay constants in the B system, where the use of the HISQ action is more difficult. The ratios of continuum-extrapolated decay constants at various unphysical values of the light-quark mass may also be useful for this approach. The analysis of B- and D-meson decay constants with Fermilab heavy quarks on the 2+1 flavor asqtad ensembles is presently being finalized [140].

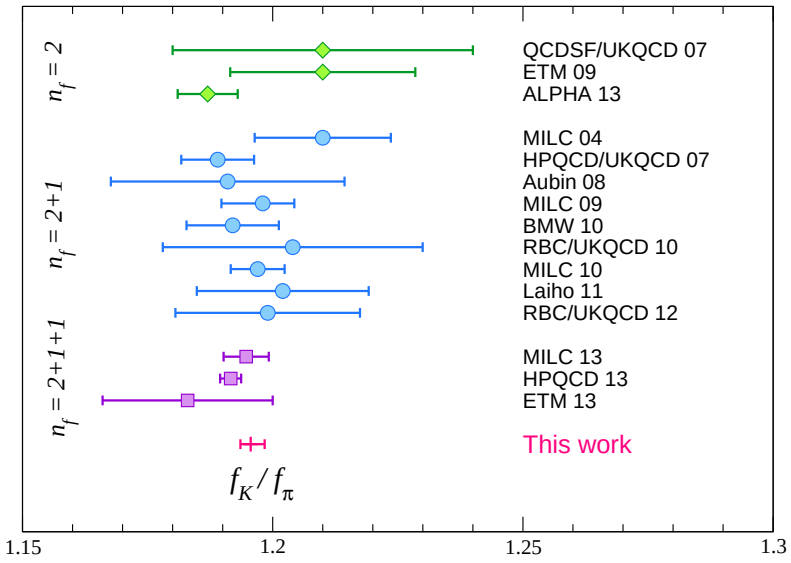

FIGURE 3.22: Unquenched lattice results for f_K/f_π [88, 115–119, 123–131]. The previous results are reviewed in [100]. Results are grouped by the number of flavors from top to bottom: $n_f = 2$ (green diamonds), $n_f = 2+1$ (blue circles), and $n_f = 2+1+1$ (purple squares). Within each grouping, the results are in chronological order. Our new result is denoted by a magenta cross and displayed at the bottom. In this plot we do not distinguish between results done in the isospin symmetric limit (degenerate up and down quarks) and results including isospin violation. The difference is small [100] and does not affect the qualitative picture. (Our result does include the up-down quark mass difference, and so is for f_{K^+}/f_{π^+}.)

3.6 Impact on CKM phenomenology

We now use our decay constant results to obtain values for CKM matrix elements within the Standard Model, and to test the unitarity of the first and second rows of the CKM matrix.

The decay-constant ratio f_{K^+}/f_{π^+} can be combined with experimental measurements of the corresponding leptonic decay widths to obtain a precise value for the ratio $|V_{us}|/|V_{ud}|$ [65]. Combining our updated result for f_{K^+}/f_{π^+} from Eq. (3.36) with recent experimental results for the leptonic branching fractions [93] and an estimate of the hadronic structure-dependent EM correction [141], we obtain

$$|V_{us}|/|V_{ud}| = 0.23081(52)_{\mathrm{LQCD}}(29)_{\mathrm{BR}(K_{\ell 2})}(21)_{\mathrm{EM}}\,. \tag{3.39}$$

Taking $|V_{ud}|$ from nuclear β decay [142], we also obtain

$$|V_{us}| = 0.22487(51)_{\mathrm{LQCD}}(29)_{\mathrm{BR}(K_{\ell 2})}(20)_{\mathrm{EM}}(5)_{V_{ud}}\,. \tag{3.40}$$

This result for $|V_{us}|$ is more precise than our recent determination from a calculation of the

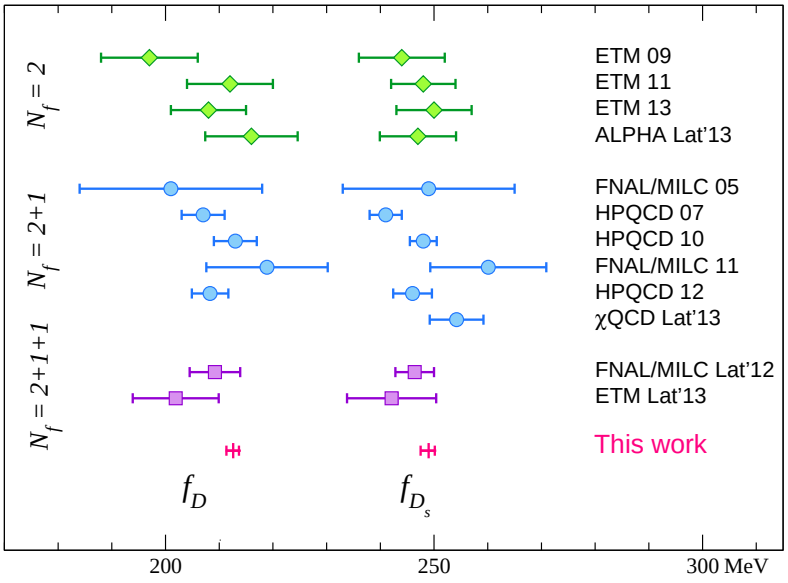

FIGURE 3.23: Unquenched lattice results for f_D and f_{D_s} [89, 112, 113, 124, 131–137]. We do not include Ref. [138] because of the small volume used, and Ref. [139] because of the lack of a continuum extrapolation. Results are grouped by the number of flavors from top to bottom: $n_f = 2$ (green diamonds), $n_f = 2 + 1$ (blue circles), and $n_f = 2 + 1 + 1$ (purple squares). Within each grouping, the results are in chronological order. Our new results are denoted by magenta pluses and displayed at the bottom. Again, we do not distinguish results in the isospin symmetric limit from those with non-degenerate up and down quarks, where we have estimated the difference in Eq. 3.35.

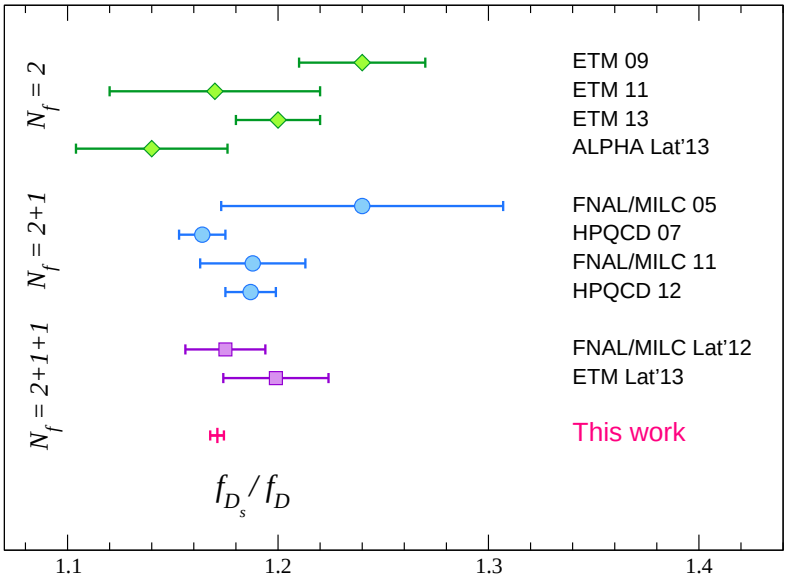

FIGURE 3.24: Unquenched lattice results for f_{D_s}/f_D [89, 112, 113, 124, 131–136]. Results are grouped by the number of flavors from top to bottom: $n_f = 2$ (green diamonds), $n_f = 2 + 1$ (blue circles), and $n_f = 2 + 1 + 1$ (purple squares). Within each grouping, the results are in chronological order. Our new result is denoted by magenta crosses and displayed at the bottom.

kaon semileptonic form factor on the physical-mass HISQ ensembles [143], and larger by 1.8σ. Figure 3.25 shows the unitarity test of the first row of the CKM matrix using our result for f_{K^+}/f_{π^+}. We find good agreement with CKM unitarity, and obtain a value for the sum of squares of elements of the first row of the CKM matrix consistent with the Standard-Model prediction zero at the level of 10^{-3}:

$$1 - |V_{ud}|^2 - |V_{us}|^2 - |V_{ub}|^2 = 0.00026(51)\,. \tag{3.41}$$

Thus our result places stringent constraints on new-physics scenarios that would lead to deviations from first-row CKM unitarity. Finally, we note that, now that the uncertainty in $|V_{us}|^2$ is approximately the same as that in $|V_{ud}|^2$, it is especially important to scrutinize the current uncertainty estimate for $|V_{ud}|$.

The D^+- and D_s-meson decay constants can be combined with experimental measurements of the corresponding leptonic decay widths to obtain $|V_{cd}|$ and $|V_{cs}|$. The values $f_{D^+}|V_{cd}| = 46.06(1.11)$ MeV and $f_{D_s}|V_{cs}| = 250.66(4.48)$ MeV in the PDG [144] are obtained from averaging the experimentally-measured decay rates into electron and muon final states including an estimate of structure-dependent Bremsstrahlung effects that lowers the $D^+ \to \mu^+\nu_\mu$ rate by $\sim 1\%$ [145, 146]. The PDG determinations of $f_{D^+}|V_{cd}|$ and $f_{D_s}|V_{cs}|$ do not, however, take into account other electroweak corrections (*c.f.* Refs. [65] and [147] and references therein). Such contributions are estimated for pion and kaon leptonic decay constants to be $\sim$ 1–2%, and the uncertainties in these corrections, in particular from the contributions that depend on the hadronic structure, lead to $\sim 0.1\%$ uncertainties in $|V_{us}|/|V_{ud}|$ and $|V_{us}|$ obtained from leptonic decays. Now that the uncertainties in the charm decay constants are at the half-a-percent level, it is timely to consider including electroweak corrections when extracting $|V_{cd}|$ and $|V_{cs}|$ from leptonic D decays, and we attempt to provide a rough estimate of their possible size here. We consider all of the contributions that have been estimated for pion and kaon leptonic decays. Not all of the necessary calculations have been performed for the charm system, however, so, where necessary, we use results for the pion and kaon system as a guide and take a generous uncertainty.

The universal long-distance EM contribution to leptonic decays of point-like charged particles was calculated by Kinoshita [148]. Evaluating this contribution for leptonic D decays into muons (because the experimental averages are dominated by measurements in the muon channel), the long-distance correction lowers both the D^+ and D_s decay rates by about 2.5%. The universal short-distance contribution to leptonic decays of charged pseudoscalar mesons, which accounts for electroweak corrections not included in the definition of G_F, was computed by Sirlin [149]. Choosing M_D for the factorization scale that enters $\ln(M_Z/\mu)$, the "Sirlin factor"

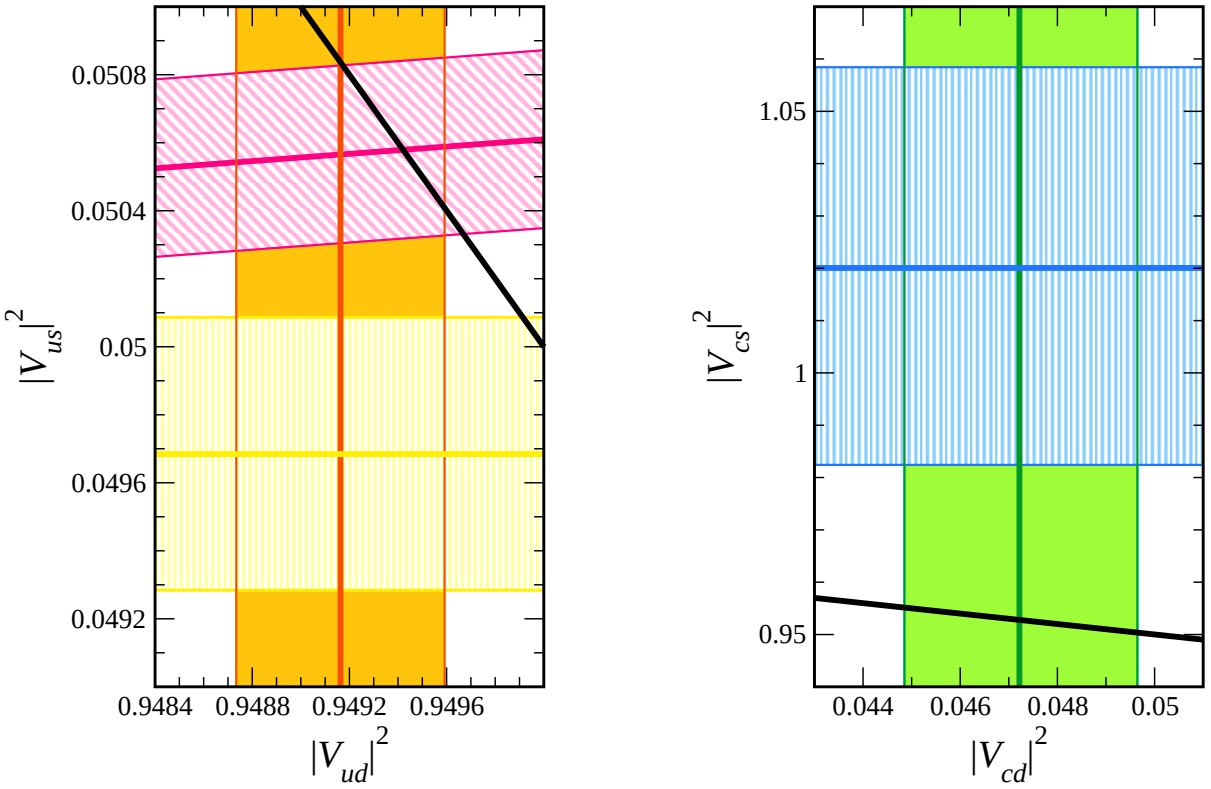

FIGURE 3.25: Unitarity tests of the Cabibbo-Kobayashi-Maskawa matrix. Left: squared magnitudes of elements of the first row of the CKM matrix. The magenta diagonal band shows $(|V_{us}|/|V_{ud}|)^2$ obtained using f_{K^+}/f_{π^+} from this work, the vertical orange band shows $|V_{ud}|^2$ from nuclear β decay [142], and the horizontal yellow band shows $|V_{us}|^2$ obtained using our recent calculation of the kaon semileptonic form factor at $q^2 = 0$ [143]. The diagonal black line is the unitary prediction, and lies well within the region of overlap of the magenta and orange bands. Right: squared magnitudes of elements of the second row of the CKM matrix. The green vertical and blue horizontal bands show $|V_{cd}|^2$ and $|V_{cs}|^2$ obtained using f_{D^+} and f_{D_s} from this work. The black diagonal line does not intersect with the region of overlap of the two colored bands, indicating a slight tension with CKM unitarity.

increases the D^+ and D_s leptonic decay rates by about 1.8%. Thus the net effect of these two known corrections is a slight decrease in the D^+ and D_s rates by less than a percent. Finally, we consider EM effects that depend on the mesons' hadronic structure. The expressions for the structure-dependent contributions to charged pion and kaon decay rates have been computed at $\mathcal{O}(e^2p^2)$ and $\mathcal{O}(e^2p^4)$ in chiral perturbation theory [150, 151]. The dominant $\mathcal{O}(e^2p^2)$ contribution takes the form $c_1^{(P)}\alpha/\pi$, and the coefficients have been estimated numerically in the large-N_c approximation to be $c_1^{(\pi)} = -2.4(5)$ and $c_1^{(K)} = -1.9(5)$ [152]. These calculations do not apply to the charm system, however, because the $D_{(s)}$-meson masses are much heavier than the pion and kaon masses, and well outside the range of validity of the light-meson chiral expansion. We therefore consider the possibility that the analogous coefficients for the D system are 2–5 times larger than for the pion and kaon system. With this assumption, we find a range of

the possible size for the hadronic correction to the D^+- and D_s-meson leptonic decay rates from 1.1–2.8%. Corrections of this size would not be negligible compared to the known short-distance and long-distance contributions; thus it is important to obtain a more reliable estimate of the contributions to charged D decays due to hadronic structure in the future.

For the determinations of $|V_{cd}|$ and $|V_{cs}|$ given here, we first adjust the experimental decay rates quoted in the PDG by the known long-distance and short-distance electroweak corrections. We then add an estimate of the uncertainty due to the unknown hadronic structure-dependent EM corrections, taking the lower estimate of 0.6%. With these assumptions, and using our results for f_{D^+} and f_{D_s} from Eqs. (3.32) and (3.33), we obtain

$$|V_{cd}| = 0.217(1)_{\rm LQCD}(5)_{\rm expt}(1)_{\rm EM}\,, \tag{3.42}$$

$$|V_{cs}| = 1.010(5)_{\rm LQCD}(18)_{\rm expt}(6)_{\rm EM}\,, \tag{3.43}$$

where “EM" denotes the error due to unknown structure-dependent EM corrections. In both cases, the uncertainty is dominated by the experimental error in the branching fractions. Thus the significant improvement in f_{D^+} and f_{D_s} does not, at present, lead to direct improvement in $|V_{cd}|$ and $|V_{cs}|$. Experimental measurements of the D^+ decay rates have improved recently [144], however, such that the error on $|V_{cd}|$ from leptonic D^+ decays is now approximately half that of $|V_{cd}|$ obtained from either neutrinos [93] or semileptonic $D \to \pi\ell\nu$ decay [153].

Our result for $|V_{cd}|$ agrees with the determination from neutrinos. Our $|V_{cd}|$ is 1.0σ lower than the determination from semileptonic D decay in Ref. [153], while our $|V_{cs}|$ is 1.1σ higher than that of Ref. [154]. Figure 3.25 shows the unitarity test of the second row of the CKM matrix using our results for f_{D^+} and f_{D_s}. We obtain a value for the sum of squares of elements of the second row of the CKM matrix of

$$1 - |V_{cd}|^2 - |V_{cs}|^2 - |V_{cb}|^2 = -0.07(4)\,, \tag{3.44}$$

showing some tension with CKM unitarity. This test will continue to become more stringent as experimental measurements of the D^+ and D_s decay rates become more precise. At present, even if our rough estimate of the uncertainty due to structure-dependent EM corrections in Eqs. (3.42) and (3.43) is too small by a factor of two, the errors on $|V_{cd}|$ and $|V_{cs}|$ would not change significantly. It will be important, however, to obtain a more reliable estimate of the contributions to charged D decays due to hadronic structure in the future.

PART II

Nonlinear Eigenvalue Problems

This part includes three chapters. In Chapter 4 ordinary differential equations are reviewed briefly, the asymptotic behavior of eigenfunctions of the Schrödinger equation is discussed, and it is explained how to generalize the concept of eigenvalue problems to nonlinear differential equations. In Chapter 5 equation $y'(x) = \cos[\pi x y(x)]$ *is investigated and its eigenvalue solutions are presented. Finally, in Chapter 6 the first and second Painlevé equations are studied.*

4 Technical Introduction to Part II

4.1 Overview of nonlinear eigenvalue problems

In the theory of ordinary differential equations, the concept of eigenvalue and eigenfunction is conventionally developed only for linear differential equations. The objective of the second part of this dissertation is to generalize this concept so that it may be applicable for nonlinear differential equations as well. The starting point is to recognize that a normalizable (square-integrable) eigenvalue solution of a linear differential equation on an infinite domain can be associated to the lack of growing terms, especially the lack of exponentially growing terms, in the asymptotic behavior of the solutions at infinity. This can be considered as a milestone to define eigenvalue problems for nonlinear differential equations. The main idea is to study special solutions of a nonlinear differential equation that are associated with instabilities. These solutions are good candidates to be investigated since they may arise as a result of missing exponentially growing terms as the solutions approach some limit curves.

The concept of a nonlinear eigenvalue problem is introduced by investigating some nonlinear differential equations. The simple-looking differential equation $y'(x) = \cos(\pi xy)$ is investigated first. A discrete set of initial conditions $y(0) = a_n$, leading to unstable separatrix behavior, are identified as the eigenvalues of the problem. This problem is discussed in derail in chapter 5. Here we only emphasize on a key feature of the eigenvalue solutions of this equation. These solutions have only an exponentially vanishing term in their asymptotic behavior as they approach their corresponding limit curves.

As solutions of special classes of nonlinear differential equations, the six Painlevé transcendents provide a rich realm to be investigated with the concept of eigenvalue problems. Their corresponding equations are presented in subsection 4.3.1, and the separatrix solution of the first

Painleveé equation is discussed in subsection 4.3.2. Similar to equation $y'(x) = \cos(\pi xy)$, the first Painleveé equation has a discrete set of critical initial conditions that give rise to unstable separatrix solutions, which appear again due to the lack of exponentially growing terms. These discrete initial conditions can be thought of as eigenvalues and the separatrices that stem from these initial conditions can be viewed as the corresponding eigenfunctions. A similar pattern is seen in the second Painlevé transcendents. The detailed study of the first and second Painlevé transcendents is presented in chapter 6.

It must be emphasized that the investigated differential equations possesses some limit curves, where the obtained eigenfunctions approach them exponentially fast in the absence of growing exponential terms. An infinitesimal change in the eigenvalues turn the growing terms on, subsequently the solutions abruptly move away from the limit curves. This is the same behavior of the eigenfunctions of the Schrödinger equation, where the limit curve is the real axis $y = 0$. As a matter of fact, in addition to the missing exponentially growing terms, these special solutions exhibit many common features with eigenfunctions of the Schrödinger equation, either the conventional one with a Hermitian Hamiltonian or with a $\mathcal{PT}$-symmetric Hamiltonian.

4.2 Eigenvalue problems in linear differential equations

This part deals with eigenvalue problems in the context of the Schrödinger equation with vanishing boundary conditions at $x = \pm\infty$. To tackle this problem, one may wish to develop a local analysis of the Schrödinger equation about $x = \infty$. But, this point is typically an irregular singular point of the equation, where one may need to study the problem in the context of asymptotic analysis. Asymptotic analysis provides an important tool to classify the solutions of the Schrödinger equation when $x \to \infty$. This leads to the concept of dominant (exponentially growing) and subdominant (exponentially vanishing) solutions. From a physical point of view, which is encoded in the boundary conditions, any acceptable solutions (eigenfunctions) must vanish at $x = \pm\infty$. The dominant terms cannot appear in the eigenfunctions either at $+\infty$ or at $-\infty$. This is a condition that holds only for a discrete set of eigenvalues. Otherwise, the dominant terms appear at least in one side of the problem.

4.2.1 Linear differential equations

An nth-order homogeneous linear differential equation has the form

$$y^{(n)}(x) + p_{n-1}(x)y^{(n-1)}(x) + \cdots + p_1(x)y^{(1)}(x) + p_0(x)y(x) = 0, \tag{4.1}$$

where $y^{(k)}(x) = d^k y/dx^k$. In an *initial-value* problem, y and its first $n-1$ derivatives are specified at one point $x = x_0$, while in a *boundary-value problem* a total of n quantities are specified at two or more points. An *eigenvalue* problem is a boundary-value problem that has *nontrivial* solutions only when a parameter E that enters the problem has special values called eigenvalues. When E is an eigenvalue of a homogeneous linear boundary-value problem, the solution to the boundary-value problem is not unique [155]. Consider the eigenvalue problem on an infinite domain

$$\begin{aligned} y'' + (E - \frac{1}{4}x^2)y &= 0 \quad (-\infty < x < \infty), \\ y(\pm\infty) &= 0\,. \end{aligned} \tag{4.2}$$

This problem has the trivial solution $y(x) \equiv 0$ for any value of E, but for special $E = n + \frac{1}{2}$, $n = 0, 1, 2, \cdots$, there are nontrivial solutions

$$y(x) = c\,\mathrm{He}_n(x)\,e^{-x^2/4}\,, \tag{4.3}$$

where c is an arbitrary constant and $\mathrm{He}_n(x)$ is the Hermite polynomial of degree n.

Equation 4.1 can be generalized from the real axis to the complex plane if the coefficient functions $p_i(x)$ make sense in the complex plane. To understand the structure of an analytic function in the complex place, it is essential to study its singularities [156]. Any singularity in $y(x)$ in the complex plane is controlled by the singularities of the coefficient functions of the differential equation. To develop a local analysis in a neighborhood of $x = x_0$, it suffices to examine the $p_i(x)$ in the neighborhood. This can be done systematically by classifying the point x_0 based on the singularities of the coefficient functions.

4.2.2 Classification of singularities of linear differential equations

Consider a point x_0 in the complex plane, where $x_0 \neq \infty$. One can classify this point as an *ordinary point*, a *regular singular point*, or an *irregular singular point* of Eq. (4.1). The local behavior of a solution of Eq. (4.1) based on this classification is summarized as [155]

- Ordinary point: The point x_0 ($x_0 \neq \infty$) is called an ordinary point of Eq. (4.1) if the coefficient functions $p_0(x), \cdots, p_{n-1}(x)$ are all analytic in a neighborhood of x_0 in the complex plane. One can show that, in the neighborhood of the ordinary point x_0, all n linearly independent solutions of Eq. (4.1) are analytic, and each of them can be expanded

in a Taylor series about x_0 as

$$y(x) = \sum_{n=0}^{\infty} a_n (x - x_0)^n. \tag{4.4}$$

- Regular singular point: The point $x0$ ($x_0 \neq \infty$) is called a regular singular point of Eq. (4.1) if not all of the coefficient functions $p_0(x), \cdots, p_{n-1}(x)$ are analytic but if all of $(x - x_0)^n p_0(x), \cdots, (x - x_0) p_{n-1}(x)$ are analytic in a neighborhood of x_0. A solution of Eq. (4.1) may be analytic at a regular singular point. If it is not analytic, its singularity must be either a pole or an algebraic or logarithmic branch point. In general, a solution has the form

$$y(x) = \sum_{i=0}^{n-1} [\ln(x - x_0)]^i (x - x_0)^{\gamma_i} A_i(x) \ , \tag{4.5}$$

  where all the functions $A_i(x)$ are analytic at x_0.

- Irregular singular point: The point x_0 ($x_0 \neq \infty$) is called an irregular singular point of Eq. (4.1) if is neither an ordinary point nor a regular singular point. There is no comprehensive theory of irregular singular points, but we can say that at an irregular singular point at least one solution is not of the form of Eq. (4.5). Typically, at an irregular singular point, all solutions exhibit an essential singularity. To analyze the local behavior of solutions near irregular singular points, one can make use of a different mathematical tool: the asymptotic power series. Although very powerful, the asymptotic power series miss a very important property. They are not convergent.

To classify the point $x_0 = \infty$, one can analytically map the point at infinity into the origin using the inversion transformation $x = 1/t$, and then classify the point $t = 0$ in the new system. The point $x_0 = \infty$ is called an ordinary, a regular singular, or an irregular singular point if the point at $t = 0$ is corresponding classified [155].

4.2.3 Asymptotic power series

Eq. (4.1) usually does not have a formal power series about an irregular singular point x_0, but a simple preliminary transformation involving exponential functions of the dependent variable x leads to a differential equation that does admit formal power series solutions [156], which is referred to as *asymptotic* power series. The asymptotic power series are typically divergent.

The power series $\sum_{n=0}^{\infty} a_n(x-x_0)^n$ is said to be asymptotic to the function $y(x)$ as $x \to x_0$ (denoted by $y(x) \sim \sum_{n=0}^{\infty} a_n(x-x_0)^n$ as $x \to x_0$) if

$$y(x) - \sum_{n=0}^{N} a_n(x-x_0)^n \ll (x-x_0)^N \quad \text{as } x \to x_0 \,, \tag{4.6}$$

for every N [155]. This definition does not imply that the asymptotic series is convergent. If the irregular singular point is at $x_0 = \infty$, the corresponding definition is $y(x) \sim \sum_{n=0}^{\infty} a_n x^{-n}$ as $x \to \infty$ if

$$y(x) - \sum_{n=0}^{N} a_n x^{-n} \ll x^{-N} \quad \text{as } x \to \infty \,, \tag{4.7}$$

for every N.

There are many subtle properties regarding the validity and uniqueness of an asymptotic power series. Here we list some of them:

- Asymptotic power series are valid in some sector as $x \to x_0$ in the complex plane. If an asymptotic power series is divergent, it can only be valid in a sector whose opening angle is less than 360° [155]. In general, one can expect to obtain a set of asymptotic relations for a function $y(x)$, each of which is valid in a wedge-shaped region about the irregular singular point.
- A function $y(x)$ can have at most one asymptotic series representation $\sum_{n=0}^{\infty} a_n(x-x_0)^n$ in a given sector S [156].
- An asymptotic series is asymptotic to a whole class of functions that differ from each other by *subdominant* functions to the asymptotic power series. A subdominant function $g(x)$, has the asymptotic expansion $g(x) \sim \sum_{n=0}^{\infty} 0(x-x_0)^n$ as $x \to x_0$.[1]

4.2.4 Stokes phenomenon and Stokes multipliers

In this part, the form of Eq. (4.1) is restricted to the Schrödinger equation, with $\hbar = 1$

$$-y''(x) + Q(x)y(x) = 0, \quad Q(x) = V(x) - E, \tag{4.8}$$

[1] A simple example for a subdominant function about the origin is $\exp(-1/x^2)$. All derivatives of this function vanish as $x \to 0$, therefore, using integration by parts, one can show that $\exp(-1/x^2) = \sum_{n=0}^{N} 0x^n + R_N(x)$, where $N \in \mathbb{N}$ and $R_N(x)$ is the remainder term. This equality would lead to a valid Taylor series if one could show that the remainder term approaches to zero as N tends to infinity for a disc $|x| < R$ with some nonzero radius R. There is not such a nonzero radius of convergence, thereby the above equality does not yield a Taylor expansion. But, it leads to the asymptotic expansion $\exp(-1/x^2) \sim \sum_{n=0}^{\infty} 0x^n$ as $x \to 0$.

with the assumption that $V(x) = x^{2m} + a_1 x^{2m-1} + \cdots + a_{2m}$, where $m \in \mathbb{N}$. There is no boundary condition imposed yet. With the polynomial potential, the point $x = \infty$ is an irregular singular point of the equation. We want to investigate the asymptotic behavior of a solution $y(x)$ of the Schrödinger as $x \to \infty$. There are two independent solutions of Eq. (4.8) with the following asymptotic behavior

$$y_{\pm}(x) \sim c_{\pm} \frac{\exp\left(\pm \int_{x_0}^{x} \sqrt{Q(t)} dt\right)}{[Q(x)]^{1/4}} \quad \text{as } x \to \infty \,. \tag{4.9}$$

These are the leading order terms in the asymptotic expansion of the solutions about the irregular singular point at infinity.

The exponent term in Eq. (4.9) can be expanded as

$$\pm \int_{x_0}^{x} \sqrt{Q(t)} dt = \pm \frac{x^{m+1}}{m+1} + \cdots \,. \tag{4.10}$$

The *principal part* of the exponent term, $\frac{1}{m+1} x^{m+1}$, determines whether a solution is subdominant (exponentially vanishing) or dominant (exponentially growing) as $x \to \infty$. When we consider this problem in the complex plane, the subdominant and the dominant solutions may change their roles in different regions, the so-called *Stokes wedges*. The exchange of the identities is called the *Stokes phenomenon* [155]. Neglecting the corrections to the right hand side of Eq. (4.10), the Stokes wedges S_k could be defined as

$$S_k = \left\{ z : \ \left| \arg z - \frac{k\pi}{m+1} \right| < \frac{\pi/2}{m+1} \right\}, \ k \in \mathbb{Z}_{2m+2} \,, \tag{4.11}$$

and the Stokes lines are the lines in the complex plane with $\arg z = \frac{(k+1/2)\pi}{m+1}$, $k \in \mathbb{Z}_{2m+2}$.[2]

It is important to emphasize that a subdominant solution in a Stokes wedge S_k, denoted by $y_k(z; E)$, is not subdominant in the neighbor Stokes wedge S_{k+1}. This can be immediately checked by investigating the principal part of the exponent of the leading order term in the asymptotic expansion. The sign of the real part of $\frac{1}{m+1} x^{m+1}$ changes as the corresponding Stokes line is crossed, consequently $y_k(z; E)$ is not subdominant in S_{k+1}. Note that this argument is only based on the leading-order behavior of the asymptotic expansion. But, a complete argument must consider the fact that an asymptotic expansion has a region of validity in the complex plane. For the case of subdominant solutions, a complete argument shows that the above conclusion is correct; *i.e.*, $y_k(z; E)$ is not subdominant in the neighboring Stokes wedge S_{k+1}. But, for the case of dominant solutions, a complete argument would suggest that a solution which is dominant in S_k might be dominant in S_{k+1} as well.

[2] For a concrete definition of the Stokes wedges and the Stokes lines, one can discuss [155, 156]. In Ref. [156], the Stokes lines are defined as certain curves beyond which a given asymptotic expansion becomes invalid.

For each Stokes wedge S_k, there exists a one-parameter family of subdominant solutions as $A\, y_k(z;E)$, where A is an arbitrary parameter and $y_k(z;E)$ is a subdominant solution normalized with one way or another. One can show that two consecutive solutions $y_k(z;E)$ and $y_{k+1}(z;E)$ (which are subdominant in S_k and S_{k+1}, respectively) are linearly independent, and then one can infer that $\{y_k, y_{k+1}\}$ constitutes a basis for the space of solutions of Eq. (4.8) [157]. Therefore, every solution of Eq. (4.8) can be expressed as a linear combination of them, in particular

$$y_{k-1}(z,E) = C_k(E)\; y_k(z,E) + \widetilde{C}_k(E)\; y_{k+1}(z,E)\;. \tag{4.12}$$

The multipliers $C_k(E)$ and $\widetilde{C}_k(E)$ are called the Stokes multipliers of y_{k-1} with respect to y_k and y_{k+1}. The Stokes multipliers are just functions of the parameter E. It would be interesting to investigate their dependence on the parameter E and study how they change as E varies.

Here we list two important properties of the Stokes multipliers of the problem [157]:

- The stokes multipliers are entire functions of E.
- $\widetilde{C}_k(E)$ never vanishes so it can be reduced to 1 by a suitable renormalization of the basis.

Therefore, by renormalizing the basis, Eq. (4.12) can be written as

$$y_{k-1}(z,E) = C_k(E)\; y_k(z,E) + y_{k+1}(z,E)\;. \tag{4.13}$$

Now, the fact that $C_k(E)$ is an entire function of E can be exploited to acquire an insightful knowledge from Eq. (4.13).

The functions $y_k(z;E)$ and $y_{k+1}(z;E)$ are subdominant in their own Stokes wedges S_k and S_{k+1}, respectively. But, they might not be subdominant in the Stokes wedge S_{k-1} . As a matter of fact, $y_k(z;E)$ cannot be subdominant in S_{k-1} at all, as explained before. Equation 4.13 assures that the expression $C_k(E)y_k(z,E) + y_{k+1}(z,E)$ is free of any exponentially growing part in S_{k-1} because the function $y_{k-1}(z;E)$ in the right side of the equation is a subdominant solution in S_{k-1}. Therefore, the function $y_{k+1}(z;E)$ posses a dominant part in S_{k-1} so that it compensates the dominant part of $C_k(E)y_k(z;E)$ for a nonvanishing Stokes multiplier. One can then infer that the function $y_{k+1}(z;E)$ does not have any exponentially growing term in S_{k-1} when $C_k(E) = 0$. Now we arrive at an important point relating the asymptotic analysis of the Schrödinger equation in the complex plane as $z \to \infty$ to the vanishing boundary condition on the real axis.

4.2.5 Zeros of the Stokes multipliers as eigenvalues

As pointed out before, the Stokes multipliers are entire functions of E. Therefore, they have discrete sets of zeros. This leads us to a remarkable conclusion that there exists a function $y_{k+1}(z;E)$ vanishing exponentially in both S_{k-1} and S_{k+1} for a discrete set of values of E, which happen to be the zeros of $C_k(E)$. This is especially important if one wishes to impose the boundary condition $y(x;E) \to 0$ as $x \to \pm\infty$. If the boundaries of the problem at $x \to \pm\infty$ are located in S_{k-1} and S_{k+1}, this set of solutions and the corresponding values of E can be identified with the eigenfunctions and eigenvalues of the Schrödinger equation.

As an example we study the parabolic cylinder equation in the complex plane $y'' + (\nu + \frac{1}{2} - z^2)y = 0$. This problem has four Stokes wedges defined in Eq. (4.11) for $m = 1$. The parabolic cylinder function $D_\nu(x)$ vanishes as $x \to +\infty$, so it can be identified with $y_0(z, \nu + \frac{1}{2})$, which is the subdominant solution in S_0. Hence, the leading asymptotic behavior of $D_\nu(z)$ is

$$D_\nu(z) \sim z^\nu e^{-z^2/4} , \quad z \to \infty; |\arg z| < \pi/4 . \tag{4.14}$$

This asymptotic behavior is valid even in a wider wedge with $|\arg z| < 3\pi/4$. But, in general, it breaks down at the Stokes lines $|\arg z| = 3\pi/4$, unless the corresponding Stokes multiplier vanishes, which happens when ν assumes special values. For the parabolic cylinder equation, Eq. (4.12) reads[3]

$$D_\nu(z) = \frac{\sqrt{2\pi}}{\Gamma(-\nu)} e^{i(\nu+1)\pi/2} D_{-\nu-1}(-iz) + e^{i\nu\pi} D_\nu(-z) . \tag{4.15}$$

It is immediately evident that the Stokes multiplier vanishes when $\nu \in \mathbb{N}$, which are the eigenvalues of the problem.

In short, this part draws a connection between eigenvalues of the Schrödinger equation and the Stokes multipliers associated with it. The zeros of the Stokes multipliers are nothing but the eigenvalues of the Schrödinger equation with vanishing boundary values at two Stokes wedges that are not adjacent.[4] These eigenvalues are discrete because they are zeros of a nonconstant

[3] Note that $D_\nu(z)$, $D_{-\nu}(z)$, and $D_{-\nu-1}(-iz)$ obey the parabolic cylinder equation $y'' + (\nu + \frac{1}{2} - z^2)y = 0$, and each of which is subdominant in a different Stokes wedges. See [155] for more discussion.

[4] The main point in the above discussion (and the example of the parabolic cylinder equation) is to show how a local analysis about infinity in the complex plane can be related to an eigenvalue problem defined on a line, *i.e.*, the real axis from physical point of view. We do not wish to consider the general case when there are many Stokes wedges in the complex plane so that $x \to \pm\infty$ cannot be located in S_{k-1} and S_{k+1}. In this case, one may be able to expand the program to find a set of solutions which vanish at the Stokes wedges corresponding to $x = \pm\infty$. Besides, in this discussion, a specific class of potentials is considered, and the reality of the eigenvalues is not discussed. For further discussion, especially about the Schrödinger equation with $\mathcal{PT}$-symmetric Hamiltonians, one can discuss [157–160].

entire function [158]. The eigenvalue solutions are inherently unstable in the sense that an infinitesimal change in the parameter E in Eq. (4.8) from an eigenvalue leads to an exponentially growing term at least in one direction as x approaches infinity on the real axis.

4.2.6 WKB approximation

WKB theory provides a global approximation to the solution of a linear differential equation whose highest derivative is multiplied by a small parameter [155]. In the case of the Schrödinger equation this small parameter is $\hbar^2$. Following Ref. [161], we introduce and use a large number $\eta = 1/\hbar$ instead of $\hbar$. Then the Schrödinger equation reads

$$\Big(-\frac{d^2}{dx^2} + \eta^2 Q(x)\Big)\psi(x;\eta) = 0, \quad Q(x) = V(x) - E \; . \tag{4.16}$$

We first investigate the problem without imposing any boundary conditions at infinity.

The starting point in the WKB approximation is to assume that a solution of Eq. (4.16) can be written in the form $e^{R(x;\eta)}$. Then, $S(x;\eta) \equiv \frac{1}{\eta}\frac{dR}{dx}$ satisfies

$$-\big(\eta^2 S^2 + \eta\frac{dS}{dx}\big) + \eta^2 Q = 0 \; . \tag{4.17}$$

Now, we assume that $S(x;\eta)$ can be expanded in powers of η^{-1} as

$$\begin{aligned} S(x;\eta) &= S_{\rm o}(x;\eta) + S_{\rm e}(x;\eta) \; , & (4.18)\\ S_{\rm e}(x;\eta) &= S_0(x) + S_2(x)\eta^{-2} + S_4(x)\eta^{-4} + \cdots \; , & (4.19)\\ S_{\rm o}(x;\eta) &= S_1(x)\eta^{-1} + S_3(x)\eta^{-3} + S_3(x)\eta^{-5} + \cdots \; . & (4.20) \end{aligned}$$

Consequently,

$$\eta^2\big(S_{\rm e} + S_{\rm o}\big)^2 + \eta\frac{d}{dx}\big(S_{\rm e} + S_{\rm o}\big) = \eta^2 Q \; . \tag{4.21}$$

Separating the odd and even powers of η^{-1}, for the odd powers we find

$$\begin{aligned} 2\eta^2 S_{\rm e}S_{\rm o} + \eta\frac{d}{dx}S_{\rm e} &= 0 \\ \Rightarrow \quad S_{\rm o} = -\frac{\frac{d}{dx}S_{\rm e}}{2\eta S_{\rm e}} &= -\frac{1}{2\eta}\frac{d}{dx}\log S_{\rm e} \; , \end{aligned} \tag{4.22}$$

and for the even powers, we obtain

$$\begin{aligned} \eta^2 S_{\rm e}^2 + \eta^2 S_{\rm o}^2 + \eta \frac{d}{dx} S_{\rm o} &= \eta^2 Q \\ \Rightarrow \quad \sqrt{S_{\rm e}} \frac{d^2}{dx^2} \Big(\frac{1}{\sqrt{S_{\rm e}}} \Big) &= \eta^2 (Q - S_{\rm e}^2) \; . \end{aligned} \tag{4.23}$$

Noticing that $-S_{\rm e}$ also obeys Eq. (4.23), the two independent solutions of the second order differential equation in Eq. (4.16) can be constructed by following formal expressions

$$\psi_{\pm}(x;\eta) = c_{\pm} \frac{1}{\sqrt{S_{\rm e}(x;\eta)}} \exp\Big(\pm \eta \int_{x_0}^{x} S_e(t;\eta) dt \Big) \; . \tag{4.24}$$

Substituting Eq. (4.19) in Eq. (4.23), we obtain

$$S_{\rm e}(x;\eta) = \sqrt{Q(x)} + \mathcal{O}(\eta^{-2}) \; . \tag{4.25}$$

Therefore, the solutions have the following leading order behavior

$$\psi_{\pm}(x;\eta) \sim c_{\pm} \frac{\exp\Big(\pm \eta \int_{x_0}^{x} \sqrt{Q(t)} dt \Big)}{[Q(x)]^{1/4}} \quad \text{as } \eta \to \infty \; , \tag{4.26}$$

where $Q(x) \neq 0$. Here are some remarks about this relation:

- Equation 4.26 is an asymptotic relation because the WKB expansion is a divergent expansion.
- Comparing Eq. (4.9) with Eq. (4.26), one can recognize that they have similar forms. The former equation is an asymptotic relation as $x \to \infty$ (*i.e.*, $Q(x) \to \infty$ for a polynomial potential), while the latter one is an asymptotic relation as $\eta \to \infty$. The former one is developed for a local analysis about $x = \infty$, but the latter one provides a global approximation, unless $Q(x) \to 0$.
- Eq. (4.26) is not valid in the vicinity of *turning points*, where $Q(x) = 0$. In a neighborhood of a simple turning point x_0, *i.e.*, a first-order zero of $Q(x)$, one can analyze the problem by replacing $Q(x)$ with $(x - x_0)$ times a constant; the Schrödinger equation reduces to the Airy equation.
- The turning points occur when $V(x) = E$. From physical point of view, the simple turning points are the borders of classically allowed regions ($V(x) < E$, *i.e.*, $Q(x) < 0$) and classically forbidden regions ($V(x) > E$ *i.e.*, $Q(x) > 0$)). In the classically allowed region,

the WKB analysis provides the leading order asymptotic behavior

$$\psi(x;\eta) \sim C\frac{\sin\Big(\eta\int_{x_0}^{x}\sqrt{-Q(t)}dt+\phi\Big)}{[-Q(x)]^{1/4}} \text{ as } \eta\to\infty\,, \tag{4.27}$$

while in the classically forbidden regions the leading order behavior is described by growing and/or decaying exponential terms as $\eta\to\infty$.

- In order to relate the solutions in classically allowed and forbidden regions, one should match them at the corresponding turning point via the Airy functions.

Now, we impose the boundary value condition that $\psi(x;\eta)\to 0$ as $x\to\pm\infty$. Let us consider the case that the potential $V(x)$ rises monotonically as $x\to\pm\infty$, and there are only two simple real turning points $x=A$ and $x=B$ with $A<B$. One can divide the real axis into five regions: two classically forbidden regions, one classically allowed region, and two regions in vicinity of the turning points. At each region, $\psi(x;\eta)$ has a form suggested by WKB theory, or the Airy equation. The process of matching these solutions leads to an approximate constraint that must be satisfied by $Q(x)$:

$$\eta\int_{A}^{B}\sqrt{E-V(t)}dt\sim(n+\tfrac{1}{2})\pi \quad \text{as } \eta\to\infty\,, \tag{4.28}$$

where $n\in\mathbb{N}$ [155]. This puts a restriction on the parameter E, otherwise the vanishing boundary values cannot be satisfied. As pointed out earlier, in the discussion of zeros of Stokes multipliers, the eigenvalue solutions are inherently unstable in the sense that an infinitesimal change in the parameter E in from an eigenvalue leads to an exponentially growing term at least in one direction as x approaches to infinity on the real axis.

4.3 Eigenvalue problems in nonlinear differential equations

4.3.1 Spontaneous singularities

A solution of a linear differential equation can only be singular at singular points of the problem, which depend only on the coefficient functions of the differential equation. Hence, its singularities occur only at fixed points independent of the initial and boundary conditions. These singularities are called *fixed* singularities. In contrast, solutions of nonlinear equations, in addition to having fixed singularities, may also exhibit new kinds of singularities which move around in the complex plane as the initial or boundary conditions vary [155]. These singularities are called *spontaneous* or *movable* singularities.

As an example, one can consider the Riccati equation $y' = y^2 + x$ with the initial condition $y(0) = a$. In a neighborhood of $x = b$, this equation may have a solution as

$$y(x) = \frac{1}{x-b} + \sum_{n=0}^{\infty} a_n (x-b)^n. \tag{4.29}$$

This is a singular solution at $x = b$, which moves as the initial condition varies. For this problem the only movable singularities are simple poles.

Similar to the solutions of $y' = y^2 + x$, the six Painlevé transcendents have movable singularities that are only ordinary poles (and not *critical* points, *i.e.*, branch points or essential singularities). The Painlevé transcendents are the solutions of the following six nonlinear second-order differential equations

$$\text{P-I}: \quad y'' = 6y^2 + x\ , \tag{4.30}$$

$$\text{P-II}: \quad y'' = 2y^3 + xy + \alpha\ , \tag{4.31}$$

$$\text{P-III}: \quad xyy'' = x\Big(y'\Big)^2 - yy' + \delta x + \beta y + \alpha y^3 + \gamma x y^4\ , \tag{4.32}$$

$$\text{P-IV}: \quad yy'' = \frac{1}{2}\Big(y'\Big)^2 + \beta + 2(x^2-\alpha)y^2 + 4xy^3 + \frac{3}{2}y^4\ , \tag{4.33}$$

$$\text{P-V}: \quad y'' = \Big(\frac{1}{2y} + \frac{1}{y-1}\Big)\Big(y'\Big)^2 - \frac{1}{x}y' + \frac{(y-1)^2}{x^2}\Big(\alpha y + \frac{\beta}{y}\Big) + \gamma\frac{y}{x} + \delta\frac{y(y+1)}{y-1}\ , \tag{4.34}$$

$$\text{P-VI}: \quad y'' = \frac{1}{2}\Big(\frac{1}{y} + \frac{1}{y-1} + \frac{1}{y-x}\Big)\Big(y'\Big)^2 - \Big(\frac{1}{x} + \frac{1}{x-1} + \frac{1}{y-x}\Big)y' + \frac{y(y-1)(y-x)}{x^2(x-1)^2}\Big(\alpha + \beta\frac{x}{y^2} + \gamma\frac{x-1}{(y-1)^2} + \delta\frac{x(x-1)}{(y-x)^2}\Big)\ . \tag{4.35}$$

Here α, β, γ and δ are complex numbers. These six differential equations do not have solutions in terms of known functions or transcendents.

4.3.2 Separatrix structure

There are many nonlinear differential equations having separatrix structure. One example is the differential equation for the first Painlevé transcendent $y'' = 6y^2 + x$. Considering only the real solutions of this equation on the real axis, one can study the asymptotic behavior of the solutions as x approaches to infinity, especially as $x \to -\infty$. It is clear that when x becomes large and negative, there can be a dominant asymptotic balance between the positive term $[y(x)]^2$ and the

negative term x, which implies that $y(x)$ can have two possible leading asymptotic behaviors:

$$y(x) \sim \pm\sqrt{-x/6} \quad (x \to -\infty), \tag{4.36}$$

which is valid because the second derivative of $\sqrt{-x/6}$ is small compared with x as $x \to -\infty$.

This problem is interesting because the asymptotic behavior $y(x) \sim -\sqrt{-x/6}$ is stable but the asymptotic behavior $y(x) \sim \sqrt{-x/6}$ is unstable. To verify this, we calculate the corrections to these two asymptotic behaviors. When x is large and negative, the solution to Eq. (4.30) oscillates about and decays slowly towards the curve $-\sqrt{-x/6}$:

$$y(x) \sim -\sqrt{-\frac{x}{6}} + \frac{-1}{48x^2} + \cdots + c\frac{1}{(-x)^{1/8}} \cos\left[\tfrac{8}{5}\sqrt[4]{\tfrac{3}{2}}(-x)^{5/4} + d\right] \quad (x \to -\infty), \tag{4.37}$$

where c and d are two arbitrary constants. The differential equation (4.30) is second order and, as expected, this asymptotic behavior contains two arbitrary constants. On the other hand, the correction to the $+\sqrt{-x/6}$ behavior has an exponential form

$$y(x) \sim \sqrt{-\frac{x}{6}} + \frac{-1}{48x^2} + \cdots + c_{\pm}\frac{1}{(-x)^{1/8}} \exp\left[\pm\tfrac{8}{5}\sqrt[4]{\tfrac{3}{2}}(-x)^{5/4}\right] \quad (x \to -\infty). \tag{4.38}$$

Thus, if $c_+ \neq 0$, nearby solutions veer away from the curve $\sqrt{-x/6}$ as $x \to -\infty$. The special solutions that decay exponentially towards $\sqrt{-x/6}$ form a one-parameter class because $c_+ = 0$. Therefore, there is a one-parameter class of initial conditions corresponding to $c_+ = 0$. One can fix the initial condition $y(0)$, then there is a discrete set of critical initial slope $y'(0)$ such that their corresponding solutions approach to $\sqrt{-x/6}$ as $x \to -\infty$.

The differential equation for the second Painlevé transcendent has similar behavior. Putting the constant α to zero for simplicity, one can write this equation as $y'' = 2y^3 + xy = (2y^2 + x)y$. An elementary asymptotic analysis shows that as $t \to -\infty$, there are three possible asymptotic behaviors for solutions $y(x)$. First, $y(x)$ can oscillate stably about the negative axis. Second, $y(x)$ can approach the curves $\pm\sqrt{-t/2}$; however, both of these asymptotic behaviors are unstable similar to the case of the first Painlevé transcendent. The equation $y'' = 2y^3 + xy$ is particularly interesting because as $t \to +\infty$, the behavior $y \to 0$ becomes unstable. Thus, it is possible to have new kinds of eigenfunctions for positive x as well. A procedure described for the first Painlevé can be used to define the eigenfunctions of the the second Painlevé, which exponentially decay to their corresponding limit curves.

The separatrix behavior is not unique for the Painlevé transcendents. As pointed out before, the first-order differential equation $y'(x) = \cos(\pi xy)$ possesses such a behavior. This equation is

a first-order nonlinear differential equation. The detailed analysis of this equation is presented in chapter 5. Then, in 6, the first and second Painlevé transcendents are discussed.

5

Nonlinear Eigenvalue Problems: A Toy Model

This chapter contains the materials published in a paper.[1] *This represents work performed by me under the overall supervision of my advisor, C. M. Bender.*

5.1 Introduction

This chapter presents a detailed asymptotic analysis of the nonlinear initial-value problem

$$y'(x) = \cos[\pi x y(x)], \quad y(0) = a. \tag{5.1}$$

This remarkable and deceptively simple looking differential equation was given as an exercise in the text by Bender and Orszag [155]. Since then, it and closely related differential equations have arisen in a number of physical contexts involving the complex extension of quantum-mechanical probability [162, 163] and the structure of gravitational inspirals [164]. The properties of solutions to this equation are strongly analogous to those of the time-independent Schrödinger eigenvalue problem.

The (linear) Schrödinger eigenvalue problem has the form

$$-\psi''(x) + V(x)\psi(x) = E\psi(x), \qquad \psi(\pm\infty) = 0, \tag{5.2}$$

where E is the eigenvalue. For simplicity, we assume that the potential $V(x)$ has one local minimum and rises monotonically to ∞ as $x \to \pm\infty$. This eigenvalue problem is not analytically

[1] C.M. Bender, A. Fring, J. Komijani, "Nonlinear Eigenvalue Problems," J. Phys. A: Math. and Theor. 47, 235204 (2014) [arXiv:1401.6161].

solvable except for special potentials, such as the harmonic oscillator potential $V(x) = x^2$. However, it is possible to find the large-n asymptotic behavior of the nth eigenvalue E_n by using semiclassical (WKB) analysis. To leading order the large-n behavior of the eigenvalues of the two-turning-point problem may be obtained from the Bohr-Sommerfeld condition

$$\int_{x_1}^{x_2} dx \sqrt{E_n - V(x)} \sim (n + 1/2)\pi \quad (n \to \infty), \tag{5.3}$$

where the turning points x_1 and x_2 are real roots of the equation $V(x) = E_n$. This WKB condition determines the eigenvalues implicitly for large n. As an example, for the anharmonic potential $V(x) = x^4$ the large-n asymptotic behavior of the eigenvalues is [165]

$$E_n \sim B n^{4/3} \quad (n \to \infty), \tag{5.4}$$

where the constant B is given by $B = 3\Gamma(3/4)\sqrt{\pi}/\Gamma(1/4)$.

The quantum eigenfunctions $\psi(x)$ exhibit several characteristic features. In the classically allowed region between the turning points ($x_1 < x < x_2$), the eigenfunctions are oscillatory and the eigenfunction corresponding to E_n has n nodes. In the classically-forbidden regions $x > x_2$ and $x < x_1$ the eigenfunctions decay exponentially and monotonically to zero as $|x| \to \infty$. Thus, at the turning points the behavior of the eigenfunctions changes abruptly from rapid oscillation to smooth exponential decay.

The solutions $y(x)$ to the nonlinear differential equation (5.1) have many features in common with the solutions $\psi(x)$ to the Schrödinger equation (5.2). For any choice of $y(0) = a$ the initial slope $y'(0)$ is 1. As x increases from 0, $y(x)$ oscillates as shown in Fig. 5.1. This regime of oscillation is analogous to a classically allowed region in quantum mechanics. Note that the number of maxima of the function $y(x)$ in the oscillatory region increases as $y(0)$ increases. With increasing x the oscillations abruptly cease and the function $y(x)$ then decays smoothly and monotonically to 0 as $x \to \infty$. This behavior resembles that of $\psi(x)$ in a classically forbidden region.

Figure 5.1 reveals that in the decaying regime the curves merge into quantized bundles. This large-x asymptotic behavior of $y(x)$ can be explained by using elementary asymptotic analysis. If we seek an asymptotic behavior of the form $y(x) \sim c/x$ ($x \to \infty$) and substitute this *ansatz* into (5.1), we find that $c = m + 1/2$ ($m = 0, 1, 2, 3, \ldots$). This is just the *leading* term in the asymptotic expansion of $y(x)$ for large x. The full series has the form

$$y(x) \sim \frac{m + 1/2}{x} + \sum_{k=1}^{\infty} \frac{c_k}{x^{2k+1}} \quad (x \to \infty). \tag{5.5}$$

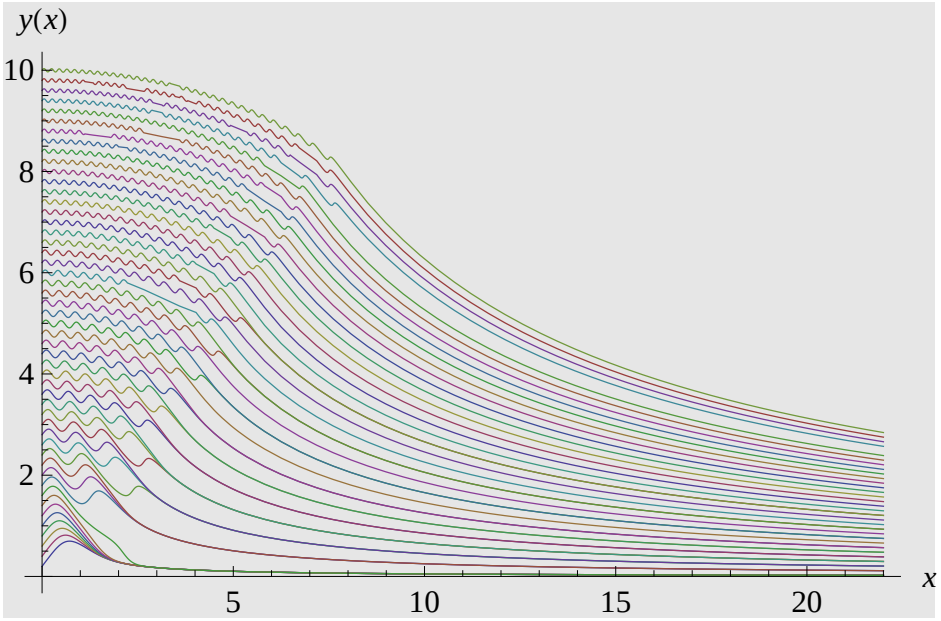

FIGURE 5.1: Numerical solutions $y(x)$ to (5.1) for $0 \leq x \leq 24$ with initial conditions $y(0) = 0.2k$ for $k = 1, 2, 3, \ldots, 50$. The solutions initially oscillate but abruptly become smoothly and monotonically decaying. In the decaying regime the solutions merge into discrete quantized bundles.

The first few coefficients are

$$\begin{aligned}
c_1 &= \frac{(-1)^m}{\pi}(m+1/2), \\
c_2 &= \frac{3}{\pi^2}(m+1/2), \\
c_3 &= (-1)^m\left[\frac{(m+1/2)^3}{6\pi} + \frac{15(m+1/2)}{\pi^3}\right], \\
c_4 &= \frac{8(m+1/2)^3}{3\pi^2} + \frac{105(m+1/2)}{\pi^4}, \\
c_5 &= (-1)^m\left[\frac{3(m+1/2)^5}{40\pi} + \frac{36(m+1/2)^3}{\pi^3} + \frac{945(m+1/2)}{\pi^5}\right], \\
c_6 &= \frac{38(m+1/2)^5}{15\pi^2} + \frac{498(m+1/2)^3}{\pi^4} + \frac{10395(m+1/2)}{\pi^6}.
\end{aligned} \tag{5.6}$$

5.1.1 Hyperasymptotic analysis

A close look at Fig. 5.1 shows a surprising result: Half of the predicted large-x asymptotic behaviors in (5.5) appear to be missing. The bundles of curves shown in Fig. 5.1 correspond only to *even* values of m. To explain what has happened to the odd-m bundles, we perform a hyperasymptotic analysis (asymptotics beyond all orders) [166]. Let $y_1(x)$ and $y_2(x)$ represent

two different curves in the mth bundle. Even though they are different curves they have exactly the same asymptotic approximation as given in (5.5). Then $Y(x) \equiv y_1(x) - y_2(x)$ satisfies the differential equation

$$\begin{aligned} Y'(x) &= \cos[\pi x y_1(x)] - \cos[\pi x y_2(x)] \\ &= -2\sin\left[\tfrac{1}{2}\pi x y_1(x) + \tfrac{1}{2}\pi x y_2(x)\right] \sin\left[\tfrac{1}{2}\pi x y_1(x) - \tfrac{1}{2}\pi x y_2(x)\right] \\ &\sim -2\sin\left[\pi\left(m+\tfrac{1}{2}\right)\right] \sin\left[\tfrac{1}{2}\pi x Y(x)\right] \quad (x\to\infty) \\ &\sim -(-1)^m \pi x Y(x) \quad (x\to\infty). \end{aligned} \tag{5.7}$$

We conclude that

$$Y(x) \sim K \exp\left[\tfrac{1}{2}(-1)^{m+1}\pi x^2\right] \quad (x\to\infty), \tag{5.8}$$

where K is an arbitrary constant. Thus, while two different curves in the same bundle have the same asymptotic expansion for large x, they differ by an exponentially small amount. This result explains why no arbitrary constant appears in the asymptotic expansion (5.5); the arbitrary constant appears in the beyond-all-orders hyperasymptotic (exponentially small) correction to this asymptotic series.

More importantly, this argument demonstrates that two curves can only be in the same bundle if m is *even*. If m is odd, the two curves *move away from one another* as x increases. Thus, while there is a bundle of infinitely many curves when m is even, we see that there is a unique and *discrete* curve, called a *separatrix*, when m is odd. The nth separatrix, whose large-x asymptotic behavior is $(2n-1/2)/x$ ($n = 1, 2, 3, \ldots$), is *unstable* for increasing x; that is, as x increases, nearby curves $y(x)$ veer away from it and become part of the bundles above or below the separatrix. This explains why there are no curves shown in Fig. 5.1 when m is odd. Ten separatrix curves are shown in Fig. 5.2.

While the separatrix curves are unstable for increasing x, they are stable for decreasing x and thus it is numerically easy to trace these curves backward from large values of x down to $x = 0$. We treat the discrete point a_n ($n = 1, 2, 3, \ldots$) at which the nth separatrix crosses the y axis as an eigenvalue. The curves $y(x)$, whose initial values $y(0) = a$ lie in the range $a_{n-1} < y(0) < a_n$, have n maxima. Our objective in this chapter is to determine analytically the large-n asymptotic behavior of the eigenvalues. We will establish that

$$a_n \sim A\sqrt{n} \quad (n\to\infty), \tag{5.9}$$

where $A = 2^{5/6}$. The constant A is a nonlinear analog of the WKB constant B in (5.4).

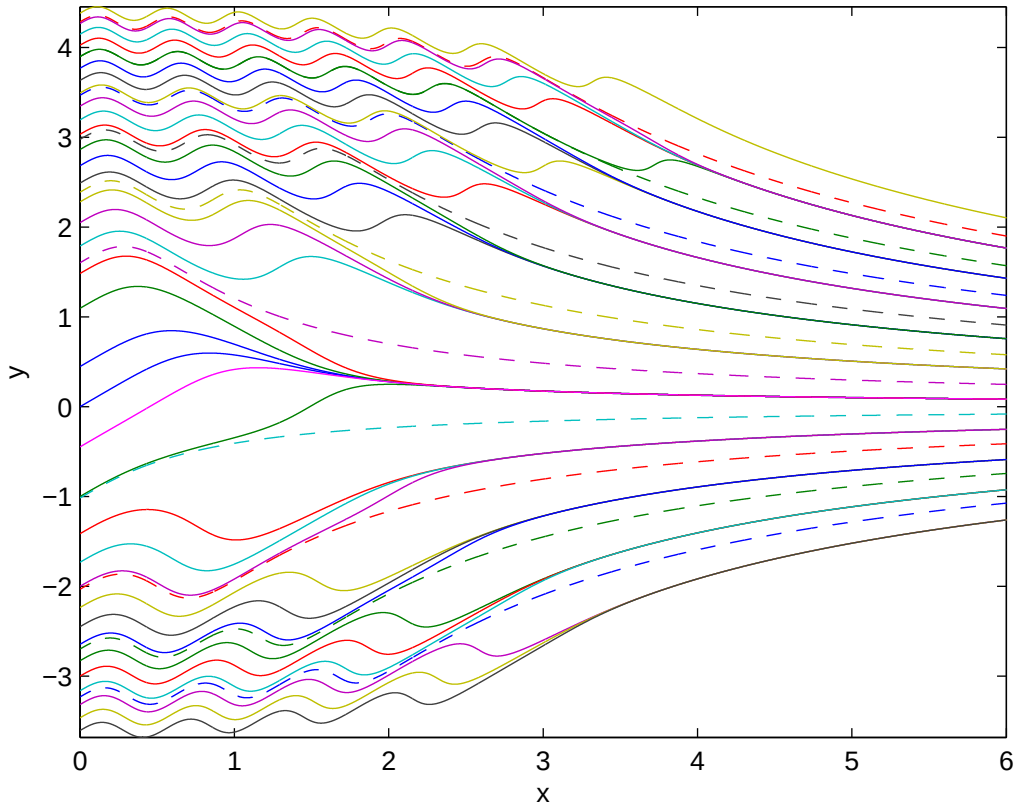

FIGURE 5.2: Numerical solutions to (5.1) showing ten separatrix curves, which cross the y axis at $a_{-3} = -3.231360$, $a_{-2} = -2.698369$, $a_{-1} = -2.032651$, $a_0 = -1.016702$, $a_1 = 1.602573$, $a_2 = 2.388358$, $a_3 = 2.976682$, $a_4 = 3.467542$, $a_5 = 3.897484$, and $a_6 = 4.284674$.

Hyperasymptotics also plays a crucial role in quantum theory. Because the Schrödinger eigenvalue problem (5.2) is second order, the asymptotic behavior of $\psi(x)$ as $x \to \infty$ contains two arbitrary constants. However, there is only *one* constant C in the WKB asymptotic approximation

$$\psi(x) \sim C[V(x) - E]^{-1/4} \exp\left[\int^x ds \sqrt{V(s) - E}\right] \quad (x \to \infty). \tag{5.10}$$

There is a second constant D, of course, but this constant multiplies the subdominant (exponentially decaying) solution, and thus this constant does not appear to any order in the WKB expansion. The constant D remains invisible except at an eigenvalue because only at an eigenvalue does the coefficient C of the exponentially growing solution (5.10) vanish *to all orders* in the large-x asymptotic expansion, leaving the physically acceptable exponentially decaying solution

$$\psi(x) \sim D[V(x) - E]^{-1/4} \exp\left[-\int^x ds \sqrt{V(s) - E}\right] \quad (x \to \infty). \tag{5.11}$$

5.1.2 Organization of this chapter

The principal thrust of the analysis in this chapter is an asymptotic study of the separatrices, which for large x are approximated by the formula in (5.5) with m odd. Thus, we let $m = 2n-1$ and we scale both the independent and dependent variables in (5.1):

$$x = \sqrt{2n - 1/2}\, t, \quad y(x) = \sqrt{2n - 1/2}\, z(t), \tag{5.12}$$

and let

$$\lambda = (2n - 1/2)\pi. \tag{5.13}$$

The resulting equation for $z(t)$ is

$$z'(t) = \cos[\lambda t z(t)]. \tag{5.14}$$

With these changes of variable, the nth separatrix [which behaves like $(2n - 1/2)/x$ as $x \to \infty$] now behaves like $1/t$ as $t \to \infty$. Also, for large λ the turning point (the point at which the oscillations cease and monotone decreasing behavior begins) is located at $t = 1$.

In Sec. 5.2 we begin by examining the differential equation (5.1) numerically. We then show numerically that for large λ the solution $z(t)$ to the scaled equation (5.14) that satisfies the initial condition $z(0) = 2^{1/3}$ is oscillatory until $t = 1$, at which point it decays smoothly like $z(t) \sim 1/t$ as $t \to \infty$. We also show that the amplitude of the oscillations is of order $1/\lambda$ for large λ. Hence, in the limit $\lambda \to \infty$ the function $z(t)$ converges to a smooth and nonoscillatory function $Z(t)$ that passes through $2^{1/3}$ at $t = 0$ and through 1 at $t = 1$. Thus, the nth eigenvalue is asymptotic to $A\sqrt{n}$ as $n \to \infty$, where $A = 2^{5/6}$. In Sec. 5.3 we perform an asymptotic calculation of $Z(t)$ correct to order $1/\lambda$ and use this result to obtain the number A in (5.9). In Sec. 5.4 we suggest that the techniques presented in this chapter may apply to many other nonlinear differential equations. As evidence, we present numerical results regarding the first Painlevé transcendent. We also conjecture that the number A in (5.9) may be related to the power-series constant P, which describes the asymptotic behavior of the zeros of partial sums of Taylor series of analytic functions.

5.2 Numerical study of (5.1) and (5.14)

We begin our analysis of (5.1) by constructing the Taylor series expansion

$$y(x) = \sum_{n=0}^{\infty} b_n x^n \tag{5.15}$$

of the solution $y(x)$. To find the Taylor coefficients b_n we substitute this expansion into the differential equation and collect powers of x. The first few Taylor coefficients are

$$\begin{aligned}
b_0 &= y(0) = a, \\
b_1 &= 1, \\
b_2 &= 0, \\
b_3 &= -\tfrac{1}{6}\pi^2 a^2, \\
b_4 &= -\tfrac{1}{4}\pi^2 a, \\
b_5 &= \tfrac{1}{120}\pi^4 a^4 - \tfrac{1}{10}\pi^2, \\
b_6 &= \tfrac{1}{18}\pi^4 a^3, \\
b_7 &= -\tfrac{1}{5040}\pi^6 a^6 + \tfrac{2}{21}\pi^4 a^2, \\
b_8 &= -\tfrac{1}{180}\pi^6 a^5 + \tfrac{31}{480}\pi^4 a, \\
b_9 &= \tfrac{1}{362880}\pi^8 a^8 - \tfrac{161}{6480}\pi^6 a^4 + \tfrac{17}{1080}\pi^4.
\end{aligned} \tag{5.16}$$

We then observe that we can reorganize and regroup the terms in the Taylor series. For example, the first terms in b_1, b_3, b_5, b_7, b_9, and so on, give rise to the function

$$\frac{1}{\pi a}\sin s$$

and the first terms in b_4, b_6, b_8, b_{10}, and so on, give rise to

$$\frac{1}{8\pi^2 a^3}\left[2s\sin(2s) + \cos(2s) - 2s^2 - 1\right],$$

where $s = \pi a x$. This partial summation of the Taylor series, a procedure used in multiple-scale perturbation theory to eliminate secular behavior [167], shows that the solution $y(x)$ is approximately a falling parabola with an oscillatory contribution whose amplitude is of order $1/a$. This is what we observe in Fig. 5.1. The partial summation suggests that a and y are both of order $\sqrt{n}$ and motivates the changes of variable (5.12) and (5.13), which give the scaled differential equation (5.14).

As λ in (5.14) tends to ∞, the oscillations disappear. (This is demonstrated in Sec. 5.3.) The resulting curve $Z(t)$, which begins at $Z(0) = 2^{1/3}$ and passes through $Z(1) = 1$, is shown as a dashed line (red in the electronic version) in Fig. 5.3 (upper panel). Also shown are the first four eigencurve (separatrix) solutions to (5.14) (blue, cyan, magenta, and green in the electronic version), which have one, two, three, and four maxima. Note that these eigensolutions rapidly approach the limiting dashed curve as the number of oscillations increases. The lower panel in

Fig. 5.3 indicates the difference between the dashed curve and the solid curves plotted in the upper panel.

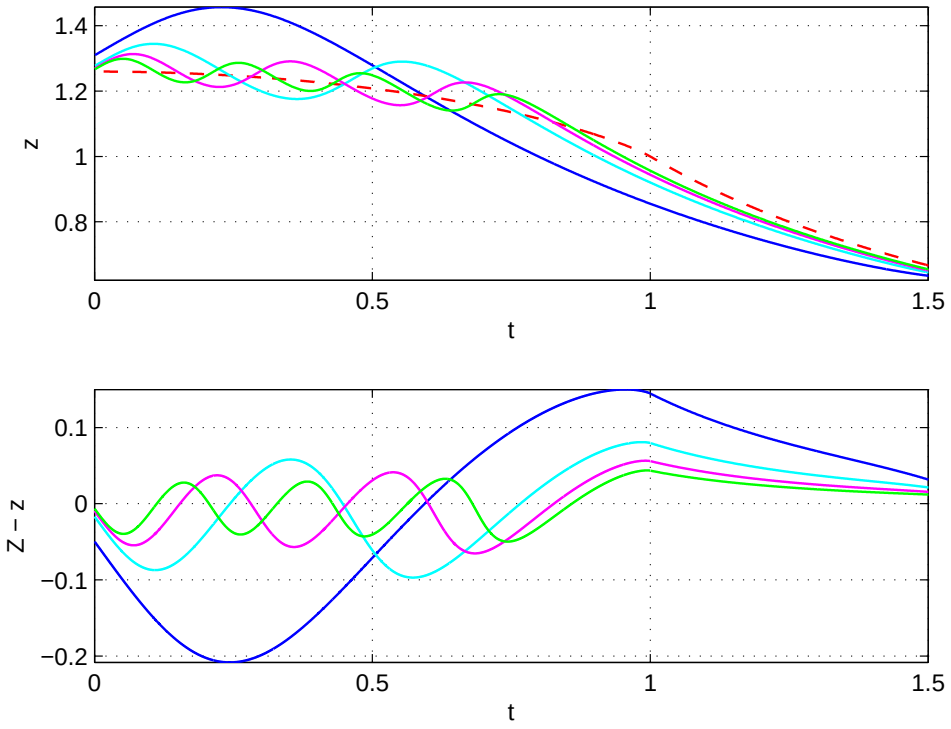

FIGURE 5.3: Upper panel: Numerical plots of the first four separatrix solutions $z(t)$ (eigensolutions) to (5.14) (blue, cyan, magenta, and green in the electronic version). These solutions have one, two, three, and four maxima. As λ increases, these curves approach the solution to (5.14) for $\lambda = \infty$ (dashed curve) (red in the electronic version). [The $\lambda = \infty$ curve is called $Z(t)$ and satisfies the differential equation (5.31).] Lower panel: A plot of the differences between the solid curves and the dashed curve.

For large values of λ the convergence to the limiting curve $Z(t)$ is dramatic. In Fig. 5.4 we plot $Z(t)$ in the upper panel and the difference between $Z(t)$ and the $n = 500,000$ separatrix curve (eigencurve) in the lower panel. Note that the difference is of order $1/n$ (10^{-6}). On the basis of these numerical calculations we used Richardson extrapolation [168] to calculate the coefficient A to an accuracy of one part in 10^{10} and we conjectured reliably that $A = 2^{5/6}$.

The convergence of $z(t)$ (which is rapidly oscillatory when $0 \leq t \leq 1$) to $Z(t)$ (which is smooth and nonoscillatory) as $\lambda \to \infty$ strongly resembles the convergence of a Fourier series. Consider, for example, the convergence of the Fourier sine series to the function $f(x) = 1$ on the interval $0 < x < \pi$. The $2N + 1$ partial sum of the Fourier sine series is

$$S_{2N+1}(x) = \frac{4}{\pi} \sum_{n=0}^{N} \frac{\sin[(2n+1)x]}{2n+1}. \tag{5.17}$$

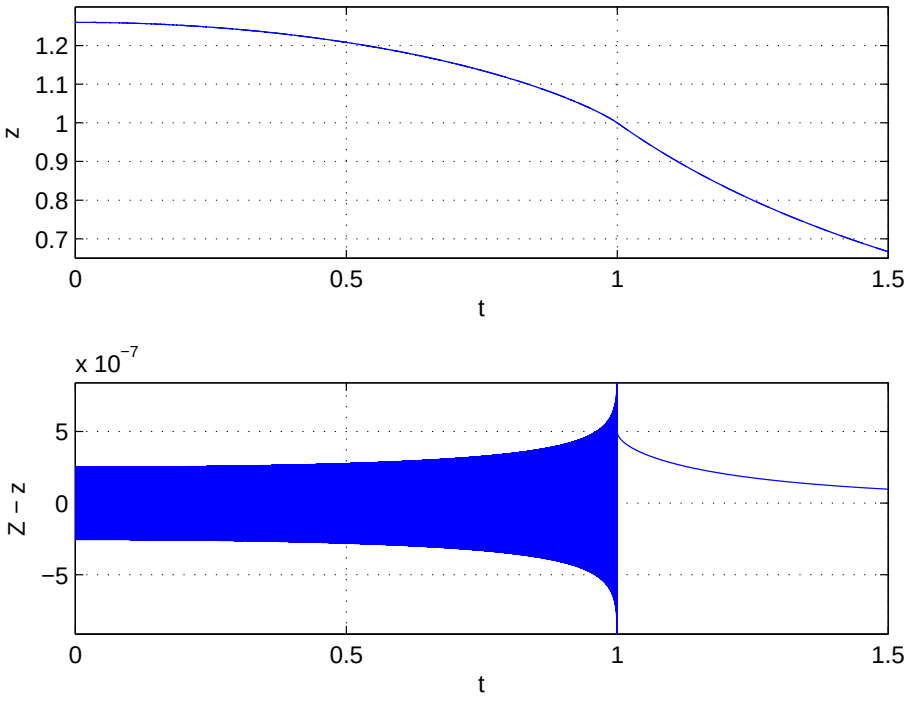

FIGURE 5.4: Upper panel: Numerical solution $z(t)$ to (5.14) corresponding to $n = 500,000$. No oscillation is visible because the amplitude of oscillation is of order $1/\lambda$ when λ is large. Lower panel: Difference between the $n = 500,000$ eigencurve $z(t)$ and the $\lambda = \infty$ curve $Z(t)$. Note that the difference is highly oscillatory and is of order 10^{-6}.

As can be inferred from Fig. 5.5, which displays the partial sums for $N = 5, 20, 80$, as N increases, $S_{2N+1}(x)$ approaches 1 (except for values of x near $x = 0$ and $x = \pi$) in a highly oscillatory fashion that strongly resembles the approach of $z(t)$ to $Z(t)$ in Fig. 5.4.

5.3 Asymptotic solution of the scaled equation (5.14)

The objective of the asymptotic analysis in this section is to solve (5.14) for large λ and to verify the result in (5.9); namely, that $A = 2^{5/6}$. We begin by converting the differential equation in (5.14) to the integral equation

$$[z(t)]^2 - [z(0)]^2 + t^2/2 + \eta(t) = \mathrm{O}(1/\lambda) \quad (\lambda \to \infty), \tag{5.18}$$

where

$$\eta(t) = \int_0^t ds\, s \cos[2\lambda s z(s)]. \tag{5.19}$$

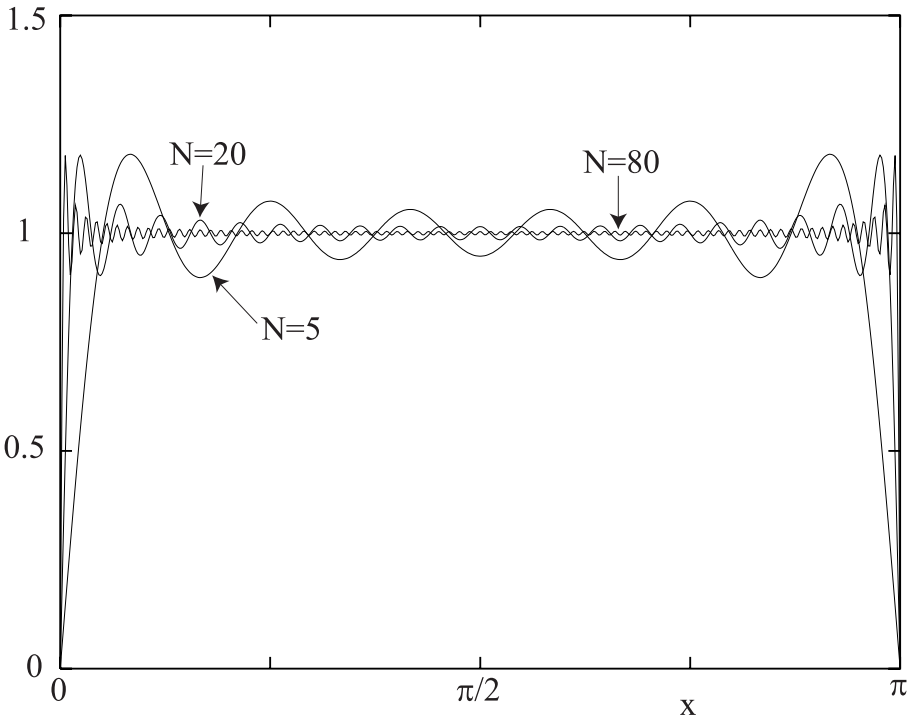

FIGURE 5.5: Convergence of the $N = 5$, 20, and 80 partial sums in (5.17) of the Fourier sine series for $f(x) = 1$. The partial sums of the Fourier series converge to 1 as $N \to \infty$ in much the same way that $z(t)$ converges to $Z(t)$ as $\lambda \to \infty$. Like the behaviors in Figs. 5.3 and 5.4, as N increases, the frequency of oscillation increases and the amplitude of oscillation approaches zero.

To obtain (5.18) we multiply (5.14) by $z(t) + tz'(t)$ and integrate from 0 to t. We then replace the quantity $[z'(t)]^2$ by $\cos^2[\lambda t z(t)]$ and use the double-angle formula for the cosine function to get $\eta(t)$ in (5.19).

The problem is now to calculate $\eta(t)$. To do so, we observe that $\eta(t)$ is just one of an infinite set of moments $A_{n,k}(t)$, which are defined as follows:

$$A_{n,k}(t) \equiv \int_0^t ds \cos[n\lambda s z(s)] \frac{s^{k+1}}{[z(s)]^k}. \tag{5.20}$$

Note that $\eta(t) = A_{2,0}(t)$.

For large λ these moments satisfy the linear difference equation

$$A_{n,k}(t) = -\tfrac{1}{2} A_{n-1,k+1}(t) - \tfrac{1}{2} A_{n+1,k+1}(t) \quad (n \geq 2). \tag{5.21}$$

To obtain this equation we multiply the integrand of the integral in (5.20) by

$$\frac{z(s)+sz'(s)}{z(s)}-\frac{sz'(s)}{z(s)}. \tag{5.22}$$

(Note that this quantity is merely an elaborate way of writing 1.) We then evaluate the first part of the resulting integral by parts and verify that it is negligible as $\lambda\to\infty$ if $t\le 1$. In the second part of the integral we replace $z'(t)$ by $\cos[\lambda t z(t)]$ and use the trigonometric identity

$$\cos(na)\cos(a)=\tfrac{1}{2}\cos[(n+1)a]+\tfrac{1}{2}\cos[(n-1)a].$$

By using repeated integration by parts, we verify that $\eta(t)$ in (5.19) can be expanded as the series

$$\eta(t)=\sum_{p=0}^{\infty}\alpha_{1,2p+1}A_{1,2p+1}(t), \tag{5.23}$$

where the coefficients $\alpha_{n,k}$ are determined by a one-dimensional random-walk process in which random walkers move left or right with equal probability but become static when they reach $n=1$. The initial condition for the random walk is that $\alpha_{n,0}=0$ if $n\ne 2$ and $\alpha_{2,0}=1$. The coefficients $\alpha_{n,k}$ obey the difference equations

$$2\alpha_{1,k}+\alpha_{2,k-1}=0, \tag{5.24}$$

$$2\alpha_{2,k}+\alpha_{3,k-1}=0, \tag{5.25}$$

$$2\alpha_{n,k}+\alpha_{n-1,k-1}+\alpha_{n+1,k-1}=0\quad(n\ge 3). \tag{5.26}$$

(Note that $\alpha_{n,k}=0$ if one of the subscripts is odd and the other is even.) The difference equations (5.25) and (5.26) can be solved in closed form, and we obtain the following exact result for $n\ge 2$:

$$\alpha_{n,k}=\frac{(-1)^n(n-1)k!}{2^k(k/2+n/2)!(k/2-n/2+1)!}, \tag{5.27}$$

which holds if n and k are both even or both odd. Finally, we use equation (5.24) to obtain

$$\alpha_{1,2p+1}=-\tfrac{1}{2}\alpha_{2,2p}=-\frac{(2p)!}{2^{2p+1}p!(p+1)!}=-\frac{\Gamma(p+1/2)}{2\sqrt{\pi}\,(p+1)!}, \tag{5.28}$$

where the duplication formula for the Gamma function was used to obtain the last equality.

Thus, the series in (5.23) for $\eta(t)$ reduces to the series of integrals

$$\eta(t) = -\frac{1}{2\sqrt{\pi}} \sum_{p=0}^{\infty} \frac{\Gamma(p+1/2)}{(p+1)!} \int_0^t ds\, z'(s) \frac{s^{2p+2}}{[z(s)]^{2p+1}},$$

which is valid for $t \leq 1$. This series can be summed in closed form:

$$\eta(t) = \int_0^t ds\, z(s)z'(s)\sqrt{1 - s^2/[z(s)]^2} - \int_0^t ds\, z(s)z'(s). \tag{5.29}$$

There is no explicit reference to λ in this expression, so we pass to the limit as $\lambda \to \infty$. In this limit the function $z(t)$, which is rapidly oscillatory (see Fig. 5.4), approaches the function $Z(t)$, which is smooth and not oscillatory. We therefore obtain from (5.18) an integral equation satisfied $Z(t)$:

$$[Z(t)]^2 - [Z(0)]^2 + \tfrac{1}{2}t^2 - \int_0^t ds\, Z(s)Z'(s) + \int_0^t ds\, Z(s)Z'(s)\sqrt{1 - s^2/[Z(s)]^2} = 0. \tag{5.30}$$

We differentiate (5.30) to obtain an elementary differential equation satisfied by $Z(t)$:

$$Z(t)Z'(t) + t + Z'(t)\sqrt{[Z(t)]^2 - t^2} = 0. \tag{5.31}$$

This differential equation is easy to solve because it is *homogeneous*; that is, the equation can be rearranged so that $Z(t)$ is always accompanied by a factor of $1/t$. Such an equation can be solved by substituting $Z(t) = tG(t)$ to reduce (5.31) to a separable differential equation for $G(t)$. The general solution for $G(t)$ is

$$\frac{K}{t^3} = \left(1 + 3[G(t)]^2\right)\left(G(t) + \sqrt{[G(t)]^2 - 1}\right) \frac{\sqrt{[G(t)]^2 - 1} - 2G(t)}{\sqrt{[G(t)]^2 - 1} + 2G(t)}, \tag{5.32}$$

where K is an arbitrary constant. The condition that $G(1) = 1$, which is obtained by substituting (5.12) into (5.5) and (5.6) and taking the limit $n \to \infty$, then determines that $K = -4$, and we obtain the exact result that $Z(0) = 2^{1/3}$. We thus conclude that $A = 2^{5/6}$. This establishes the principal result of this chapter.

5.4 Discussion and description of future work

5.4.1 First Painlevé transcendent

We believe that the asymptotic approach developed in this chapter may be applicable to many nonlinear differential equations having separatrix structure. One example is the differential equation for the first Painlevé transcendent

$$y''(x) = [y(x)]^2 + x. \tag{5.33}$$

How do solutions to this equation behave as $x \to -\infty$? It is clear that when x becomes large and negative, there can be a dominant asymptotic balance between the positive term $[y(x)]^2$ and the negative term x, which implies that $y(x)$ can have two possible leading asymptotic behaviors:

$$y(x) \sim \pm\sqrt{-x} \quad (x \to -\infty), \tag{5.34}$$

which is valid because the second derivative of $\sqrt{-x}$ is small compared with x as $x \to -\infty$.

This problem is interesting because the asymptotic behavior $y(x) \sim -\sqrt{-x}$ is stable but the asymptotic behavior $y(x) \sim \sqrt{-x}$ is unstable. To verify this, we calculate the corrections to these two asymptotic behaviors. When x is large and negative, the solution to (5.33) oscillates about and decays slowly towards the curve $-\sqrt{-x}$ [155]:

$$y(x) \sim -\sqrt{-x} + c(-x)^{-1/8} \cos\left[\tfrac{4}{5}\sqrt{2}(-x)^{5/4} + d\right] \quad (x \to -\infty), \tag{5.35}$$

where c and d are two arbitrary constants. The differential equation (5.33) is second order and, as expected, this asymptotic behavior contains two arbitrary constants.

On the other hand, the correction to the $+\sqrt{-x}$ behavior has an exponential form

$$y(x) \sim \sqrt{-x} + c_{\pm}(-x)^{-1/8} \exp\left[\pm\tfrac{4}{5}\sqrt{2}(-x)^{5/4}\right] \quad (x \to -\infty). \tag{5.36}$$

Thus, if $c_+ \neq 0$, nearby solutions veer away from the curve $\sqrt{-x}$ as $x \to -\infty$. The special solutions that decay exponentially towards $\sqrt{-x}$ form a one-parameter and not a two-parameter class because $c_+ = 0$. The vanishing of c_+ gives an eigenvalue condition on the choice of initial slope $y'(0)$. For each value of $y(0)$ there is a set of eigencurves (separatrices). These curves correspond to a discrete set of initial slopes $y'(0)$ [169].

We have performed a numerical study of the solutions to (5.33) that satisfy the initial conditions $y(0) = 1$ and $y'(0) = a$. There is a discrete set of eigencurves whose initial positive slopes are $a_1 = 0.231955$, $a_2 = 3.980669$, $a_3 = 6.257998$, $a_4 = 8.075911$, $a_5 = 9.654843$, $a_6 = 11.078201$, $a_7 = 12.389217$, $a_8 = 13.613878$, $a_9 = 14.769304$, $a_{10} = 15.867511$, $a_{11} = 16.917331$, $a_{12} = 17.925488$. (There is also an infinite discrete set of *negative* eigenvalues.) The first two of these curves are shown in the left panel and the next two are shown in the right panel of Fig. 5.6. Note that the separatrix curves do not just exhibit n maxima as do the dashed curves in Fig. 5.2. Rather, these curves pass through increasingly many double poles. The curve corresponding to a_1 approaches $+\sqrt{-x}$ from above and the curve corresponding to a_2 approaches $+\sqrt{-x}$ from below. The curves corresponding to a_3 and a_4 also approach $+\sqrt{-x}$ from above and below, but these curves first pass through one double pole. Similarly, the curves corresponding to a_5 and a_6 pass through two double poles, and the curves corresponding to a_{2n-1} and a_{2n} pass through n double poles. The key feature of these separatrix curves is that after passing through n double poles, they approach the curve $+\sqrt{-x}$ exponentially fast as $x \to -\infty$. If $y'(0)$ lies in between two eigenvalues, the curve either oscillates about and approaches the stable asymptotic curve $-\sqrt{-x}$ as in the left panel of Fig. 5.7 or else it lies above the unstable asymptotic curve $+\sqrt{-x}$ and passes through an infinite number of double poles as in the right panel of Fig. 5.7.

We have used Richardson extrapolation [168] to find the behavior of the numbers a_n for large n, and we obtain a result very similar in structure to that in (5.9). Specifically, we find that

$$a_n \sim C n^{3/5} \quad (n \to \infty), \tag{5.37}$$

where $C = 4.28373$. The constant C appears to be universal in that it is seems to be the same for all values of $y(0)$. We are currently trying to apply our analytical asymptotic methods to this problem to find an analytic calculation for the number C.

5.4.2 Conjectural connection with the power-series constant

There is a possible link between this work and the power-series constant P in the theory of complex variables; P is defined as follows. Let $\mathcal{F}$ be the class of functions $f(z)$ that are analytic in the unit circle $|z| < 1$ but singular on the unit circle. If $f \in \mathcal{F}$, the radius of convergence of the Taylor series $f(z) = \sum_{k=0}^{\infty} a_k z^k$ is 1. The nth partial sum

$$S_n(z) = \sum_{k=0}^{n} a_k z^k \tag{5.38}$$

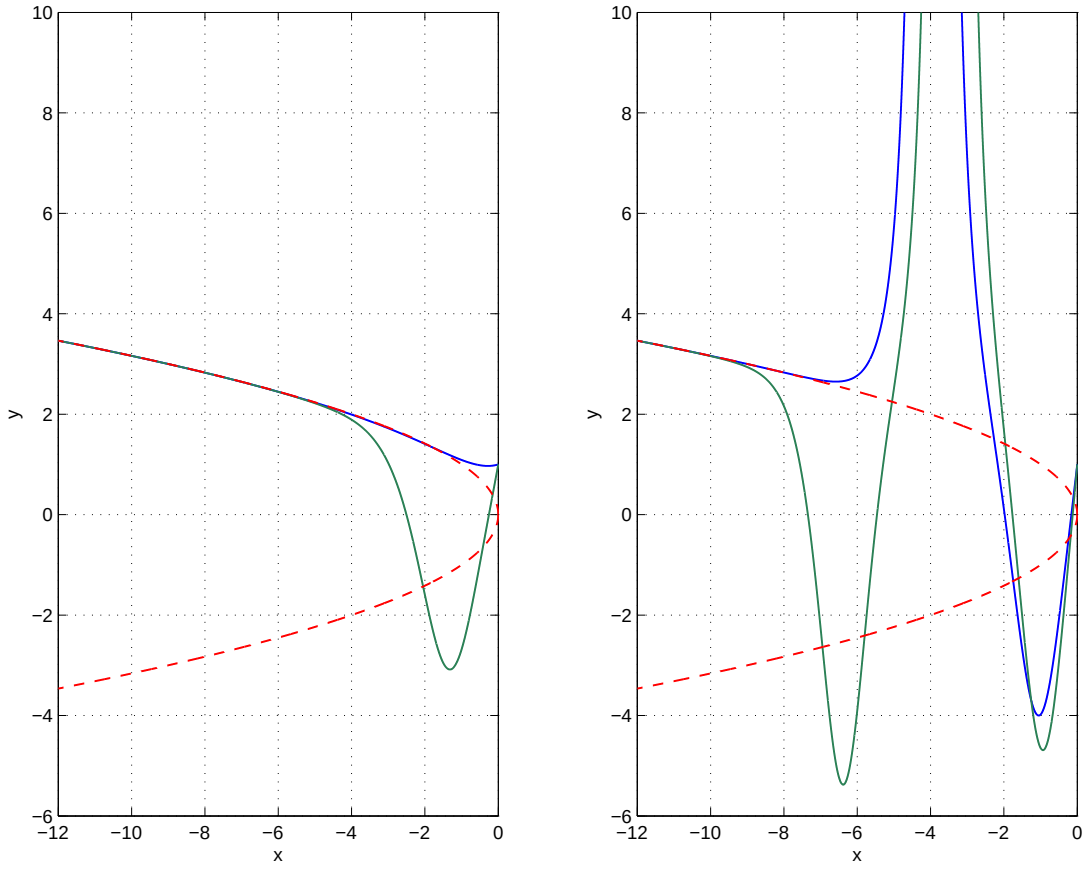

FIGURE 5.6: Eigencurve solutions to the first Painlevé transcendent. The eigencurves pass through $y(0) = 1$ and the slopes of the curves at $x = 0$ are the eigenvalues a_n. As $x \to -\infty$, the eigencurves approach $+\sqrt{-x}$ exponentially rapidly. Left panel: first two eigencurves corresponding to the eigenvalues $a_1 = 0.231955$ and $a_2 = 3.980669$. The a_1 curve approaches $+\sqrt{-x}$ from above and the a_2 curve approaches $+\sqrt{-x}$ from below. Right panel: The next two eigencurves for the Painlevé transcendent corresponding to the eigenvalues $a_3 = 6.257998$ and $a_4 = 8.075911$. Note that the second pair of eigenvalues passes through one double pole before approaching the curve $+\sqrt{-x}$.

of the Taylor series is a polynomial in z. We define the real number $\rho_n(f)$ as the modulus of the zero of $S_n(z)$ that is most distant from the origin. Next, we define the *infimum limit* $\rho(f)$ of the sequence of numbers $\rho_n(f)$:

$$\rho(f) \equiv \liminf_{n\to\infty} \rho_n(f) = \lim_{n\to\infty} \left[\inf_{k>n} \rho_k(f) \right]. \tag{5.39}$$

Finally, we define the power series constant P as the *supremum* of $\rho(f)$ over all functions f in $\mathcal{F}$:

$$P \equiv \sup_{f\in\mathcal{F}} \rho(f). \tag{5.40}$$

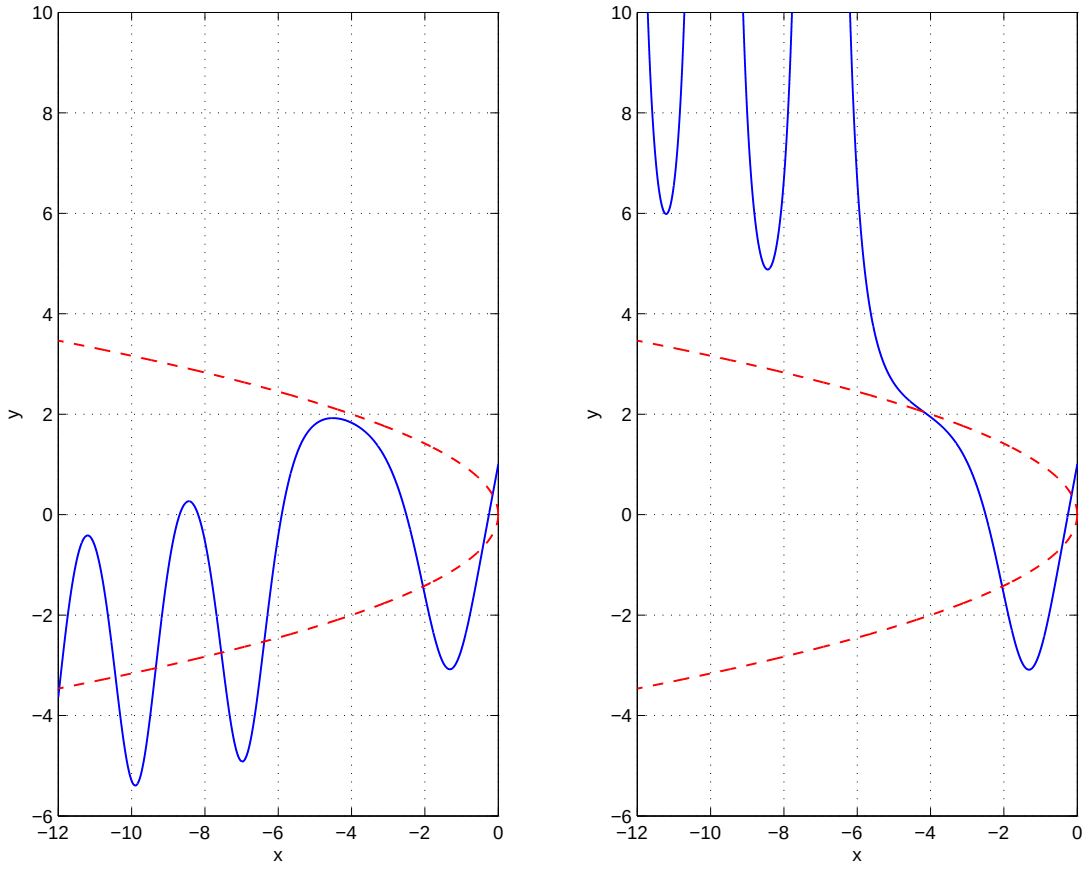

FIGURE 5.7: Non-eigenvalue solutions to the first Painlevé transcendent. If $y(0) = 1$ but $y'(0)$ is not one of the eigenvalues a_n, the curve either oscillates about and approaches the stable asymptotic curve $-\sqrt{-x}$ as in the left panel or else it lies above the unstable asymptotic curve $+\sqrt{-x}$ and passes through an infinite number of double poles as in the right panel.

The quest to determine P was initiated by Hayman [170]. The precise value of P is still not known, but lower and upper bounds on P have been established. The power series constant was known to lie in the interval $1 \leq P \leq 2$ until Clunie and Erdös [171] improved these bounds to $\sqrt{2} \leq P \leq 2$, and Buckholtz [172] sharpened these bounds to $1.7 \leq P \leq 12^{1/4}$. These bounds were further optimized by Frank (as explained in Ref. [172]) to

$$1.7818 \leq P \leq 1.82. \tag{5.41}$$

The bounds (5.41) appear to be the best known to date.

To illustrate, we compute $\rho(f)$ for some specific functions. For the class of functions

$$f_\tau(z) = \sum_{k=0}^{\infty} \exp[i\pi\tau(k^2+k)]\, z^k \tag{5.42}$$

the sequence $\rho_n(f)$ has a limit as $n \to \infty$. For example, it is easy to show that for $\tau = 1/4$,

$$f_{1/4}(z) = \left(1 + iz - iz^2 - z^3\right) / \left(1 + z^4\right). \tag{5.43}$$

For this function we get $\rho_{20}\left(f_{1/4}\right) \approx 1.69999$, $\rho_{21}\left(f_{1/4}\right) \approx 1.70000$, $\rho_{22}\left(f_{1/4}\right) \approx 1.70001$, $\rho_{23}\left(f_{1/4}\right) \approx 1.70002$, $\rho_{24}\left(f_{1/4}\right) \approx 1.70002$, $\rho_{25}\left(f_{1/4}\right) \approx 1.70002$. This sequence converges to the zero of largest modulus, $z = -\left(1 + i + \sqrt{2i-4}\right)/2$, of the function $f_{1/4}(z)$. This limit is close to the value of P. The function

$$f_{3/8}(z) = \left(1 + e^{3i\pi/4}z + e^{i\pi/4}z^2 + iz^3 - iz^4 - e^{i\pi/4}z^5 - e^{3i\pi/4}z^6 - z^7\right) / \left(1 + z^8\right) \tag{5.44}$$

gives a $\rho(f)$ that is even closer to P: $\rho\left(f_{3/8}\right) \approx 1.7804$. In general, to determine $\rho(f)$ accurately we terminate the Taylor series at sufficiently large n and evaluate $\rho_n(f)$. In Fig. 5.8 we display our numerical results for $\rho_{50}(f_\tau)$ obtained from the partial sum $S_{50}(z)$. The maximum values are $\rho_{50}(f_{0.3780}) = \rho_{50}(f_{0.8780}) \approx 1.7818$, which agree with the best known lower bound for P to the precision of the computation.

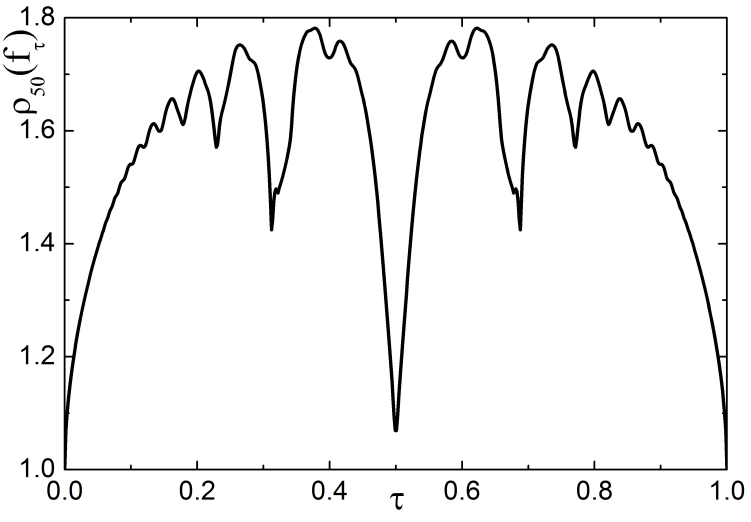

FIGURE 5.8: Plot of $\rho_{50}(f_\tau)$ as a function of τ. At the optimal value of the parameter τ the maximum of the curve is close to 1.7818.

It is not always true that the sequence $\rho_n(f)$ has a limit. The infimum limit in (5.39) is used because it always produces a definite limit, even if the ordinary limit is ambiguous. For

example, the function $f(z) = (1-z/10)/(1-z^4)$ gives the partial sequence ..., $\rho_{40}(f) \approx 1.00362$, $\rho_{41}(f) = 10$, $\rho_{42}(f) = \infty$, $\rho_{43}(f) = \infty$, $\rho_{44}(f) \approx 1.00328$, $\rho_{45}(f) = 10$, $\rho_{46}(f) = \infty$, $\rho_{47}(f) = \infty$, $\rho_{48}(f) \approx 1.00307$, $\rho_{49}(f) = 10$, ... (We adopt the convention in Ref. [172] that $\rho_n(f) = \infty$ when the partial sum $S_n(z)$ is a polynomial of degree less than n.) There is no definite limit for this sequence $\rho_n(f)$, but the infimum limit gives $\rho(f) = 1$, which is well below the value of P.

It is astonishing that A in (5.9) agrees with the best known lower bound for the power-series constant P in (5.41). There is a plausible connection between the P and the asymptotic behavior of eigenvalues: On one hand, P is associated with the zero of largest modulus of a polynomial, namely, the nth partial sum of a Taylor series. On the other hand, a conventional linear eigenvalue problem of the form $H\psi = E\psi$ may be solved by introducing a basis and replacing the operator H by an $n \times n$ matrix H_n. We then determine the eigenvalues numerically by calculating the zeros of the secular polynomial $\mathrm{Det}(H_n - IE)$. Finding the asymptotic behavior of the high-energy eigenvalues corresponds to finding the largest zero of the secular polynomial as n, the degree of the polynomial, tends to infinity. We do not know whether our constant $2^{5/6}$ agrees exactly with the lower bound on P and we leave this observation as coincidence. We hope to elaborate on the precise relation in a future chapter [173].

5.4.3 Final comments

In this chapter we have focused on separatrix behavior, which is a consequence of instabilities of nonlinear differential equations. We have interpreted separatrices as being eigenfunctions (eigencurves). The corresponding eigenvalues are the initial conditions that specify the separatrix curves. For the differential equation $y'(x) = \cos[\pi x y(x)]$, we have shown that the nth eigenvalue grows like $2^{1/3}\sqrt{2n}$ for large n. We have also done a numerical study of eigenvalues and separatrices associated with the first Painlevé transcendent. To the currently known precision, the number $2^{5/6}$ appears in another asymptotic context, namely, as the lower bound 1.7818 on the power series constant P. We conjecture that the number $2^{5/6}$ may even be the exact value of P.

We have studied here the asymptotic behavior of large eigenvalues. For linear eigenvalue problems this limit is accessible by using WKB theory but for the nonlinear eigenvalue problem studied here the large-eigenvalue limit is accessible because the problem becomes *linear* in this limit; indeed, the large-eigenvalue separatrix curve was found by reducing the problem to a *linear* random walk problem that can be solved exactly. The strategy of transforming a nonlinear problem to an equivalent linear problem is reminiscent of the Hopf-Cole substitution that reduces the nonlinear Burgers equation to the linear diffusion equation, the inverse-scattering analysis

that reduces the nonlinear Korteweg-de Vries equation to a linear integral equation, of the Bäcklund transformation that linearizes some integrable nonlinear wave equations. We believe that the techniques introduced here to determine the asymptotic behavior of large eigenvalues may apply to other nonlinear differential equations having instabilities and separatrix behavior.

6

Nonlinear Eigenvalue Problems: Painlevé Transcendents

This chapter contains the materials of a submitted paper.[1] *This represents work performed by me under the overall supervision of my advisor, C. M. Bender.*

6.1 Introduction

The famous Painlevé transcendents are six nonlinear second-order differential equations whose key features are that their movable (spontaneous) singularities are poles (and not, for example, branch points or essential singularities). There is a vast literature on these remarkable differential equations [161, 174–180]. These equations have arisen many times in mathematical physics; for a small sample, see Refs. [181–188]. This chapter considers the first and second Painlevé transcendents, referred to here as P-I and P-II. The initial-value problem (IVP) for the P-I differential equation is

$$y''(t) = 6[y(t)]^2 + t, \qquad y(0) = c,\ y'(0) = b \tag{6.1}$$

and the IVP for P-II (we have set an arbitrary additive constant to 0) is

$$y''(t) = 2[y(t)]^3 + ty(t), \qquad y(0) = c,\ y'(0) = b. \tag{6.2}$$

Many asymptotic studies of the Painlevé transcendents have been published, but in this chapter we present a simple numerical and asymptotic analysis that to our knowledge has not appeared in the literature. This analysis concerns the initial conditions that give rise to special

[1] C. M. Bender and J. Komijani, "Painlevé Transcendents and PT-Symmetric Hamiltonians," arXiv:1502.04089 [math-ph].

unstable separatrix solutions of P-I and P-II. Our asymptotic analysis verifies the numerical results given in this chapter for P-I and P-II as well as some preliminary numerical calculations that were presented in an earlier chapter on nonlinear differential-equation eigenvalue problems [189].

The main idea, originally introduced in Ref. [189], is that a nonlinear differential equation may have a discrete set of *critical* initial conditions that give rise to unstable separatrix solutions. These discrete initial conditions can be thought of as eigenvalues and the separatrices that stem from these initial conditions can be viewed as the corresponding eigenfunctions. The objective in Ref. [189] was to find the large-n (semiclassical) asymptotic behavior of the nth eigenvalue. The general analytical approach that was proposed was to simplify the nonlinear differential problem to a linear problem that could be used to determine the leading asymptotic behavior of the eigenvalues as $n \to \infty$.

A toy model was used in Ref. [189] to explain the concept of a nonlinear eigenvalue problem. This model makes use of the elementary first-order differential equation problem

$$y'(t) = \cos[\pi t\, y(t)], \quad y(0) = a. \tag{6.3}$$

It was shown that the solutions to this initial-value problem pass through n maxima before vanishing like $1/t$ as $t \to \infty$. As the initial condition $a = y(0)$ increases past special critical values a_n, the number of maxima jumps from n to $n+1$. At these critical values the solution $y(t)$ to (6.3) is an unstable separatrix curve in the following sense: At values of $y(0)$ infinitesimally below a_n the solution merges with a bundle of stable solutions all having n maxima and when $y(0)$ is infinitesimally above a_n the solution merges with a bundle of stable solutions all having $n+1$ maxima. The challenge is to determine the asymptotic behavior of the critical values a_n for large n. (This generic problem is the analog of a semiclassical high-energy approximation in quantum mechanics.) To solve this problem it was shown that for large n, the nonlinear differential equation problem (6.3) reduces to a *linear* one-dimensional random-walk problem. The random-walk problem was solved exactly, and it was shown analytically that

$$a_n \sim 2^{5/6}\sqrt{n} \quad (n \to \infty). \tag{6.4}$$

Kerr subsequently found an alternative solution to this asymptotics problem and verified (6.4) [190].

The nonlinear eigenvalue problem described above is similar in many respects to the linear eigenvalue problem for the time-independent Schrödinger equation. For a potential $V(x)$ that

rises as $x \to \pm\infty$, the eigenfunctions $\psi(x)$ of the Schrödinger eigenvalue problem

$$-\psi''(x) + V(x)\psi(x) = E\psi(x), \quad \psi(\pm\infty) = 0, \tag{6.5}$$

are unstable with respect to small changes in the eigenvalue E; that is, if E is increased or decreased slightly, $\psi(x)$ abruptly ceases to obey the boundary conditions [and thus is not normalizable (square integrable)]. Furthermore, like the eigenfunctions (separatrix curves) of (6.3), the eigenfunction $\psi_n(x)$ corresponding to the nth eigenvalue has n oscillations in the classically allowed region before decreasing monotonically to 0 in the classically forbidden region.

This chapter considers four eigenvalue problems. First, for P-I we find the large-n behavior of the positive eigenvalues b_n for the initial condition $y(0) = 0$, $y'(0) = b_n$ and also the large-n behavior of the negative eigenvalues c_n for the initial condition $y(0) = c_n$, $y'(0) = 0$. We show that

$$b_n \sim B_{\rm I} n^{3/5} \quad \text{and} \quad c_n \sim C_{\rm I} n^{2/5}.$$

Second, for P-II we show that for large n the asymptotic behaviors of b_n and c_n are given by

$$b_n \sim B_{\rm II} n^{2/3} \quad \text{and} \quad c_n \sim C_{\rm II} n^{1/3}.$$

We determine the constants $B_{\rm I}$, $C_{\rm I}$, $B_{\rm II}$, and $C_{\rm II}$ both numerically and analytically.

This chapter is organized as follows. In Sec. 6.2 we obtain the constants $B_{\rm I}$ and $C_{\rm I}$ by using numerical techniques and in Sec. 6.3 we do so analytically by reducing the large-eigenvalue problem to the *linear* time-independent Schrödinger equation for the cubic $\mathcal{PT}$-symmetric Hamiltonian $H = \frac{1}{2}p^2 + ix^3$. Next, we study the eigenvalue problem for the second Painlevé transcendent. In Sec. 6.4 we present a numerical determination of the large-n behavior of the eigenvalues and in Sec. 6.5 we verify the numerical results in Sec. 6.4 by using asymptotic analysis to reduce the nonlinear large-eigenvalue problem for P-II to the linear Schrödinger equation for the quartic $\mathcal{PT}$-symmetric Hamiltonian $H = \frac{1}{2}p^2 - \frac{1}{2}x^4$. In Sec. 6.6 we make some brief concluding remarks.

6.2 Numerical analysis of the first Painlevé transcendent

In Ref. [189] there is a brief numerical study of the initial-value problem for the first Painlevé transcendent (6.1). It is easy to see that there are two possible asymptotic behaviors as $t \to -\infty$; the solutions to the P-I equation can approach either $+\sqrt{-t/6}$ or $-\sqrt{-t/6}$. An elementary asymptotic analysis shows that if the solution $y(t)$ approaches $-\sqrt{-t/6}$, the solution oscillates stably about this curve with slowly decreasing amplitude [155]. However, while the curve $+\sqrt{-t/6}$

is a possible asymptotic behavior, this behavior is *unstable* and nearby solutions tend to veer away from it. We define the eigenfunction solutions to the first Painlevé transcendent as those solutions that *do* approach $+\sqrt{-t/6}$ as $t \to -\infty$. These separatrix solutions resemble the eigenfunctions of conventional quantum mechanics in that they exhibit n oscillations before settling down to this asymptotic behavior. However, because the P-I equation is nonlinear, these oscillations are violent; the nth eigenfunction passes through $[n/2]$ double poles where it blows up before it smoothly approaches the curve $+\sqrt{-t/6}$. (The symbol $[n/2]$ means greatest integer in $n/2$.)

One can specify two different kinds of eigenvalue problems for P-I, each of which is fundamentally related to the instability of the asymptotic behavior $+\sqrt{-t/6}$. One can (i) fix the initial value $y(0)$ and look for (discrete) values of the initial slopes $y'(0) = b$ that give rise to solutions approaching $+\sqrt{-t/6}$, or else (ii) one can fix the initial slope $y'(0)$ and look for the (discrete) initial values of $y(0) = c$ that give rise to solutions approaching $+\sqrt{-t/6}$.

6.2.1 Initial-slope eigenvalues for Painlevé I

Let us examine the numerical solutions to the initial-value problem for the P-I equation (6.1) for $t < 0$. To find these solutions we use Runge-Kutta to integrate down the negative-real axis. When we approach a double pole and the solution becomes large and positive, we estimate the location of the pole and integrate along a semicircle in the complex-t plane around the pole. We then continue integrating down the negative-real axis. We choose the fixed initial value $y(0) = 0$ and allow the initial slope $y'(0) = b$ to have increasingly positive values. (We only present results for positive initial slope; the behavior for negative initial slope is analogous and describing it would be repetitive.) Our numerical analysis shows that the particular choice of $y(0)$ is not crucial; for *any* fixed $y(0)$ the large-n asymptotic behavior of the initial-slope eigenvalues b_n is the same.

We find that above the critical value $b_1 = 1.851854034$ (the first eigenvalue) there is a continuous interval of b for which $y(t)$ first has a minimum and then has an infinite sequence of double poles (see Fig. 6.1, left panel). However, if b increases past the next critical value $b_2 = 3.004031103$ (the second eigenvalue), the character of the solutions changes abruptly and $y(t)$ oscillates stably about $-\sqrt{-t/6}$ (Fig. 6.1, right panel). When b exceeds the critical value $b_3 = 3.905175320$ (the third eigenvalue), the solutions again exhibit an infinite sequence of poles (Fig. 6.2, left panel). When b increases past the fourth critical value $b_4 = 4.683412410$ (fourth eigenvalue), the solutions once again oscillate stably about $-\sqrt{-t/6}$ (Fig. 6.2, right panel). Our numerical analysis indicates that there is an infinite sequence of critical points (eigenvalues) at

which the P-I solutions alternate between infinite sequences of double poles and stable oscillation about $-\sqrt{-t/6}$.

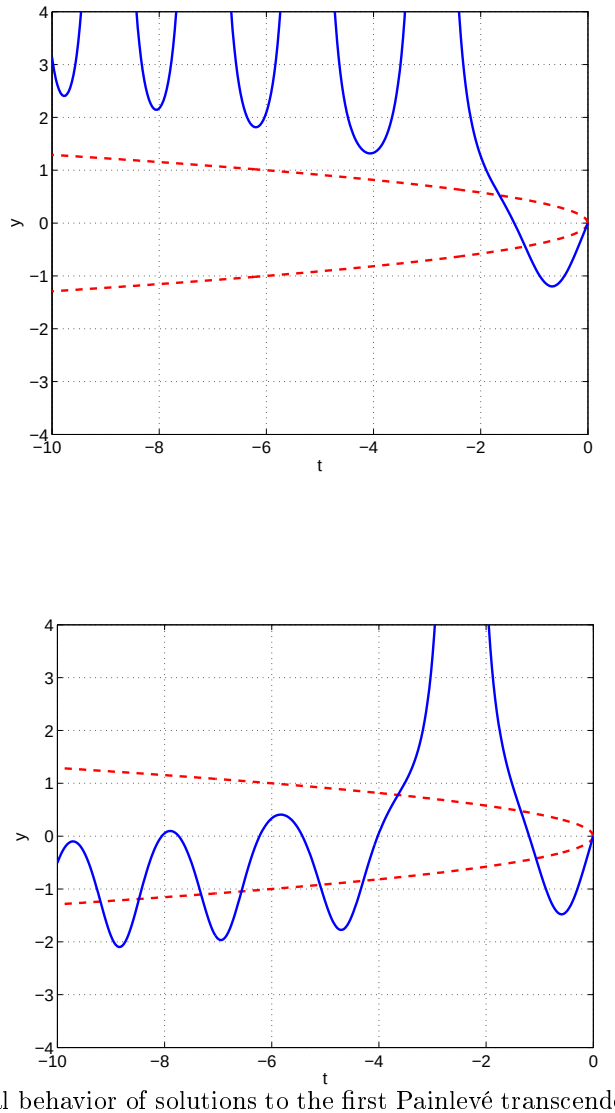

FIGURE 6.1: Typical behavior of solutions to the first Painlevé transcendent $y(t)$ for the initial conditions $y(0) = 0$ and $b = y'(0)$. In the left panel $b = 2.504031103$, which lies between the eigenvalues $b_1 = 1.851854034$ and $b_2 = 3.004031103$. In the right panel $b = 3.504031103$, which lies between the eigenvalues $b_2 = 3.004031103$ and $b_3 = 3.905175320$. The dashed curves are $y = \pm\sqrt{-t/6}$. In the left panel the solution $y(t)$ has an infinite sequence of double poles and in the right panel the solution oscillates stably about $-\sqrt{t/6}$.

The solutions that arise when $y'(0)$ is at an eigenvalue have a completely different (and unstable) character from those in Figs. 6.1 and 6.2. These special solutions pass through a *finite* number of double poles (analogous to the oscillatory behavior of quantum-mechanical bound-state eigenfunctions in the classically allowed region of a potential well) and then undergo a turning-point-like transition in which the poles cease and $y(t)$ exponentially approaches the limiting curve $+\sqrt{-t/6}$. The solutions arising from the first and second critical points b_1 and b_2

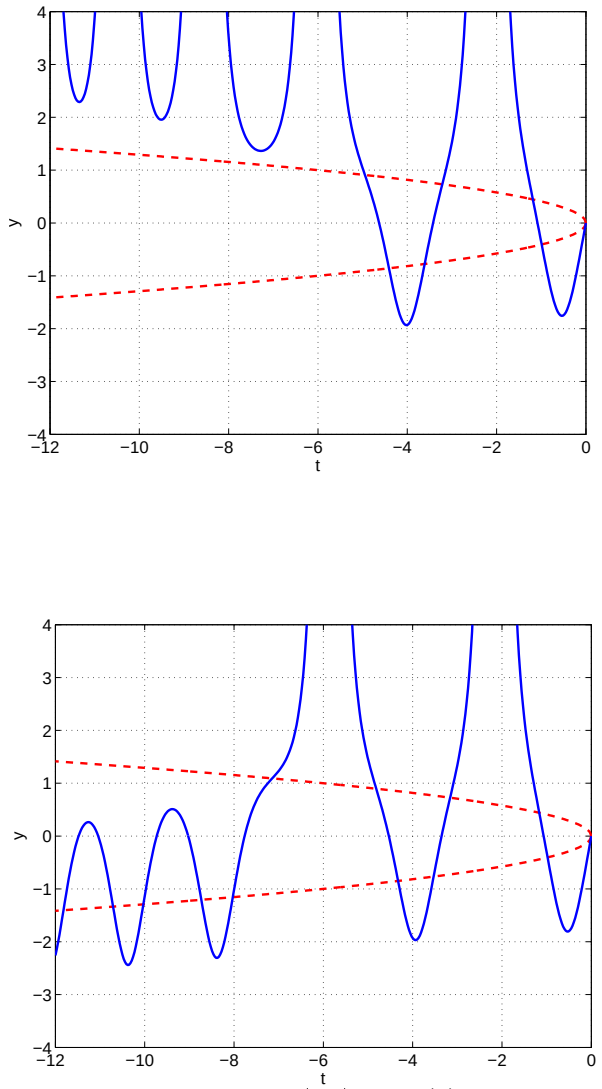

FIGURE 6.2: Solutions to the P-I equation (6.1) for $y(0) = 0$ and $b = y'(0)$. Left panel: $b = 4.583412410$, which lies between the eigenvalues $b_3 = 3.905175320$ and $b_4 = 4.6834124103$. Right panel: $b = 4.783412410$, which lies between the eigenvalues $b_4 = 4.683412410$ and $b_5 = 5.383086722$.

are shown in Fig. 6.3, those arising from the third and fourth critical points b_3 and b_4 are shown in Fig. 6.4, and those arising from the tenth and eleventh critical points b_{10} and b_{11} are shown in Fig. 6.5. The critical points are analogous to eigenvalues because they give rise to *unstable* separatrix solutions; if $y'(0)$ changes by an infinitesimal amount above or below a critical value, the character of the solutions changes abruptly and the solutions exhibit the two possible generic behaviors shown in Figs. 6.1 and 6.2.

In Ref. [189] a numerical asymptotic study of the critical values b_n for $n \gg 1$ was performed by using Richardson extrapolation [191]. [In Ref. [189] the initial value was chosen to be $y(0) = 1$ rather than $y(0) = 0$ as in the current chapter. However, as emphasized above, if $y(0)$ is held

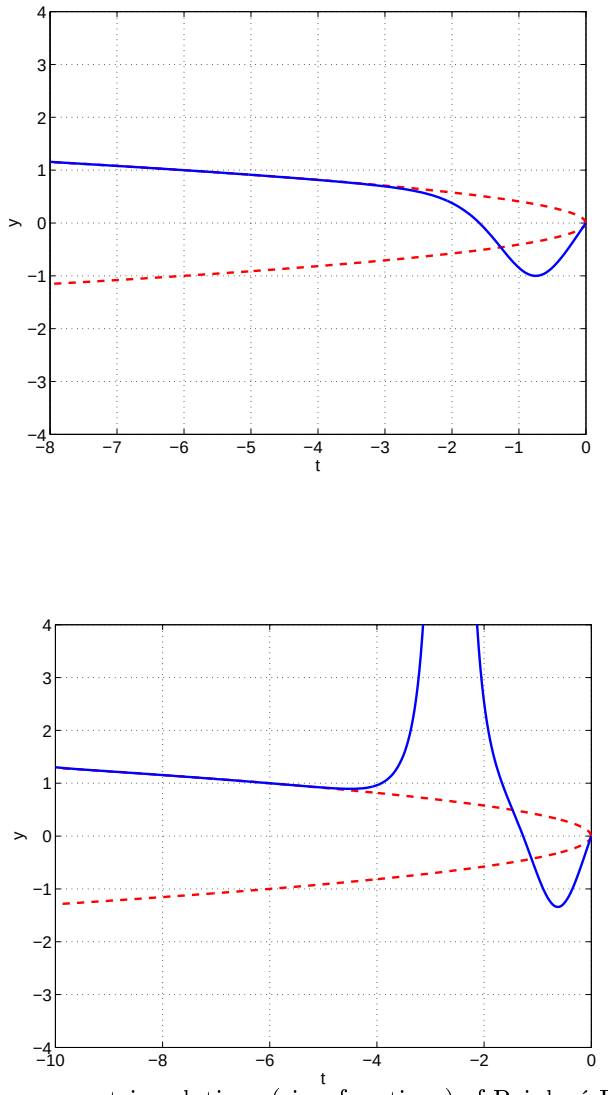

FIGURE 6.3: First two separatrix solutions (eigenfunctions) of Painlevé I with initial condition $y(0) = 0$. Left panel: $y'(0) = b_1 = 1.851854034$; right panel: $y'(0) = b_2 = 3.004031103$. The dashed curves are $y = \pm\sqrt{-t/6}$.

fixed, we find that the large-n asymptotic behavior of the initial slope b_n is insensitive to the choice of $y(0)$.] It was found in Ref. [189] that for large n, the nth critical value had the asymptotic behavior

$$y_n'(0) = b_n \sim B_{\rm I} n^{3/5} \quad (n \to \infty). \tag{6.6}$$

In Ref. [189] the constant $B_{\rm I}$ was determined numerically to an accuracy of about four or five decimal places. However, we have now performed a more accurate numerical determination of the constant $B_{\rm I}$ by applying fifth-order Richardson extrapolation to the first eleven eigenvalues,

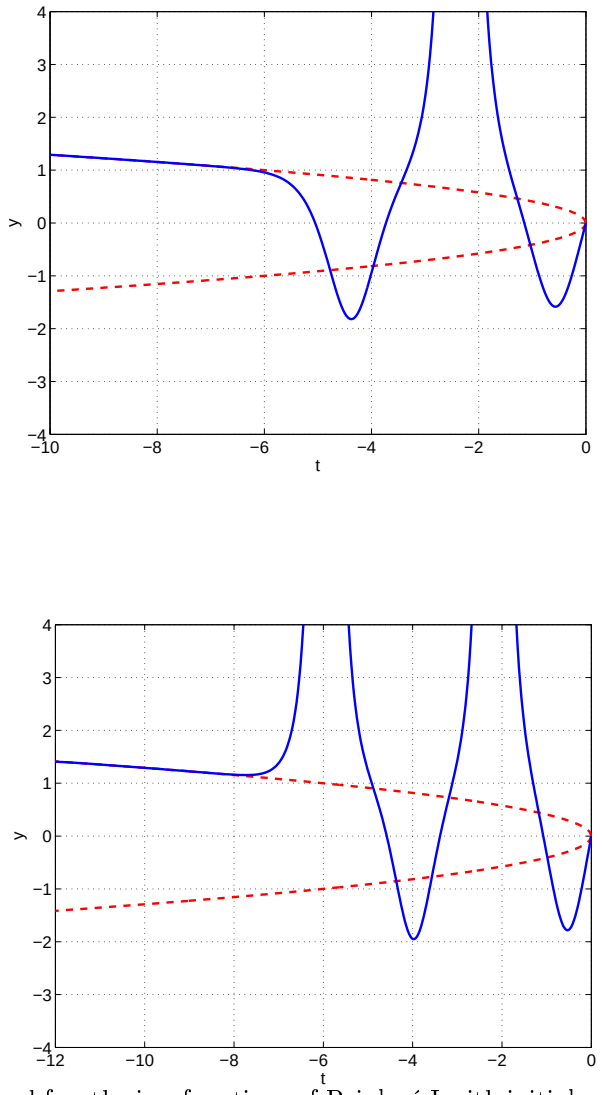

FIGURE 6.4: Third and fourth eigenfunctions of Painlevé I with initial condition $y(0) = 0$. Left panel: $y'(0) = b_3 = 3.905175320$; right panel: $y'(0) = b_4 = 4.683412410$.

and we have found the value of B_{I} accurate to one part in nine decimal places:

$$B_{\mathrm{I}} = 2.09214674. \tag{6.7}$$

On the basis of our numerical analysis, we can say with confidence that the underlined digit lies in the range from 3 to 5, so our determination of B_{I} is accurate to one part in 2×10^8.

6.2.2 Initial-value eigenvalues for Painlevé I

If we hold the initial slope fixed at $y'(0) = 0$ and allow the initial value $y(0) = c$ to become increasingly negative, we find that there is a sequence of negative eigenvalues c_n for which

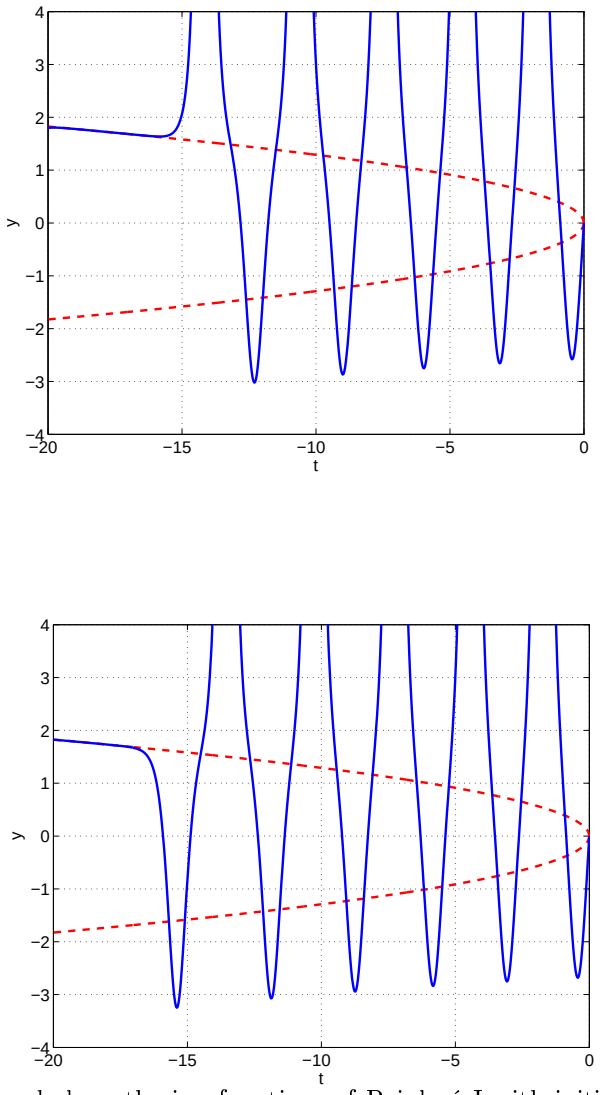

FIGURE 6.5: Tenth and eleventh eigenfunctions of Painlevé I with initial condition $y(0) = 0$. Left panel: $y'(0) = b_{10} = 8.244932302$; right panel: $y'(0) = b_{11} = 8.738330156$. Note that as n increases, the eigenfunctions pass through more and more double poles before exhibiting a turning-point-like transition and approaching the limiting curve $+\sqrt{-t/6}$ exponentially rapidly. This behavior is analogous to that of the eigenfunctions of a time-independent Schrödinger equation for a particle in a potential well; the higher-energy eigenfunctions exhibit more and more oscillations in the classically allowed region before entering the classically forbidden region, where they decay exponentially.

the solutions behave like the eigenfunction separatrix solutions in Figs. 6.3–6.5. The first four eigenfunctions are plotted in Figs. 6.6 and 6.7.

Applying fourth-order Richardson extrapolation to the first 15 eigenvalues, we find that for large n the sequence of initial-value eigenvalues c_n is asymptotic to $C_{\rm I} n^{2/5}$, where the numerical value of the constant $C_{\rm I}$ is

$$C_{\rm I} = -1.0304844. \tag{6.8}$$

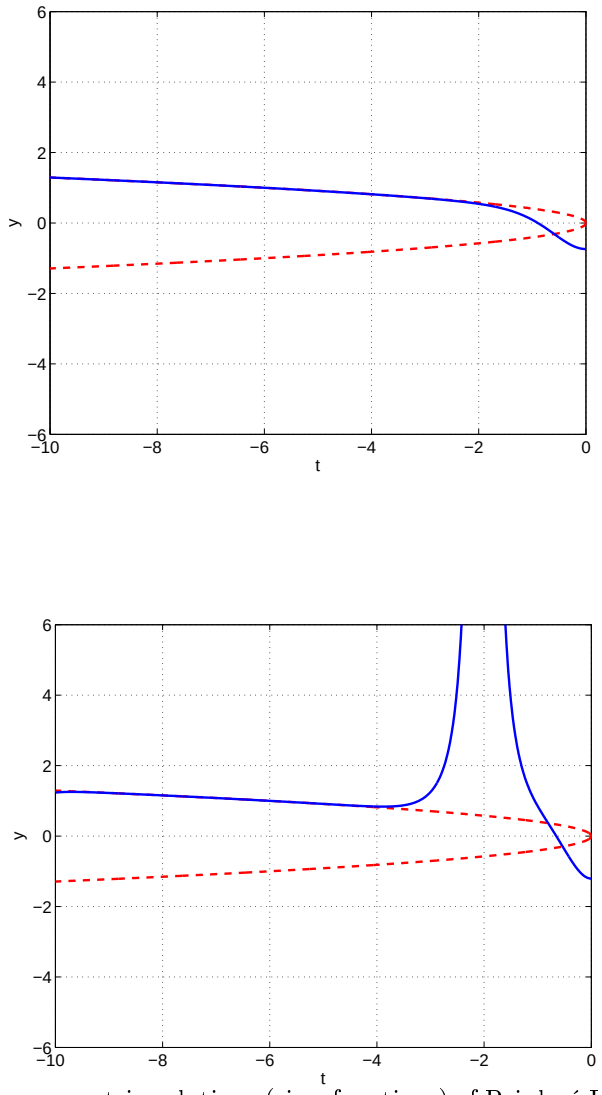

FIGURE 6.6: First two separatrix solutions (eigenfunctions) of Painlevé I with fixed initial slope $y'(0) = 0$. Left panel: $y(0) = c_1 = -0.7401954236$; right panel: $y(0) = c_2 = -1.206703845$. The dashed curves are $y = \pm\sqrt{-t/6}$.

We are confident that the final digit is accurate to an error of ± 1 and thus $C_{\rm I}$ is determined to an accuracy of one part in 10^7.

6.3 Asymptotic calculation of $B_{\rm I}$ and $C_{\rm I}$

In this section we present an analytic calculation of $B_{\rm I}$ and $C_{\rm I}$ in (6.7) and (6.8). To begin, we multiply the P-I differential equation in (6.1) by $y'(t)$ and integrate from $t = 0$ to $t = x$. We get

$$H \equiv \tfrac{1}{2}[y'(x)]^2 - 2[y(x)]^3 = \tfrac{1}{2}[y'(0)]^2 - 2[y(0)]^3 + I(x), \tag{6.9}$$

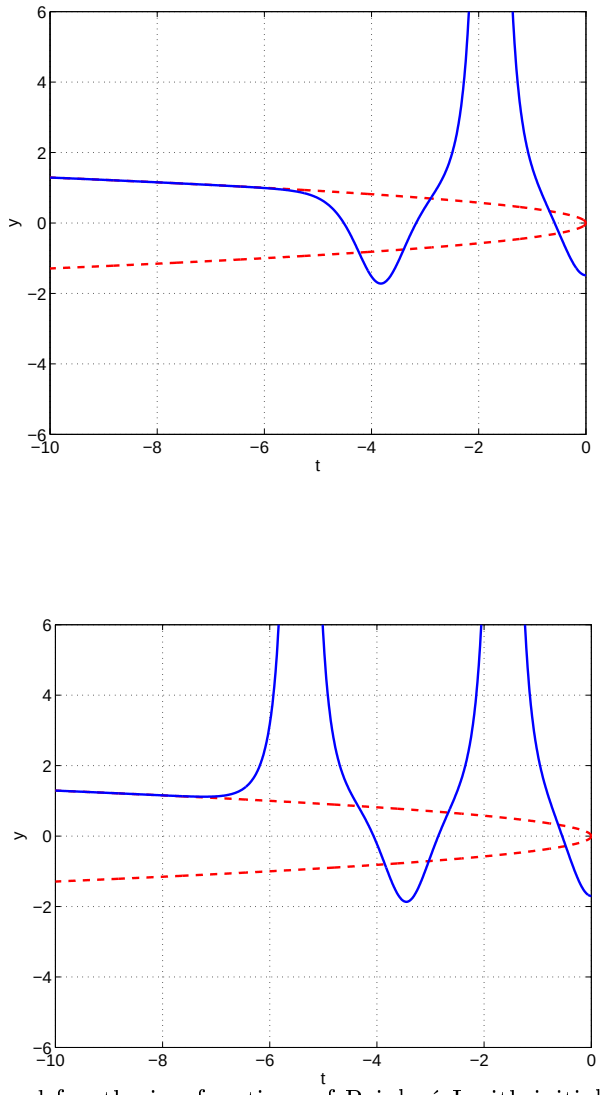

FIGURE 6.7: Third and fourth eigenfunctions of Painlevé I with initial slope $y'(0) = 0$. Left panel: $y(0) = c_3 = -1.484375587$; right panel: $y(0) = c_4 = -1.69951765$.

where $I(x) = \int_0^x dt\, ty'(t)$. Note that the path of integration is the same as that used to calculate $y(t)$ numerically in Sec. 6.2; it follows the negative-real axis until is gets near a pole, at which point it makes a semicircular detour in the complex-t plane to avoid the pole.

If we evaluate $I(x)$ for large $|x|$ in the classically allowed region (just before the poles abruptly cease at the turning point), we find that as $n \to \infty$, $I(x)$ fluctuates and becomes small compared with H. This is not surprising because $I(x)$ receives many positive and negative contributions from the poles. [In fact, by calculating $I(x)$ as $x \to -\infty$, we can see a clear signal of an eigenvalue; as $y'(0) = b$ passes an eigenvalue, $I(x)$ goes from having positive to negative (or negative to positive) fluctuations but at an eigenvalue $I(x)$ is smooth and not fluctuating.] Thus, for large n we treat the fluctuating quantity $I(x)$ as small, and if we do so we can interpret

H as a time-independent quantum-mechanical Hamiltonian. [The isomonodromic properties of H when $I(x)$ is not neglected were studied in Ref. [161].]

We conclude that the large-n (semiclassical) behavior of the eigenvalues [that is, the initial conditions in (6.1)] can be determined by solving the *linear* quantum-mechanical eigenvalue problem $\hat{H}\psi = E\psi$, where $\hat{H} = \frac{1}{2}\hat{p}^2 - 2\hat{x}^3$. To find these eigenvalues we rotate $\hat{H}$ into the complex plane [192] and obtain the well-studied $\mathcal{PT}$-symmetric Hamiltonian [193]

$$\hat{H} = \tfrac{1}{2}\hat{p}^2 + 2i\hat{x}^3. \tag{6.10}$$

The large eigenvalues of this Hamiltonian can be found by using the complex WKB techniques discussed in detail in Ref. [193]. For the general class of $\mathcal{PT}$-symmetric Hamiltonians $\hat{H} = \frac{1}{2}\hat{p}^2 + g\hat{x}^2\,(i\hat{x})^\epsilon$ $(\epsilon \geq 0)$, the WKB approximation to the nth eigenvalue $(n \gg 1)$ is given by

$$E_n \sim \frac{1}{2}(2g)^{2/(4+\epsilon)} \left[\frac{\Gamma\left(\frac{3}{2} + \frac{1}{\epsilon+2}\right)\sqrt{\pi}\, n}{\sin\left(\frac{\pi}{\epsilon+2}\right)\Gamma\left(1 + \frac{1}{\epsilon+2}\right)} \right]^{(2\epsilon+4)/(\epsilon+4)}. \tag{6.11}$$

Thus, for H in (6.10) we take $g = 2$ and $\epsilon = 1$ and obtain the asymptotic behavior

$$E_n \sim 2\left[\sqrt{3\pi}\,\Gamma\left(\tfrac{11}{6}\right) n/\Gamma\left(\tfrac{1}{3}\right)\right]^{6/5} \quad (n \to \infty). \tag{6.12}$$

Since $\hat{H}$ in (6.10) is time independent, we can evaluate H in (6.9) for fixed $y(0)$ and large $y'(0) = b_n$ and obtain the result that

$$b_n \sim \sqrt{2E_n} = B_{\rm I} n^{3/5} \quad (n \to \infty), \tag{6.13}$$

which verifies (6.6). We then read off the analytic value of the constant $B_{\rm I}$:

$$B_{\rm I} = 2\left[\sqrt{3\pi}\,\Gamma\left(\tfrac{11}{6}\right)/\Gamma\left(\tfrac{1}{3}\right)\right]^{3/5}, \tag{6.14}$$

which agrees with the numerical result in (6.7). Also, if we take the initial slope $y'(0)$ to vanish and take the initial condition $y(0) = c_n$ to be large, we obtain an analytic expression for $C_{\rm I}$,

$$C_{\rm I} = -\left[\sqrt{3\pi}\,\Gamma\left(\tfrac{11}{6}\right)/\Gamma\left(\tfrac{1}{3}\right)\right]^{2/5}, \tag{6.15}$$

which agrees with the numerical result in (6.8).

6.4 Numerical analysis of the second Painlevé transcendent

To understand the behavior of solutions to the initial-value problem in (6.2) for Painlevé II, we follow the procedure used in Sec. 6.2 to study P-I. An elementary asymptotic analysis shows that as $t \to -\infty$, there are three possible asymptotic behaviors for solutions $y(t)$. First, $y(t)$ can oscillate stably about the negative axis. Second, $y(t)$ can approach the curves $\pm\sqrt{-t/2}$; however, both of these asymptotic behaviors are unstable.

If we numerically integrate (6.2), we observe that when t becomes large and negative, a typical solution to the P-II initial-value problem either oscillates about the negative axis or passes through an infinite sequence of simple poles. However, it is also possible to find special eigenfunction solutions that pass through only a finite number of poles and then approach either the positive or the negative branches of the square-root curves. These eigenfunctions obey the boundary conditions $y(0) = 0$ and $y'(0) = \pm b$. [Note that P-II is symmetric under $y \to -y$, so there are two sets of eigenfunctions, one for each sign of $y'(0)$.] We study these eigenfunctions numerically in Subsec. 6.4.1. The P-II equation is particularly interesting because as $t \to +\infty$, the behavior $y \to 0$ becomes unstable. Thus, it is possible to have new kinds of eigenfunctions for positive t as well. We seek eigenfunctions that satisfy $y'(0) = 0$ and $y(0) = c$ and examine the positive-c eigenfunctions numerically in Subsec. 6.4.2.

6.4.1 Initial-slope eigenvalues for Painlevé II

Similar to what we found in Sec. 6.2, if we choose $y(0) = 0$, there are critical values $y'(0) = b_n$ at which the solutions $y(t)$ change their character. In Figs. 6.8 and 6.9 we plot the solutions to the P-II equation for the initial condition $y(0) = 0$ and $y'(0) = b$ for $b_1 < b < b_2$, $b_2 < b < b_3$, $b_3 < b < b_4$, and $b_4 < b < b_5$. Note that in these figures the character of the solution alternates between having an infinite sequence of simple poles and oscillating stably about $y(t) = 0$. However, when $y'(0) = b$ is at a critical value (eigenvalue) b_n, the solution $y(t)$ passes through a *finite* number $[n/2]$ of simple poles and then approaches either $+\sqrt{-t/2}$ or $-\sqrt{-t/2}$. These eigenfunctions (separatrices) are plotted in Figs. 6.10, 6.11, and 6.12 for $n = (1, 2)$, $(3, 4)$, and $(20, 21)$.

Note that the eigenfunctions in Figs. 6.10, 6.11, and 6.12 alternate between approaching the upper-unstable branch $+\sqrt{-t/2}$ or the lower-unstable branch $-\sqrt{-t/2}$, and thus there are actually two sequences of eigenvalues, one for even n and one for odd n. Using Richardson extrapolation, we find that the sequences of eigenvalues b_{2n} and b_{2n+1} have the same asymptotic

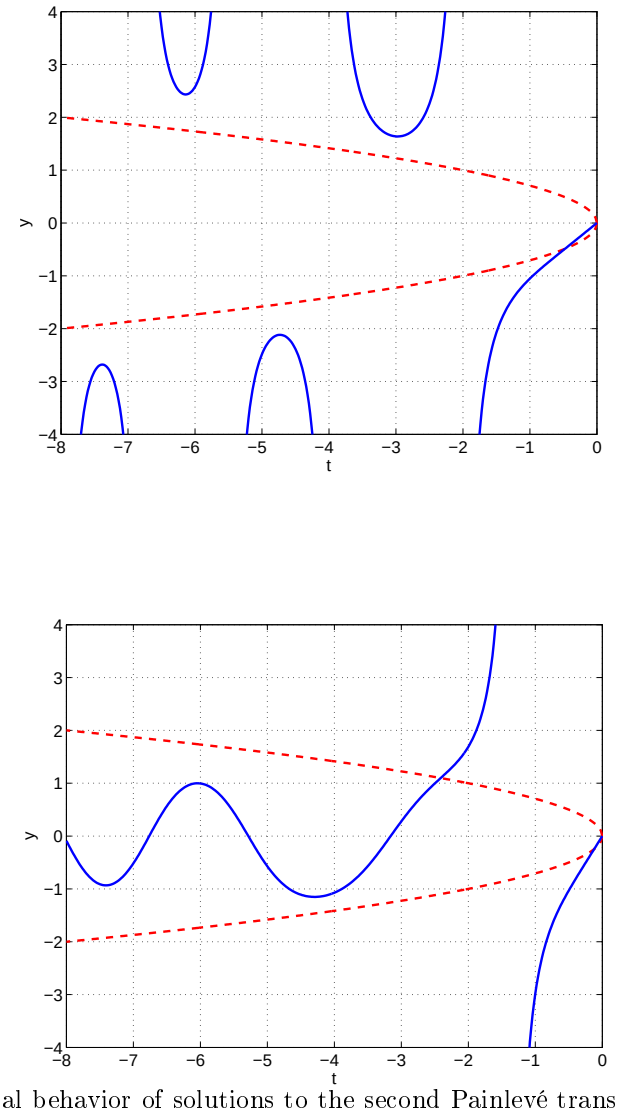

FIGURE 6.8: Typical behavior of solutions to the second Painlevé transcendent for the initial conditions $y(0) = 0$ and $b = y'(0)$. In the left panel $b = 1.028605106$, which lies between the eigenvalues $b_1 = 0.5950825526$ and $b_2 = 1.528605106$. In the right panel $b = 2.028605106$, which lies between the eigenvalues $b_2 = 1.528605106$ and $b_3 = 2.155132869$. In the left panel the solution $y(t)$ has an infinite sequence of simple poles and in the right panel the solution oscillates stably about $-\sqrt{t/6}$. The dashed curves are the functions $\pm\sqrt{-t/2}$.

behavior

$$b_{2n} \sim b_{2n+1} \sim B_{\mathrm{II}} n^{2/3} \quad (n \to \infty). \tag{6.16}$$

Our numerical calculations give

$$B_{\mathrm{II}} = 1.8624128. \tag{6.17}$$

The numerical data for P-II are slightly more noisy than those for P-I, and fourth-order Richardson extrapolation only gives the underlined eighth digit as 8 ± 2.

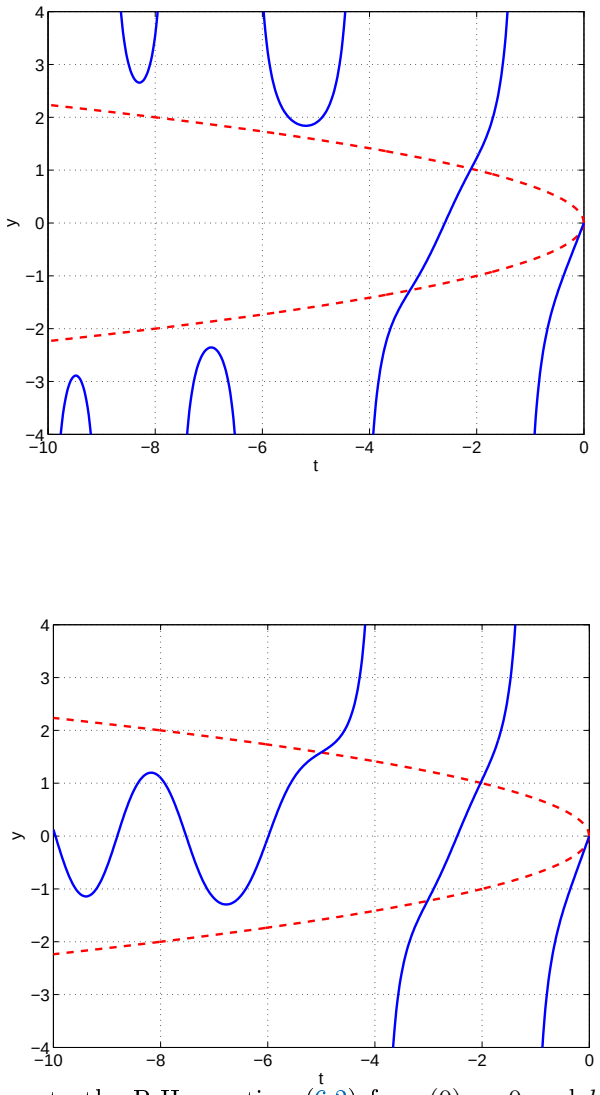

FIGURE 6.9: Solutions to the P-II equation (6.2) for $y(0) = 0$ and $b = y'(0)$. Left panel: $b = 2.600745985$, which lies between the eigenvalues $b_3 = 2.155132869$ and $b_4 = 2.700745985$. Right panel: $b = 2.800745985$, which lies between the eigenvalues $b_4 = 2.700745985$ and $b_5 = 3.195127590$.

6.4.2 Initial-value eigenvalues for Painlevé II

Next, we plot the positive-t solutions to P-II for vanishing initial slope and positive initial condition for $t \geq 0$. As $t \to \infty$, the nth eigenfunction passes through n simple poles before it approaches zero monotonically. In Figs. 6.13, 6.14, and 6.15 we plot the six eigenfunctions corresponding to $n = (1, 2)$, $(3, 4)$, and $(13, 14)$. (Because of the symmetry of P-II, for every positive eigenvalue there is a corresponding negative eigenvalue. We do not plot the negative-eigenvalue solutions.)

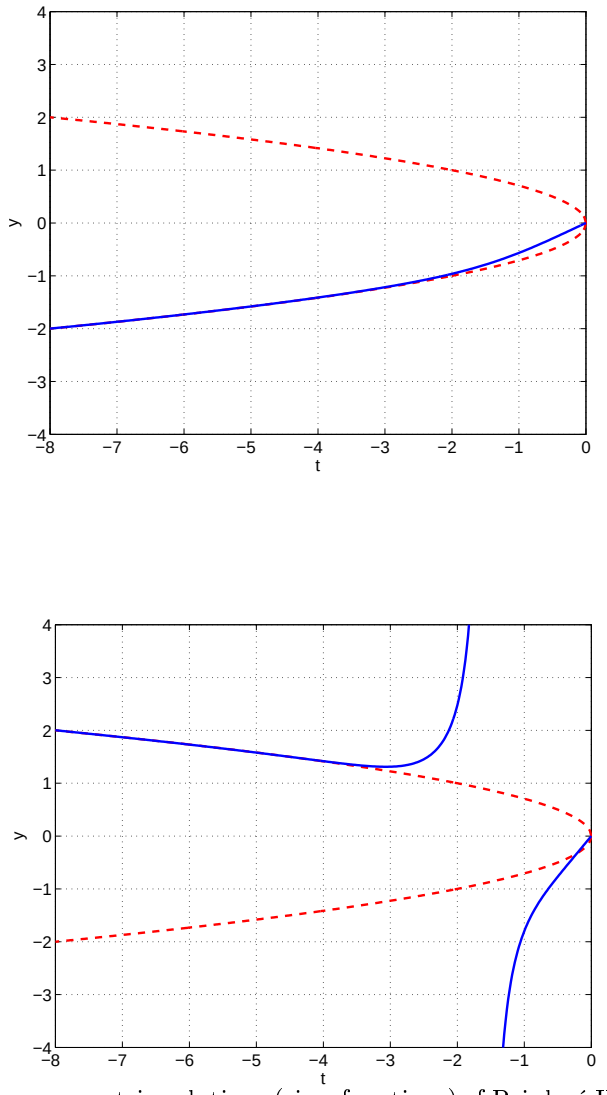

FIGURE 6.10: First two separatrix solutions (eigenfunctions) of Painlevé II with initial condition $y(0) = 0$. Left panel: $y'(0) = b_1 = 0.5950825526$; right panel: $y'(0) = b_2 = 1.528605106$. The dashed curves are $\pm\sqrt{-t/2}$.

Using fourth-order Richardson we determine that for large n, $c_n \sim C_{\rm II} n^{1/3}$, where

$$C_{\rm II} = 1.21581165. \tag{6.18}$$

The last digit 5 has an uncertainty of ± 1.

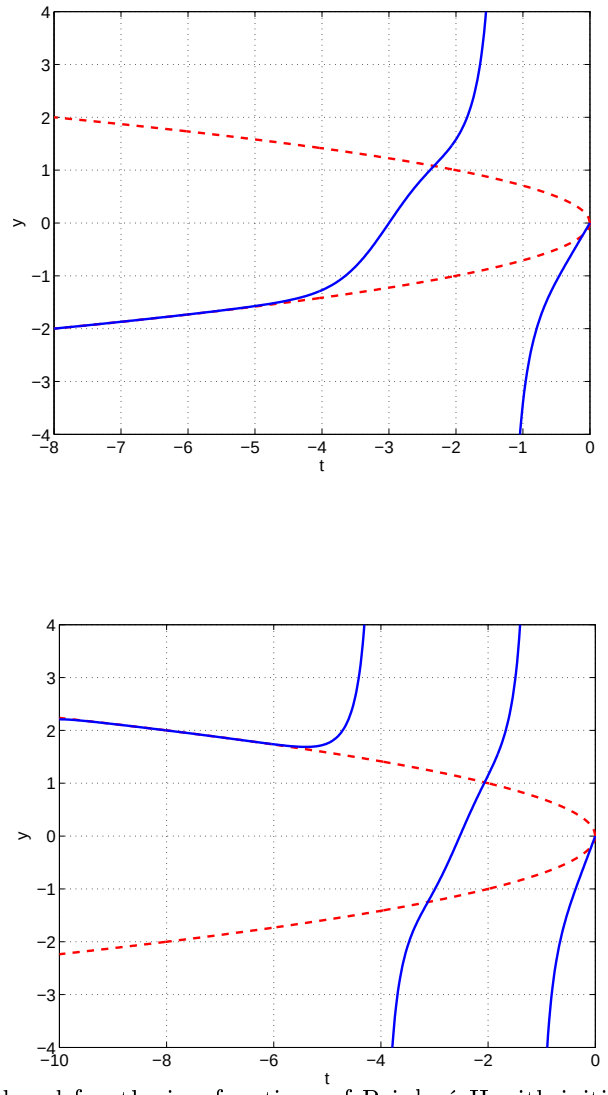

FIGURE 6.11: Third and fourth eigenfunctions of Painlevé II with initial condition $y(0) = 0$. Left panel: $y'(0) = b_3 = 2.155132869$; right panel: $y'(0) = b_4 = 2.700745985$.

6.5 Asymptotic calculation of $B_{\rm II}$ and $C_{\rm II}$

To obtain analytic expressions for $B_{\rm II}$ in (6.17) and $C_{\rm II}$ in (6.18), we follow the same procedure as in Sec. 6.3 for P-I. We multiply the P-II differential equation in (6.2) by $y'(t)$ and integrate from $t = 0$ to $t = x$, where x is in the turning-point region which the simple poles stop. The result is

$$H \equiv \tfrac{1}{2}[y'(x)]^2 - \tfrac{1}{2}[y(x)]^4 = \tfrac{1}{2}[y'(0)]^2 - \tfrac{1}{2}[y(0)]^4 + I(x), \tag{6.19}$$

where $I(x) = \int_0^x dt\, t y(t) y'(t)$. The path of integration is the same as that used to calculate P-II numerically in Sec. 6.4; it follows the negative-real axis until it gets near a simple pole, at which point it makes a semicircular detour in the complex-t plane to avoid the pole. Again, as

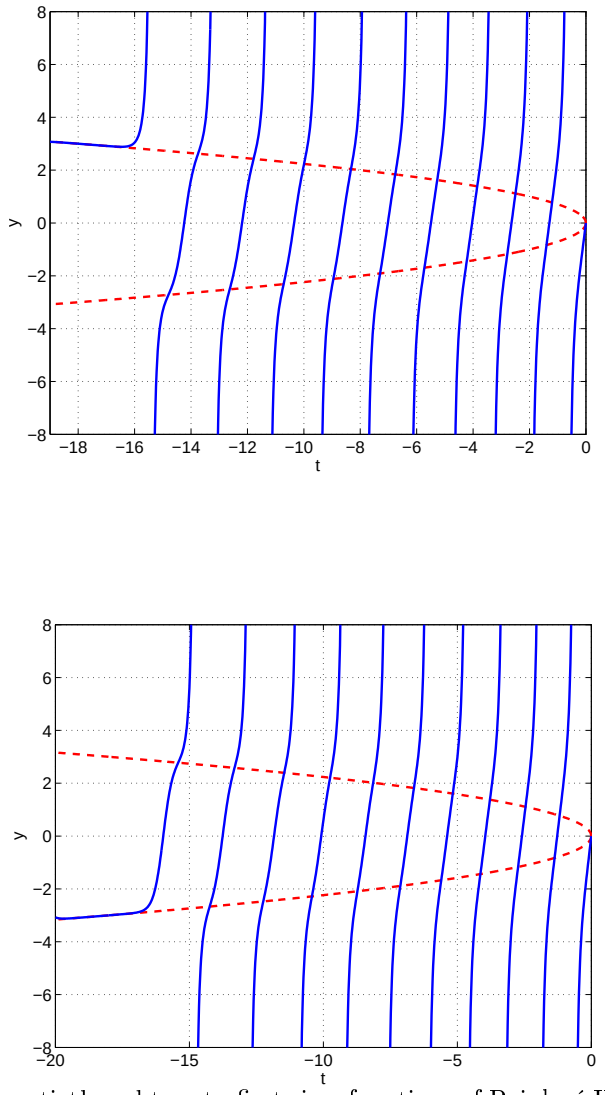

FIGURE 6.12: The twentieth and twenty-first eigenfunctions of Painlevé II with initial condition $y(0) = 0$. Left panel: $y'(0) = b_{20} = 8.499476190$; right panel: $y'(0) = b_{21} = 8.787666814$.

in Sec. 6.3, we argue that along this path the integrand of $I(x)$ is oscillatory and because of cancellations we may neglect $I(x)$ when n is large.

We treat H as the $\mathcal{PT}$-symmetric quantum-mechanical Hamiltonian

$$\hat{H} = \tfrac{1}{2}\hat{p}^2 - \tfrac{1}{2}\hat{x}^4 \tag{6.20}$$

and we use (6.11) with $g = 1/2$ and $\epsilon = 2$ to obtain the formula

$$E_n \sim \tfrac{1}{2}\left[3n\sqrt{2\pi}\Gamma\left(\tfrac{3}{4}\right)/\Gamma\left(\tfrac{1}{4}\right)\right]^{4/3} \tag{6.21}$$

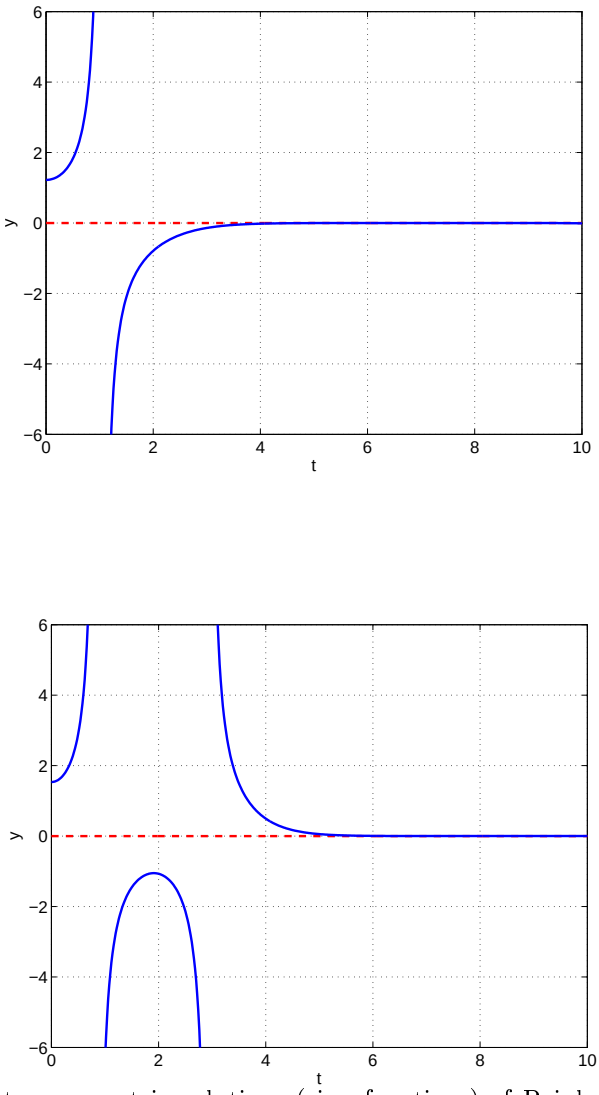

FIGURE 6.13: First two separatrix solutions (eigenfunctions) of Painlevé II with fixed initial slope $y'(0) = 0$. Left panel: $y(0) = c_1 = 1.222873339$; right panel: $y(0) = c_2 = 1.533883935$.

for the large eigenvalues of $\hat{H}$. Finally, we calculate the eigenvalues b_n by using

$$\sqrt{2E_n} \sim \left[3n\sqrt{2\pi}\Gamma\left(\tfrac{3}{4}\right)/\Gamma\left(\tfrac{1}{4}\right)\right]^{2/3} \quad (n \to \infty). \tag{6.22}$$

This result allows us to identify the value of $B_{\rm II}$ in (6.17) as

$$B_{\rm II} = \left[3\sqrt{2\pi}\Gamma\left(\tfrac{3}{4}\right)/\Gamma\left(\tfrac{1}{4}\right)\right]^{2/3}. \tag{6.23}$$

This result agrees with the numerical determination in (6.17).

To calculate C_{II} we observe from Figs. 6.13-6.15 that the initial value $y(0)$ is positive. However, if we neglext $I(x)$ and assume a vanishing initial slope, we see that the right side of

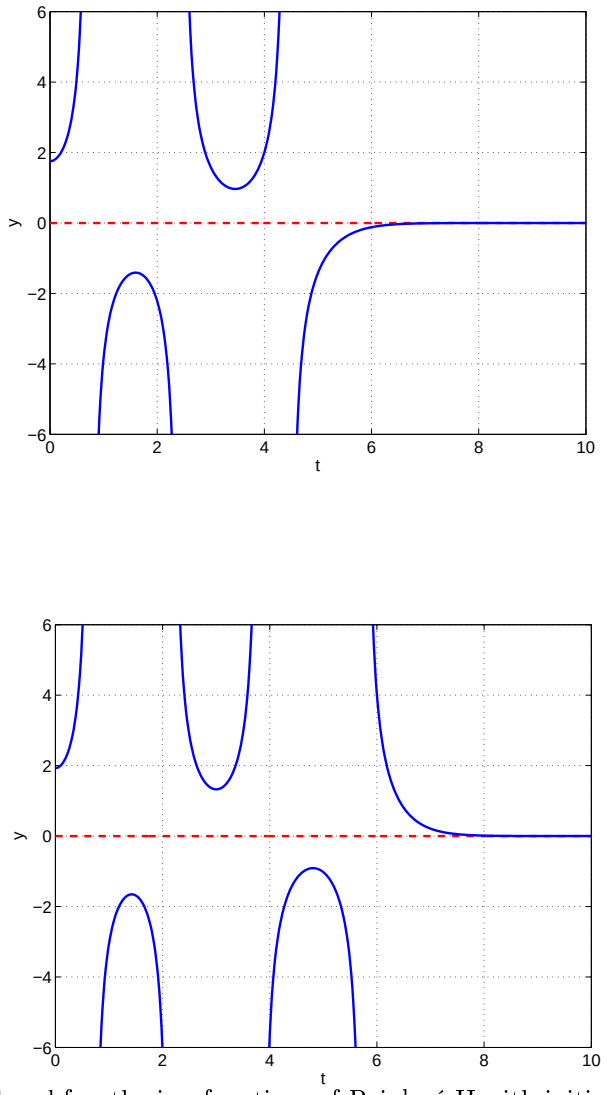

FIGURE 6.14: Third and fourth eigenfunctions of Painlevé II with initial slope $y'(0) = 0$. Left panel: $y(0) = c_3 = 1.754537281$; right panel: $y(0) = c_4 = 1.93061783$.

(6.19) negative. Thus, as we did for the cubic Hamiltonian $\frac{1}{2}\hat{p}^2 - 2\hat{x}^3$, we perform a complex rotation of the coupling constant to convert the quartic Hamiltonian to the form

$$\hat{H} = \tfrac{1}{2}\hat{p}^2 + \tfrac{1}{2}\hat{x}^4. \tag{6.24}$$

This is the conventional Hermitian quartic-anharmonic-oscillator Hamiltonian, and does not belong to the class of $\mathcal{PT}$-symmetric Hamiltonians $\hat{H} = \frac{1}{2}\hat{p}^2 + g\hat{x}^2(i\hat{x})^\epsilon$. A WKB calculation gives the large-eigenvalue approximation

$$E_n \sim \left[3n\sqrt{\pi}\Gamma\left(\tfrac{3}{4}\right)/\Gamma\left(\tfrac{1}{4}\right)\right]^{4/3} \quad (n \to \infty). \tag{6.25}$$

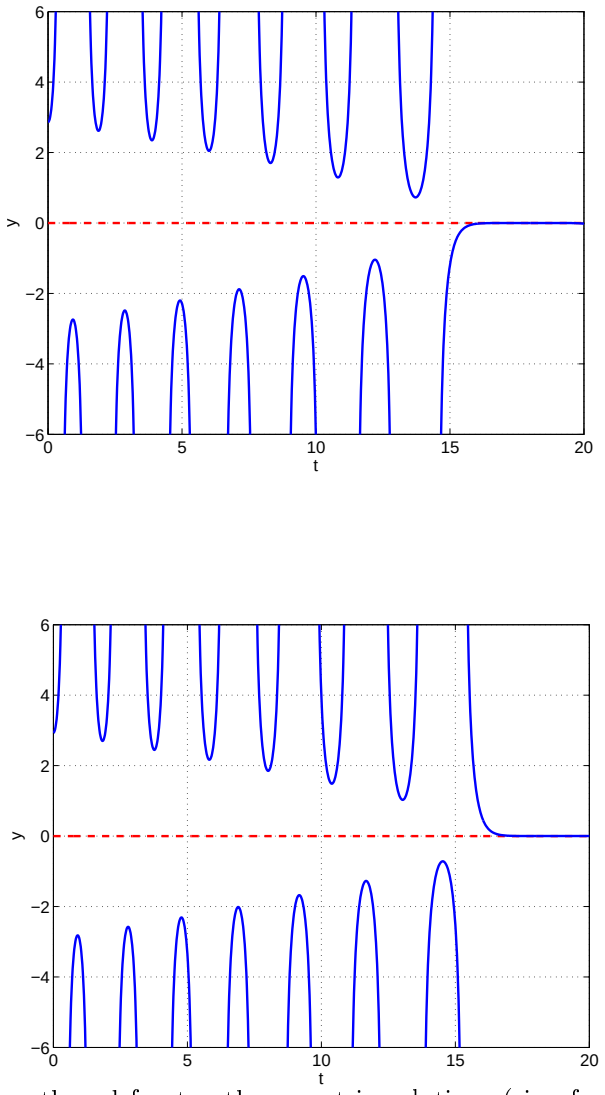

FIGURE 6.15: Thirteenth and fourteenth separatrix solutions (eigenfunctions) of Painlevé II with fixed initial slope $y'(0) = 0$. Left panel: $y(0) = c_1 = 2.858869051$; right panel: $y(0) = c_2 = 2.9303576515$.

Thus, we read off the value of C_{II}:

$$C_{II} = \left[3\sqrt{\pi}\Gamma\left(\tfrac{3}{4}\right)/\Gamma\left(\tfrac{1}{4}\right)\right]^{1/3}, \tag{6.26}$$

which agrees exactly with the numerical result in (6.18).

6.6 Brief concluding remarks

In this chapter we have shown that the first two Painlevé equations, P-I and P-II, exhibit instabilities that are associated with separatrix solutions. The initial conditions that give rise to these separatrix solutions are eigenvalues. We have calculated the semiclassical (large-eigenvalue) behavior of the eigenvalues in two ways, first by using numerical techniques and then by using asymptotic methods to reduce the initial-value problems for the nonlinear P-I and P-II equations to linear eigenvalue problems associated with the time-independent Schrödinger equation. The agreement between these two approaches is exact.

The obvious continuation of this work is to examine the next four Painlevé equations, P-III — P-VI, to see if there are instabilities, separatrices, and eigenvalues for these equations as well. However, the techniques we have applied here may also be useful for other nonlinear differential equations such as the Thomas-Fermi equation $y''(x) = [y(x)]^{3/2}/\sqrt{x}$, which is posed as a boundary-value problem satisfying the boundary conditions $y(0) = 1$ and $y(\infty) = 0$. The solution to this problem is *unstable* with respect to small changes in the initial data; if the initial slope $y'(0)$ is varied by a small amount, the solution develops a spontaneous singularity at some positive value a. A leading-order local analysis suggests that this singularity is a fourth-order pole of the form $400(x-a)^{-4}$. However, this singularity is not a pole. Indeed, a higher-order local analysis indicates that there is a logarithmic-branch-point singularity at $x = a$ as well and thus the solutions to the Thomas-Fermi equation live on multisheeted Riemann surfaces. It would be interesting to see if our work on nonlinear eigenvalue problems extends beyond meromorphic functions.

Bibliography

[1] Georgi, H. Heavy quark effective field theory.

[2] Kogut, J. B., and Susskind, L. Hamiltonian Formulation of Wilson's Lattice Gauge Theories. *Phys.Rev. D11* (1975), 395–408.

[3] Banks, T., et al. Strong Coupling Calculations of the Hadron Spectrum of Quantum Chromodynamics. *Phys.Rev. D15* (1977), 1111.

[4] Susskind, L. Lattice Fermions. *Phys.Rev. D16* (1977), 3031–3039.

[5] Wilson, K. G. Confinement of Quarks. *Phys.Rev. D10* (1974), 2445–2459.

[6] Rothe, H. Lattice gauge theories: An Introduction. *World Sci.Lect.Notes Phys. 43* (1992), 1–381.

[7] Kluberg-Stern, H., Morel, A., Napoly, O., and Petersson, B. Flavors of Lagrangian Susskind Fermions. *Nucl.Phys. B220* (1983), 447.

[8] Bazavov, A., Toussaint, D., Bernard, C., Laiho, J., DeTar, C., et al. Nonperturbative QCD simulations with 2+1 flavors of improved staggered quarks. *Rev.Mod.Phys. 82* (2010), 1349–1417.

[9] Neubert, M. Effective field theory and heavy quark physics. 149–194.

[10] Manohar, A. V. Effective field theories. *Lect.Notes Phys. 479* (1997), 311–362.

[11] Georgi, H. Effective field theory. *Ann.Rev.Nucl.Part.Sci. 43* (1993), 209–252.

[12] Ecker, G. Effective field theories.

[13] Polchinski, J. Effective field theory and the Fermi surface.

[14] Rothstein, I. Z. TASI lectures on effective field theories.

[15] Scherer, S. Introduction to chiral perturbation theory. *Adv.Nucl.Phys. 27* (2003), 277.

[16] Weinberg, S. Phenomenological Lagrangians. *Physica A96* (1979), 327.

[17] Golterman, M. Applications of chiral perturbation theory to lattice QCD. 423–515.

[18] A. Manohar and M. Wise, *Heavy Quark Physics*, Cambridge University Press (2000).

[19] Symanzik, K. Continuum Limit and Improved Action in Lattice Theories. 1. Principles and phi**4 Theory. *Nucl.Phys. B226* (1983), 187.

[20] Kronfeld, A. S. Uses of effective field theory in lattice QCD: Chapter 39 in At the Frontiers of Particle Physics, Handbook of QCD.

[21] Sharpe, S. R. B(K) Using staggered fermions: An update. *Nucl.Phys.Proc.Suppl. 34* (1994), 403–406.

[22] Lee, W.-J., and Sharpe, S. R. Partial flavor symmetry restoration for chiral staggered fermions. *Phys.Rev. D60* (1999), 114503.

[23] Aubin, C., and Bernard, C. Pion and kaon masses in staggered chiral perturbation theory. *Phys.Rev. D68* (2003), 034014.

[24] Aubin, C., and Bernard, C. Pseudoscalar decay constants in staggered chiral perturbation theory. *Phys.Rev. D68* (2003), 074011.

[25] C. Aubin and C. Bernard, Phys. Rev. D73 014515 (2006) [arXiv:hep-lat/0510088v3].

[26] McNeile, C., Davies, C., Follana, E., Hornbostel, K., and Lepage, G. High-Precision f_{B_s} and HQET from Relativistic Lattice QCD. *Phys.Rev. D85* (2012), 031503.

[27] Bazavov, A., et al. Scaling studies of QCD with the dynamical HISQ action. *Phys.Rev. D82* (2010), 074501.

[28] Bazavov, A., et al. Pseudoscalar meson physics with four dynamical quarks. *PoS LATTICE2012* (2012), 159.

[29] Bazavov, A., et al. Lattice QCD ensembles with four flavors of highly improved staggered quarks. *Phys.Rev. D87*, 5 (2013), 054505.

[30] Bernard, C., et al. Tuning Fermilab Heavy Quarks in 2+1 Flavor Lattice QCD with Application to Hyperfine Splittings. *Phys.Rev. D83* (2011), 034503.

[31] Laiho, J., and Van de Water, R. S. $B \to D^* \ell\nu$ and $B \to D\ell\nu$ form factors in staggered chiral perturbation theory. *Phys.Rev. D73* (2006), 054501.

[32] E. Follana *et al.* [HPQCD Collaboration], Phys. Rev. D **75**, 054502 (2007) [hep-lat/0610092].

[33] E. Follana, C. T. H. Davies, G. P. Lepage and J. Shigemitsu [HPQCD Collaboration and UKQCD Collaboration], Phys. Rev. Lett. **100**, 062002 (2008) [arXiv:0706.1726].

[34] A. Bazavov *et al.* [Fermilab Lattice and MILC Collaborations], PoS LATTICE **2012**, 159 (2012) [arXiv:1210.8431 [hep-lat]].

[35] C. McNeile, C. T. H. Davies, E. Follana, K. Hornbostel and G. P. Lepage, Phys. Rev. D **85**, 031503 (2012) [arXiv:1110.4510 [hep-lat]].

[36] C. Bernard *et al.* [Fermilab Lattice and MILC Collaborations], Phys. Rev. D **83**, 034503 (2011) [arXiv:1003.1937 [hep-lat]].

[37] W. Lee and S. Sharpe Phys. Rev. **D60**, 114503 (1999) [arXiv:hep-lat/9905023].

[38] C. Aubin and C. Bernard, Phys. Rev. D **68**, 034014 (2003) [arXiv:hep-lat/0304014] and Phys. Rev. D **68**, 074011 (2003) [arXiv:hep-lat/0306026].

[39] A. Bazavov *et al.* [MILC Collaboration], Phys. Rev. D**87**, 054505 (2013) [arXiv:1212.4678[hep-lat]].

[40] A. X. El-Khadra, A. S. Kronfeld and P. B. Mackenzie, Phys. Rev. D **55**, 3933 (1997) [arXiv:hep-lat/9604004].

[41] G. P. Lepage and B. A. Thacker, Nucl. Phys. Proc. Suppl. **4**, 199 (1988); B. A. Thacker and G. P. Lepage, Phys. Rev. D **43**, 196 (1991).

[42] C. van den Doel and J. Smit, Nucl. Phys. B **228**, 122 (1983); M. Golterman and J. Smit, Nucl. Phys. B **245**, 61 (1984).

[43] C. Bernard, M. Golterman and Y. Shamir, Phys. Rev. D **77**, 074505 (2008) [arXiv:0712.2560 [hep-lat]].

[44] K. Symanzik, Nucl. Phys. B **226**, 187 (1983).

[45] C. Bernard, M. Golterman and Y. Shamir, Phys. Rev. D **73**, 114511 (2006) [hep-lat/0604017].

[46] S. Prelovsek, Phys. Rev. D **73**, 014506 (2006) [hep-lat/0510080].

[47] Y. Shamir, Phys. Rev. D **71**, 034509 (2005) [hep-lat/0412014].

[48] Y. Shamir, Phys. Rev. D **75**, 054503 (2007) [hep-lat/0607007].

[49] C. Bernard, Phys. Rev. D **73**, 114503 (2006) [hep-lat/0603011].

[50] S. R. Sharpe, PoS **LAT2006**, 022 (2006) [hep-lat/0610094].

[51] A. S. Kronfeld, PoS **LAT2007**, 016 (2007) [arXiv:0711.0699 [hep-lat]].

[52] M. Golterman, PoS **CONFINEMENT8**, 014 (2008) [arXiv:0812.3110 [hep-ph]].

[53] G. C. Donald, C. T. H. Davies, E. Follana and A. S. Kronfeld, Phys. Rev. D **84**, 054504 (2011) [arXiv:1106.2412 [hep-lat]].

[54] S. R. Sharpe, Phys Rev. D **46**, 3146 (1992) [arXiv:hep-lat/9205020].

[55] A. Bazavov *et al.* [Fermilab Lattice and MILC Collaborations], talks at *Lattice 2013*, Mainz, Germany, July 29–Aug. 3, 2013, to be published in Proceedings of Science, and work in progress.

[56] A. Bazavov, C. Bernard, C. M. Bouchard, C. DeTar, M. Di Pierro, A. X. El-Khadra, R. T. Evans and E. D. Freeland *et al.* [Fermilab Lattice and MILC Collaborations], Phys. Rev. D **85**, 114506 (2012) [arXiv:1112.3051].

[57] C. G. Boyd and B. Grinstein, Nucl. Phys. B442, 205 (1995), [arXiv:hep-ph/9402340].

[58] C. Aubin and C. Bernard, Phys. Rev. D76, 014002 (2007) [arXiv:hep-lat/0704.0795].

[59] J. Laiho and R. S. Van de Water, Phys. Rev. D **73**, 054501 (2006) [hep-lat/0512007].

[60] S. R. Sharpe and R. S. Van de Water, Phys. Rev. D **71**, 114505 (2005) [arXiv:hep-lat/0409018].

[61] A. Bazavov *et al.* [MILC Collaboration], Phys. Rev. D **82**, 074501 (2010) [arXiv:1004.0342 [hep-lat]].

[62] I. W. Stewart, Nucl. Phys. B529, 62 (1998) [arXiv:hep-ph/9803227].

[63] D. Becirevic *et al.*, Phys. Rev. D68, 074003 (2003) [arXiv:hep-lat/0305001].

[64] D. Arndt and C. J. D. Lin, Phys. Rev. D70, 014503 (2004) [arXiv:hep-lat/0403012].

[65] W. J. Marciano, Phys. Rev. Lett. **93**, 231803 (2004) [hep-ph/0402299].

[66] C. Aubin *et al.* [MILC Collaboration], Phys. Rev. D **70**, 114501 (2004) [hep-lat/0407028].

[67] A. Bazavov *et al.* [MILC Collaboration], Phys. Rev. Lett. **110**, 172003 (2013) [arXiv:1301.5855 [hep-ph]].

[68] E. Follana *et al.* [HPQCD Collaboration], Phys. Rev. D **75**, (2007) 054502 [hep-lat/0610092].

[69] A. Bazavov *et al.* [MILC Collaboration], PoS(LATTICE 2008) 033 [arXiv:0903.0874]; A. Bazavov *et al.*, PoS(LATTICE 2009) 123 [arXiv:0911.0869]; PoS(LATTICE 2010) 320 [arXiv:1012.1265].

[70] A. Bazavov *et al.*, Phys. Rev. D **82**, 074501 (2010) [arXiv:1004.0342].

[71] A. Bazavov *et al.* [MILC Collaboration], Phys. Rev. **D87**, 054505 (2013) [arXiv:1212.4768].

[72] E. Marinari, G. Parisi and C. Rebbi, Nucl. Phys. B **190**, 734 (1981).

[73] S. Prelovsek. Phys. Rev. D**73**, 014506 (2006).

[74] C. Bernard, Phys. Rev. D**73**, 114503 (2006).

[75] C. Bernard, M. Golterman, and Y. Shamir. Phys. Rev. D**73**, 114511 (2006).

[76] C. Bernard, C. DeTar, Z. Fu, and S. Prelovsek. Phys. Rev. D**76**, 094504 (2007).

[77] Y. Shamir. Phys. Rev. D**71**, 034509 (2005).

[78] Y. Shamir. Phys. Rev. D**75**, 054503 (2007).

[79] E. Follana, A. Hart, and C.T.H. Davies. Phys. Rev.Lett. **93**, 241601 (2004).

[80] S. Dürr, C. Hoelbling, and U. Wenger. Phys. Rev. D**70**, 094502 (2004).

[81] S. Dürr and C. Hoelbling. Phys. Rev. D**71**, 054501 (2005).

[82] K. Y. Wong and R.M. Woloshyn. Phys. Rev. D**71**, 094508 (2005).

[83] S. Dürr and C. Hoelbling. Phys. Rev. D**74**, 014513 (2006).

[84] G. Donald, C.T.H. Davies, E. Follana, and A.S. Kronfeld. Phys. Rev. D**84**, 054504 (2011).

[85] W. -J. Lee and S. R. Sharpe, Phys. Rev. D **60**, 114503 (1999) [hep-lat/9905023].

[86] J. Komijani and C. Bernard, PoS(LATTICE 2012) 199 [arXiv:1211.0785]; C. Bernard and J. Komijani, Phys. Rev. D88, 094017 (2013) [arXiv:1309.4533].

[87] A. Bazavov *et al.* [Fermilab Lattice and MILC Collaborations], PoS(LATTICE 2013) 405 [arXiv:1312.0149].

[88] A. Bazavov *et al.*, Rev. Mod. Phys. **82**, 1349 (2010) [arXiv:0903.3598].

[89] J.A. Bailey *et al.* [Fermilab Lattice and MILC Collaborations], PoS(LATTICE 2011) 320 [arXiv:1112.3978]; A. Bazavov *et al.* [Fermilab Lattice and MILC Collaborations], Phys. Rev. D **85** 114506 (2012) [arXiv:1112.3051].

[90] S. Aoki *et al.*, Phys.Rev. D62 (2000) 094501.

[91] G.W. Kilcup and S.W. Sharpe, Nucl. Phys. **B283** (1987) 493.

[92] E. Follana *et al.* [HPQCD and UKQCD Collaborations], Phys. Rev. D **75**, 054502 (2007) [arXiv:hep-lat/0610092].

[93] J. Beringer *et al.* [Particle Data Group], Phys. Rev. D **86**, 010001 (2012).

[94] G.P. Lepage, In: From Actions to Answers: Proceedings of the 1989 Theoretical Advanced Study Institute in Elementary Particle Physics, eds. T. DeGrand and D. Toussaint (World Scientific, Singapore, 1990) p. 197.

[95] S. R. Sharpe, Phys. Rev. D **56**, 7052 (1997) [Erratum-ibid. D **62**, 099901 (2000)] [hep-lat/9707018].

[96] C. Davies *et al.*, Nucl. Phys. Proc. Suppl. **119**, 595 (2003) [hep-lat/0209122].

[97] S. Basak *et al.* [MILC Collaboration], PoS(LATTICE 2012) 137 [arXiv:1210.8157 [hep-lat]].

[98] S. Basak *et al.* [MILC Collaboration], PoS CD **12**, 030 (2013) [arXiv:1301.7137 [hep-lat]].

[99] S. Basak et al. (MILC Collaboration), PoS(LATTICE 2014) 116 [arXiv:1409.7139].

[100] S. Aoki, Y. Aoki, C. Bernard, T. Blum, G. Colangelo, M. Della Morte, S. Dürr and A. X. El Khadra *et al.*, arXiv:hep-lat/1310.8555.

[101] A. Bazavov *et al.* [Fermilab Lattice and MILC Collaborations], Phys. Rev. D **85**, 114506 (2012) [arXiv:1112.3051].

[102] C. G. Boyd and B. Grinstein, Nucl. Phys. **B442**, 205 (1995) [arXiv:hep-ph/9402340].

[103] I. W. Stewart, Nucl. Phys. B **529**, 62 (1998) [hep-ph/9803227]; D. Becirevic, S. Prelovsek and J. Zupan, Phys. Rev. D **68**, 074003 (2003) [hep-lat/0305001].

[104] A. Bazavov *et al.* [MILC Collaboration], PoS(LATTICE 2011) 107 [arXiv:1111.4314 [hep-lat]], and work in progress.

[105] C. Aubin and C. Bernard, Phys. Rev. D76, 014002 (2007) [arXiv:hep-lat/0704.0795].

[106] D. Arndt and C. J. D. Lin, Phys. Rev. D70, 014503 (2004) [arXiv:hep-lat/0403012].

[107] T. Appelquist and J. Carazzone, Phys. Rev. D **11**, 2856 (1975).

[108] D. Becirevic and F. Sanfilippo, Phys. Lett. **B721**, 94 (2013) [arXiv:1210.5410]; K. U. Can, G. Erkol, M. Oka, A. Ozpineci, and T. T. Takahashi, Phys. Lett. **B719**, 103 (2013) [arXiv:1210.0869].

[109] W. Detmold, C. J. D. Lin, and S. Meinel, Phys. Rev. D**85**, 114508 (2012) [arXiv:1203.3378].

[110] W. Bernreuther and W. Wetzel, Nucl. Phys. B **197**, 228 (1982) [Erratum-ibid. B **513**, 758 (1998)].

[111] A. Manohar and M. Wise, *Heavy Quark Physics*, Cambridge University Press (2000).

[112] C. Davies *et al.* [HPQCD Collaboration], Phys. Rev. D **82**, 114504 (2010) [arXiv:1008.4018].

[113] H. Na *et al.* [HPQCD Collaboration], Phys. Rev. D **86** 054510 (2012) [arXiv:1206.4936].

[114] B. Blossier *et al.* [ETM Collaboration], Phys. Rev. D **82**, 114513 (2010) [arXiv:1010.3659 [hep-lat]].

[115] C. Aubin *et al.* [MILC Collaboration] Phys. Rev. **D** 70, 114501 (2004) [arXiv:hep-lat/0407028].

[116] Y. Aoki *et al.* [RBC/UKQCD Collaboration], Phys. Rev. D**83** (2011) 074508 [arXiv:1011.0892].

[117] S. Dürr *et al.* [BMW Collaboration], Phys. Rev. D **81**, 054507 (2010) [arXiv:1001.4692].

[118] J. Laiho and R.S. Van de Water, PoS(LATTICE 2011) 293 [arXiv:1112.4861].

[119] R. Arthur *et al.*, Phys. Rev. D **87** (2013) 094514 [arXiv:1208.4412].

[120] N. Carrasco *et al.*, Nucl. Phys. **B887**, 19 (2014) [arXiv:1403.4504 [hep-lat]].

[121] S. Dürr and G. Koutsou, Phys. Rev. Lett. **108**, 122003 (2012) [arXiv:1108.1650 [hep-lat]].

[122] C. T. H. Davies, C. McNeile, K. Y. Wong, E. Follana, R. Horgan, K. Hornbostel, G. P. Lepage and J. Shigemitsu *et al.*, Phys. Rev. Lett. **104**, 132003 (2010) [arXiv:0910.3102 [hep-ph]].

[123] G. Schierholz *et al.*, PoS(LATTICE 2007) 133.

[124] B. Blossier *et al.*, JHEP **0907**, (2009) 043 [arXiv:0904.0954].

[125] S. Lottini [ALPHA Collaboration], PoS(LATTICE 2013) 315 [arXiv:1311.3081].

[126] E. Follana, C. T. H. Davies, G. P. Lepage and J. Shigemitsu [HPQCD/UKQCD Collaboration], Phys. Rev. Lett. **100** (2008) 062002 [arXiv:0706.1726].

[127] C. Aubin, J. Laiho and R.S. Van de Water, PoS(LATTICE 2008) 105 [arXiv:0810.4328].

[128] A. Bazavov *et al.* [MILC Collaboration], PoS(LATTICE 2010) 074 [arXiv:1012.0868].

[129] A. Bazavov *et al.* [MILC Collaboration], Phys. Rev. Lett. **110**, 172003 (2013) [arXiv:1301.5855].

[130] R.J. Dowdall, C.T.H. Davies, G.P. Lepage and C. McNeile [HPQCD Collaboration], Phys. Rev. D **88** (2013) 074504, [arXiv:1303.1670];

[131] L. Riggio *et al.*, PoS(LATTICE 2013) 314 [arXiv:1311.3080].

[132] C. Aubin *et al.* [Fermilab lattice and MILC Collaborations], Phys. Rev. Lett. **95**, 122002(2005) [arXiv:hep-lat/0506030].

[133] E. Follana *et al.* [HPQCD Collaboration], Phys. Rev. Lett. **100**, 062002 (2008) [arXiv:0706.1726].

[134] P. Dimopoulos *et al.* [ETM Collaboration], JHEP **01**, 046 (2012) [arXiv:1107.1441].

[135] A. Bazavov *et al.* [Fermilab Lattice and MILC Collaborations], PoS(LATTICE 2012) 159 [arXiv:1210.8431].

[136] J. Heitger *et al.*, PoS(LATTICE 2013) 475 [arXiv:1312.7693].

[137] Y.B. Yang *et al.*, PoS(LATTICE 2013) 500 [arXiv:1401.1487].

[138] W.P. Chen *et al.*, [arXiv:1404.3648].

[139] Y. Namekawa *et al.* [PACS-CS Collaboration], Phys. Rev. D **84** (2011) 074505 [arXiv:1104.4600].

[140] A. Bazavov *et al.* [Fermilab Lattice and MILC Collaborations], *in preparation.*

[141] M. Antonelli *et al.*, Eur. Phys. J. C **69**, 399 (2010) [arXiv:1005.2323 [hep-ph]].

[142] J. C. Hardy and I. S. Towner, Phys. Rev. C **79**, 055502 (2009) [arXiv:0812.1202 [nucl-ex]].

[143] A. Bazavov *et al.* [Fermilab Lattice and MILC Collaborations], Phys. Rev. Lett. **112**, 112001 (2014) [arXiv:1312.1228 [hep-ph]].

[144] J. L. Rosner and S. Stone, arXiv:1309.1924 [hep-ex].

[145] G. Burdman, J. T. Goldman and D. Wyler, Phys. Rev. D **51**, 111 (1995) [hep-ph/9405425].

[146] B. A. Dobrescu and A. S. Kronfeld, Phys. Rev. Lett. **100**, 241802 (2008) [arXiv:0803.0512 [hep-ph]].

[147] V. Cirigliano, G. Ecker, H. Neufeld, A. Pich and J. Portoles, Rev. Mod. Phys. **84**, 399 (2012) [arXiv:1107.6001 [hep-ph]].

[148] T. Kinoshita, Phys. Rev. Lett. **2**, 477 (1959).

[149] A. Sirlin, Nucl. Phys. B **196**, 83 (1982).

[150] M. Knecht, H. Neufeld, H. Rupertsberger and P. Talavera, Eur. Phys. J. C **12**, 469 (2000) [hep-ph/9909284].

[151] V. Cirigliano and I. Rosell, JHEP **0710**, 005 (2007) [arXiv:0707.4464 [hep-ph]].

[152] S. Descotes-Genon and B. Moussallam, Eur. Phys. J. C **42**, 403 (2005) [hep-ph/0505077].

[153] H. Na *et al.*, Phys. Rev. D **84**, 114505 (2011) [arXiv:1109.1501 [hep-lat]].

[154] H. Na, C. T. H. Davies, E. Follana, G. P. Lepage and J. Shigemitsu, Phys. Rev. D **82**, 114506 (2010) [arXiv:1008.4562 [hep-lat]].

[155] Bender, C., and Orszag, S. *Advanced mathematical methods for scientists and engineers.* International series in pure and applied mathematics. McGraw-Hill, 1978.

[156] Wasow, W. *Asymptotic expansions for ordinary differential equations.* Courier Corporation, 2002.

[157] Tai, T. D. On the simpleness of zeros of stokes multipliers. *Journal of Differential Equations 223*, 2 (2006), 351 – 366.

[158] Shin, K. C. On the reality of the eigenvalues for a class of pt-symmetric oscillators. *Communications in mathematical physics 229*, 3 (2002), 543–564.

[159] Delabaere, E., and Rasoamanana, J.-M. Resurgent deformations for an ordinary differential equation of order 2. *Pacific journal of mathematics 223*, 1 (2006), 35–93.

[160] Sibuya, Y. *Global theory of a second order linear ordinary differential equation with a polynomial coefficient*, vol. 18. Elsevier, 1975.

[161] Kawai, T., and Takei, Y. *Algebraic analysis of singular perturbation theory*, vol. 227. American Mathematical Soc., 2005.

[162] C. M. Bender, D. W. Hook, P. N. Meisinger, and Q. Wang, Phys. Rev. Lett. **104**, 061601 (2010).

[163] C. M. Bender, D. W. Hook, P. N. Meisinger, and Q. Wang, Ann. Phys. **325**, 2332-2362 (2010).

[164] J. Gair, N. Yunes, and C. M. Bender, J. Math. Phys. **53**, 032503 (2012).

[165] See Ref. [155], chap. 10.

[166] For a discussion of hyperasymptotics see M. V. Berry and C. J. Howls, Proc. Roy. Soc. A **430**, 653 (1990); M. V. Berry in *Asymptotics Beyond All Orders*, ed. by H. Segur, S. Tanveer, and H. Levine (Plenum, New York, 1991), pp. 1-14.

[167] See Ref. [155], chap. 11.

[168] See Ref. [155], chap. 8.

[169] A detailed study of the asymptotic behavior of the Painlevé transcendents may be found in M. Jimbo and T. Miwa, Physica D **2**, 407 (1981). Separatrix behavior of the first Painlevé transcendent is mentioned briefly in A. A. Kapaev, Differential Equations **24**, 1107 (1989).

[170] See Problem 7.7 in W. K. Hayman, *Research Problems in Function Theory* [Athlone Press (University of London), London, 1967].

[171] J. Clunie and P. Erdös, Proc. Roy. Irish Acad. **65**, 113 (1967).

[172] J. D. Buckholtz, Michigan Math. J. **15**, 481 (1968).

[173] C. M. Bender, A. Fring, and J. Komijani, work in progress.

[174] E. L. Ince, *Ordinary Differential Equations* (Dover, New York, 1956).

[175] A detailed study of the asymptotic behavior of the Painlevé transcendents may be found in M. Jimbo and T. Miwa, Physica D **2**, 407 (1981).

[176] Separatrix behavior of the first Painlevé transcendent is mentioned briefly in A. A. Kapaev, Differential Equations **24**, 1107 (1989).

[177] P. A. Clarkson, J. Comp. Appl. Math. **153**, 127 (2003).

[178] D. Maseoro, *Essays on the Painlevé First Equation and the Cubic Oscillator*, PhD Thesis, SISSA (2010).

[179] O. Costin, R. D. Costin, and M. Huang, *Tronquée solutions of the Painlevé equation* P_1 (2013, unpublished).

[180] A. S. Fokas, A. R. Its, A. A. Kapaev, and V. Y. Novokshonov, *Painlevé Transcendents: The Riemann-Hilbert Approach*, (American Mathematical Society, New York, 2006).

[181] The spin-spin correlation function for the two-dimensional Ising model for temperatures near T_c is described by P-III. See T. T. Wu, B. M. McCoy, C. A. Tracy, and E. Barouch, Phys. Rev. B **13**, 316 (1976).

[182] For all temperatures the diagonal correlation function for the Ising model in two dimensions $\langle \sigma_{0,0}\sigma_{N,N}\rangle$ is given in terms of P-VI. See M. Jimbo and T. Miwa, Proc. Jap. Acad. **56A**, 405 (1980) and **57A**, 347 (1981).

[183] E. Brézin and V. A. Kazakov, Phys. Lett. B **236**, 144 (1990).

[184] M. Douglas and S. Shenker, Nucl. Phys. B **335**, 635 (1990).

[185] D. Gross and A. Migdal, Nucl. Phys. B **340**, 333 (1990).

[186] G. Moore, Comm. Math. Phys. **133**, 261 (1990).

[187] G. Moore, Prog. Theor. Phys. Suppl. **102**, 255 (1990).

[188] A. S. Fokas, A. R. Its, and A. V. Kitaev, Comm. Math. Phys. **147**, 395 (1992).

[189] C. M. Bender, A. Fring, and J. Komijani, J. Phys. A: Math. Theor. **47**, 235204 (2014).

[190] O. S. Kerr, J. Phys. A: Math. Theor. **47**, 368001 (2014).

[191] See Ref. [155], Chap. 8.

[192] For a discussion of complex scaling (complex rotation of coordinates) see W. P. Reinhardt, Ann. Rev. Phys. Chem. **33**, 223 (1982).

[193] C. M. Bender and S. Boettcher, Phys. Rev. Lett. **80**, 5243 5246 (1998).

APPENDICES

A

The QCD Action in Euclidean Space-Time

Under the Wick rotation $x_0 \to -ix_4$ and $\partial_0 \to i\partial_4$. Then the QCD Lagrangian and action in Minkowski and Euclidean space-time are related by

$$\mathcal{L}_{\mathrm{M}} = -\mathcal{L}_{\mathrm{E}} \,, \qquad S_{\mathrm{M}} = iS_{\mathrm{E}} \,. \tag{A.1}$$

The fermionic part of the QCD action in Minkowski space-time is

$$S_{\mathrm{fermion}} = \sum_{f=1}^{N_f} \sum_{c=1}^{3} \int d^4x \; \bar{\psi}_{f,c}(\not{D} - m_f)\psi_{f,c} \,, \qquad \not{D} = i\gamma^\mu(\partial_\mu - ig_S A_\mu) \,, \tag{A.2}$$

and its gauge part is

$$S_{\mathrm{gauge}} = -\int d^4x \frac{1}{2} \operatorname{Tr} F^{\mu\nu} F_{\mu\nu} \,, \qquad F_{\mu\nu} = \partial_\mu A_\nu - \partial_\nu A_\mu - ig_S[A_\mu, A_\nu] \,. \tag{A.3}$$

The γ^μ matrices satisfy the following anticommutation relation

$$\{\gamma^\mu, \gamma^\nu\} = 2g^{\mu\nu}. \tag{A.4}$$

In Euclidea space-time, it is convenient to use the Hermitean choice $\gamma_4^{\mathrm{E}} = \gamma^0$ and $\gamma_j^{\mathrm{E}} = -i\gamma^j$ with the following anticommutation relation [6]

$$\{\gamma_\mu^{\mathrm{E}}, \gamma_\nu^{\mathrm{E}}\} = 2\delta_{\mu\nu}. \tag{A.5}$$

Then the fermionic part of the QCD action in Euclidean space-time is given by

$$S^{\text{Eucl.}}_{\text{fermion}} = \sum_{f=1}^{N_f} \sum_{c=1}^{3} \int d^4x \; \bar{\psi}_{f,c}(\not{D} + m_f)\psi_{f,c} \; , \qquad \not{D} = \gamma^{\text{E}}_{\mu}(\partial_\mu - ig_S A_\mu) \; , \tag{A.6}$$

and its gauge part is

$$S^{\text{Eucl.}}_{\text{gauge}} = + \int d^4x \frac{1}{2} \operatorname{Tr} F_{\mu\nu} F_{\mu\nu} \; , \qquad F^{\text{Eucl.}}_{\mu\nu} = \partial_\mu A_\nu - \partial_\nu A_\mu - ig_S[A_\mu, A_\nu] \; . \tag{A.7}$$

Note that the form of $(\partial_\mu - ig_S A_\mu)$ does not change when making the transition to the Euclidean space-time, since both ∂_0 and A_0 follow the same rule: $\partial_0 \to i\partial_4$ and $A_0 \to iA_4$ [6]. In Lattice QCD the Euclidean space-time is understood, so we drop any labels reminding us of this.

Two-point Correlation Functions in Staggered Fermions

The one component-staggered fermion fields $\chi(x)$, with x in the dimensionless lattice units, can be assembled into Dirac fields $\psi(y)$, living on 2^4 hypercubes of the original lattice, labeled by y, with corners $x = 2y + A$, where $A_\mu = 0, 1$. We say y is in blocked-lattice units since it refers to the whole 2^4 hypercube. The one component-staggered fermion fields $\chi(x)$ living at the sites within each block can be assembled into Dirac fields $q(y)$ as

$$\begin{aligned} \psi(y)_{\alpha i} &= \frac{1}{8}\sum_A (\Gamma_A)_{\alpha i}\, U_A(y)\, \chi(2y+A)\,, \\ \bar{\psi}(y)_{\alpha i} &= \frac{1}{8}\sum_A \bar{\chi}(2y+A)\, U_A^\dagger(y)\, (\Gamma_A^*)_{\alpha i}\,, \end{aligned} \tag{B.1}$$

where α and i label the Dirac and taste indices, respectively, Γ_A is defined in Eq. (1.30), and $U_A(y)$ is a product of the gauge links over some fixed path from $2y$ to $2y + A$. The bilinear fermions operators, with spin structure $\gamma_s = \Gamma_s$ and taste structure $\xi_t = \Gamma_t^*$ are defined by

$$\mathcal{O}_{st} = \bar{\psi}(y)(\gamma_s \otimes \xi_t)\psi(y) = \frac{1}{16}\sum_{A,B} \bar{\chi}(2y+A)\, U_A^\dagger(y)\, U_B(y)\, \chi(2y+B)\, \frac{1}{4}\,\mathrm{Tr}\left(\Gamma_A^\dagger \Gamma_s \Gamma_B \Gamma_t^\dagger\right). \tag{B.2}$$

The bilinear fermion operator becomes local by choosing $\Gamma_t = \Gamma_s$ due to the fact that the trace over the product of matrices forces A and B to be identical. This allows us to define a 4-vector local current as

$$J_{\mu,\mathrm{local}} = \bar{\psi}(y)(\gamma_\mu \otimes \xi_\mu)\psi(y) = \frac{1}{16}\sum_A \bar{\chi}(2y+A)\, \alpha_\mu(A)\, \chi(2y+A), \tag{B.3}$$

where

$$\alpha_\mu(A) = (-1)^{A_1+\cdots+A_4+A_\mu}\,. \tag{B.4}$$

Choosing $\Gamma_t = I$, we have a 4-vector taste-singlet current (point-split current) as

$$J_{\mu,I} = \bar{\psi}(y)(\gamma_\mu \otimes I)\psi(y) = \frac{1}{16}\sum_{A,B} \bar{\chi}(2y+A)\, U_A^\dagger(y)\, \eta_\mu(A)\, U_B(y)\, \chi(2y+B)\, \big(\delta_{A+\hat{\mu},B} + \delta_{A-\hat{\mu},B}\big), \tag{B.5}$$

where

$$\eta_\mu(A) = (-1)^{A_1+\cdots+A_{\mu-1}},\ \eta_1(A) = 1\ . \tag{B.6}$$

B.1 Two-point Correlation Functions

The two-point correlation function of χ and $\bar{\chi}$ at infinite spatial volume and time can be written as

$$C^{[2]}_{AA'}(y;y') \equiv \langle \chi(2y+A)\bar{\chi}(2y'+A')\rangle = \int_{-\pi}^{+\pi} \frac{d^4p}{(2\pi)^4}\, K^{-1}_{AA'}(p)\, e^{ip.(y-y')}\ . \tag{B.7}$$

Here, both y and p are in blocked-lattice units. For the free case we have [6]

$$K^{-1}_{AA'}(p) = \frac{-i\sum_\mu \Gamma^\mu_{AA'}(p)\ \sin(\frac{p_\mu}{2}) + M\delta_{AA'}}{\sum_\mu \sin^2(\frac{p_\mu}{2}) + M^2}\ , \tag{B.8}$$

where M is the fermion mass in lattice units, and

$$\Gamma^\mu_{AA'}(p) = e^{ip.(A-A')/2}\big(\delta_{A+\hat{\mu},A'} + \delta_{A-\hat{\mu},A'}\big)\eta_\mu(A)\ , \tag{B.9}$$

where $\eta_\mu(A)$, defined in Eq. (B.6), is the remnant phase of the original Dirac structure. Note that in Eq. (B.7) the momentum p is the momentum associated with the hypercube-blocks, labeled by y, rather the original lattice cites with component $x = 2y + A$.

Projecting the free propagator to the spatial momentum $\mathbf{p}$, we obtain

$$\sum_{\mathbf{y}} e^{-i\mathbf{p}.\mathbf{y}}\, C^{[2]}_{AA'}(\mathbf{y}, y_4; y') = e^{-i\mathbf{p}.\mathbf{y}'}\, \mathbf{K}^{-1}_{AA'}(\mathbf{p}; y_4 - y'_4)\ , \tag{B.10}$$

where

$$\begin{aligned}\mathbf{K}^{-1}_{AA'}(\mathbf{p}; y_4 - y'_4) &= \int_{-\pi}^{+\pi} \frac{dp_4}{2\pi}\, K^{-1}_{AA'}(\mathbf{p}, p_4)\, e^{ip_4.(y_4-y'_4)} \\ &= \frac{e^{-E(\mathbf{p})|y_4-y'_4|}}{s\sqrt{1+s^2}}\big(-i\sum_\mu \Gamma^\mu_{AA'}(\hat{p})\ \sin(\frac{\hat{p}_\mu}{2}) + M\delta_{AA'}\big)\ ,\end{aligned} \tag{B.11}$$

where $s = \sqrt{M^2 + \sin^2 \frac{\mathbf{p}}{2}}$, $E(\mathbf{p}) = 2\sinh^{-1}(s)$, and $\hat{p}$ denotes the momentum of an on-shell particle as $\hat{p} = (\mathbf{p}, \hat{p}_4)$, where $\hat{p}_4 = iE(\mathbf{p})\ \mathrm{sgn}(y_4 - y'_4)$. Note that $\hat{p}_4 = iE(\mathbf{p})\ \mathrm{sgn}(A_4 - A'_4)$ if $y_4 = y'_4$, and the dependence on $\hat{p}_4$ vanishes when $y_4 = y'_4$ as well as $A_4 = A'_4$.) Similarly one can show that

$$\sum_{\mathbf{y}'} C^{[2]}_{AA'}(y; \mathbf{y}', y'_4)\ e^{i\mathbf{p}'.\mathbf{y}'} = \mathbf{K}^{-1}_{AA'}(\mathbf{p}'; y_4 - y'_4)\ e^{i\mathbf{p}'.\mathbf{y}}\ . \tag{B.12}$$

Now we can construct the two-point correlation function of the spin-taste (hypercube) fermions ψ and $\bar{\psi}$ as

$$G^{[2]}_{\alpha i,\alpha' i'}(y; y') \equiv \langle \psi_{\alpha i}(y) \bar{\psi}_{\alpha' i'}(y') \rangle = \frac{1}{64} \sum_{A,A'} (\Gamma_A)_{\alpha i}\ U_A(y)\ C^{[2]}_{AA'}(y; y')\ U^{\dagger}_{A'}(y')\ (\Gamma^*_{A'})_{\alpha' i'}\ . \tag{B.13}$$

For the free case we have

$$G^{[2]}_{\alpha i,\alpha' i'}(y; y') = \frac{1}{64} \sum_{A,A'} (\Gamma_A)_{\alpha i}\ C^{[2]}_{AA'}(y; y')\ (\Gamma^*_{A'})_{\alpha' i'} \tag{B.14}$$

$$= \int_{-\pi}^{+\pi} \frac{d^4p}{(2\pi)^4}\ S_{\alpha i,\alpha' i'}(p)\ e^{ip.(y-y')}\ . \tag{B.15}$$

To calculate $S(p)$ we use the identity

$$\frac{1}{4} \sum_{A} (\Gamma_A)_{\alpha i} (\Gamma^*_A)_{\beta j} = \delta_{\alpha\beta}\delta_{ij}\ , \tag{B.16}$$

and also the following relations

$$\sum_{A} \cos\Big(\frac{p.(A - A')}{2}\Big) \big(\delta_{A+\hat{\mu},A'} + \delta_{A-\hat{\mu},A'}\big) \eta_\mu(A)\ \Gamma_A = \cos\Big(\frac{p.\hat{\mu}}{2}\Big)\ \gamma_\mu\ \Gamma_{A'}\ , \tag{B.17}$$

$$\sum_{A} \sin\Big(\frac{p.(A - A')}{2}\Big) \big(\delta_{A+\hat{\mu},A'} + \delta_{A-\hat{\mu},A'}\big) \eta_\mu(A)\ \Gamma_A = \sin\Big(\frac{p.\hat{\mu}}{2}\Big)\ \gamma_5\ \Gamma_{A'}\ \xi^*_5 \xi^*_\mu\ , \tag{B.18}$$

where $\xi_\mu = \gamma^*_\mu$ and $\xi_5 = \gamma^*_5 = \gamma_5$. It should be emphasized that we use ξ matrices on the right hand side of the $\Gamma_{A'}$ because the column index of $\Gamma_{A'}$ is a taste index rather than a Dirac index. To derive the above equalities, it is enough to consider that for a given A' there is only one surviving value of A. Putting all the components together we obtain

$$S_{\alpha i,\alpha' i'}(p) = \frac{1}{16} \frac{-i \sum_\mu \sin(\frac{p_\mu}{2})\ \big[\cos(\frac{p_\mu}{2})(\gamma_\mu)_{\alpha\alpha'}\delta_{ii'} + i \sin(\frac{p_\mu}{2})(\gamma_5)_{\alpha\alpha'}\ (\xi^*_5\xi^*_\mu)_{i'i}\big] + M\delta_{\alpha\alpha'}\delta_{ii'}}{\sum_\mu \sin^2 \frac{p_\mu}{2} + M^2}, \tag{B.19}$$

which can be written as

$$S(p) = \frac{1}{16}\frac{\sum_\mu \left[\frac{-i}{2}\sin(p_\mu)\ (\gamma_\mu \otimes I) + \sin^2(\frac{p_\mu}{2})\ (\gamma_5 \otimes \xi_\mu\xi_5)\right] + M(I\otimes I)}{\sum_\mu \sin^2\frac{p_\mu}{2} + M^2}\ . \tag{B.20}$$

Note that we are using the Euclidean set of γ-matrices, which are Hermitian. This relation can be expressed as

$$S(p) = \frac{1}{16}\frac{\sum_\mu -i\sin(\frac{1}{2}p_\mu)\ \Gamma^\mu_{\text{s-t}}(p) + M}{\sum_\mu \sin^2(\frac{1}{2}p_\mu) + M^2}\ , \tag{B.21}$$

where

$$\Gamma^\mu_{\text{s-t}}(p) \equiv (\gamma_\mu \otimes I)\exp\left[i\tfrac{1}{2}p_\mu(\gamma_\mu\gamma_5 \otimes \xi_\mu\xi_5)\right]\ . \tag{B.22}$$

Projecting the free propagator to the spatial momentum $\mathbf{p}$, we obtain

$$\sum_{\mathbf{y}} e^{-i\mathbf{p}.\mathbf{y}}\ G^{[2]}_{\alpha i,\alpha' i'}(\mathbf{y}, y_4; y') = e^{-i\mathbf{p}.\mathbf{y}'}\ \mathbf{S}_{\alpha i,\alpha' i'}(\mathbf{p}; y_4 - y'_4)\ , \tag{B.23}$$

where

$$\begin{aligned}\mathbf{S}(\mathbf{p}; y_4 - y'_4) &= \int_{-\pi}^{+\pi}\frac{dp_4}{2\pi}\ S(\mathbf{p}, p_4)\ e^{ip_4.(y_4-y'_4)} \\ &= \frac{1}{16}\ \frac{e^{-E(\mathbf{p})|y_4-y'_4|}}{s\sqrt{1+s^2}} \\ &\quad\times\Big(\sum_\mu\left[\frac{-i}{2}\sin(\hat{p}_\mu)\ (\gamma_\mu\otimes I) + \sin^2(\frac{\hat{p}_\mu}{2})\ (\gamma_5\otimes\xi_\mu\xi_5)\right] + M(I\otimes I)\Big)\end{aligned} \tag{B.24}$$

where $s = \sqrt{M^2 + \sin^2\frac{\mathbf{p}}{2}}$, $E(\mathbf{p}) = 2\sinh^{-1}(s)$, $\hat{p} = (\mathbf{p}, \hat{p}_4)$ and $\hat{p}_4 = iE(\mathbf{p})\ \text{sgn}(y_4 - y'_4)$. Eq. (B.24) is valid only if $y_4 \neq y'_4$, otherwise it reads

$$\begin{aligned}\mathbf{S}(\mathbf{p}; 0) &= \int_{-\pi}^{+\pi}\frac{dp_4}{2\pi}\ S(\mathbf{p}, p_4) \\ &= \frac{1}{16}(1 - \frac{s}{\sqrt{1+s^2}})(\gamma_5\otimes\xi_4\xi_5)\ + \frac{1}{16}\ \frac{1}{s\sqrt{1+s^2}} \\ &\quad\times\Big(\sum_j\left[\frac{-i}{2}\sin(\hat{p}_j)\ (\gamma_j\otimes I) + \sin^2(\frac{\hat{p}_j}{2})\ (\gamma_5\otimes\xi_j\xi_5)\right] + M(I\otimes I)\Big).\end{aligned} \tag{B.25}$$

(Note that $(1 - s/\sqrt{1+s^2})(\gamma_5\otimes\xi_4\xi_5)$ does not vanish in the naive continuum limit as $s \to 0$.) Similarly, one can show

$$\sum_{\mathbf{y}'} G^{[2]}_{\alpha i,\alpha' i'}(y; \mathbf{y}', y'_4)\ e^{i\mathbf{p}'.\mathbf{y}'} = \mathbf{S}_{\alpha i,\alpha' i'}(\mathbf{p}'; y_4 - y'_4)\ e^{i\mathbf{p}'.\mathbf{y}}\ . \tag{B.26}$$

C

Reduction to Irreducible Tensors

In Sec. 2.3.2, we need to reduce a 3-index tensor to irreducible Lorentz representations in order to find the type-B2 chiral form for the current. The reduction is done explicitly here. For present convenience we work in Euclidean space and use Euclidean rotational symmetry (plus parity) instead of Lorentz symmetry, so we do not have to worry about upper and lower indices.

Consider a tensor $X^{\alpha\beta\rho}$, which may be taken to be traceless on the second two indices $X^{\alpha\lambda\lambda} = 0$, where sum over λ is implied.[1] The tracelessness may be assumed because the trace term will simply reproduce type-A contributions, as in the discussion of $\mathcal{L}^{B2}_{2,a^2}$. In addition, we may just consider the reduction of the part of X that is symmetric on the second two indices,

$$Y^{\alpha\beta\rho} \equiv \frac{1}{2}\left(X^{\alpha\beta\rho} + X^{\alpha\rho\beta}\right) \tag{C.1}$$

since we will ultimately be interested in writing only the element $X^{\mu\nu\nu}$ in terms of irreducible tensors, and the antisymmetric part will not contribute.

The tensor Y transforms as the product of a vector (on the first index) and a traceless symmetric tensor (on the second and third indices). To see what representations appear, we use the fact that $SO(4) = SU(2) \times SU(2)$ to denote irreducible tensors by their spin under the two $SU(2)$ factors. A vector is the $(\frac{1}{2}, \frac{1}{2})$ representation, while a traceless, symmetric two-index tensor is the $(1, 1)$ representation. The product thus contains $(\frac{3}{2}, \frac{3}{2})$, $(\frac{3}{2}, \frac{1}{2}) \oplus (\frac{1}{2}, \frac{3}{2})$, and $(\frac{1}{2}, \frac{1}{2})$, where parity interchanges the two $SU(2)$ factors, making a single representation out of the second component. The highest representation must be symmetric, and $(\frac{3}{2}, \frac{3}{2})$ corresponds to a completely symmetric, three index tensor $S^{\alpha\beta\rho}$, which is traceless on any pair of indices: $S^{\alpha\lambda\lambda} = S^{\lambda\alpha\lambda} = S^{\lambda\lambda\alpha} = 0$. The $(\frac{3}{2}, \frac{1}{2}) \oplus (\frac{1}{2}, \frac{3}{2})$ is a traceless three index tensor $A^{\alpha\beta\rho}$ of mixed

[1] In what follows λ will be used as a summation index, and sum over it is always implied when it appears twice. However, all other indices are not summed over, even when they appear more than once.

symmetry, antisymmetric on the first two indices (say). The $(\frac{1}{2},\frac{1}{2})$ is a vector W^ρ, formed from only the nonvanishing trace of Y:

$$W^\rho = Y^{\lambda\lambda\rho} = Y^{\lambda\rho\lambda} \ . \tag{C.2}$$

Constructing $S^{\alpha\beta\rho}$ and $A^{\alpha\beta\rho}$, we have

$$S^{\alpha\beta\rho} = \frac{1}{3}\left(Y^{\alpha\beta\rho} + Y^{\beta\rho\alpha} + Y^{\rho\alpha\beta}\right) - \frac{1}{9}\left(\delta^{\beta\rho}\, Y^{\lambda\lambda\alpha} + \delta^{\alpha\rho}\, Y^{\lambda\lambda\beta} + \delta^{\alpha\beta}\, Y^{\lambda\lambda\rho}\right) \ , \tag{C.3}$$

$$A^{\alpha\beta\rho} = \frac{1}{2}\left(Y^{\alpha\beta\rho} - Y^{\beta\alpha\rho}\right) - \frac{1}{6}\left(\delta^{\alpha\rho}\, Y^{\lambda\lambda\beta} - \delta^{\beta\rho}\, Y^{\lambda\lambda\alpha}\right) \ . \tag{C.4}$$

From the $SU(2)\times SU(2)$ quantum numbers, S and A should each be 16-dimensional. Checking this for S is straightforward; for A, the following identity is helpful:

$$A^{\alpha\beta\rho} + A^{\beta\rho\alpha} + A^{\rho\alpha\beta} = 0 \ . \tag{C.5}$$

Solving Eqs. (C.2) through (C.4) for $Y^{\alpha\beta\rho}$ gives the reduction

$$Y^{\alpha\beta\rho} = S^{\alpha\beta\rho} + \frac{2}{3}\left(A^{\alpha\beta\rho} - A^{\rho\alpha\beta}\right) + \frac{1}{9}\left(2\,\delta^{\alpha\rho}\, W^\beta + 2\,\delta^{\alpha\beta}\, W^\rho - \delta^{\beta\rho}\, W^\alpha\right) \ . \tag{C.6}$$

The particular case of interest is the reduction of $X^{\mu\nu\nu}$. From Eqs. (C.1) and (C.6), we have

$$X^{\mu\nu\nu} = S^{\mu\nu\nu} + \frac{4}{3}A^{\mu\nu\nu} + \frac{1}{9}\left(4\,\delta^{\mu\nu}\, W^\nu - W^\mu\right) \ . \tag{C.7}$$

D

Expansion of Φ_0 in terms of $1/m_Q$

Equation (3.8) contains the effects of hyperfine splittings (*e.g.*, $M_D^* - M_D$) and flavor splittings (*e.g.*, $M_{D_s} - M_D$), but no other $1/m_Q$ effects. Boyd and Grinstein [102] find some other contributions at the same order as hyperfine and flavor splittings. However, one can show that most of these terms only produce $1/m_Q$ corrections to the LECs relevant to the pseudoscalar-meson decay constants. (Some of the terms violate heavy-quark spin symmetry, and therefore give different contributions to the pseudoscalar and vector-meson decay constants at this order, but we are not concerned with vector-meson decay constants here.) Following Eq. (20) of Ref. [102], at the order of $\mathcal{O}(1/m_Q, m_q^0)$ where m_q is a light quark mass, the $1/m_Q$ terms can be included by replacing Φ_0 by $\Phi_0(1+\text{const}/m_Q)$. This dependence can be simply absorbed in Φ_0 for a fixed value of m_Q. However, in our analysis the charm mass varies by about 10%, which leads to a correction comparable to that produced by terms of $\mathcal{O}(m_q) \sim \mathcal{O}(m_\pi^2)$. Therefore, replacing Φ_0 by $\Phi_0(1+\text{const}/m_Q)$ in Eq. (3.8) should be considered a NLO correction. At this order the rate for $D^* \to D\pi$ is governed by $g_\pi(1+\text{const}/m_Q)$ instead of g_π, which is already taken into account by incorporating the range $g_\pi = 0.53(8)$ in the fits. We do not allow any further dependence of g_π on m_Q in our analysis, because this dependence is formally NNLO.

On each ensemble, we have data with two different values of the valence charm mass: m_c' and $0.9m_c'$, where m_c' is the charm sea mass of the ensemble. In Fig. D.1, the ratio of Φ_D at m_c' to Φ_D at $0.9m_c'$ is shown in terms of m_v for our four lattice spacings. The fact that $\Phi_D(m_c')/\Phi_D(0.9m_c')$ does not vary much as a function of the light valence-quark mass is evidence that the $1/m_Q$ effects can be absorbed in the overall factor in front of the full one-loop result as discussed above. On the other hand, Φ_D computed at m_c' and at $0.9m_c'$ are highly correlated so that their ratio is known precisely. Since our fits take the correlations into account, the p values will be low unless the chiral form is able to reproduce the ratio to high accuracy. Therefore, the expansion of the

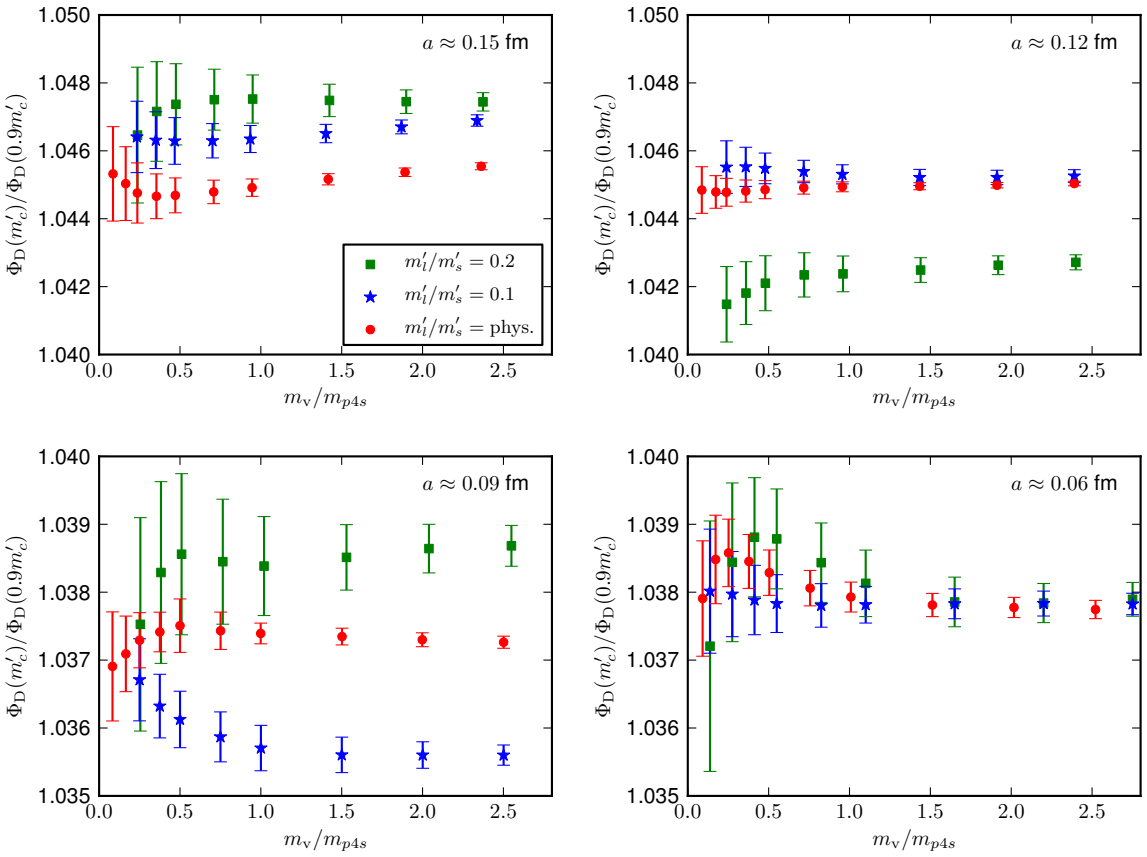

FIGURE D.1: The ratio $\Phi_D(m'_c)/\Phi_D(0.9m'_c)$ (where m'_c is the charm sea mass of the ensembles) as a function of m_v, the light valence-quark mass. The upper left panel shows data at $a \approx 0.15$ fm. The upper right panel shows the data at $a \approx 0.12$ fm from the ensembles with m_s tuned close to its physical value. In the second row, we show $a \approx 0.09$ fm (left) and $a \approx 0.06$ fm (right) data.

overall factor, Φ_0, in terms of $1/m_Q$ needs to be taken beyond the first order; for acceptable fits we need to introduce a $1/m_Q^2$ term as well as the $1/m_Q$ term, as indicated in Eq. (3.21). Furthermore, good fits require the LEC k_1 in Eq. (3.21) to have generic dependence on a; such dependence for k_2 is also strongly preferred by the fits.

Note finally that Fig. D.1 shows a roughly 4% difference between Φ_D at m'_c and at $0.9m'_c$. As claimed in the discussion above Eq. (3.21), this is comparable to the chiral NLO effects of a nonzero pion mass, which may be estimated from the fits shown in Fig. 3.17. Indeed, those fits imply that the difference between the physical value of Φ_{D^+} and its value in the (two-flavor) chiral limit is roughly 3%.